



UNIVERSIDAD DE SEVILLA
Escuela Técnica Superior de Ingeniería

PhD Thesis:
STUDY OF THE UNFOLDING FAILURE
OF CURVED COMPOSITE LAMINATES

A THESIS SUBMITTED BY
JUAN MANUEL GONZÁLEZ CANTERO

FOR THE DEGREE OF DOCTOR OF PHILOSOPHY IN THE
UNIVERSIDAD DE SEVILLA

SUPERVISED BY

ENRIQUE GRACIANI DÍAZ
FEDERICO PARÍS CARBALLO

2017

Abstract

The use of composite materials in structural applications has been considerably increased in the last years. This increment has introduced the use of composite laminates in complex components including highly curved zones. Highly curved laminates are prone to unfolding failure, a delamination caused by a bending moment which tries to flatten the curvature.

Unfolding failure is classically associated to the Interlaminar Normal Stress (INS), which is characterized by the InterLaminar Tensile Strength (ILTS). The ILTS is typically obtained by a four-point bending test applied to an L-shaped specimen with all the plies oriented at 0° . If this test procedure is applied to composite laminates with differently oriented plies an apparent ILTS is obtained. The apparent ILTS exhibits a thickness-dependence which has not been physically explained yet.

INS may be obtained by using FEM. Notwithstanding, analytical models are desirable for obtaining lower modelling and calculation times. Nowadays, analytical models have shown high errors in the calculation of the INS for some kinds of geometries and loading states. These errors are due to a free-edge effect associated with the curvature changes, e.g., in the joint of a curved part with a straight arm. Differences in INS values due to a change of curvature may be even of a 100% with respect to the actual value.

The PhD project has studied, in a first stage, the four-point bending test, which is the one typically employed for ILTS determination, obtaining a non-linear model for the calculation of the load-displacement and load-bending moment distributions. The model has been successfully correlated with experimental results.

The second stage of the PhD has been focused to the INS calculation, developing two different bi-dimensional models based on a series expansion of the displacement and a higher-order moments definition in the stresses. The first model is based in monomials, with very low computational times and a good accuracy, and the second model is based in Legendre polynomials, with still low computational times and a very high accuracy. Both models have allowed the change-of-curvature problem to be solved and to

analyse in detail the different parameters involving the stresses distribution near to free-edges.

The third stage of the PhD has been focused on the expansion of the bi-dimensional models to obtain a three-dimensional model in order to consider also the effect of the torsion and the anticlastic effect combined with the curvature, as well as the effect of the finite width of the specimens. This model let us also to calculate accurately the out-of-plane stress state.

Finally, in the fourth stage of the PhD, the stress calculation methodologies developed have been used for the data reduction of an existing test campaign. Results suggest that in laminates with a low apparent ILTS, intralaminar failures in the matrix direction may have taken place before delamination. Comparing the load causing the failure with the predictions made for the first intralaminar/interlaminar failure, and observing the crack locations in tested coupons, a feasible explanation for the thickness dependence has been found. This explanation consists in distinguishing two kinds of unfolding failures: first, the traditional unfolding initiated by the INS and, second, the newly defined induced unfolding, which is initiated by a failure associated to intralaminar stresses that propagates as a delamination due to the presence of the high INS.

Based in the previous results, some optimization guidelines have been defined for the design and sizing of curved composite laminates based in the unfolding failure.

Acknowledgements

I wish to thank Federico París and Enrique Graciani for their support which has made possible this project.

Special thanks and recognition are also due to FIDAMC, the Spanish Foundation for the Development, Application and Research on Composite Materials, whose support has contributed to the development of the project.

A special recognition goes to Airbus Group Innovations (AGI) for the opportunity of working in one of its main researching centres in Germany, the Airbus Group Chair of Seville for its support and Airbus Operations S.L. for its collaboration in the project.

Finally, I wish to thank my family, my friends and my partners in FIDAMC for their support.

Contents

List of Figures	11
List of Acronyms	15
1 Introduction	17
1.1 Motivations and aims of the project	19
1.2 State of the art in stresses calculation in curved laminates	22
1.3 State of the art in failure criteria	26
1.3.1 Failure initiation criteria	27
1.3.2 Failure propagation criteria	29
1.4 Thesis overview	30
2 Analysis of the four-point bending test	33
2.1 Standardized testing procedure for assessment of ILTS	34
2.2 Non-linear model for obtaining the bending moment	36
2.3 Simplification of the non-linear model	48
2.4 Comparison of the non-linear model with experimental results	50
2.5 Comparison of the non-linear model with the ASTM procedure	53
3 Bi-dimensional models for evaluating interlaminar stresses	55
3.1 Theoretical basis of the regularized models	56
3.2 Approximations of the regularized models	61
3.3 Theoretical basis of the non-regularized models	67
3.4 Monomials based model (MBM)	71
3.4.1 Development of the MBM for straight beams	72
3.4.2 Development of the MBM for curved beams	82
3.4.3 MBM numerical limitations	90
3.5 Legendre polynomials based model (LPBM)	91
3.5.1 Characteristics of the Legendre polynomials	92
3.5.2 Development of the LPBM for straight beams	95
3.5.3 Development of the LPBM for curved beams	99

3.6	Resolution of the regularized problem by using the non-regularized models	104
3.7	Resolution of the homogeneous problem	107
3.8	Resolution of the joints between components	109
3.8.1	Continuity of the circumferential stresses between components	110
3.8.2	Continuity of the shear stresses between components	111
3.8.3	Continuity of the circumferential displacements between components	112
3.8.4	Continuity of the transverse displacements between components	114
3.8.5	Application of the boundary conditions and the continuity conditions	116
3.9	Results of the non-regularized models and validation by FEM	117
3.9.1	L-shaped beam under bending moment	117
3.9.2	L-shaped beam under a compressive load	119
3.9.3	Joggle under a tensile load	121
3.10	Numerical characteristics of the MBM and LPBM non regularized models	123
3.11	Regularization distance	125
3.12	Off-topic applications of the non regularized models	129
3.12.1	Joint of beams with different material properties	129
3.12.2	Non-regularized effects due to the boundary conditions	131
3.12.3	Non-regularized effects due to punctual loads	133
4	Three-dimensional models for evaluating interlaminar stresses	137
4.1	3D model with double regularization for singly-curved beams under bending moment and residual strains	139
4.1.1	Theoretical development	141
4.1.2	Loads application and boundary conditions	149
4.1.3	Particular cases	156
4.2	Analysis of the effect of residual stresses in the unfolding failure	161
4.2.1	Homogeneous anisotropic materials	162
4.2.2	Composite laminates	164
4.2.3	Finite elements comparison	166
4.3	Analysis of the three-dimensional effects over the unfolding failure	166
4.3.1	Homogeneous anisotropic materials	167
4.3.2	Composite laminates	169
4.3.3	Finite elements comparison	170
4.4	Three-dimensional non-regularized models	173

4.4.1	Development of the 3D non-regularized model in flat laminates	175
4.4.2	Development of the 3D non-regularized model in curved laminates	190
4.5	Applications of the 3D non-regularized models	209
4.5.1	Through-the-width distributions	209
4.5.2	Free-edge effects	211
5	Failure mechanisms involved in the unfolding failure	215
5.1	The concept of the induced unfolding failure mechanism	216
5.2	Experimental results	218
5.2.1	Traditional unfolding	219
5.2.2	Induced unfolding	220
6	Design recommendations	227
6.1	Evaluation of the maximum bending moment with the combination of traditional and induced unfolding	228
6.2	Optimization recommendations based on both failure mechanisms	234
7	Concluding remarks and future developments	237
A	Matrices of the differential equation of the 2D non-regularized models	243
A.1	MBM matrices for the straight beam	243
A.2	MBM matrices for the curved beam	244
A.3	LPBM matrices for the straight beam	245
A.4	LPBM matrices for the curved beam	246
B	Matrices expressions of the 3D non-regularized models	247
B.1	Stiffness matrices for the flat laminate	247
B.2	Auxiliary matrices for the flat laminate	249
B.3	Stiffness matrices for the curved laminate	250
B.4	Auxiliary matrices for the curved laminate	256
	Bibliography	263
	Curriculum Vitae	275

List of Figures

1.1	When the laminate is opened by a bending moment the plies try to separate.	18
1.2	Example of thickness dependence of the apparent ILTS obtained from quasi-isotropic laminates.	20
1.3	INS colour plot in a L-shaped beam loaded under end bending moment. (a) Regularized stresses. (b) Non-regularized stresses.	22
1.4	Comparison between the Kim and Soni criterion and the Brewer and Lagace criterion.	28
2.1	Four-point bending test set-up.	34
2.2	Beam approximation of the specimen in a four-point bending test.	36
2.3	Deformed configuration of beam 1.	37
2.4	Deformed configuration of beam 2 and beam 3.	42
2.5	Numerical and experimental force-displacement relations in SP1.	52
2.6	Numerical and experimental force-displacement relations in SP2.	52
3.1	Geometry and loads considered in the regularized models of a curved beam.	57
3.2	Loads considered in the approximation of the regularized models of a curved beam.	62
3.3	Definition of the curvilinear coordinate system.	68
3.4	Examples of geometries where the non-regularized models can be applied. Global coordinate system definition.	70
3.5	Decomposition of the section in several constant-curvature beams.	71
3.6	Straight beam.	73
3.7	(a) Clockwise curved beam. (b) Counter-clockwise curved beam.	83

3.8	Condition number of $\hat{\mathbf{K}}_{\sigma}$ depending on the thickness.	91
3.9	Legendre polynomials up to $i = 5$	93
3.10	Regularized solution of the non-regularized models for the bending moment loading.	105
3.11	Regularized solution of the non-regularized models for the axial force loading.	106
3.12	Regularized solution of the non-regularized models for the shear force loading.	107
3.13	L-shaped beam under bending moment.	117
3.14	Maximum INS in the L-shaped beam under bending moment.	118
3.15	Maximum ISS in the L-shaped beam under bending moment.	119
3.16	L-shaped beam under a compressive load.	120
3.17	Maximum INS in the L-shaped beam under compressive load.	120
3.18	Maximum ISS in the L-shaped beam under compressive load.	121
3.19	Joggle under a tensile load.	121
3.20	Maximum INS in the joggle under tensile load.	122
3.21	Maximum ISS in the joggle under tensile load.	123
3.22	Computational times of the MBM. (a) Depending on N_p for $n = 9$. (b) Depending on n for $N_p = 8$	124
3.23	Computational times of the LPBM. (a) Depending on N_p for $n = 20$. (b) Depending on n for $N_p = 1$	124
3.24	Complex plane representation of $\sqrt{\lambda_{\min}}$	128
3.25	Regularization distances for a single-ply laminate depending on the orientation.	128
3.26	Joint of two beams with different material properties, axially loaded.	129
3.27	Axial stress at the joint of two different materials.	130
3.28	Stresses in the joint of two different materials. (a) Shear stress. (b) Through-thickness stress in both sides.	131
3.29	Axial stress in an embedment under tensile load.	132
3.30	Stresses in an embedment under tensile load. (a) Shear stress. (b) Through-thickness stress.	132
3.31	Axial stress in an embedment under bending moment.	133
3.32	Stresses in an embedment under bending moment. (a) Shear stress. (b) Through-thickness stress.	134
3.33	Three-point bending test configuration.	134
3.34	Axial stress in the top and bottom of a three-point bending test sample.	135
3.35	Shear stress in a three-point bending test.	136
4.1	Geometry of the studied problem and parameters definition.	140

4.2	Deformations associated to the strain constant parameters.	149
4.3	Residual stresses in a 45° single ply laminate with $\Delta T = -160^\circ\text{C}$. (a) Circumferential, axial and shear stresses. (b) Interlaminar normal stress.	163
4.4	Residual stresses in a 45° single ply laminate with $\Delta T = -160^\circ\text{C}$ expressed in the material axes. (a) Stress in the fibre direction. (b) Stresses in the orthotropic matrix directions and shear stress.	163
4.5	Maximum radial stress for $\Delta T = -160^\circ\text{C}$ depending on the orientation of the single ply laminate.	164
4.6	Radial stresses due to the temperature increment in different stacking sequences.	165
4.7	Radial stresses due to the temperature increment in different geometries. (a) Increment of the number of plies. (b) Increment of the mean radius.	166
4.8	Validation of the model (continuous line) with finite elements results (asterisks) in the homogeneous case of 45°. (a) In-plane stresses. (b) Interlaminar stresses.	167
4.9	Maximum radial stress for $M_0 = -1 \text{ Nm/m}$ depending on the orientation of the single ply laminate.	168
4.10	Stresses in a 35° single ply laminate under $M_0 = -1 \text{ Nm/m}$ for (a) the free torsion model and (b) the constrained model.	169
4.11	Differences between 45° plies and -45° plies when both are used in a laminate, showed in a [45 -45 -45 45] stacking sequence. (a) Free torsion model, (b) Constrained model.	170
4.12	Validation of the models (continuous and discontinuous lines) by using $M_0 = -1 \text{ N}$ with finite elements results (asterisks) in the homogeneous case of 45°.	171
4.13	Validation of the models (continuous and discontinuous lines) by using $M_0 = -1.2 \text{ N}$ and comparing with FE results (asterisks) in the homogeneous case of 45°.	172
4.14	Section studied with the 3D model.	174
4.15	Distributed forces and moments distribution through the width: (a) bending moment $M_s(y)$, (b) axial force $N_s(y)$	210
4.16	Distributed forces and moments distribution through the width: (a) anticlastic bending moment $M_y(y)$, (b) torsional moment $M_{ys}(y)$	211
4.17	INS obtained in the interface between a 0° and a 90° ply in a laminate [0,90] _s under axial load.	212
4.18	INS obtained in the interface between a 0° and a 90° ply for different model orders.	213

4.19	ISS obtained in the interface between a 0° and a 90° ply in a laminate $[0,90]_S$ under axial load.	213
5.1	Propagation of intralaminar cracks as delaminations causing the induced unfolding.	217
5.2	Induced unfolding initiated by a fibre compressive failure.	218
5.3	Apparent ILTS of the coupons respect to the thickness.	220
5.4	Maximum stress in the matrix direction of the coupons respect to the thickness.	221
5.5	Location of the delaminations in a CP1 coupon.	222
5.6	Location of the delaminations in a CP2/CP3 coupon.	223
5.7	Location of the delaminations in a CP4 coupon.	223
5.8	Location of the delaminations in a CP5 coupon.	224
5.9	Location of the delaminations in a CP6 coupon.	225
6.1	Analytical bending moment in the traditional unfolding, M_{TU} , for $R = t$	229
6.2	Analytical bending moment in the induced unfolding, M_{IU} , for $R = t$	230
6.3	Analytical bending moment, M_{\max} , for $R = t$	230
6.4	Analytical bending moment in the traditional unfolding, M_{TU} , for $R = 2t$	231
6.5	Analytical bending moment in the induced unfolding, M_{IU} , for $R = 2t$	232
6.6	Analytical bending moment, M_{\max} , for $R = 2t$	232
6.7	Analytical bending moment in the traditional unfolding, M_{TU} , for $R = 3t$	233
6.8	Analytical bending moment in the induced unfolding, M_{IU} , for $R = 3t$	233
6.9	Analytical bending moment, M_{\max} , for $R = 3t$	234

List of Acronyms

2D	—	Bi-dimensional.
3D	—	Three-dimensional.
CBS	—	Curved Beam Strength.
CBT	—	Classical Beam Theory.
CFRP	—	Carbon fibre reinforced plastic.
CLT	—	Classical Laminate Theory.
FE	—	Finite Elements.
FEM	—	Finite Elements Method.
FSDT	—	First-order Shear Deformation Theory.
ILCS	—	Interlaminar compressive strength.
ILSS	—	Interlaminar shear strength.
ILTS	—	Interlaminar tensile strength.
INS	—	Interlaminar normal stress.
ISS	—	Interlaminar shear stresses.
LPBM	—	Legendre polynomials based model.
MBM	—	Monomials based model.
RD	—	Regularization distance.
UD	—	Unidirectional.

Chapter 1

Introduction

Nowadays, composite materials are used in many different sectors and applications, from the aeronautical and automotive sectors to the rail and marine sectors. In their origins, composite materials were used mainly in lightweight structures involving thin laminates where the curvature radius is much higher than the thickness and the interlaminar stresses are typically neglected due to their extremely low values. Notwithstanding, in the last years the use of this kind of materials has been considerably increased, requiring to incorporate the use of composite laminates in more complex components, where thicker laminates and highly-curved laminates are included. The introduction of the composite materials in this kind of components and structures has caused the apparition of new failure mechanisms which were not previously considered. The unfolding failure is found within those failure mechanisms.

The unfolding failure consists in a delamination given in highly-curved and moderately-curved oriented-fibre composite laminates which is produced preliminarily by the interlaminar stresses induced by the curvature. This kind of failure is generally associated with an opening bending moment. When a curved component is loaded under a bending moment which tries to open the curvature trying to give a flatter geometry to the curved laminate the plies try to separate like the pages of a book, see Figure 1.1. This effect is due to the different length between the plies located at the lowest and at the highest radius. Interlaminar normal stresses (INS) appear as the opposition of the plies to be separated, and, when they are high enough, the delamination involving the unfolding failure is produced. Some examples of composite laminates including the aforementioned highly-curved parts and, therefore, prone to the unfolding failure, are the L-shaped beams, the T-shaped beams, the Ω -shaped beams, the joggles or the corrugated laminates [1, 2].

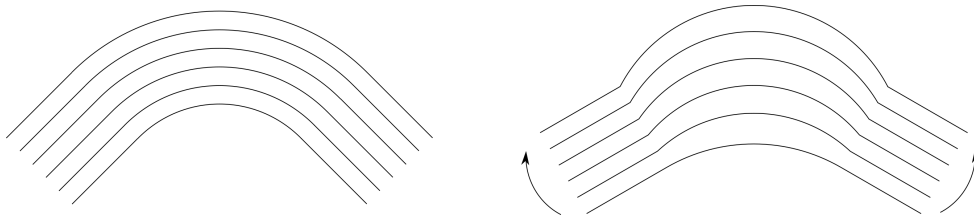


Figure 1.1: When the laminate is opened by a bending moment the plies try to separate.

The unfolding failure is a failure mechanism, mainly characteristic of the composite laminates. This fact is due to the low strength of these materials in the interlaminar direction (typically in the range of 40-80 MPa in CFRP with epoxy resins) respect to the intralaminar direction (which, for CFRP in the fibre direction, is typically in the range of 2000-3000 MPa). Thus, through-the-thickness failures are considerably more probable in this kind of materials than in isotropic materials in which strength is the same in all directions.

The unfolding failure prediction is typically carried out in three different steps. The first step consists in obtaining the loads and boundary conditions of the curved laminate. This step is conditioned by the model used in the second step, which consists in the stress calculation. The stress calculation may be done by a Finite Element (FE) model or by analytical procedures. Thus, if a bi-dimensional analytical model is considered for the stress calculation, the loads obtained in the first step must be compatible with this model. In many cases non-linearities must be considered for the loads calculation, e.g., in the four-point bending test [3]. Finally, once the stresses have been calculated, a failure criterion is applied.

The current PhD project is focused mainly in the second step. Different analytical stress calculation methodologies are developed in the context of the interlaminar stresses in curved laminates in order to reduce the computational times (in comparison with the FE models) and to improve the accuracy (in comparison with the nowadays analytical procedures which present high errors). The third step, relative to the failure criteria, is also studied with the detailed analysis of the failure mechanism involving the delamination of the unfolding failure, which is validated with some experimental results.

The state of the art for the second and third steps in the unfolding failure prediction is analysed individually in the following sections, after introducing the motivations and aims of the project. The first step is not

commented in those sections while its analysis depends on each kind of problem. Notwithstanding, in the present document the particular case of the four-point bending problem is analysed in further chapters due to its importance for the experimental estimation of the InterLaminar Tensile Strength (ILTS).

1.1 Motivations and aims of the project

The Thesis is oriented to analyse two main problems that have been found in the calculation of the unfolding failure reserve factor in typical components used in the aeronautical industry. The first problem is a thickness dependence of the ILTS, which is typically obtained with a four-point bending test over a curved composite laminate. This thickness dependence is widely observed in the unfolding calculations in the aeronautical companies and it is not demonstrated physically. The second problem is the lack of accuracy of the analytical models when applied to some kinds of loading states. These loading states are dominated by non-regularized effects which are not taken into account in the traditional analytical calculations, and nowadays are obtained typically by using a detailed FE model. However, an analytical or semi-analytical procedure is desired to improve the computational times allowing to reduce times in design problems.

When a quasi-isotropic composite laminate is tested according to the four-point bending test standardized in the procedure ASTM D 6415/D 6415M [3], a curved beam strength (CBS) is obtained as the bending moment per unit of width applied to the curved zone of the L-sectioned beam at the instant of the failure. Considering this bending moment and by using a certain analytical or numerical calculation method for calculating the stresses (e.g., Ko and Jackson's equations [4] or Kedward's formula [1]), a maximum INS may be obtained at the instant of failure. The four-point bending test has neglectable interlaminar shear stresses (ISS) in the curved zone, and then, the traditional delamination failure criteria (e.g., the Kim and Soni criterion [5]), which depends generally on the INS and the ISS, may be applied as a maximum stress failure criterion. Therefore, considering that the failure is due to the INS as has been traditionally done, the maximum INS at the instant of failure may be considered as an apparent ILTS.

The apparent ILTS, obtained as commented before from quasi-isotropic laminates, has typically shown a thickness dependence as shown in the example of Figure 1.2, where thinner specimens have lower strengths than thicker ones. This thickness dependence is shown by Edwards and Thompson [6]. In the Figure, the apparent ILTS has been expressed non-dimensionally re-

spect to the strength in direction 2 (matrix in-plane direction of a ply), S_{22} . The cause of this thickness dependence has not been physically explained yet although it is widely observed in the aeronautical sector. In this way, nowadays applications obtain the apparent ILTS from the four-point bending test depending on the thickness, and it is used when it is applied to other loading states and other kind of specimens (such as T-shaped beams or joggles). The application of this dependency to this other kind of specimens has not been demonstrated to be valid and it may cause errors in the estimation of the final failure. Hence, it requires a deeper study of the stresses and the failure mechanisms to determine the cause of the thickness dependence.

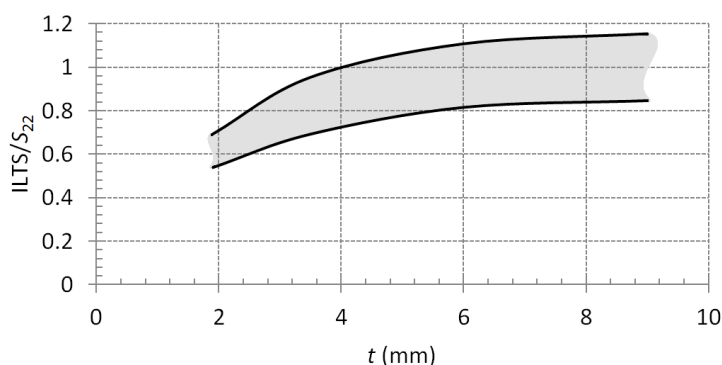


Figure 1.2: Example of thickness dependence of the apparent ILTS obtained from quasi-isotropic laminates.

The thickness dependence has not been shown in unidirectional laminates $[0]_n$, as can be seen in the unidirectional specimens of Hoffmann et al. [7]. Furthermore, it is neither observed in some fabric composites, as can be seen in the results of the maximum INS obtained by Avalon and Donaldson [8].

The thickness dependence is against the size effects explained by Wisnom [9]. In accordance with the size effects, thicker laminates should have lower ILTS. Hoffmann et al. [7] tried to demonstrate the size effects in the ILTS. Notwithstanding, the ILTS obtained in the composite laminates was not that expected, obtaining the lowest strength in the thinnest specimens and the highest strength in the medium thickness specimens, which is also against the apparent ILTS distribution of Figure 1.2, where a decrement of the ILTS is obtained also in the medium thickness specimens.

Edwards and Thompson [6] attributed the thickness dependence to the fact that, due to manufacturing defects, the curved specimens have small

interlaminar cracks or delaminations prior to the tests, and these delaminations propagate at a lower load than the corresponding to the ILTS value, causing the apparent ILTS to become lower than the real one.

Makeev et al. [10] studied the role of the porosity in the delamination, showing that, with a small increment in the porosity and in the void size, the strength may decrease significantly. In this way, other possible explanation for the decrease in the strength in thinner laminates may be given by considering the presence of a more significant void content in those specimens.

Fletcher et al. [11,12] and Kim et al. [13] assumed that the delamination is highly dominated by the free-edge effects, using a resin edge to reduce the free-edge effects and to improve the strength. Following their reasoning, other possible explanation consists in the free-edge effect, it requiring a deeper study on these stress concentrators respect to the thickness.

Regarding the second motivation of the Thesis, consisting in the lack of accuracy in the stress state obtained by the analytical methodologies for some loading states, it may be due to several causes. Traditional analytical methodologies calculate only the regularized stress state, which consists in considering the curved laminate isolated, and generally loaded only under end loads, although some authors consider also distributed loads. However, there are some effects which may cause perturbations in the stresses obtaining a non-regularized stress state. This is the case, e.g., of the free-edge effects, where the free-edge boundary condition causes a stress concentration in a localized zone near to the edge.

Other cause for the appearance of non-regularized stresses is the change of curvature of the laminate. Highly curved laminates are commonly linked with flat laminates. This is the case of the L-shaped beam, where the curved part of the L is joined to two straight arms, or the case of a joggle, where several curvature changes are given along the section.

Considering the particular case of a L-shaped beam loaded under an end bending moment, if a traditional stress calculation method is used, such as the Ko and Jackson's equations [4], the curved part of the section has a constant INS in the circumferential direction, while null INS are given in the straight arms. Therefore, a discontinuity is given at the joint of the curved part with the arms, see Figure 1.3(a), where the solution obtained with Ko and Jackson's equations is depicted. This discontinuity is given in all the components of stresses and displacements, and not only in the INS. Hence, the stress tensor is modified by non-regularized effects causing a smooth variation of the stresses between the straight arm and the curved part in order to accomplish the equilibrium equations and the compatibility of the displacements, see Figure 1.3(b). This effect has been shown by Most et al. [14] and it is studied in the current Thesis.

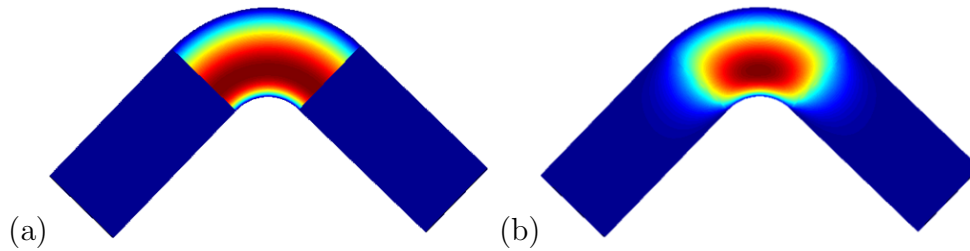


Figure 1.3: INS colour plot in a L-shaped beam loaded under end bending moment. (a) Regularized stresses. (b) Non-regularized stresses.

The non-regularized effects due to the change of curvature are localized near to the section where it takes place, modifying the stresses respect to the regularized ones only in this zone. Therefore, they are especially important in laminates with a short curved part respect to the thickness, or when the maximum regularized value is obtained near to the change of curvature.

The aims of the Thesis are oriented to improve the calculation and prediction of the unfolding failure in curved composite laminates. The first aim of the project is oriented to develop a novel analytical procedure for obtaining the stresses in curved laminates, in order to predict the non-regularized effects without requiring a FE model. The use of an analytical procedure allows the stresses to be obtained with a satisfactory accuracy in smaller computational times than FE, which is especially useful for optimization problems where many evaluations of the stresses have to be done. Second, an explanation for the thickness dependence is looked for, trying to find the real failure mechanism involving the unfolding failure, in order to develop a new, more realistic, failure criterion. Moreover, the first objective helps to the resolution of the second one, as a satisfactory accuracy in the stress calculation is required for understanding the failure mechanism of the component.

1.2 State of the art in stresses calculation in curved laminates

The calculation of composite laminates is based on the Classical Laminate Theory (CLT) [15, chap. 4] and on the First-order Shear Deformation Theory (FSDT) [16], which consist in a plate theory where the composite laminate is approximated by homogeneous equivalent material through the stiffness matrix A-B-D, and where the INS is neglected. Therefore, this

theory cannot be applied directly to the highly-curved laminates for obtaining the interlaminar stress. Notwithstanding, the CLT may be applied to curved laminates for obtaining the intralaminar stresses with a good accuracy (see [17], for instance), or for obtaining the deformation of curved laminates under different kind of loads (see [18], for instance).

Lekhnitskii et al. [19, chap. 3] obtained the closed-form solution of the through-the-thickness stresses in curved bi-dimensional beams made by homogeneous anisotropic material under end load and bending moment. Hence, it cannot be applied to composite laminates while composite laminates are heterogeneous at a laminate level (non-homogeneities associated with the presence of fibre and matrix inside each ply are not considered in the present document). Notwithstanding, many authors have approximated the laminate by homogeneous equivalent material and have applied the Lekhnitskii's equations [20–23] to determine the INS.

The maximum INS for a curved beam under bending moment obtained by using the Lekhnitskii's equations has been approximated by a closed form equation given by Kedward et al. [1]. This equation is independent of the stiffness properties of the material, depending only on the bending moment and on the geometrical parameters, and being only accurate when the circumferential stiffness is lesser than 20 times the radial stiffness. The INS caused by an axial force may be neglected while the dominant load for those stresses is the bending moment. With reference to the shear problem, the maximum of the ISS may be approximated by the maximum ISS in a flat laminate, given by Cui et al. [24].

The extension of the Lekhnitskii's equations to a laminate problem was solved by Ko and Jackson [4], allowing the effect of the stacking sequence over the INS distribution to be obtained. Ko and Jackson's equations constitute a linear system of equations where the number of equations depends on the number of plies N_p , so that it requires to solve $3N_p$ equations for the bending moment and $8N_p$ equations for the end load (which may be decomposed in end axial force and end shear force). Smidt [25] and Sheno and Wang [26] developed a similar model to the Ko and Jackson's equations, applied to curved sandwich beams under bending load.

Some authors have been working in the last years in the development of simpler models to solve the INS in curved laminates considering the stacking sequence. One of the main objectives of those models is to obtain approximations of the Ko and Jackson's equations which may be implemented in a FE software to calculate the INS in curved laminates. Other objectives for obtaining approximated models are to calculate problems which cannot be solved with Ko and Jackson's equations, such as double-curvature problems, three-dimensional cases or distributed loads (e.g., pressure), or to

reduce computational times, e.g., for solving optimization problems.

The CLT may be extended for calculating the INS from the in-plane stresses by using the equilibrium equations. Notwithstanding, the CLT applied to curved laminates requires a modification of the A-B-D matrix so that considering the different lengths of the plies in the inner and outer radius. This modification implies logarithmic expressions in the terms of the stiffness matrix which has been presented by several authors as Qatu [27], Kress et al. [28] or Guedes and Sá [29].

Other approximated models begin with the Kirchoff assumption used in the CLT and consider different hypothesis. That is the case of Kress [30] and Kress et al. [28], who used the aforementioned assumption only in the circumferential displacements, calculating the expression of the through-the-thickness displacements.

Some authors have considered the hypothesis of thin laminates $t \ll R$ (where t is the thickness and R is the mean radius) in the development of an approximated model for curved beams, as Rodríguez de la Cruz et al. [31] for sandwich curved beams, Lin and Hsieh [17] for variable curvature beams, Vargas et al. [32] for studying the thermal and mechanical stresses in unsymmetrical curved laminates or Bruno et al. [33] for studying the delamination propagation in curved laminates. Those models have a high accuracy when the $t \ll R$ hypothesis is accomplished.

The series expansion in the displacements and/or the stresses is one of the most used approximations for calculating the stresses in thicker curved laminates where $t \sim R$. Carrera et al. [34] presented a compilation of several methods based on series expansions in the displacements, not only for curved laminates. Those models usually start from the Timoshenko theory [35, 36] expanding the displacements with additional terms.

The most basic series expansion is done by using monomial functions in the thickness, as is the case of Matsunaga [37, 38]. Other authors have preferred a Fourier series as Ren [39], who expanded the INS by using a Fourier series of sines, or the use of zig-zag functions as Carrera [40] and Icardi and Ferrero [41]. More advanced models including series expansions are based in more complex numerical techniques as the differential quadrature method [42, 43] or the higher-order shear deformation theory [44, 45].

Those analytical procedures have been compared with experimental results in several loading states and geometries. For example, Cui and Ruiz [46] and Wisnom et al. [47] tested C-specimens under combined shear, axial and bending loads, Cui et al. [24] tested curved beams under pure bending, and McRobbie et al. [48] tested open-rings of composite laminates and sandwiches under bending due to end loads.

Many of the mentioned analytical approximations are oriented to develop

elements for a FE software. Finite elements allows the INS in curved laminates to be accurately obtained, but they require to refine the mesh in the interlaminar direction in a three-dimensional model [49]. The refinement of the mesh in the interlaminar direction requires also refining the mesh in the intralaminar plane in order to maintain the aspect ratio, so the final model has an excessive number of elements consuming too much computational time to obtain the solution.

In that way, many authors have worked in the development of new elements for curved composites which do not require so much interlaminar refinement to obtain accurate INS. Rattanawangcharoen [50] developed a three-dimensional element with the main aim of analysing weakly bonded cylindrical panels. Kress and Winkler [51] developed a shell element for corrugated laminates. Cinefra and Carrera [52] and Vidal et al. [53] developed cylindrical shell elements using a layerwise theory. Finally, Fraternali and Bilotti [54] developed non-linear elements for curved laminates.

The calculation of the INS may be also influenced by the residual stresses due to the manufacturing process and the cooling of the laminate after the curing process. The different mechanisms producing residual stresses are summarized by Wisnom et al. [55]. The residual stresses have been typically associated to the in-plane stresses and interlaminar residual stresses have been typically neglected, except in the free-edges. However, when the laminate is curved, residual INS appear due, as the residual in-plane stresses, to the different expansion coefficients between the plies. Those residual INS in curved laminates were shown experimentally and numerically by Kim and Lee [56] and by Takagaki et al. [57] in the case of cylindrical laminates, and analytically by Huang and Tauchert [58] in doubly-curved laminates.

Notwithstanding, the aforementioned analytical and numerical procedures do not consider other effects which may influence in a high percentage the stress distributions. Those procedures consider typically the curved laminate isolated, calculating only the regularized stresses. However, some factors may cause a non-regularized distribution near to a particular focus. One of those focuses is the change of curvature, as shown by Most et al. [14]. The compatibility and equilibrium in a joint between two laminates with different curvature cause a perturbation over their stress distributions, which is especially important in the case of INS. Therefore, the change of curvature is an important factor to be considered in the unfolding calculation.

The change of curvature is related also with the laminates of variable curvature or with the doubly-curved laminates. The double curvature in thick laminates has been widely studied in the literature, where the works of Qatu [59], Asadi et al. [60,61] and Tornabene et al. [62] may be mentioned.

The most well-known non-regularized focus is the free-edge of the lami-

nate. The free-edge effect is the result of the null stresses boundary condition in the free-edge of the laminates, which, due to the different stiffnesses between the different plies causes a stress concentration with theoretically infinite stresses near to the edge, in order to accomplish the equilibrium and displacements compatibility.

The free-edge effects have been highly studied in the literature. The typical cases considered in the study of the free-edge effects are the cross-ply laminate $[0,90]_S$ and the angle-ply laminate $[\pm 45]_S$. First mentions of the existence of the free-edge was commented by Pipes and Pagano [63]. A closed form approximation for the calculation of these free-edge effects in the cross-ply laminate was developed by Pipes and Pagano [64], Pagano [65] and Becker [66]. A closed form approximation for the cross-ply and also for the angle-ply laminates was developed by Kassapoglou and Lagace [67]. A wider study of the free-edge in composite laminates may be found in Mittelstedt and Becker [68]. Finally, another model for the free-edge calculation, based on a series expansion of the displacements by using Legendre polynomials but oriented to a finite element modelling, has been developed by Wenzel et al. [69].

The delamination of composite materials has been traditionally associated with the free-edge effects (see Kant and Swaminathan [70] for instance). It is considered that when the free-edge effect is dominant enough the crack initiated at the free-edge may propagate interlaminarily in an unstable way causing the final delamination in the laminate. This effect applied to the unfolding failure in curved laminates is analysed by Fletcher et al. [11, 12] and Kim et al. [13], who have studied the influence of introducing a resin edge in the free boundary to reduce the free-edge effects.

1.3 State of the art in failure criteria

Once the stresses have been obtained by using one of the different analytical or numerical models presented in the previous section, a failure criteria must be applied to predict when the failure is initiated and, when applicable, to predict if the crack will propagate.

Therefore, two kind of failure criteria may be differentiated: the failure initiation criteria and the failure propagation criteria. Those different failure criteria are summarized by Orifici et al. [71]. The free-edge effects are usually treated using failure propagation criteria since they have associated singular stresses similar to those associated with a crack in the linear elastic fracture mechanics theory.

1.3.1 Failure initiation criteria

The failure initiation criteria may be expressed depending on stresses or depending on strains. However, the stresses-based failure criteria have imposed over the strain-based failure criteria. In this way, the most basic failure criterion consists in the maximum stress criterion, where each stress is considered independently and compared to its corresponding allowable. In this way, a maximum stress delamination criterion considers that the delamination is produced when the INS reach its allowable value or when any of the two ISS reaches its corresponding interlaminar shear strength.

Hashin [72] developed a quadratic criterion, given by an ellipsoid in terms of the INS and the two ISS. This failure criterion is valid only for the tensile zone of the INS, the strength being required to be changed in the criterion for the compression zone. Brewer and Lagace [73] developed a similar criterion, which distinguishes the tensile and compressive zones of the INS by two independent ellipsoids. This criterion was reformulated by Most et al. [14].

Other quadratic criterion is given by Kim and Soni [5], who used a translated ellipsoid for the INS and the ISS, considering the different tensile and compressive strengths. The Kim and Soni criterion in the interlaminar tensile zone is highly dependent on the interlaminar compressive strength (ILCS), which is difficult to obtain experimentally. The Brewer and Lagace criterion does not have this dependency while it considers two independent ellipsoids in the tensile and compressive sides. For comparison reasons, the Kim and Soni criterion and the Brewer and Lagace criterion are depicted in Figure 1.4 for a bi-dimensional case (considering only one ISS, the ellipsoids being then depicted as ellipses). The shear stress has an allowable given by S_τ , the ILTS is defined as S_{33}^t and the ILCS is defined as S_{33}^c .

Other authors have considered in their criteria that the in-plane stresses may affect to the delamination failure. On the one hand, some of those criteria are based on the consideration of the fibre direction stress in the delamination. Several criteria considering the fibre direction stress are exposed by Tong [74]. These criteria are applied, in particular, for adhesively bonded composite double lap joints. The application of these criteria in scenarios different to those in which they were developed, may imply a wrong prediction, as when applying to the present studied problem of curved laminates. On the other hand, other authors have considered the stresses in the resin in all the directions for predicting the delamination. This is the case of Wisnom et al. [75], who considered a matrix effective stress for estimating the through-the-thickness failure. This effective stress is calculated from the matrix principal stresses, which are obtained by considering that the matrix stress in the fibre direction is obtained by factoring down the composite

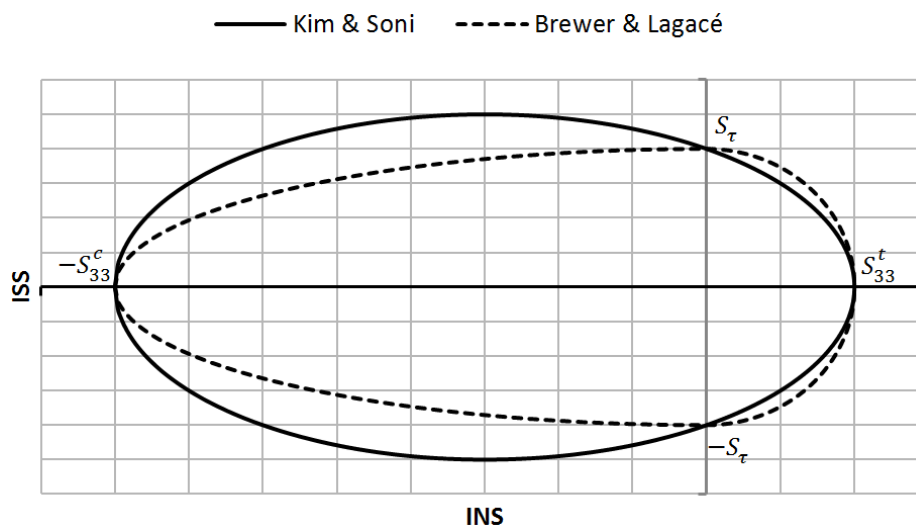


Figure 1.4: Comparison between the Kim and Soni criterion and the Brewer and Lagacé criterion.

stress by the ratio of matrix modulus to the fibre direction modulus, and that the rest of stresses remains the same than in the ply. This criterion has been used by several authors, such as H el enon et al. [76], who applied the criterion to a T-shaped beam to estimate the delamination load.

For the application of the different initiation failure criteria the different strengths are required. The interlaminar shear strength (ILSS) is typically obtained by using a three point bending test, which is standardized by the testing procedure ASTM D 2344/D 2344M [77]. The ILTS may be obtained by different procedures, which are summarized by Makeev et al. [10].

The typical experimental procedure to obtain the ILTS consists in a four-point bending test applied to a curved beam, which is standardized by the testing procedure ASTM D 6415/D 6415M [3]. The testing procedure establishes a L-shaped specimen with all the plies oriented at 0° (defining the 0° direction as the curved direction and the 90° direction as the through-the-width direction) for obtaining the ILTS. In the case of different stacking sequences than the $[0]_n$ laminate the CBS is obtained as the maximum bending moment that the curved laminate can bear.

The ILTS may be obtained also by a three-point bending test [78] using a thick enough laminate so that the specimen is bent in the interlaminar direction. The use of the three-point bending test to obtain the ILTS is explained by Makeev et al. [10, 79], and it requires to modify the geometry respect to the geometry specified by the procedure ASTM D 2344/D 2344M

[77] in order to obtain the desired failure mechanism. However, to the author knowledge, this method has not been used for characterizing the interlaminar properties of the material.

Finally, the ILTS may be also obtained by using a tensile test in the interlaminar direction. The tensile test in the interlaminar direction is standardized by the testing procedure ASTM D 7291/D 7291M [80], and it is carried out by adhesively bonding the composite specimen to the metal tabs and applying a tensile force in the bonded faces, perpendicular to the through-the-thickness direction. It requires analysing carefully that the failure is produced in the through-the-thickness direction of the laminate and not in the adhesive joint with the tabs. A similar kind of specimen for determining the ILTS through a tensile test but without adhesive bondings was developed by Hoffmann et al. [81, 82].

However, the results of the ILTS obtained with the tensile test are very different to the results of the ILTS obtained with the curved beam in the four-point bending test. This is due to the size effect. The tensile test has a volume of material under high stresses higher than the curved beam has, and then the ILTS obtained by using a tensile test is lower than the ILTS obtained in the four-point bending test of a curved beam.

The size effect affects to the strength of the materials depending on the volume of material under high stresses (see [9, 83, 84] for instance). The size effect is usually modelled by the Weibull distribution [85]. The Weibull distribution is usually used for representing the strength of brittle materials, where the failure is dominated by the presence of defects which are statistically distributed. The size effects in the through-the-thickness strength properties were analysed by Hoffmann et al. [7]. However, he obtained a big difference in the case of the tensile INS at failure load, not obtaining a satisfactory correlation with the size effects predictions.

1.3.2 Failure propagation criteria

The crack propagation problem requires a different kind of study based in fracture mechanics, with the concept of the strain energy release rate. The crack propagation has been analysed also in the last years by using FEM with cohesive elements.

Although the crack propagation is not studied in the present document, as a reference, Lu et al. [86] studied the crack propagation in curved beams under pure bending moment, Wimmer and Pettermann [87] studied the crack propagation and the stability of the propagation in composite laminates applying it to the particular case of a L-shaped laminate, Wimmer et al. [88, 89] studied the initiation and propagation of the cracks in L-shaped

laminates, Gözlüklü and Coker [90] studied the dynamic delamination of L-shaped laminates using cohesive elements and Gözlüklü et al. [91] used also the cohesive elements in L-shaped beams and compared it with experimental results obtained with a high-speed camera. Additionally, Gözlüklü et al. [91] showed that the delamination process in L-shaped laminates is very quick. The L-shaped laminate is completely delaminated in only $20\mu\text{s}$.

The free-edge effect may be analysed by using also the strain energy release rate and cohesive elements, but some authors have developed stress based criteria for the failure propagation from a free-edge effect. This is the case of Kim and Soni criterion [92], which considers that the failure appears when the integral of the INS from a distance of the free-edge defined as the ply thickness, until a distance defined as the laminate thickness divided by the ply thickness, reaches the ILTS.

1.4 Thesis overview

The thesis is ordered following the three main steps in the unfolding calculation. The first step, consisting in the load calculation, is studied in Chapter 2. In particular, the four-point bending test standardized by the procedure ASTM D 6415/D 6415M [3], analysing the calculation of the bending moment in the angular part of the sample from the load applied in the test, is studied.

The bending moment is the input parameter used later in the stress calculation methods, the accuracy in the calculation of this parameter being then extremely important. Furthermore, the test is highly non-linear due to the change in the contact-point of the rollers with the coupons. Therefore, a new non-linear methodology to analyse the test and to obtain the force-displacement and the force-bending moment relations is developed. The force-displacement relation may be used also to correlate the accuracy of the model with experimental results. This model has been presented by the author in [93]. With this study, a deeper knowledge about the four-point bending test is obtained.

The second step in the unfolding calculation consists in the calculation of the stresses. The stresses calculation is divided in two different Chapters. Chapter 3 is based in bi-dimensional models. It includes, first, a summary of the theoretical bases of the traditional methods (Lekhnitskii's equations and Ko and Jackson's equations). After that, an approximated model for calculating the regularized stresses in an isolated curved laminate is developed. This regularized model has been published in [94], and it is developed in the present document with a matrix notation which lets us to expand it

later to obtain the non-regularized model.

The last part of Chapter 3 is dedicated to develop the bi-dimensional non-regularized models. Two different non-regularized models are developed based on a series expansion of the displacements by using different functions. The first model uses monomial functions in the development [95], similarly to the model developed by Matsunaga [38] but using a different definition of the transverse displacements, whereas the second model uses Legendre polynomials [96].

Chapter 4 develops different three-dimensional models for the stress calculation including the residual stresses due to the manufacturing process. The first model, consisting in a regularized three-dimensional model, is an extension of the model developed by Spencer et al. [97] for the calculation of the thermal residual stresses in curved laminates, including also the stresses due to the bending moment and other loading states. The model has been explained by the author in [98], and results of the model have been presented in [99]. The second model is an extension of the bi-dimensional non-regularized model developed in Chapter 3 to the three-dimensional problem. This non-regularized model enables including effects such as the free-edge effects or the anticlastic effect.

Both Chapters 3 and 4 are mainly oriented to get an efficient and reliable model to evaluate the INS in highly-curved laminates considering the non-regularized effects due to the change of curvature and three-dimensional effects. These non-regularized effect may be obtained also with FEM. However, FEM requires complex models for obtaining a satisfactory accuracy, requiring high computational times and, therefore, it is not practical for a design of components point of view. However, detailed FEM models have been used in this Thesis for the validation of the developed solutions.

The last step in the unfolding calculation consists in the application of a failure criterion. In this way, the failure mechanisms involving the unfolding failure are studied in Chapter 5. A new failure mechanism is explored, called induced unfolding, where the delamination is not initiated by the INS. The induced unfolding is produced by an intralaminar failure that, when propagating, produce the delamination of the laminate.

Therefore, two kind of unfolding failures are defined: the traditional unfolding, initiated by an interlaminar failure, and the induced unfolding, initiated by an intralaminar failure. The induced unfolding applied to the experimental results permits explaining the thickness dependence of the ILTS in composite laminates. Furthermore, it is consistent with the results obtained over fabric CFRP and UD laminates. The idea of the induced unfolding has been presented by the author in [100]. Chapter 5 shows some experimental evidences of the existence of the aforementioned induced un-

folding.

Finally, Chapter 6 summarizes the main results obtained in the previous Chapters in order to develop some design recommendations for curved composite laminates prone to unfolding failure.

The PhD project has been developed in the facilities of FIDAMC, the Spanish Foundation for Research, Development and Application of Composite Materials, with the academic supervision of the University of Seville.

Chapter 2

Analysis of the four-point bending test

The traditional unfolding failure is associated with the interlaminar normal stresses (INS). The unfolding failure is generally caused by a bending moment which tries to open the curvature, causing that the different plies try to separate and inducing interlaminar tensile stresses.

Hence, the traditional unfolding failure is mainly characterized by the interlaminar tensile strength (ILTS). There are several procedures to assess the ILTS property, which are summarized by Makeev et al. [10]. The simplest method to obtain this strength consists in a tensile test in the interlaminar direction, which is standardized by the test procedure ASTM D7291 [80]. Several authors, such as Hoffmann et al. [81], have characterized the ILTS using this procedure. Makeev et al. [10] showed that the ILTS obtained using this procedure is highly dominated by the size effects, it being different from the one obtained using different procedures and not being very representative for a curved specimen.

The curved beam ILTS is obtained by using a four-point bending test, which is standardized by the test procedure ASTM D6415 [3]. This test procedure is complexer than the tensile test [80] but it is more widely used since it is less affected by the size effects. Notwithstanding, the curved beam is prone to manufacturing defects in form of porosity. Several authors such as Makeev et al. [10] and Jackson and Martin [101] have commented the effect of the porosity over the ILTS. Furthermore, this testing procedure has shown a thickness dependence of the ILTS, which have not been physically explained yet (see Edwards and Thompson [6]). The topic of the thickness dependence is dealt with in Chapter 5.

The present Chapter studies the four-point bending test since it is the most common testing procedure for obtaining the ILTS, which is a key

parameter in the analysis of unfolding failure. After analysing the testing procedure, a non-linear model for obtaining the bending moment in the curved part of the sample from the applied load is developed and finally it is compared with the methodology proposed by the ASTM procedure and compared with some experimental results.

2.1 Standardized testing procedure for assessment of ILTS

The most widely used testing procedure for assessment of ILTS of composite materials is the four-point bending test, whose testing configuration is schematically depicted in Figure 2.1. The geometry of the specimen is determined by the mean radius of the curved part R , the thickness t and the angle in the undeformed configuration φ_i . The opening angle of the L-shaped section is obtained as $\Theta_i = 180^\circ - 2\varphi_i$, so for a typical shape with $\Theta_i = 90^\circ$ the angle φ_i has a value of 45° .

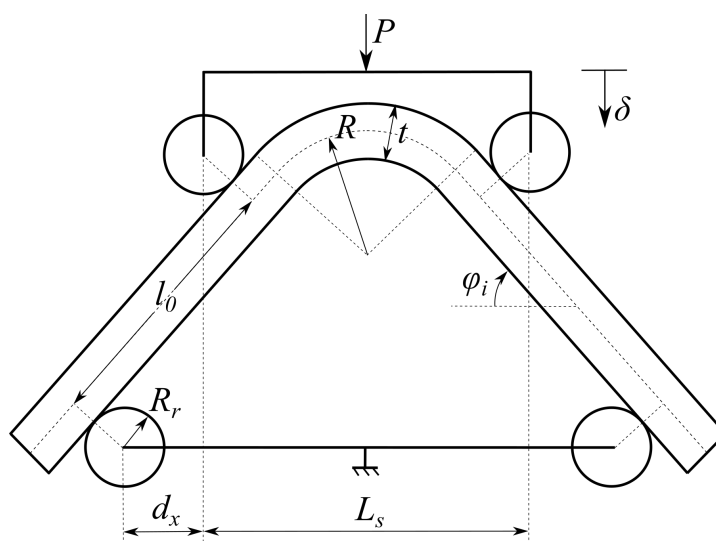


Figure 2.1: Four-point bending test set-up.

The testing set-up is defined by the radius of the rollers R_r , the distance between the upper rollers L_s and the horizontal distance between one upper roller and the nearest downer roller d_x . The distance l_0 (indicated in Figure 2.1) is calculated from the previous values as follows:

$$l_0 = \frac{d_x + (2R_r + t) \sin \varphi_i}{\cos \varphi_i}. \quad (2.1)$$

The total applied load per unit of width is denominated as P and the relative displacements of the rollers is denominated as δ .

This testing procedure includes the complexity of being highly non-linear due to the change of the position of the points where the rollers contact the sample when the load is increased, so a large displacements model is required. This non-linearity affects to the calculation of the bending moment in the curved part of the sample, which is required for calculating the INS and therefore for obtaining the ILTS from the failure load.

The testing procedure ASTM D 6415/D 6415M [3] estimates this non-linearity by using the hypothesis of considering that the arms of the L-shaped specimens remain straight during the loading process and turn to an angle φ (which for a null load has a value of φ_i) which is obtained from the experimental displacement δ . Therefore, the bending moment obtained from the testing procedure at the failure load does not depend only on this failure load, it depending also on the displacement measured at failure. In this way, the procedure does not need the stiffness property of the material as an input while both load and displacements are obtained experimentally.

Considering the undeformed shape, the bending moment (per unit of width) is obtained from the applied load (per unit of width) as follows:

$$M_0^{us} = -\frac{P}{2 \cos \varphi_i} l_0 = -\frac{P}{2 \cos \varphi_i} \frac{d_x + (2R_r + t) \sin \varphi_i}{\cos \varphi_i}. \quad (2.2)$$

Considering that the straight arm remains straight and turn to a new angle φ , the corrected bending moment yield:

$$M_0 = -\frac{P}{2 \cos \varphi} \frac{d_x + (2R_r + t) \sin \varphi}{\cos \varphi}, \quad (2.3)$$

where the new angle φ is obtained from the displacement δ as follows:

$$d_y = d_x \tan \varphi_i + \frac{2R_r + t}{\cos \varphi_i} - \delta, \quad (2.4a)$$

$$\varphi = \arcsin \left(\frac{-d_x(2R_r + t) + d_y \sqrt{d_x^2 + d_y^2 - 4R_r^2 - 4R_r t - t^2}}{d_x^2 + d_y^2} \right). \quad (2.4b)$$

Once the bending moment is obtained the stresses are calculated typically by using the Lekhtniskii's equations [19, chap. 3] or the Ko and Jackson

equations [4]. The calculation of the stresses from the loads are analysed in further chapters.

The testing procedure ASTM D 6415/D 6415M [3] recommends the use of the Kedward's formula [1], an approximation of the Lekhnitskii's INS maximum value:

$$\sigma_{r,max} = -\frac{3M_0}{t\sqrt{4R^2 - t^2}}. \quad (2.5)$$

The approach of considering that the straight arms remain straight may be very conservative when the non-linearity is very pronounced, like in the thinner specimens. Therefore, for improving the calculation of the bending moment, a novel non-linear model is developed in the following sections.

2.2 Non-linear model for obtaining the bending moment

In order to improve the calculation of the bending moment in a four-point bending test a novel model considering the non-linearities due to the large displacements is developed. The non-linearities are considered by calculating the contact point of the rollers with the specimen in the deformed configuration.

The specimen is modelled by using a Timoshenko beam model [35, 36] and considering the symmetry of the problem according to Figure 2.2.

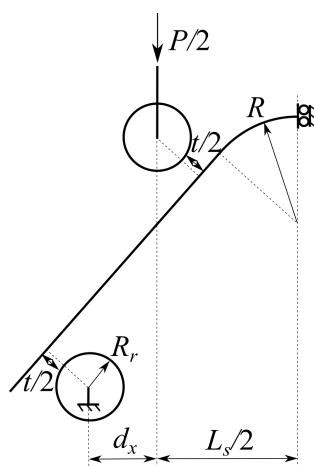


Figure 2.2: Beam approximation of the specimen in a four-point bending test.

The whole beam is divided in 3 different beams. Beam 1 is defined as the part of the beam located between the two rollers, beam 2 is defined as the part of the beam located between the inner roller and the beginning of the curved part, and beam 3 is defined as the curved part. Furthermore, point 0 is defined as the point of contact with the outer roller, point 1 is defined as the point of contact with the inner roller, point 2 is defined as the point of joint between beam 2 and 3, and point 3 is defined as the symmetry point of the whole beam.

Beginning with the analysis of beam 1, the deformed configuration is depicted in Figure 2.3.

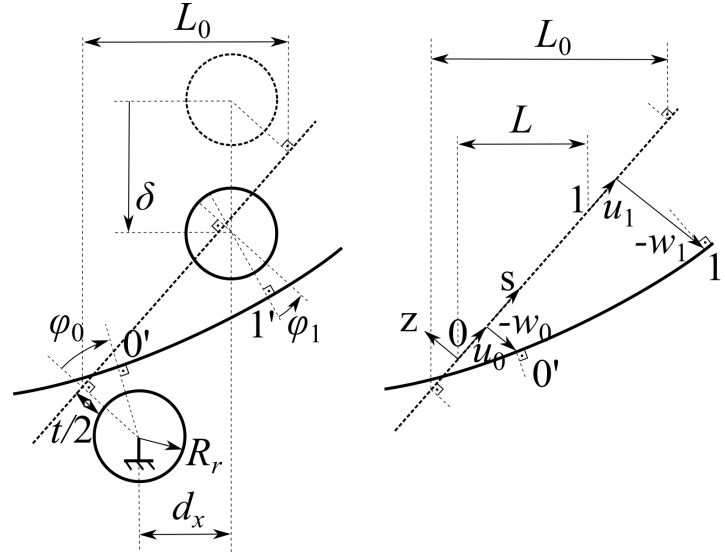


Figure 2.3: Deformed configuration of beam 1.

Let us assume that when the upper roller is displaced a distance δ in the vertical direction, the deformed shape has an angular change in the slope of the mean line at point 0 defined by φ_0 and an angular change in the slope at point 1 defined by φ_1 . The initial horizontal distance between the contact points translated to the mean line of the beam is called L_0 . This horizontal distance in the deformed shape, translated to the undeformed one according to Figure 2.3, is called L . The translation from the undeformed shape to the deformed shape is done by using the displacements at point 0, u_0 and w_0 , and the displacements at point 1, u_1 and w_1 .

In accordance with Timoshenko beam theory and defining the coordinate system (s, z) shown in Figure 2.3, the displacements are approximated considering that plane sections remain plane:

$$u(s, z) = u^0(s) + z\phi(s), \quad w(s, z) = w^0(s). \quad (2.6)$$

In this way, considering the displacements given in equation (2.6) and considering large displacements the angles φ_0 and φ_1 are calculated as:

$$\varphi_0 = \arctan \phi_0, \quad \varphi_1 = \arctan \phi_1, \quad (2.7)$$

where $\phi_0 = \phi(0)$ and $\phi_1 = \phi(L)$, with $\phi(s)$ being the slope change of the section. Considering a large displacements model, $\phi(s)$ is the tangent corresponding to $\varphi(s)$.

By using the definition of the displacements (2.6), the strains can be written as:

$$\varepsilon_s = \frac{du^0(s)}{ds} + z\frac{d\phi(s)}{ds}, \quad \varepsilon_z = 0, \quad (2.8a)$$

$$\gamma_{sz} = \phi(s) + \frac{dw^0(s)}{ds}. \quad (2.8b)$$

In accordance with Figure 2.3, distance L may be calculated as:

$$L = d_x + \hat{R}_r(\sin(\varphi_i - \varphi_o) + \sin(\varphi_i - \varphi_1)) + (w_1 - w_o) \sin \varphi_i + (u_o - u_1) \cos \varphi_i, \quad (2.9)$$

where the parameter \hat{R}_r is defined as:

$$\hat{R}_r = R_r + \frac{t}{2}. \quad (2.10)$$

Substituting (2.7) into (2.9):

$$L = d_x + \hat{R}_r \left(\frac{\sin \varphi_i - \phi_o \cos \varphi_i}{\sqrt{1 + \phi_o^2}} + \frac{\sin \varphi_i - \phi_1 \cos \varphi_i}{\sqrt{1 + \phi_1^2}} \right) + (w_1 - w_o) \sin \varphi_i + (u_o - u_1) \cos \varphi_i, \quad (2.11)$$

The vertical force applied by the rollers is $P/2$, and then considering that the applied load in the outer roller has an angle $\varphi_i - \varphi_o$ and applying the load translated to the undeformed configuration, it holds that:

$$N(s) = -\frac{P \sin \varphi_o}{2 \cos(\varphi_i - \varphi_o)}, \quad Q(s) = -\frac{P \cos \varphi_o}{2 \cos(\varphi_i - \varphi_o)}, \quad (2.12a)$$

$$M(s) = -\frac{P \cos \varphi_o}{2 \cos(\varphi_i - \varphi_o)} s, \quad (2.12b)$$

where $N(s)$ is the axial force, $Q(s)$ is the shear force and $M(s)$ is the bending moment.

Substituting (2.7) into (2.12):

$$N(s) = -\frac{P\phi_o}{2(\cos \varphi_i + \phi_o \sin \varphi_i)}, \quad Q(s) = -\frac{P}{2(\cos \varphi_i + \phi_o \sin \varphi_i)}, \quad (2.13a)$$

$$M(s) = -\frac{P}{2(\cos \varphi_i + \phi_o \sin \varphi_i)}s. \quad (2.13b)$$

The constitutive equations of the material in a 2D approach yield for a ply p (with $p = 1, 2, \dots, N_p$):

$$\sigma_s = C_{11}^p \varepsilon_s + C_{13}^p \varepsilon_z, \quad \sigma_z = C_{13}^p \varepsilon_s + C_{33}^p \varepsilon_z, \quad (2.14a)$$

$$\tau_{sz} = C_{55}^p \gamma_{sz}, \quad (2.14b)$$

where C_{ij}^p , for $i, j = 1, 3$ and $i = j = 5$, are the stiffnesses of a ply p in the local coordinate system (s, z) considering a bi-dimensional assumption.

Introducing the definition of the strains (2.8) and integrating the constitutive equations (2.14), the classical stiffness matrix A-B-D and the stiffness C are obtained (see Jones [15], Chapter 4) applied to a bi-dimensional problem:

$$\begin{bmatrix} N(s) \\ M(s) \end{bmatrix} = \begin{bmatrix} A & B \\ B & D \end{bmatrix} \begin{bmatrix} du^0(s)/ds \\ d\phi(s)/ds \end{bmatrix}, \quad (2.15a)$$

$$Q(s) = C \left(\phi(s) + \frac{dw(s)}{ds} \right), \quad (2.15b)$$

where the components A , B and D are given by:

$$A = \sum_{p=1}^{N_p} C_{11}^p (z_p - z_{p-1}), \quad (2.16a)$$

$$B = \sum_{p=1}^{N_p} C_{11}^p \frac{1}{2} (z_p^2 - z_{p-1}^2), \quad (2.16b)$$

$$D = \sum_{p=1}^{N_p} C_{11}^p \frac{1}{3} (z_p^3 - z_{p-1}^3), \quad (2.16c)$$

and the stiffness C is modified by considering a parabolic distribution of the shear stress:

$$C = \sum_{p=1}^{N_p} C_{55}^p \frac{3}{2} \left(z_p - z_{p-1} - \frac{4}{3t^2} (z_p^3 - z_{p-1}^3) \right). \quad (2.17)$$

For the sake of simplicity only symmetrical laminates are considered, and, as a consequence, $B = 0$.

Hence, the displacement component $\phi(s)$ is obtained integrating equation (2.15a), considering (2.13b), as follows:

$$\frac{d\phi(s)}{ds} = \frac{M(s)}{D} \longrightarrow \phi(s) = \frac{P}{4D(\cos \varphi_i + \phi_o \sin \varphi_i)} \left(\frac{L^2}{\cos^2 \varphi_i} - s^2 \right) + \phi_1, \quad (2.18)$$

where ϕ_1 is the value of $\phi(s)$ at point 1 ($\phi_1 = \phi(L/\cos \varphi_i)$).

Considering that $\phi(0) = \phi_0$ the next equation for the force P is obtained:

$$P = \frac{4D(\phi_o - \phi_1) \cos^2 \varphi_i (\cos \varphi_i + \phi_o \sin \varphi_i)}{L^2}. \quad (2.19)$$

The displacement component $u(s)$ is obtained integrating equation (2.15a), considering (2.13a), as follows:

$$\frac{du(s)}{ds} = \frac{N(s)}{A} \longrightarrow u(s) = \frac{P\phi_o}{2A(\cos \varphi_i + \phi_o \sin \varphi_i)} \left(\frac{L}{\cos \varphi_i} - s \right) + u_1, \quad (2.20)$$

where u_1 is the value of $u(s)$ at point 1.

Considering that $u(0) = u_0$ the following expression is obtained:

$$(u_0 - u_1) \cos \varphi_i = \frac{PL\phi_o}{2A(\cos \varphi_i + \phi_o \sin \varphi_i)}. \quad (2.21)$$

Finally, integrating equation (2.15b), the transversal displacement yields:

$$w(s) = \frac{P}{2C(\cos \varphi_i + \phi_o \sin \varphi_i)} \left(\frac{L}{\cos \varphi_i} - s \right) + \phi_1 \left(\frac{L}{\cos \varphi_i} - s \right) + \frac{P}{4D(\cos \varphi_i + \phi_o \sin \varphi_i)} \left(\frac{2L^3}{3 \cos^3 \varphi_i} - \frac{L^2}{\cos^2 \varphi_i} s + \frac{s^3}{3} \right) + w_1, \quad (2.22)$$

where w_1 is the value of $w(s)$ at point 1.

Considering that $w(0) = w_0$ the following expression is obtained:

$$w_1 - w_0 = -\frac{P}{2C(\cos \varphi_i + \phi_o \sin \varphi_i)} \frac{L}{\cos \varphi_i} - \frac{P}{4D(\cos \varphi_i + \phi_o \sin \varphi_i)} \frac{2L^3}{3 \cos^3 \varphi_i} - \phi_1 \frac{L}{\cos \varphi_i}. \quad (2.23)$$

Substituting (2.19) in (2.23), yields:

$$(w_1 - w_0) \sin \varphi_i = -\frac{PL \tan \varphi_i}{2C(\cos \varphi_i + \phi_o \sin \varphi_i)} - \frac{L}{3}(2\phi_o + \phi_1) \tan \varphi_i. \quad (2.24)$$

Therefore, the length L is obtained by substituting (2.21) and (2.24) into (2.9), yielding:

$$L = \frac{d_x + \hat{R}_r \left(\frac{\sin \varphi_i - \phi_o \cos \varphi_i}{\sqrt{1 + \phi_o^2}} + \frac{\sin \varphi_i - \phi_1 \cos \varphi_i}{\sqrt{1 + \phi_1^2}} \right)}{1 + \frac{1}{3}(2\phi_o + \phi_1) \tan \varphi_i + \frac{P}{2(\cos \varphi_i + \phi_o \sin \varphi_i)} \left(\frac{\tan \varphi_i}{C} - \frac{\phi_o}{A} \right)}. \quad (2.25)$$

Notice that considering a null load P and, therefore, null values of ϕ_o and ϕ_1 , the initial length yield:

$$L_0 = d_x + 2\hat{R}_r \sin \varphi_i. \quad (2.26)$$

Beam 2 is defined between point 1, with a change in the slope of φ_1 as seen previously, and point 2, with a change in the slope of φ_2 . The deformed configuration is depicted in Figure 2.4.

A local coordinate system (s_2, z) is defined in accordance with Figure 2.4, where $s_2 = s - (L/\cos \varphi_i)$.

According to Figure 2.4, the length of beam 2, given by the length of the projection of the deformed beam 2 onto the undeformed configuration, is given by L_2 as follows:

$$L_2 = \frac{L_s}{2} - R \sin \varphi_i - \hat{R}_r \sin(\varphi_i - \varphi_1) - w_1 \sin \varphi_i + u_1 \cos \varphi_i. \quad (2.27)$$

Substituting (2.7) into (2.27):

$$L_2 = \frac{L_s}{2} - R \sin \varphi_i - \frac{\hat{R}_r(\sin \varphi_i - \phi_1 \cos \varphi_i)}{\sqrt{1 + \phi_1^2}} - w_1 \sin \varphi_i + u_1 \cos \varphi_i. \quad (2.28)$$

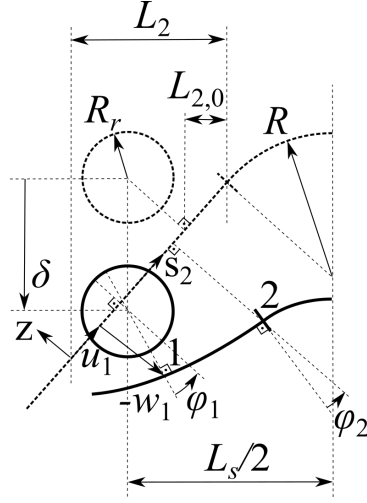


Figure 2.4: Deformed configuration of beam 2 and beam 3.

Considering that the applied load in the inner roller has an angle $\varphi_i - \varphi_1$, that the vertical force applied by the roller is $P/2$, and applying the load projected to the undeformed configuration the forces and the bending moment can be written as:

$$N(s_2) = -\frac{P(\phi_o - \phi_1) \cos \varphi_i}{2(\cos \varphi_i + \phi_o \sin \varphi_i)(\cos \varphi_i + \phi_1 \sin \varphi_i)}, \quad (2.29a)$$

$$Q(s_2) = \frac{P(\phi_o - \phi_1) \sin \varphi_i}{2(\cos \varphi_i + \phi_o \sin \varphi_i)(\cos \varphi_i + \phi_1 \sin \varphi_i)}, \quad (2.29b)$$

$$M(s_2) = -\frac{P}{2(\cos \varphi_i + \phi_o \sin \varphi_i)} \frac{L}{\cos \varphi_i} + \frac{P(\phi_o - \phi_1) \sin \varphi_i}{2(\cos \varphi_i + \phi_o \sin \varphi_i)(\cos \varphi_i + \phi_1 \sin \varphi_i)} s_2. \quad (2.29c)$$

Defining N_2 , Q_2 and M_2 as the axial force, the shear force and bending moment, respectively, evaluated at $s_2 = L_2/\cos \varphi_i$ (which coincides with the beginning of the curved part), yields:

$$N_2 = -\frac{P(\phi_o - \phi_1) \cos \varphi_i}{2(\cos \varphi_i + \phi_o \sin \varphi_i)(\cos \varphi_i + \phi_1 \sin \varphi_i)}, \quad (2.30a)$$

$$Q_2 = -N_2 \tan \varphi_i, \quad (2.30b)$$

$$M_2 = \frac{P}{2(\cos \varphi_i + \phi_o \sin \varphi_i) \cos \varphi_i} \left(\frac{(\phi_o - \phi_1) \sin \varphi_i}{(\cos \varphi_i + \phi_1 \sin \varphi_i)} L_2 - L \right). \quad (2.30c)$$

Substituting (2.30) in (2.29):

$$N(s_2) = N_2, \quad Q(s_2) = -N_2 \tan \varphi_i, \quad (2.31a)$$

$$M(s_2) = M_2 - N_2 \tan \varphi_i \left(s_2 - \frac{L_2}{\cos \varphi_i} \right). \quad (2.31b)$$

Hence, the displacement component $\phi(s_2)$ is obtained integrating equation (2.15a), considering (2.31b), as follows:

$$\begin{aligned} \frac{d\phi(s_2)}{ds_2} = \frac{M(s_2)}{D} \longrightarrow \phi(s_2) = \frac{M_2}{D} \left(s_2 - \frac{L_2}{\cos \varphi_i} \right) - \\ \frac{N_2 \tan \varphi_i}{D} \left(\frac{s_2^2}{2} - \frac{L_2}{\cos \varphi_i} s_2 + \frac{L_2^2}{2 \cos^2 \varphi_i} \right) + \phi_2. \end{aligned} \quad (2.32)$$

Considering the boundary condition $\phi(0) = \phi_1$ in (2.32), the following expression is obtained:

$$\phi_1 = \phi_2 - \frac{M_2}{D} \frac{L_2}{\cos \varphi_i} - \frac{N_2 L_2^2 \tan \varphi_i}{D 2 \cos^2 \varphi_i}. \quad (2.33)$$

The displacement component $u(s_2)$ is obtained integrating equation (2.15a), considering (2.31a), as follows:

$$\frac{du(s_2)}{ds_2} = \frac{N(s_2)}{A} \longrightarrow u(s_2) = \frac{N_2}{A} \left(s_2 - \frac{L_2}{\cos \varphi_i} \right) + u_2. \quad (2.34)$$

Considering the boundary condition $u(0) = u_1$ in (2.34), the following expression is obtained:

$$u_1 \cos \varphi_i = u_2 \cos \varphi_i - \frac{N_2 L_2}{A}. \quad (2.35)$$

Finally, integrating equation (2.15b) the transversal displacement can be written as:

$$\begin{aligned} \frac{dw(s_2)}{ds_2} = \frac{Q(s_2)}{C} - \phi(s_2) \longrightarrow w(s_2) = \frac{N_2 \tan \varphi_i}{C} \left(\frac{L_2}{\cos \varphi_i} - s_2 \right) - \\ \frac{M_2}{D} \left(\frac{s_2^2}{2} - \frac{L_2}{\cos \varphi_i} s_2 + \frac{L_2^2}{2 \cos^2 \varphi_i} \right) + \phi_2 \left(\frac{L_2}{\cos \varphi_i} - s_2 \right) + \\ \frac{N_2 \tan \varphi_i}{D} \left(\frac{s_2^3}{6} - \frac{L_2}{\cos \varphi_i} \frac{s_2^2}{2} + \frac{L_2^2}{2 \cos^2 \varphi_i} s_2 - \frac{L_2^3}{6 \cos^3 \varphi_i} \right) + w_2. \end{aligned} \quad (2.36)$$

Considering the boundary condition $w(0) = w_1$ in (2.36), the following expression is obtained:

$$w_1 = w_2 + \frac{N_2 \tan \varphi_i}{C} \frac{L_2}{\cos \varphi_i} - \frac{M_2}{D} \frac{L_2^2}{2 \cos^2 \varphi_i} - \frac{N_2 \tan \varphi_i}{D} \frac{L_2^3}{6 \cos^3 \varphi_i} + \phi_2 \frac{L_2}{\cos \varphi_i}. \quad (2.37)$$

Beam 3 is defined as the curved part. The deformed shape of beam 3 is observed also in Figure 2.4. A local coordinate system (θ, z) is defined, where θ is an angular coordinate with origin at point 2, and z is the through-thickness coordinate with origin at the mean line.

The equilibrium equations of the forces and the bending moment in beam 3 give a distribution of the forces and the bending moment as follows:

$$N(\theta) = N_2 \cos \theta - Q_2 \sin \theta, \quad (2.38a)$$

$$Q(\theta) = N_2 \sin \theta + Q_2 \cos \theta, \quad (2.38b)$$

$$M(\theta) = M_2 + R(N_2(1 - \cos \theta) + Q_2 \sin \theta), \quad (2.38c)$$

where R is the mean radius of the curved part.

Therefore, evaluating the forces and the bending moment at $\theta = \varphi_i$ and substituting (2.30), the central point of the beam has the following loads:

$$N_3 = -\frac{P(\phi_o - \phi_1)}{2(\cos \varphi_i + \phi_o \sin \varphi_i)(\cos \varphi_i + \phi_1 \sin \varphi_i)}, \quad Q_3 = 0, \quad (2.39a)$$

$$M_3 = \frac{P}{2(\cos \varphi_i + \phi_o \sin \varphi_i)} \left(-\frac{L}{\cos \varphi_i} + (L_2 \tan \varphi_i + R(1 - \cos \varphi_i)) \frac{\phi_o - \phi_1}{\cos \varphi_i + \phi_1 \sin \varphi_i} \right). \quad (2.39b)$$

Considering the definition of the displacements (2.6), the strains can be written as:

$$\varepsilon_s = \frac{R}{R+z} \left(\frac{1}{R} \frac{du^0(\theta)}{d\theta} + \frac{z}{R} \frac{d\phi(\theta)}{d\theta} + \frac{w^0(\theta)}{R} \right), \quad \varepsilon_z = 0, \quad (2.40a)$$

$$\gamma_{sz} = \frac{R}{R+z} \left(\phi(\theta) - \frac{u^0(\theta)}{R} + \frac{1}{R} \frac{dw^0(\theta)}{d\theta} \right). \quad (2.40b)$$

Introducing the definition of the strains (2.40) in the constitutive equations (2.14) and integrating the circumferential stress to obtain the axial force and the bending moment, the stiffness matrix \hat{A} - \hat{B} - \hat{D} and the stiffness \hat{C} are obtained (see [94]):

$$\begin{bmatrix} N(\theta) \\ M(\theta) \end{bmatrix} = \begin{bmatrix} \hat{A} & \hat{B} \\ \hat{B} & \hat{D} \end{bmatrix} \begin{bmatrix} \frac{1}{R} \frac{du^0(\theta)}{d\theta} + \frac{w^0(\theta)}{R} \\ \frac{1}{R} \frac{d\phi(\theta)}{d\theta} \end{bmatrix}, \quad (2.41a)$$

$$Q(\theta) = \hat{C} \left(\phi(\theta) - \frac{u^0(\theta)}{R} + \frac{1}{R} \frac{dw^0(\theta)}{d\theta} \right), \quad (2.41b)$$

where the components \hat{A} , \hat{B} and \hat{D} are given by:

$$\hat{A} = \sum_{p=1}^{N_p} \left[RC_{11}^p \log \left(\frac{R + z_p}{R + z_{p-1}} \right) \right], \quad (2.42a)$$

$$\hat{B} = \sum_{p=1}^{N_p} \left[RC_{11}^p \left(z_p - z_{p-1} - R \log \left(\frac{R + z_p}{R + z_{p-1}} \right) \right) \right], \quad (2.42b)$$

$$\hat{D} = \sum_{p=1}^{N_p} \left[RC_{11}^p \left(R^2 \log \left(\frac{R + z_p}{R + z_{p-1}} \right) + \frac{z_p}{2} (z_p - 2R) - \frac{z_{p-1}}{2} (z_{p-1} - 2R) \right) \right], \quad (2.42c)$$

and the stiffness \hat{C} is modified by considering a parabolic distribution multiplied by $R/(R + z)$ of the shear stress:

$$\hat{C} = \sum_{p=1}^{N_p} \left[\frac{3}{2} RC_{55}^p \left(\log \left(\frac{R + z_p}{R + z_{p-1}} \right) - \frac{4}{t^2} \left(R^2 \log \left(\frac{R + z_p}{R + z_{p-1}} \right) + \frac{z_p}{2} (z_p - 2R) - \frac{z_{p-1}}{2} (z_{p-1} - 2R) \right) \right) \right]. \quad (2.43)$$

Notice that the curvature implies a not null \hat{B} matrix even in symmetric laminates.

The compliance equation (2.41a) is inverted and yields:

$$\begin{bmatrix} \frac{1}{R} \frac{du^0(\theta)}{d\theta} + \frac{w^0(\theta)}{R} \\ \frac{1}{R} \frac{d\phi(\theta)}{d\theta} \end{bmatrix} = \begin{bmatrix} \frac{1}{EA} & -\frac{1}{EV} \\ -\frac{1}{EV} & \frac{1}{EI} \end{bmatrix} \begin{bmatrix} N(\theta) \\ M(\theta) \end{bmatrix}, \quad (2.44)$$

where:

$$EA = \frac{\hat{D}}{\hat{A}\hat{D} - \hat{B}^2}, \quad EV = \frac{\hat{B}}{\hat{A}\hat{D} - \hat{B}^2}, \quad EI = \frac{\hat{A}}{\hat{A}\hat{D} - \hat{B}^2}. \quad (2.45)$$

Integrating the second equation of (2.44) associated with $\phi(\theta)$ and considering the boundary condition $\phi(0) = \phi_2$ it yields:

$$\phi(\theta) = R \frac{M_2\theta + R(N_2(\theta - \sin\theta) + Q_2(1 - \cos\theta))}{EI} - R \frac{N_2 \sin\theta + Q_2(\cos\theta - 1)}{EV} + \phi_2. \quad (2.46)$$

Considering the global boundary condition $\phi(\varphi_i) = 0$ and using (2.30b), the angle ϕ_2 can be written as:

$$\phi_2 = \frac{RN_2 \tan \varphi_i}{EV} - \frac{R}{EI}(M_2\varphi_i + RN_2(\varphi_i - \tan \varphi_i)). \quad (2.47)$$

Substituting $w^0(\theta)$ obtained from the first equation of (2.44) into (2.41b) yields:

$$u^0(\theta) + \frac{d^2 u^0(\theta)}{d\theta^2} = R \left(\phi(\theta) - \frac{Q(\theta)}{\hat{C}} + \frac{1}{EA} \frac{dN(\theta)}{d\theta} - \frac{1}{EV} \frac{dM(\theta)}{d\theta} \right). \quad (2.48)$$

Substituting (2.46) and (2.38) into (2.48) and integrating the remaining equation and the first equation of (2.44), the mean-line displacements can be written as:

$$\begin{aligned} u^0(\theta) = & R \left((M_2 + RN_2) \left(\frac{R}{EI} \theta - \left(\frac{R}{EI} + \frac{1}{EV} \right) \sin \theta \right) + \right. \\ & \left(\phi_2 + \left(\frac{R}{EV} + \frac{R^2}{EI} \right) Q_2 \right) (1 - \cos \theta) - \left(\frac{R^2}{EI} + \frac{R}{EV} + \frac{1}{\hat{C}} \right) N_2 \sin \theta + \\ & \left. \left(\frac{R^2}{EI} + \frac{2R}{EV} + \frac{1}{EA} + \frac{1}{\hat{C}} \right) \frac{\theta}{2} (N_2 \cos \theta - Q_2 \sin \theta) \right) + u_2 \cos \theta - w_2 \sin \theta, \end{aligned} \quad (2.49a)$$

$$\begin{aligned} w^0(\theta) = & R \left(\left(\frac{R}{EI} + \frac{1}{EV} \right) (M_2 + RN_2)(\cos \theta - 1) + \left(\frac{Q_2}{\hat{C}} - \phi_2 \right) \sin \theta + \right. \\ & \left. \left(\frac{R^2}{EI} + \frac{2R}{EV} + \frac{1}{EA} + \frac{1}{\hat{C}} \right) \frac{\theta}{2} (N_2 \sin \theta + Q_2 \cos \theta) \right) + u_2 \sin \theta + w_2 \cos \theta, \end{aligned} \quad (2.49b)$$

where the boundary conditions applied are $u^0(0) = u_2$ and $w^0(0) = w_2$.

The global boundary condition of $u^0(\theta)$ is given by $u^0(\varphi_i) = 0$. However, the remaining global boundary condition is given by the null vertical displacement of the outer roller. For the sake of simplicity, this boundary condition is changed by doing a solid rigid displacement of the model so that $w^0(\varphi_i) = 0$. In this way, applying both boundary conditions and considering (2.30b) and (2.47), u_2 and w_2 yield:

$$u_2 = R \left((M_2 + RN_2) \left(\left(\frac{R}{EI} + \frac{1}{EV} \right) \sin \varphi_i - \frac{R}{EI} \varphi_i \right) + \left(\frac{R^2}{EI} + \frac{R}{EV} + \frac{1}{\hat{C}} \right) N_2 \tan \varphi_i - \left(\frac{R^2}{EI} + \frac{2R}{EV} + \frac{1}{EA} + \frac{1}{\hat{C}} \right) \frac{\varphi_i}{2} N_2 \right), \quad (2.50a)$$

$$w_2 = R \left((M_2 + RN_2) \left(\frac{R}{EI} + \frac{1}{EV} \right) (\cos \varphi_i - 1) + \left(\frac{R^2}{EI} + \frac{2R}{EV} + \frac{1}{EA} + \frac{1}{\hat{C}} \right) \frac{\varphi_i}{2} N_2 \tan \varphi_i \right), \quad (2.50b)$$

Hence, the problem resolution is closed with the non-linear equations system defined by (2.19), (2.25), (2.28), (2.30a), (2.30c), (2.33), (2.35), (2.37), (2.47), (2.50a) and (2.50b). The problem is solved beginning with the value of a parameter, e.g., beginning with a given value of the applied force P .

Once the problem has been solved, the vertical displacement between the rollers, δ , can be written as:

$$\delta = d_x \tan \varphi_i + \frac{2R}{\cos \varphi_i} - R_r (\cos(\varphi_i - \varphi_o) + \cos(\varphi_i - \varphi_1)) - L \tan \varphi_i + (u_o - u_1) \sin \varphi_i + (w_o - w_1) \cos \varphi_i, \quad (2.51)$$

where, substituting (2.7), (2.21) and (2.24) yields:

$$\delta = d_x \tan \varphi_i + \frac{2R}{\cos \varphi_i} - R_r \left(\frac{\cos \varphi_i + \phi_o \sin \varphi_i}{\sqrt{1 + \phi_o^2}} + \frac{\cos \varphi_i + \phi_1 \sin \varphi_i}{\sqrt{1 + \phi_1^2}} \right) - L \tan \varphi_i + \frac{PL}{2(\cos \varphi_i + \phi_o \sin \varphi_i)} \left(\frac{\phi_o \tan \varphi_i}{A} + \frac{1}{C} \right) + \frac{L}{3}(2\phi_o + \phi_1) \quad (2.52)$$

2.3 Simplification of the non-linear model

The model developed in the previous section is complex to solve due to the non-linearity of the equations. In the present section, several hypotheses are applied, which have been verified previously to be applicable in typical configurations using CFRP laminates, in order to obtain a closed-form solution of the model. Considering the hypothesis $A \ll C \ll D/t^2$, $R_2 N_2 \ll M_2$, $EV \ll REI$, $(\phi_0 - \phi_1)L_2 \ll L$ and $\phi_1^2 \ll 1$, the equations are simplified as follows:

$$P = \frac{4D(\phi_0 - \phi_1) \cos^2 \varphi_i (\cos \varphi_i + \phi_0 \sin \varphi_i)}{L^2}, \quad (2.53a)$$

$$L = \frac{d_x + \hat{R}_r \left(\frac{\sin \varphi_i - \phi_0 \cos \varphi_i}{\sqrt{1 + \phi_0^2}} + \sin \varphi_i - \phi_1 \cos \varphi_i \right)}{1 + \frac{1}{3}(2\phi_0 + \phi_1) \tan \varphi_i}, \quad (2.53b)$$

$$L_2 = \frac{L_s}{2} - R \sin \varphi_i - \hat{R}_r (\sin \varphi_i - \phi_1 \cos \varphi_i) - w_1 \sin \varphi_i + u_1 \cos \varphi_i, \quad (2.53c)$$

$$N_2 = -\frac{P(\phi_0 - \phi_1) \cos \varphi_i}{2(\cos \varphi_i + \phi_0 \sin \varphi_i)(\cos \varphi_i + \phi_1 \sin \varphi_i)}, \quad (2.53d)$$

$$M_2 = \frac{-PL}{2(\cos \varphi_i + \phi_0 \sin \varphi_i) \cos \varphi_i}, \quad (2.53e)$$

$$\phi_1 = \phi_2 - \frac{M_2}{D} \frac{L_2}{\cos \varphi_i}, \quad (2.53f)$$

$$w_1 = w_2 - \frac{M_2}{D} \frac{L_2^2}{2 \cos^2 \varphi_i} + \phi_2 \frac{L_2}{\cos \varphi_i}, \quad (2.53g)$$

$$\phi_2 = -\frac{R}{EI} M_2 \varphi_i, \quad (2.53h)$$

$$u_1 = u_2 = M_2 \frac{R^2}{EI} (\sin \varphi_i - \varphi_i), \quad (2.53i)$$

$$w_2 = M_2 \frac{R^2}{EI} (\cos \varphi_i - 1). \quad (2.53j)$$

Substituting (2.53h) and (2.53j) in (2.53g) and (2.53f):

$$\phi_1 = -M_2 \left(\frac{R}{EI} \varphi_i + \frac{1}{D} \frac{L_2}{\cos \varphi_i} \right), \quad (2.54)$$

$$w_1 = M_2 \left(\frac{R^2}{EI} (\cos \varphi_i - 1) - \frac{1}{D} \frac{L_2^2}{2 \cos^2 \varphi_i} - \frac{R \varphi_i}{EI} \frac{L_2}{\cos \varphi_i} \right). \quad (2.55)$$

Substituting (2.53a) in (2.53e):

$$\phi_1 = \frac{M_2 L}{2D \cos \varphi_i} + \phi_o. \quad (2.56)$$

For typical test configurations, the distance L_2 is very small compared with the distance L and it may be approximated by being invariant with the value of the initial length:

$$L_2 = \frac{L_s}{2} - R \sin \varphi_i - \hat{R}_r \sin \varphi_i. \quad (2.57)$$

Dividing (2.53d) between (2.53e) and substituting (2.56):

$$N_2 = \frac{-M_2^2 \cos \varphi_i}{2D(\cos \varphi_i + \phi_1 \sin \varphi_i)}. \quad (2.58)$$

Therefore, neglecting the angle ϕ_1 and substituting in (2.39a), the axial force in the central point may be approximated by:

$$N_3 = -\frac{M_2^2}{2D \cos \varphi_i}. \quad (2.59)$$

Substituting (2.56) in (2.54) and in (2.53b):

$$\phi_o = -M_2 \left(\frac{R}{EI} \varphi_i + \frac{1}{D \cos \varphi_i} \left(L_2 + \frac{L}{2} \right) \right), \quad (2.60)$$

$$L = \frac{d_x + \hat{R}_r \left(\frac{\sin \varphi_i - \phi_o \cos \varphi_i}{\sqrt{1 + \phi_o^2}} + \sin \varphi_i - \phi_o \cos \varphi_i - \frac{M_2 L}{2D} \right)}{1 + \left(\phi_o + \frac{M_2 L}{6D \cos \varphi_i} \right) \tan \varphi_i}. \quad (2.61)$$

Using the Taylor expansion in $\phi_o = 0$ in the numerator of (2.61) and neglecting the powers higher or equal than two (considering $\phi_o \ll 1$):

$$L = \frac{d_x + \hat{R}_r \left(2 \sin \varphi_i - 2 \phi_o \cos \varphi_i - \frac{M_2 L}{2D} \right)}{1 + \left(\phi_o + \frac{M_2 L}{6D \cos \varphi_i} \right) \tan \varphi_i}. \quad (2.62)$$

Substituting (2.60) in (2.62) and developing the equation:

$$L = d_x + \left(\frac{R}{EI} \varphi_i + \frac{1}{D \cos \varphi_i} \left(L_2 + \frac{L}{3} \right) \right) M_2 L \tan \varphi_i + \hat{R}_r \left(2 \sin \varphi_i + 2M_2 \left(\frac{R}{EI} \varphi_i \cos \varphi_i + \frac{1}{D} \left(L_2 + \frac{L}{4} \right) \right) \right). \quad (2.63)$$

which constitutes a second-order equation in L which may be solved analytically:

$$L = \frac{-B_L - \sqrt{B_L^2 - 4A_L C_L}}{2A_L}, \quad (2.64)$$

$$A_L = \frac{M_2}{3D \cos \varphi_i} \tan \varphi_i, \quad (2.65)$$

$$B_L = \frac{L_2 M_2}{D \cos \varphi_i} \tan \varphi_i + \frac{R M_2}{EI} \varphi_i \tan \varphi_i + \frac{\hat{R}_r M_2}{2D} - 1, \quad (2.66)$$

$$C_L = d_x + 2\hat{R}_r \left(\sin \varphi_i + \frac{R M_2}{EI} \varphi_i \cos \varphi_i + \frac{M_2 L_2}{D} \right). \quad (2.67)$$

Therefore, the resolution of the model is reduced to consider a given value of the bending moment in the symmetry point $M_3 \cong M_2 < 0$ and calculating the length L from (2.64), where the length L_2 is given by (2.57). Once L has been obtained the angle ϕ_0 is obtained from (2.60) and the angle ϕ_1 from (2.54). Finally, the load necessary to obtain the bending moment M_3 is calculated from (2.53a), and the displacement of the rollers is given by (2.52). If desired, the axial force at the central point is given by (2.59). If the input parameter is the load P instead of the bending moment M_3 , it is necessary to do an iterative process to obtain the desired load.

2.4 Comparison of the non-linear model with experimental results

For the validation of the non-linear model, the results obtained with it are compared with experimental results. The experimental tests have been carried out by Ramírez [102]. The tests have been carried out over a standard CFRP which has been previously characterized, obtaining the material properties given in Table 2.1.

E_{11}	152 GPa	E_{22}	8.7 GPa
ν_{12}	0.37	G_{12}	10 GPa

Table 2.1: Ply properties

Two kinds of specimens are considered:

- Specimen SP1: $[45,0,0,0,-45]_s$, $t = 2$ mm, $R = 6$ mm, $W = 27$ mm.

- Specimen SP2: $[45,0,0,-45,90,45,0]_S$, $t = 2.7$ mm, $R = 6.35$ mm, $W = 27$ mm.

The 0° direction is defined as the curved direction, while the 90° direction is defined as the through-the-width direction.

The test configuration is defined by a roller radius of $R_r = 5$ mm, and the distances are $L_s = 22$ mm and $d_x = 7$ mm.

Three coupons of each kind of specimen are tested, which are numbered as SPx.y, where x indicates the type of the specimen (1 or 2) and y indicates the number of coupon (from 1 to 3).

The numerical evaluation has been carried out by considering the hypotheses of Plane Strain and Plane Stress for obtaining the constitutive equations (2.14) from the 3D constitutive equations. Additionally, the Classic Laminate Theory (CLT) has been applied to obtain the classical 6x6 A-B-D matrix (see for instance [15], Chapter 4) and, considering that the out-of-plane forces and moments are null (the forces and moments associated to the transverse stress σ_y and the shear stress τ_{sy} , where y is the through-the-width coordinate), so that an equivalent 2x2 A-B-D matrix for equation (2.15a) may be obtained by using the aforementioned consideration.

Figures 2.5 and 2.6 show for SP1 and SP2 specimens respectively the numerical results obtained with the Plane Strain assumption, the Plane Stress assumption and with the 2x2 A-B-D matrix obtained from the 6x6 A-B-D matrix of the CLT. Those numerical results are compared with the experimental results obtained in the tests.

Notice that the Plane Stress assumption is not physically realistic as it implies discontinuities in the through-the-width normal strain. Furthermore, in laminates with $\pm 45^\circ$, Plane Strain assumption is also non realistic as implies discontinuities in the through-the-width interlaminar shear stress. Therefore, only the model based on the CLT A-B-D matrix is physically realistic.

It may be observed that the results of the model evaluated with the stiffness properties of the CLT are always located between the results of the Plane Strain assumption and the Plane Stress assumption. The Plane Strain assumption is the stiffest assumption, and the Plane Stress assumption is the less stiff assumption. It can be obtained that the range between both Plane Strain and Plane Stress assumptions is higher when higher is the number of $\pm 45^\circ$ plies. Notwithstanding, the model based on the CLT is usually nearer to the Plane Stress model.

The experimental results show a high agreement with the model based on the CLT approximation. It shows a high accuracy of this assumption compared with the Plane Strain and the Plane Stress assumptions, especially

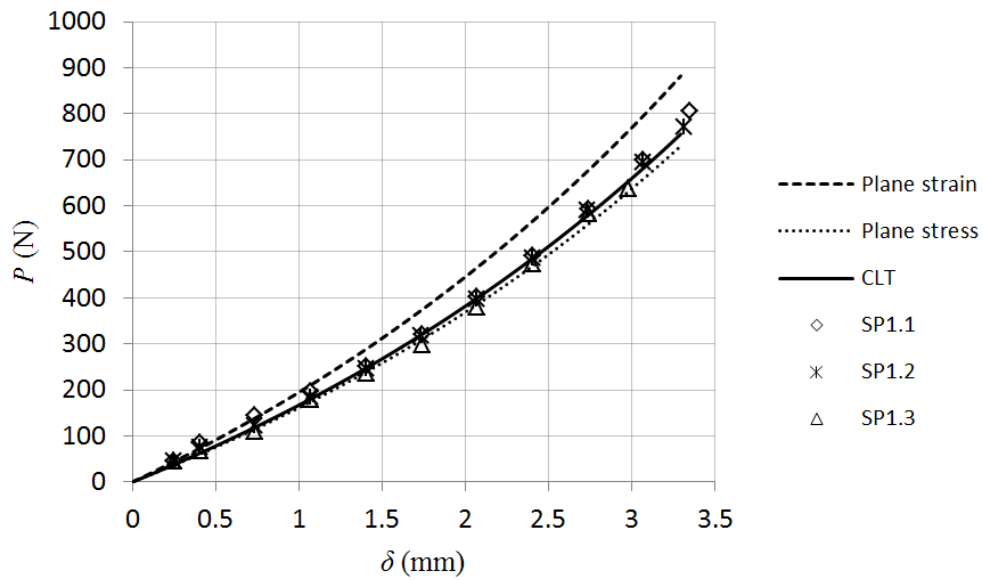


Figure 2.5: Numerical and experimental force-displacement relations in SP1.

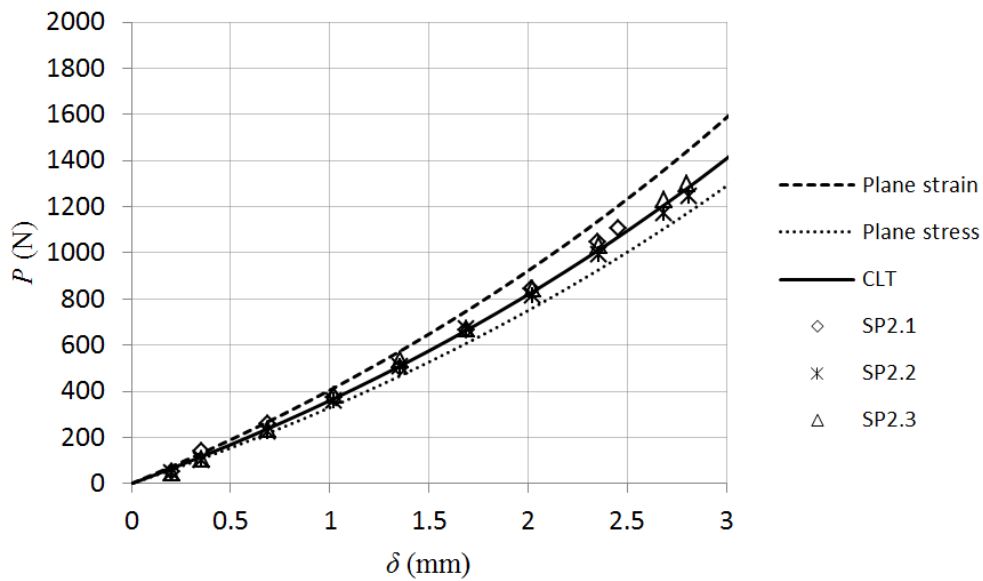


Figure 2.6: Numerical and experimental force-displacement relations in SP2.

in laminates with a high percentage of $\pm 45^\circ$ plies.

The non-linearity and the slope of the curves modified by the change of the point of contact of the specimen with the rollers are captured with a

high accuracy by the analytical model.

2.5 Comparison of the non-linear model with the ASTM procedure

The model developed may be used to monitor the test in real time, validating that the experimental results are according to the analytical results and detecting if any kind of defects or errors are present during the test. However, the main utility of the model is not the monitoring of the test, but the calculation of the bending moment from the applied load.

The calculation of the stresses involving the unfolding failure is done by means of the bending moment, so high errors in this calculation implies a poor estimation of the unfolding failure and, according to it, a poor estimation of the ILTS by using the four-point bending test, which is normalized by the procedure ASTM D6415 [3].

The ASTM procedure requires both load and displacement experimental parameters to estimate the ILTS. However, the analytical procedure developed in the present Chapter only requires one of the two parameters (force or displacement), and the other parameter can be calculated. This is useful for comparison with the experimental load-displacement distribution and validation of the accuracy of the model.

In this way, both analytical and ASTM procedures are applied to the experimental specimens SP1 and SP2 commented in the previous section. For introducing the data in the ASTM procedure, specimens SP1 are considered to fail, based on the experimental results, at a mean load of $P_1 = 790$ N with a displacement $\delta_1 = 3.4$ mm, and specimens SP2 are considered to fail, based on the experimental results, at a mean load of $P_2 = 1270$ N with a displacement $\delta_2 = 2.8$ mm.

The analytical procedure developed in the present document applied to the specimens SP1 using the load P_1 results in an slope $\phi_0 = 0.124$, an slope $\phi_1 = 0.041$ and a total bending moment $M_{SP1} = 11.7$ Nm. These slopes, by using (2.7), imply an angle $\varphi_0 = 0.123$ rad and $\varphi_1 = 0.041$ rad. By using the ASTM procedure, the angle ϕ obtained is 0.698 rad, which implies an increment $\varphi_i - \phi = 0.0982$ rad, which is located between the angles φ_0 and φ_1 . Therefore, by using 2.3, the bending moment obtained according to the ASTM procedure yields $M_{SP1}^{ASTM} = 12.1$ Nm, which is a 3% higher than the one obtained from the non-linear model developed in the present document.

The analytical procedure developed in the present document applied to the specimens SP2 using the load P_2 results in an slope $\phi_0 = 0.0965$, an slope $\phi_1 = 0.0289$ and a total bending moment $M_{SP1} = -20.6$ Nm. These

slopes, by using (2.7), imply an angle $\varphi_0 = 0.0962$ rad and $\varphi_1 = 0.0289$ rad. By using the ASTM procedure, the angle ϕ obtained is 0.7221 rad, which implies an increment $\varphi_i - \phi = 0.0764$ rad, which is located between the angles φ_0 and φ_1 . Therefore, by using (2.3), the bending moment obtained according to the ASTM procedure yields $M_{SP_1}^{ASTM} = 21.1$ Nm, which is a 2% higher than the one obtained from the non-linear model developed in the present document.

Therefore, for the present specimens, the ASTM procedure has very low errors in the calculation of the bending moment applied to the curved zone, presenting a high accuracy. These errors may be higher for specimens with a lower bending stiffness. Notwithstanding, the ASTM procedure requires to obtain the experimental displacement, which is a difficult task in view of the test set-up. An inaccurate experimental measurement of the failure displacement may imply errors in the bending moment calculation higher than the ones presented in the aforementioned experimental results. In contrast, the present analytical method requires only the experimental load, which is easily obtained with a high accuracy from the experimental tests.

Chapter 3

Bi-dimensional models for evaluating interlaminar stresses

The unfolding failure, which is traditionally associated to the interlaminar tensile stresses, is typically calculated using two different techniques. The first technique consists in the use of a FE software, which requires a highly refined mesh in the thickness of the laminate. If the mesh in the thickness has to be refined for obtaining a good accuracy in the interlaminar stresses it implies also a refinement in the in-plane direction. This fact causes that a very high number of elements are needed in the numerical model and, hence, high calculation times are required for obtaining a good estimation of the interlaminar stresses. Furthermore, the high calculation times hinder the optimization of geometries and stacking sequences.

The second technique consists in the use of analytical solutions. The typical analytical solutions are based in bi-dimensional approximations, which reduce the scope of applications. Furthermore, traditional calculation methods for the interlaminar stresses are regularized models. Regularized stresses and strains are defined as the stresses and strains far enough from a perturbation. A typical example of a perturbation is given by the free edge effect, where a stress concentrator is given. However, this is not the only perturbation present. In the case of the traditional sections prone to unfolding failure, another kind of perturbation is given by curvature changes, e.g., in a L-sectioned beam where the curved zone is joint to the straight arms. This effect has been observed numerically by Most et al. [14].

The perturbation due to the change of curvature allows equalling the displacements and stresses between both parts, while the regularized solutions are not similar. Respect to the interlaminar normal stress (INS), the INS has a through-the-thickness distribution in the section of the change of curvature given approximately (for the case of a bending moment loading)

by the average distribution between the regularized one of one side and the regularized one of the adjacent side. When another kind of load is applied, the INS distribution is also reduced in the side where the highest values are given. It implies that when the maximum regularized value of the INS is given just at the joint, the non-regularized value is actually much lower due to the change of curvature perturbation and, therefore, regularized models may underestimate the failure.

Accordingly, there is a necessity to introduce a non-regularized analytical model which allows calculating in a quicker and more accurate way the non-regularized stresses, getting a similar accuracy that of the detailed FE models, but with lower computational times. This chapter develops two non-regularized models based on a series expansion of the displacements and on the definition of higher-order moments in the stresses. Before that, the basis of the regularized models developed by Lekhnitskii [19, chap. 3] and Ko and Jackson [4] are presented, as well as an approximation of the regularized model based on the Timoshenko beam theory developed by the authors [94], which constitutes the first-order model of the non-regularized models.

3.1 Theoretical basis of the regularized models

The models developed by Lekhnitskii [19, chap. 3] and Ko and Jackson [4] are developed in the present section to make the notation uniform with the notation used in the project.

Regularized models developed by Lekhnitskii [19, chap. 3] and Ko and Jackson [4] constitute the solution of an isolated curved beam loaded under end axial and shear forces, $N(0) = N_0$ and $Q(0) = Q_0$, and bending moment, $M(0) = M_0$, see Fig. 3.1. These forces and moment are defined from the circumferential and shear stresses, $\sigma_\theta(r, \theta)$ and $\tau_{r\theta}(r, \theta)$, as follows:

$$N(\theta) = \int_{R^-}^{R^+} \sigma_\theta(r, \theta) dr, \quad M(\theta) = \int_{R^-}^{R^+} (r - R) \sigma_\theta(r, \theta) dr, \quad (3.1a)$$

$$Q(\theta) = \int_{R^-}^{R^+} \tau_{r\theta}(r, \theta) dr, \quad (3.1b)$$

where r is the radial coordinate, θ the circumferential coordinate, R is the mean radius, R^- is the inner radius, R^+ is the outer radius and t is the thickness. Notice that forces and the moment are integrated only across the

thickness and not along the width (defining the width as the out-of-plane dimension), so they are actually forces and moment per unit width.

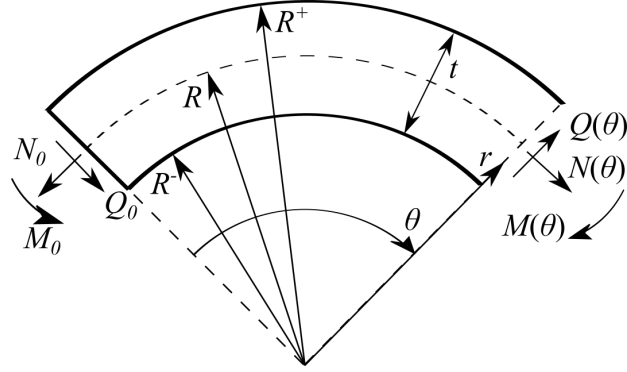


Figure 3.1: Geometry and loads considered in the regularized models of a curved beam.

Boundary conditions at the ends of the curved beam assure only that the mean value and the bending moment of the stress distribution are equals to the applied loads. Therefore, the solution is only accurate at a particular distance from the ends. That distance is denominated Regularization Distance (RD) and is analysed in a further section.

The forces and the moment have a circumferential distribution due to the equilibrium equations as follows:

$$N(\theta) = N_0 \cos \theta - Q_0 \sin \theta, \quad (3.2a)$$

$$Q(\theta) = Q_0 \cos \theta + N_0 \sin \theta, \quad (3.2b)$$

$$M(\theta) = M_0 + R(N_0 - N(\theta)). \quad (3.2c)$$

Lekhnitskii's equations were developed for anisotropic homogeneous materials, considering the stress-strain relations of the material given by the following equations:

$$\varepsilon_\theta(r, \theta) = \frac{1}{E_\theta} \sigma_\theta(r, \theta) - \frac{\nu_{\theta r}}{E_\theta} \sigma_r(r, \theta), \quad (3.3a)$$

$$\varepsilon_r(r, \theta) = -\frac{\nu_{\theta r}}{E_\theta} \sigma_\theta(r, \theta) + \frac{1}{E_r} \sigma_r(r, \theta), \quad (3.3b)$$

$$\gamma_{r\theta}(r, \theta) = \frac{1}{G_{r\theta}} \tau_{r\theta}(r, \theta), \quad (3.3c)$$

where E_r is the radial stiffness, E_θ the circumferential stiffness, $G_{r\theta}$ is the shear stiffness in the bi-dimensional plane and $\nu_{\theta r}$ is the Poisson ratio. These

stiffness constants are obtained from the three-dimensional properties of the material by doing a bi-dimensional assumption such as plane stress or plane strain.

Ko and Jackson's equations are developed for a composite laminate, where the plies are anisotropic and homogeneous, considered orthotropic when expressed in the polar coordinate system in the bi-dimensional plane. The stress-strain relations for each ply p are given also by equations (3.3) but with different stiffness properties for each ply, yielding:

$$\varepsilon_\theta(r, \theta) = \frac{1}{E_\theta^p} \sigma_\theta^p(r, \theta) - \frac{\nu_{\theta r}^p}{E_\theta^p} \sigma_r^p(r, \theta), \quad (3.4a)$$

$$\varepsilon_r(r, \theta) = -\frac{\nu_{\theta r}^p}{E_\theta^p} \sigma_\theta^p(r, \theta) + \frac{1}{E_r^p} \sigma_r^p(r, \theta), \quad (3.4b)$$

$$\gamma_{r\theta}(r, \theta) = \frac{1}{G_{r\theta}^p} \tau_{r\theta}^p(r, \theta). \quad (3.4c)$$

The strain-stress relations given in (3.4) are inverted as follows:

$$\sigma_\theta^p(r, \theta) = C_{\theta\theta}^p \varepsilon_\theta(r, \theta) + C_{r\theta}^p \varepsilon_r(r, \theta), \quad (3.5a)$$

$$\sigma_r^p(r, \theta) = C_{r\theta}^p \varepsilon_\theta(r, \theta) + C_{rr}^p \varepsilon_r(r, \theta), \quad (3.5b)$$

$$\tau_{r\theta}^p(r, \theta) = G_{r\theta}^p \gamma_{r\theta}(r, \theta), \quad (3.5c)$$

where C_{ij}^p ($i, j = r, \theta$) are defined as the stiffness constants of the bi-dimensional ply p .

The resolution of the equations consists, first, in expressing (by using the polar coordinate system) the stresses in a ply p depending on the Airy function $F_p(r, \theta)$, ensuring that equilibrium equations are automatically accomplished:

$$\sigma_\theta^p(r, \theta) = \frac{\partial^2 F_p(r, \theta)}{\partial r^2}, \quad (3.6a)$$

$$\sigma_r^p(r, \theta) = \frac{1}{r} \frac{\partial F_p(r, \theta)}{\partial r} + \frac{1}{r^2} \frac{\partial^2 F_p(r, \theta)}{\partial \theta^2}, \quad (3.6b)$$

$$\tau_{r\theta}^p(r, \theta) = -\frac{\partial^2}{\partial \theta \partial r} \left(\frac{F_p(r, \theta)}{r} \right). \quad (3.6c)$$

The compatibility equation in the bi-dimensional problem expressed in polar coordinates yields:

$$\frac{\partial}{\partial r} \left(r^2 \frac{\partial \varepsilon_\theta(r, \theta)}{\partial r} \right) + \frac{\partial^2 \varepsilon_r(r, \theta)}{\partial \theta^2} - r \frac{\partial \varepsilon_r(r, \theta)}{\partial r} - \frac{\partial^2 (r \gamma_{r\theta}(r, \theta))}{\partial \theta \partial r} = 0. \quad (3.7)$$

The compatibility equation can be expressed, depending on the stresses, substituting (3.3) in (3.7), which yields:

$$\begin{aligned} & \frac{1}{E_\theta^p} r^2 \frac{\partial^2 \sigma_\theta^p(r, \theta)}{\partial r^2} - \frac{\nu_{\theta r}^p}{E_\theta^p} r^2 \frac{\partial^2 \sigma_r^p(r, \theta)}{\partial r^2} - \frac{\nu_{\theta r}^p}{E_\theta^p} \frac{\partial^2 \sigma_\theta^p(r, \theta)}{\partial \theta^2} + \frac{1}{E_r^p} \frac{\partial^2 \sigma_r^p(r, \theta)}{\partial \theta^2} \\ & + \frac{2 + \nu_{\theta r}^p}{E_\theta^p} r \frac{\partial \sigma_\theta^p(r, \theta)}{\partial r} - \frac{E_\theta^p + 2\nu_{\theta r}^p E_r^p}{E_r^p E_\theta^p} r \frac{\partial \sigma_r^p(r, \theta)}{\partial r} - \frac{1}{G_{r\theta}^p} \frac{\partial^2 (r\tau_{r\theta}^p(r, \theta))}{\partial \theta \partial r} = 0. \end{aligned} \quad (3.8)$$

Substituting (3.6) in (3.8), a single equation is obtained for the Airy function $F_p(r, \theta)$, which has to be solved introducing the boundary conditions of the problem.

The simplification done by Lekhnitskii and Ko and Jackson consists in considering that stresses and strains depends only on the radial coordinate when the curved beam is loaded under a bending moment, and considering that stresses and strains depends also on the circumferential coordinate with the shape of $\cos \theta$ and $\sin \theta$ when it is loaded also under an end axial and shear forces. It implies that the resulting stresses are the regularized ones. The simplification is carried out supposing an Airy function $F_p(r, \theta) = F_0^p(r) + F_1^p(r) \cos \theta + F_2^p(r) \sin \theta$, which is introduced into (3.6) and (3.8) obtaining the following equations:

$$\frac{d}{dr} \left(r^2 \frac{d^3 F_0^p(r)}{dr^3} \right) - \kappa_p^2 r \frac{d}{dr} \left(\frac{1}{r} \frac{dF_0^p(r)}{dr} \right) = 0, \quad (3.9a)$$

$$\frac{d}{dr} \left(r^2 \frac{d^3 F_i^p(r)}{dr^3} \right) - (\beta_p^2 - 1) \frac{d}{dr} \left(r \frac{d}{dr} \left(\frac{F_i^p(r)}{r} \right) \right) = 0, \quad i = 1, 2, \quad (3.9b)$$

where:

$$\kappa_p = \sqrt{\frac{E_\theta^p}{E_r^p}} = \sqrt{\frac{C_{\theta\theta}^p}{C_{rr}^p}}, \quad (3.10a)$$

$$\begin{aligned} \beta_p &= \sqrt{\frac{E_\theta^p}{G_{r\theta}^p} + \frac{E_\theta^p - 2\nu_{\theta r}^p E_r^p}{E_r^p} + 1} \\ &= \sqrt{\frac{C_{\theta\theta}^p (C_{rr}^p + G_{r\theta}^p) - (C_{r\theta}^p)^2 - 2C_{r\theta}^p G_{r\theta}^p}{C_{rr}^p C_{r\theta}^p} + 1}. \end{aligned} \quad (3.10b)$$

The solution of equations (3.9), neglecting the terms which do not affect to the stresses, yields:

$$\begin{cases} F_0^p(r) = F_{0,0}^p r^2 + F_{0,1}^p r^{1+\kappa_p} + F_{0,2}^p r^{1-\kappa_p}, & \text{if } \kappa_p \neq 1, \\ F_0^p(r) = F_{0,0}^p r^2 + F_{0,1}^p r^2 \log r + F_{0,2}^p \log r, & \text{if } \kappa_p = 1, \end{cases} \quad (3.11a)$$

$$F_i^p(r) = F_{i,0}^p r \log r + F_{i,1}^p r^{1+\beta_p} + F_{i,2}^p r^{1-\beta_p}, \quad i = 1, 2. \quad (3.11b)$$

Finally, Ko and Jackson closed their equations by the calculation of $F_{i,j}$, with $i, j = 0, 1, 2$, by applying the boundary conditions. Considering that the laminate is composed by N_p plies, there are $3N_p$ unknown variables in the θ non-dependant terms, $3N_p$ terms in the $\cos \theta$ terms and $3N_p$ unknown variables in the $\sin \theta$ terms, so $9N_p$ equations are required to close the problem.

The first block of equations is given by the compatibility between plies, with establishes the continuity of the radial and circumferential displacements, $u_r(r, \theta)$ and $u_\theta(r, \theta)$, constituting a total of $2N_p - 2$ equations for each kind of θ -dependant term, i.e., $6N_p - 6$ equations.

The second block of equations is given by the equilibrium equations between plies, which establishes the continuity of shear and radial stresses, $\tau_{r\theta}(r, \theta)$ and $\sigma_r(r, \theta)$. Notice that, as it is demonstrated in [4], the shear stress equilibrium is accomplished if the radial one is accomplished. Therefore, these equations constitute a total of $3N_p - 3$ equations.

The third block of equations is given by the null radial boundary conditions of the radial stress, given by $\sigma_r(R^-, \theta) = \sigma_r(R^+, \theta) = 0$ (the shear stress boundary condition $\tau_{r\theta}(R^-, \theta) = \tau_{r\theta}(R^+, \theta) = 0$ is automatically accomplished if the radial stress one is accomplished). Applying these equations to each kind of term a total of 6 equations is given.

Finally, the last 3 equations are given by the applied axial and shear loads, $N(0)$ and $Q(0)$, and the bending moment, $M(0)$.

These $9N_p$ linear equations can be implemented in a numerical software so that stresses and strains can be easily obtained in very short computational times.

Lekhnitskii's equations can be obtained by considering a single-ply laminate ($N_p = 1$), so that the stresses yield, if $\kappa \neq 1$:

$$\begin{aligned} \sigma_\theta(r, \theta) = & \frac{N(\theta)}{r g_N} \left((1 + \beta) \left(\frac{r}{R^+} \right)^\beta + (1 - \beta) \left(\frac{R^-}{r} \right)^\beta - 1 - \left(\frac{R^-}{R^+} \right)^\beta \right) \\ & + \frac{M(\theta) + RN(\theta)}{(R^+)^2 g_M} \left(1 - \frac{1 - c^{\kappa+1}}{1 - c^{2\kappa}} \kappa \left(\frac{r}{R^+} \right)^{\kappa-1} + \frac{1 - c^{\kappa-1}}{1 - c^{2\kappa}} \kappa \left(\frac{R^-}{r} \right)^{\kappa+1} \right), \end{aligned} \quad (3.12a)$$

$$\begin{aligned} \sigma_r(r, \theta) = & \frac{N(\theta)}{r g_N} \left(\left(\frac{r}{R^+} \right)^\beta + \left(\frac{R^-}{r} \right)^\beta - 1 - \left(\frac{R^-}{R^+} \right)^\beta \right) \\ & + \frac{M(\theta) + RN(\theta)}{(R^+)^2 g_M} \left(1 - \frac{1 - c^{\kappa+1}}{1 - c^{2\kappa}} \left(\frac{r}{R^+} \right)^{\kappa-1} - \frac{1 - c^{\kappa-1}}{1 - c^{2\kappa}} \left(\frac{R^-}{r} \right)^{\kappa+1} \right), \end{aligned} \quad (3.12b)$$

$$\tau_{r\theta}(r, \theta) = \frac{Q(\theta)}{r g_N} \left(\left(\frac{r}{R^+} \right)^\beta + \left(\frac{R^-}{r} \right)^\beta - 1 - \left(\frac{R^-}{R^+} \right)^\beta \right), \quad (3.12c)$$

where:

$$g_M = \frac{1 - c^2}{2} - \frac{\kappa}{\kappa + 1} \frac{(1 - c^{\kappa+1})^2}{1 - c^{2\kappa}} + \frac{\kappa c^2}{\kappa - 1} \frac{(1 - c^{\kappa-1})^2}{1 - c^{2\kappa}}, \quad c = \frac{R^+}{R^-}, \quad (3.13a)$$

$$g_N = \frac{2}{\beta} \left(1 - \left(\frac{R^-}{R^+} \right)^\beta \right) + \left(1 + \left(\frac{R^-}{R^+} \right)^\beta \right) \log \frac{R^-}{R^+}. \quad (3.13b)$$

3.2 Approximations of the regularized models

The previously presented regularized models are very difficult to extend to the non-regularized cases. The author has developed an approximated model of the regularized problem [94] which provides the basis for the following non-regularized models.

In the literature, the most used approximation of the regularized model was given by Kedward et al. [1], who estimate with the following expression the maximum radial stress in a section loaded mainly by a bending moment per unit of width, M :

$$\max \sigma_r(r) \simeq \frac{3M}{2t\sqrt{R^+R^-}}. \quad (3.14)$$

This approximation is widely used, even in composite laminates, e.g., in the four point bending test ASTM procedure [3], where it is indicated that the approximation is accurate only in the cases with $\kappa_p^2 < 20$.

Other examples of approximations of the regularized models were developed by Qatu [27] and Kress et al. [28], as beam models or extensions of the Classical Laminate Theory. The model developed by the author [94] is based also on a beam model, by considering a layerwise model. In [94] two kinds of models are developed, one for thin laminates ($t \ll R$) and one

for thick laminates ($t \sim R$). The thin laminates model let us to obtain the following approximation of the maximum radial stress in the case of a homogeneous material:

$$\max \sigma_r(r) \simeq \frac{12M}{t^3}(R - \sqrt{R^+R^-}). \quad (3.15)$$

Equations (3.15) and (3.14) give similar results for thin laminates. Notwithstanding, differences are lower than 3% for $R/t < 1.5$.

Respect to the thick beam model, it is developed in the present section with a matrix notation, which is easier to implement numerically and constitutes the first order model of the non-regularized models developed in the following sections.

The problem exposed in [94] consists in an isolated 2D curved composite beam (see Fig. 3.2) under end axial and shear forces per unit of width, $N_0 = N(0)$ and $Q_0 = Q(0)$, and an end moment per unit of width, $M_0 = M(0)$. The beam is also under non-uniform external pressure per unit of width, $\sigma^+(\theta)$ and $\sigma^-(\theta)$, and shear distributed loads per unit of width, $\tau^+(\theta)$ and $\tau^-(\theta)$, in the outer and inner radius, R^+ and R^- . The consideration of these distributed loads is an improvement respect to the Lekhnitskii's equations and Ko and Jackson's equations, which do not include them.

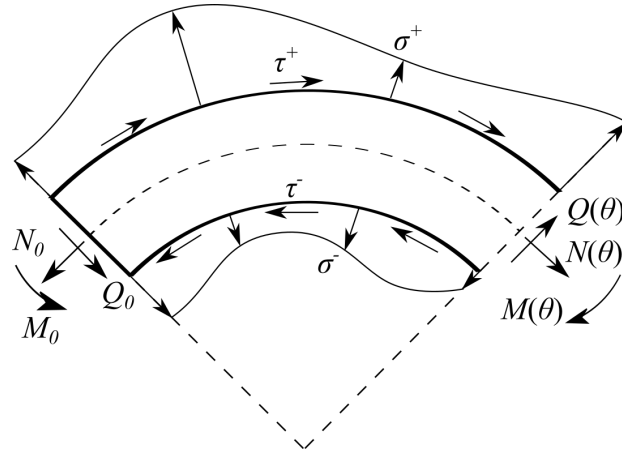


Figure 3.2: Loads considered in the approximation of the regularized models of a curved beam.

A circumferential coordinate, θ , and a radial coordinate, r , are considered as shown in Fig. 3.1. The curved beam has a mean radius R and a thickness t .

The axial and shear forces and the bending moment are defined from the circumferential and shear stresses, σ_θ and $\tau_{r\theta}$, by equations (3.1).

Mean line distributed loads are calculated from the distributed outer and inner radius boundary conditions as follows:

$$q(\theta) = \frac{1}{R} (R^+ \tau^+(\theta) - R^- \tau^-(\theta)), \quad (3.16a)$$

$$p(\theta) = \frac{1}{R} (R^+ \sigma^+(\theta) - R^- \sigma^-(\theta)), \quad (3.16b)$$

$$m(\theta) = \frac{t}{2R} (R^+ \tau^+(\theta) + R^- \tau^-(\theta)), \quad (3.16c)$$

where $q(\theta)$ is the mean line shear distributed load, $p(\theta)$ is the mean line radial distributed load and $m(\theta)$ is the mean line distributed bending moment.

In this way the equilibrium equations of the forces and the bending moment are given by:

$$\frac{dN(\theta)}{d\theta} + Q(\theta) + Rq(\theta) = 0, \quad (3.17a)$$

$$\frac{dM(\theta)}{d\theta} + R \frac{dN(\theta)}{d\theta} + Rm(\theta) + R^2q(\theta) = 0, \quad (3.17b)$$

$$\frac{dQ(\theta)}{d\theta} + Rp(\theta) = N(\theta). \quad (3.17c)$$

Forces $N(\theta)$, $Q(\theta)$ and $M(\theta)$ are obtained directly from these equations. The forces vector, $\mathbf{M}_T(\theta)$, is defined as follows:

$$\mathbf{M}_T(\theta) = \begin{bmatrix} N(\theta) \\ M(\theta) \end{bmatrix}. \quad (3.18)$$

The model developed in [94] considered the Timoshenko hypothesis applied over each lamina, and the conclusion obtained was that this hypothesis is applied then over the whole section, so the displacements are approached by:

$$u_\theta(\theta, r) = u_o(\theta) + (r - R)u_1(\theta), \quad u_r(\theta, r) = w_1(\theta), \quad (3.19)$$

where $u_\theta(\theta, r)$ is the circumferential displacement and $u_r(\theta, r)$ the radial one.

The elasticity strain equation for the circumferential strain in polar coordinates is given by:

$$\varepsilon_\theta(\theta, r) = \frac{1}{r} \frac{\partial u_\theta(\theta, r)}{\partial r} + \frac{u_r(\theta, r)}{r}. \quad (3.20)$$

Substituting (3.19) in (3.20), the circumferential strain yield:

$$\varepsilon_\theta(\theta, r) = \frac{R}{r} e_N(\theta) + \frac{R}{r} (r - R) e_M(\theta), \quad (3.21a)$$

$$e_N(\theta) = \frac{1}{R} \frac{du_o(\theta)}{d\theta} + \frac{w_1(\theta)}{R}, \quad e_M(\theta) = \frac{1}{R} \frac{du_1(\theta)}{d\theta}, \quad (3.21b)$$

where $e_N(\theta)$ and $e_M(\theta)$ are the Classical Beam Theory (CBT) axial and bending strains.

The strains vector, $\mathbf{e}_T(\theta)$, is defined as follows:

$$\mathbf{e}_T(\theta) = \begin{bmatrix} e_N(\theta) \\ e_M(\theta) \end{bmatrix}. \quad (3.22)$$

Therefore, equation (3.21a) can be expressed in matrix notation as follows:

$$\varepsilon_\theta(\theta, z) = \mathbf{T}^T(r) \mathbf{e}_T(\theta), \quad \mathbf{T}^T(r) = \begin{bmatrix} \frac{R}{r} & \frac{R}{r}(r-R) \end{bmatrix}. \quad (3.23)$$

Neglecting the radial strain (due to the hypothesis of the constant value of the radial displacement) the relation between the circumferential stress and the strains in a ply p , according to (3.5), depends on the stiffness of the ply, $C_{\theta\theta}^p$, as follows:

$$\sigma_\theta^p(\theta, z) = C_{\theta\theta}^p \varepsilon_\theta(\theta, z) = C_{\theta\theta}^p \mathbf{T}^T(r) \mathbf{e}_T(\theta) = (\mathbf{S}_\theta^p(r))^T \mathbf{e}_T(\theta). \quad (3.24)$$

Plies are enumerated beginning with $p = 1$ in the ply situated in the lower radius up to $p = N_p$ located in the outer radius.

Couplings between shear and axial stresses and strains are not given, since the material is considered to be orthotropic in the θ - r axes. Therefore, the relation between the circumferential stress and the strain vector is given by $\mathbf{S}_\theta^p(r)$, defined according to (3.24) as follows:

$$\mathbf{S}_\theta^p(r) = C_{\theta\theta}^p \mathbf{T}(r) = \frac{R}{r} C_{\theta\theta}^p \begin{bmatrix} 1 \\ r-R \end{bmatrix}. \quad (3.25)$$

Integrating the circumferential stress in order to obtain the forces vector, next expression is obtained:

$$\begin{aligned} \mathbf{M}_T(\theta) &= \int_{R^-}^{R^+} \begin{bmatrix} 1 \\ r-R \end{bmatrix} \sigma_\theta^p(r, \theta) dr \\ &= \int_{R^-}^{R^+} \begin{bmatrix} 1 \\ r-R \end{bmatrix} (\mathbf{S}_\theta^p(r))^T \mathbf{e}_T(\theta) dr = \hat{\mathbf{K}}_\sigma \mathbf{e}_T(\theta), \end{aligned} \quad (3.26)$$

where the equivalent homogeneous material stiffness matrix is given by:

$$\hat{\mathbf{K}}_\sigma = \begin{bmatrix} A' & B' \\ B' & D' \end{bmatrix}, \quad (3.27)$$

with:

$$A' = \sum_{p=1}^{N_p} \left(C_{\theta\theta}^p R \log \left(\frac{R_p^+}{R_p^-} \right) \right), \quad (3.28a)$$

$$B' = \sum_{p=1}^{N_p} \left(C_{\theta\theta}^p R \left(R_p^+ - R_p^- - R \log \left(\frac{R_p^+}{R_p^-} \right) \right) \right), \quad (3.28b)$$

$$D' = \sum_{p=1}^{N_p} \left(C_{\theta\theta}^p R \left(R^2 \log \left(\frac{R_p^+}{R_p^-} \right) + \frac{R_p^+ - R_p^-}{2} (R_p^+ + R_p^- - 4R) \right) \right), \quad (3.28c)$$

where R_p^+ and R_p^- are the values of r at the outer and inner radius respectively for the ply p and N_p is the number of plies. Notice that $R_p^+ = R_{p+1}^-$. The curvature radius causes a coupling effect between the axial and bending parameters ($B' \neq 0$) even when a symmetric laminate is given.

Substituting (3.26) in (3.24), the circumferential stress can be calculated from the axial force and the bending moment as follows:

$$\sigma_\theta^p(\theta, r) = (\mathbf{S}_\theta^p(r))^T \hat{\mathbf{K}}_\sigma^{-1} \mathbf{M}_T(\theta). \quad (3.29)$$

Once the circumferential stress has been obtained, the other stresses can be calculated by equilibrium. The equilibrium equations of the elasticity in polar coordinates are given by:

$$\frac{\partial \sigma_\theta}{\partial \theta} + \frac{1}{r} \frac{\partial (r^2 \tau_{r\theta})}{\partial r} = 0, \quad (3.30a)$$

$$\frac{\partial (r \sigma_r)}{\partial r} + \frac{\partial \tau_{r\theta}}{\partial \theta} = \sigma_\theta. \quad (3.30b)$$

Thus, substituting (3.29) in (3.30) and integrating, the shear and radial stresses are given by:

$$\tau_{r\theta}^p(\theta, r) = \tau_{r\theta}^p(R_p^-, \theta) \left(\frac{R_p^-}{r} \right)^2 - (\mathbf{S}_{r\theta}^p(r))^T \hat{\mathbf{K}}_\sigma^{-1} \frac{d\mathbf{M}_T(\theta)}{d\theta}, \quad (3.31a)$$

$$\begin{aligned} \sigma_r^p(\theta, r) = & \sigma_r^p(R_p^-, \theta) \frac{R_p^-}{r} + \frac{d\tau_{r\theta}^p(R_p^-, \theta)}{d\theta} \frac{R_p^-}{r} \left(\frac{R_p^-}{r} - 1 \right) \\ & + (\mathbf{S}_{r,1}^p(r))^T \hat{\mathbf{K}}_\sigma^{-1} \mathbf{M}_T(\theta) + (\mathbf{S}_{r,2}^p(r))^T \hat{\mathbf{K}}_\sigma^{-1} \frac{d^2 \mathbf{M}_T(\theta)}{d\theta^2}, \end{aligned} \quad (3.31b)$$

where:

$$\mathbf{S}_{r\theta}^p(r) = \frac{1}{r^2} \int_{R_p^-}^r r' \mathbf{S}_{\theta}^p(r') dr' = \frac{C_{\theta\theta}^p R}{r^2} \left[\begin{array}{c} r - R_p^- \\ \frac{r - R_p^-}{2} (r + R_p^- - 2R) \end{array} \right], \quad (3.32a)$$

$$\mathbf{S}_{r,1}^p(r) = \frac{1}{r} \int_{R_p^-}^r \mathbf{S}_{\theta}^p(r') dr' = \frac{C_{\theta\theta}^p R}{r} \left[\begin{array}{c} \log \frac{r}{R_p^-} \\ r - R_p^- - R \log \frac{r}{R_p^-} \end{array} \right], \quad (3.32b)$$

$$\begin{aligned} \mathbf{S}_{r,2}^p(r) &= \frac{1}{r} \int_{R_p^-}^r \mathbf{S}_{r\theta}^p(r') dr' \\ &= \frac{C_{\theta\theta}^p R}{r} \left[\begin{array}{c} \log \frac{r}{R_p^-} + \frac{R_p^-}{r} - 1 \\ \frac{r}{2} - R_p^- - \left(R - \frac{R_p^-}{2} \right) \frac{R_p^-}{r} + R \left(1 - \log \frac{r}{R_p^-} \right) \end{array} \right], \end{aligned} \quad (3.32c)$$

where $\mathbf{S}_{r\theta}^p(r)$ relates the shear stress with the derivative of the strains vector, $\mathbf{S}_{r,1}^p(r)$ relates the radial stress with the strain vector and $\mathbf{S}_{r,2}^p(r)$ relates the radial stress with the second derivative of the strain vector.

The boundary conditions for $\tau_{r\theta}^p(R_p^-, \theta)$ and $\sigma_r^p(R_p^-, \theta)$ are obtained from the previous lamina $p-1$ so that $\tau_{r\theta}^p(R_p^-, \theta) = \tau_{r\theta}^{p-1}(R_{p-1}^+, \theta)$ and $\sigma_r^p(R_p^-, \theta) = \sigma_r^{p-1}(R_{p-1}^+, \theta)$, beginning with a boundary condition for the first ply $p=1$ of $\sigma_r^1(R^-, \theta) = \sigma^-(\theta)$ and $\tau_{r\theta}^1(R^-, \theta) = \tau^-(\theta)$. The boundary conditions of $\sigma_r^{N_p}(R^+, \theta) = \sigma^+(\theta)$ and $\tau_{r\theta}^{N_p}(R^+, \theta) = \tau^+(\theta)$ are automatically satisfied.

In conclusion, the equations of the method may be easily solved to calculate the stresses in two simple steps. The first step consists in the calculation of the axial force and the bending moment from equations (3.17). For example, in the case of constant distributed loads ($q(\theta) = q_0$, $p(\theta) = p_0$, $m(\theta) = m_0$) the forces and the bending moment yield:

$$N(\theta) = (N_0 - Rp_0) \cos \theta - (Q_0 + Rq_0) \sin \theta + Rp_0, \quad (3.33a)$$

$$Q(\theta) = (Q_0 + Rq_0) \cos \theta + (N_0 - Rp_0) \sin \theta - Rq_0, \quad (3.33b)$$

$$M(\theta) = M_0 + R(N_0 - N(\theta)) - R(m_0 + Rq_0)\theta. \quad (3.33c)$$

Once forces and moment have been obtained, the second step is to calculate stresses. Circumferential stress is directly obtained from equation (3.29). Shear stress is calculated recursively from (3.31a), beginning with a boundary condition of $\tau_{r\theta}(R^-, \theta) = \tau^-(\theta)$. Deriving equation (3.31a) respect to θ , $d\tau_{r\theta}(r, \theta)/d\theta$ is obtained recursively too, beginning with a boundary condition of $d\tau_{r\theta}(R^-, \theta)/d\theta = d\tau^-(\theta)/d\theta$. Finally, the radial stress

is obtained recursively from (3.31b) beginning with a boundary condition $\sigma_r(R^-, \theta) = \sigma^-(\theta)$.

In the resolution procedure it is necessary to define three important matrices and vectors:

- $\mathbf{M}_T(\theta)$ vector, containing the axial force and the bending moment.
- Stiffness matrix $\hat{\mathbf{K}}_\sigma$, relating the axial force and the bending moment with the mean section strains.
- $\mathbf{S}^p(r)$ vectors, relating the stresses with the mean section strains and their derivatives. They are calculated from the stress-strain relations and the $\mathbf{T}(r)$ vector, which relates the strain with the mean section strains.

If the matrix equations are developed in conventional form by multiplying the matrices, equations of the model given by [94] are obtained, as the same hypotheses have been considered. Therefore, results of the present model are the same than those presented in the aforementioned reference. Some comparisons with the Lekhnitskii's equations, the Ko and Jackson's equations and FE results can be found in [103].

3.3 Theoretical basis of the non-regularized models

The non-regularized models developed in the present project are based on a series expansion of the displacements. Several authors have tried to model several kinds of structural problems based also in series expansions. Carrera et al. [34] presented a compilation of several methods based on series expansions in the displacements applied to vibration analysis. Several kinds of those models are commented in Chapter 1.

Among the models based on monomials, the one developed by Matsunaga [37] is of special interest in the present work. Matsunaga considers, for flat laminates, a series expansion with monomial functions in the in-plane displacements, including $n + 1$ terms in these displacements, and another series expansion with monomial functions in the out-of-plane displacement, including n terms in this displacement. The approximation by using one order less in the out-of-plane displacement than in the in-plane ones is typical also in the first order models, such as the Timoshenko beam theory [35,36] or the CLT [15]. Later, Matsunaga applied his model to curved laminates [38]

by using also a series expansion with monomial functions in the two displacements.

Matsunaga's model uses a series expansion based on monomial functions in the displacements in the next way:

$$u_s(s, z) = u_o(s) + zu_1(s) + \sum_{i=2}^{\infty} z^i u_n(s), \quad (3.34a)$$

$$u_z(s, z) = w_1(s) + \sum_{i=2}^{\infty} z^{i-1} w_n(s), \quad (3.34b)$$

where a curvilinear coordinate system (s, z) is used (see Fig. 3.3), defined by the axial coordinate s and the through-thickness coordinate z . This curvilinear coordinate system is related with the previously defined polar coordinate system (θ, r) by the relations $s = R\theta$ and $z = r - R$.

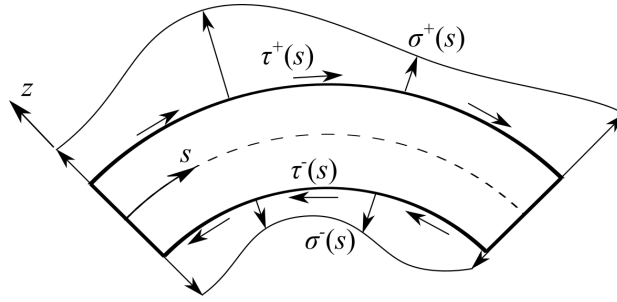


Figure 3.3: Definition of the curvilinear coordinate system.

Approximating the displacements by a n -order model instead of the infinite summation:

$$u_s(s, z) = u_o(s) + zu_1(s) + \sum_{i=2}^n z^i u_i(s), \quad (3.35a)$$

$$u_z(s, z) = w_1(s) + \sum_{i=2}^n z^{i-1} w_i(s). \quad (3.35b)$$

Notice that the through-thickness displacement, $u_z(s, z)$, is approximated with one order less than the axial displacement, $u_s(s, z)$.

The present model is based on a similar series expansion but by using different functions in the series expansion in the different displacements, which allows an easier and a more efficient numerical resolution of the problem to be performed. Furthermore, Matsunaga used a secondary series expansion

in the parameters that has been suppressed in the present model. In this way, axial displacement is expanded by using functions $f_i^s(z)$, and through-thickness displacements are expanded by using different functions $f_i^z(z)$, so they yield:

$$u_s(s, z) = u_o(s) + zu_1(s) + \sum_{i=2}^n f_i^s(z)u_i(s), \quad (3.36a)$$

$$u_z(s, z) = w_1(s) + \sum_{i=2}^n f_i^z(z)w_i(s). \quad (3.36b)$$

Different kinds of non-regularized models can be chosen depending on the functions used in the series expansion of the axial displacements, $f_i^s(z)$. The present document develops two kind of models. The first one is based on monomial functions ($f_i^s(z) = z^i$), and is called monomials based model (MBM). Due to numerical instabilities in the stiffness matrix of the MBM, a second model is developed based on Legendre polynomials ($f_i^s(z) = p_i(2z/t)$, where $p_i(2z/t)$ is the i -th Legendre polynomial), and is called Legendre polynomials based model (LPBM).

The functions used for the through-thickness displacement, $f_i^z(z)$, are determined by the shear strains. In the CBT, which constitutes the first order model, axial strain depends on two CBT 1D strain components given in (3.21b), shear strain depends only on one CBT 1D strain component and the through-thickness strain is neglected. If a n -th order model is chosen it is desirable to increment in $n - 1$ components each strain, so that the axial strain is defined by $n + 1$ components, the through-thickness strain is defined by $n - 1$ components and the shear strain is defined by n components. In that way, the condition to determine the functions for the series expansion in the through-thickness displacement is that shear strain depends only on n components.

The aim of developing these non-regularized models is to estimate the perturbation introduced by a change of curvature, so that a more accurate stresses distribution may be obtained in this kind of geometries. The geometries considered consist in a section of a curved composite laminate, treated as a chain of constant curvature beams. Each beam may be composed by different materials or different stacking sequences, but all beams must have the same thickness, which is constant along the axial coordinate. In that way, some examples of geometries in which the model can be applied are sections of L-shaped components, Ω -shaped components, joggles or corrugated laminates (see Fig. 3.4).

Notice that typically the sections end in a long enough straight part in which stresses tend to their regularized values. Therefore, they can be

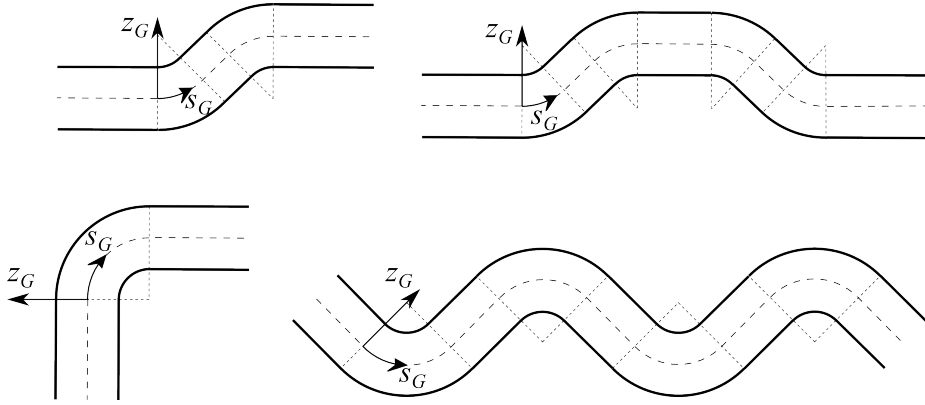


Figure 3.4: Examples of geometries where the non-regularized models can be applied. Global coordinate system definition.

considered semi-infinite. Another kind of boundary conditions can be chosen at the ends of the chain, e.g., an embedded end.

A global coordinate system (s_G, z_G) is considered in the whole section as shown in Fig. 3.4. The axial coordinate s_G is a curvilinear coordinate along the mean line of the section. The origin is located in the first joint of the chain in the case of a semi-infinite end beam, and it is oriented towards the following joint. The through-thickness coordinate z_G has its origin in the mean line and the orientation of it can be chosen by the user.

The section can be decomposed in several constant-curvature beams, and a local coordinate system (s_k, z_k) is considered for each component k (see Fig. 3.5), where s_k has the same sense than s_G but with its origin in the joint with the previous beam, and z_k coincides with the global through-thickness coordinate z_G . Therefore, three kinds of components can be considered:

- Straight beams (Beams 1, 3 and 5 in Fig. 3.5).
- Clockwise curved beams, which have a local through-thickness coordinate z_k defined in the same sense than the radial coordinate (Beam 2 in Fig. 3.5).
- Counter-clockwise curved beams, which have a local through-thickness coordinate z_k defined positive towards the center of curvature (Beam 4 in Fig. 3.5).

The problem is solved by considering each component isolated and considering arbitrary stresses boundary conditions applied at both ends of the components (or applied at the only one end for the case of the semi-infinite

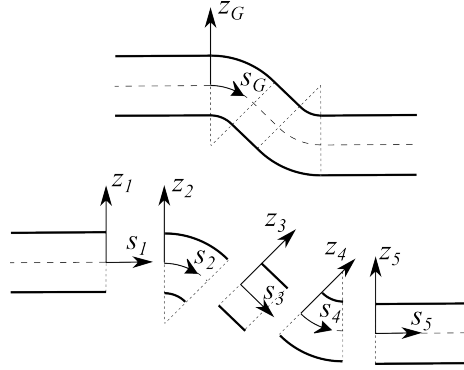


Figure 3.5: Decomposition of the section in several constant-curvature beams.

end components). Displacements and stresses are obtained in the component depending on the arbitrary boundary conditions. Finally, the arbitrary boundary conditions are calculated by imposing continuity of the displacements and the stresses at both sides of every joint of the chain of beams.

3.4 Monomials based model (MBM)

The first model developed in this Thesis can be obtained by choosing the monomials functions as $f_i^s(z)$ functions, similarly to what is done in the Matsunaga models [37,38]. The difference with these models is given in the definition of the $f_i^z(s)$ functions, which are not necessarily monomials.

Therefore, the MBM is based on an approximation of the displacements as follows:

$$u_s(s, z) = u_o(s) + zu_1(s) + \sum_{i=2}^n z^i u_i(s), \quad (3.37a)$$

$$u_z(s, z) = w_1(s) + \sum_{i=2}^n f_i^z(z) w_i(s). \quad (3.37b)$$

However, as will be seen later, for a better numerical resolution it is recommendable to use non-dimensional parameters, at least non-dimensional displacements and lengths and optionally non-dimensional stresses and pressures. Numerical errors are minimized when displacements and lengths are adimensionalized with the half of the thickness. Non-dimensional parameters are marked with an upper bar in the magnitude, so if u is a generic

displacement/length and σ is a generic stress/pressure, the non-dimensional parameters \bar{u} and $\bar{\sigma}$ respectively are defined as:

$$\bar{u} = \frac{2u}{t}, \quad \bar{\sigma} = \frac{\sigma}{E_{\text{ref}}}, \quad (3.38)$$

where t is the thickness and E_{ref} is a reference stiffness, e.g., the stiffness in the fibre direction.

Hence, the series expansion using non-dimensional parameters can be developed alternatively to 3.37 as follows:

$$\bar{u}_s(\bar{s}, \bar{z}) = \bar{u}_o(\bar{s}) + \bar{z}\bar{u}_1(\bar{s}) + \sum_{i=2}^n \bar{z}^i \bar{u}_i(\bar{s}), \quad (3.39a)$$

$$\bar{u}_z(\bar{s}, \bar{z}) = \bar{w}_1(\bar{s}) + \sum_{i=2}^n \bar{f}_i^z(\bar{z}) \bar{w}_i(\bar{s}). \quad (3.39b)$$

For the sake of simplicity, the bar indicating the non-dimensional magnitudes is obviated in the present section while all the magnitudes used are non-dimensional unless it is said otherwise. Nevertheless, the model can be implemented also with the dimensional magnitudes, obtaining a worse numerical behaviour.

The model is developed for the isolated beam under arbitrary boundary conditions, and in the next sections the joint to other beams will be analysed. The model is developed first for the case of straight beams, and after that it is developed for curved beams, jointly for both clockwise and counter-clockwise curved beams.

This model has been published by the author in [95] considering only end loads applied. However, the model developed here considers also distributed loads in the transverse boundaries.

3.4.1 Development of the MBM for straight beams

A straight beam with thickness t (considered non-dimensional with value $t = 2$) and length L_k is studied (see Figure 3.6). A local non-dimensional coordinate system s_k and z_k is used as defined in Figure 3.5.

The beam is loaded under distributed transverse and shear loads in the positive boundary of z_k , $\sigma^+(s_k)$ and $\tau^+(s_k)$, and under distributed transverse and shear loads in the negative boundary of z_k , $\sigma^-(s_k)$ and $\tau^-(s_k)$. Arbitrary stresses boundary conditions are applied in $s_k = 0$, given by $\sigma_s^0(z_k)$ and $\tau_s^0(z_k)$, and in $s_k = L_k$, given by $\sigma_s^L(z_k)$ and $\tau_s^L(z_k)$.

For the sake of simplicity, the index k indicating the component is suppressed in the following.

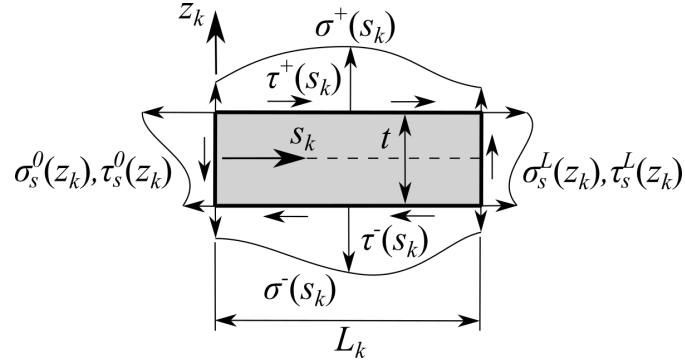


Figure 3.6: Straight beam.

Displacements

The longitudinal and through-thickness displacements approximation of the straight beam is given by equations (3.39), where the axial displacements have been approximated by a series expansion by using monomial functions. The functions $f_i^z(z)$ used for the through-thickness displacements have to be determined.

The series expansion can be expressed in matrix notation by the definition of the following vectors of length $n - 1$:

$$\mathbf{u}^T(s) = [u_2(s) \quad u_3(s) \quad \dots \quad u_n(s)], \quad (3.40a)$$

$$\mathbf{w}^T(s) = [w_2(s) \quad w_3(s) \quad \dots \quad w_n(s)], \quad (3.40b)$$

$$\mathbf{f}_s^T(z) = [z^2 \quad z^3 \quad \dots \quad z^n], \quad (3.40c)$$

$$\mathbf{f}_z^T(z) = [f_2^z(z) \quad f_3^z(z) \quad \dots \quad f_n^z(z)]. \quad (3.40d)$$

Therefore, equation (3.39) can be expressed as follows:

$$u_s(s, z) = u_o(s) + zu_1(s) + \mathbf{f}_s^T(z)\mathbf{u}(s), \quad (3.41a)$$

$$u_z(s, z) = w_1(s) + \mathbf{f}_z^T(z)\mathbf{w}(s). \quad (3.41b)$$

Strains

Strains equations in the local Cartesian coordinate system yield:

$$\varepsilon_s(s, z) = \frac{\partial u_s(s, z)}{\partial s}, \quad \varepsilon_z(s, z) = \frac{\partial u_z(s, z)}{\partial z}, \quad (3.42a)$$

$$\gamma_{sz}(s, z) = \frac{\partial u_s(s, z)}{\partial z} + \frac{\partial u_z(s, z)}{\partial s}. \quad (3.42b)$$

First, functions $f_i^z(z)$ may be determined by the aforementioned condition which imposes that the shear strain depends only on n 1D components. Substituting (3.41) in (3.42b) shear strain yields:

$$\gamma_{sz}(s, z) = u_1(s) + \frac{d\mathbf{f}_s^T(z)}{dz}\mathbf{u}(s) + \frac{\partial w_1(s)}{\partial s} + \mathbf{f}_z^T(z)\frac{\partial \mathbf{w}(s)}{\partial s}. \quad (3.43)$$

The derivative of functions $\mathbf{f}_s(z)$ can be expressed as follows:

$$\frac{d\mathbf{f}_s(z)}{dz} = \mathbf{H}_\gamma \hat{\mathbf{f}}_s(z), \quad (3.44)$$

where $\hat{\mathbf{f}}_s(z)$ is a vector similar to $\mathbf{f}_s(z)$ but with all components being a monomial one order lower:

$$\hat{\mathbf{f}}_s^T(z) = [z \quad z^2 \quad \dots \quad z^{n-1}], \quad (3.45)$$

and matrix \mathbf{H}_γ is a diagonal matrix defined by its components H_{ij}^γ , with $i, j = 2, 3, \dots, n$:

$$H_{ij}^\gamma = i\delta_{ij}, \quad (3.46)$$

where δ_{ij} denotes the Kronecker delta, equal to 1 when $i = j$ and to 0 otherwise.

Hence, choosing $\mathbf{f}_z^T(z) = \hat{\mathbf{f}}_s^T(z)$, the shear strain can be expressed depending only on n 1D components. Accordingly, the series expansion in the through-thickness displacement is done also by using monomial functions, and the approximation of the displacements employed in the straight beam case remains the same than in the Matsunaga model for this kind of beams [37].

Therefore, strains may be expressed as follows:

$$\varepsilon_s(s, z) = e_N(s) + ze_M(s) + \mathbf{f}_s^T(z)\mathbf{e}_s(s), \quad (3.47a)$$

$$\gamma_{sz}(s, z) = e_Q(s) + \hat{\mathbf{f}}_s^T(z)\mathbf{e}_\gamma(s), \quad (3.47b)$$

$$\varepsilon_z(s, z) = \hat{\hat{\mathbf{f}}}_s^T(z)\mathbf{e}_z(s), \quad (3.47c)$$

where $e_N(s)$, $e_M(s)$ and $e_Q(s)$ are the CBT 1D strain components, and $\mathbf{e}_s(s)$, $\mathbf{e}_\gamma(s)$ and $\mathbf{e}_z(s)$ are the higher-order 1D strain components, which yield:

$$e_N(s) = \frac{du_0(s)}{ds}, \quad (3.48a)$$

$$e_M(s) = \frac{du_1(s)}{ds}, \quad (3.48b)$$

$$e_Q(s) = u_1(s) + \frac{dw_1(s)}{ds}, \quad (3.48c)$$

$$\mathbf{e}_s(s) = \frac{d\mathbf{u}(s)}{ds}, \quad (3.48d)$$

$$\mathbf{e}_\gamma(s) = \frac{d\mathbf{w}(s)}{ds} + \mathbf{H}_\gamma^T \mathbf{u}(s), \quad (3.48e)$$

$$\mathbf{e}_z(s) = \mathbf{H}_z^T \mathbf{w}(s), \quad (3.48f)$$

where $\hat{\mathbf{f}}_s(z)$ is a vector similar to $\hat{\mathbf{f}}_s(z)$ but with all components being a monomial one order lower, and matrix \mathbf{H}_z is a diagonal matrix defined by its components H_{ij}^z , with $i, j = 2, 3, \dots, n$:

$$\hat{\mathbf{f}}_s^T(z) = [1 \quad z \quad \dots \quad z^{n-2}], \quad (3.49a)$$

$$H_{ij}^z = (i-1) \delta_{ij}. \quad (3.49b)$$

Matrix \mathbf{H}_z has been obtained from the derivative of $\hat{\mathbf{f}}_s(z)$ as follows:

$$\frac{d\hat{\mathbf{f}}_s(z)}{dz} = \mathbf{H}_z \hat{\mathbf{f}}_s(z). \quad (3.50)$$

Equilibrium

The 2D equilibrium equations expressed in the local Cartesian coordinate system yield:

$$\frac{\partial \sigma_s(s, z)}{\partial s} + \frac{\partial \tau_{sz}(s, z)}{\partial z} = 0, \quad (3.51a)$$

$$\frac{\partial \sigma_z(s, z)}{\partial z} + \frac{\partial \tau_{sz}(s, z)}{\partial s} = 0. \quad (3.51b)$$

In the CBT, axial stress is approximated from the axial force $N(s)$ and the bending moment $M(s)$, shear stress is approximated from the shear force $Q(s)$ and the through-thickness stress is neglected. The higher-order model extends the approximation of the stresses by including $n-1$ additional terms in each stress, similarly to what has been done in the strains side. CBT forces and moment and higher-order moments expressed directly in matrix notation are defined by:

$$N(s) = \int_{-t/2}^{t/2} \sigma_s(s, z) dz, \quad M(s) = \int_{-t/2}^{t/2} \sigma_s(s, z) z dz, \quad (3.52a)$$

$$Q(s) = \int_{-t/2}^{t/2} \tau_{sz}(s, z) dz, \quad (3.52b)$$

$$\mathbf{M}_s(s) = \int_{-t/2}^{t/2} \sigma_s(s, z) \mathbf{f}_s(z) dz, \quad (3.52c)$$

$$\mathbf{M}_\tau(s) = \int_{-t/2}^{t/2} \tau_{sz}(s, z) \mathbf{f}_\tau(z) dz, \quad (3.52d)$$

$$\mathbf{M}_z(s) = \int_{-t/2}^{t/2} \sigma_z(s, z) \mathbf{f}_\sigma(z) dz. \quad (3.52e)$$

Notice that the axial higher-order moments have been defined by using the monomial functions included in $\mathbf{f}_s(z)$, but the shear and the transverse higher-order moments are defined by using different functions, included in vectors $\mathbf{f}_\tau(z)$ and $\mathbf{f}_\sigma(z)$, respectively, that have to be determined.

Equilibrium equations of the CBT forces can be obtained by integrating in the thickness both 2D equilibrium equations (3.51) and considering the boundary conditions in $z = \pm t/2$:

$$\frac{dN(s)}{ds} + \tau^+(s) - \tau^-(s) = 0, \quad (3.53a)$$

$$\frac{dQ(s)}{ds} + \sigma^+(s) - \sigma^-(s) = 0. \quad (3.53b)$$

The CBT bending moment equilibrium equation can be obtained by integrating in the thickness equation (3.51a), multiplied by z :

$$\frac{dM_s(s)}{ds} + \frac{t}{2} (\tau^+(s) + \tau^-(s)) = Q(s). \quad (3.54)$$

The CBT forces, $N(s)$ and $Q(s)$, and moment, $M(s)$, are obtained directly by integrating equations (3.53) and (3.54) and introducing the boundary conditions given by:

$$N(0) = N_0 = \int_{-t/2}^{t/2} \sigma_s^0(z) dz, \quad M(0) = M_0 = \int_{-t/2}^{t/2} \sigma_s^0(z) z dz, \quad (3.55a)$$

$$Q(0) = Q_0 = \int_{-t/2}^{t/2} \tau_{sz}^0(z) dz. \quad (3.55b)$$

Boundary conditions of these CBT forces and moment in $s = L$ are in equilibrium with the boundary conditions in $s = 0$ and, therefore, they are automatically accomplished with equations (3.53) and (3.54) if boundary condition in $s = 0$ are given.

The higher-order moments equilibrium equation in the axial direction is obtained by integrating equation (3.51a) multiplied by $\mathbf{f}_s(z)$:

$$\begin{aligned} \frac{d\mathbf{M}_s(s)}{ds} + \mathbf{f}_s\left(\frac{t}{2}\right)\tau^+(s) - \mathbf{f}_s\left(-\frac{t}{2}\right)\tau^-(s) \\ = \int_{-t/2}^{t/2} \frac{d\mathbf{f}_s(z)}{dz} \tau_{sz}(s, z) dz. \end{aligned} \quad (3.56)$$

Considering equation (3.44) and defining $\mathbf{f}_\tau(z)$ as the same functions used in the series expansion of the shear strain (3.47b), $\mathbf{f}_\tau(z) = \mathbf{f}_z(z) = \hat{\mathbf{f}}_s(z)$, equation (3.56) yields:

$$\frac{d\mathbf{M}_s(s)}{ds} + \mathbf{f}_s\left(\frac{t}{2}\right)\tau^+(s) - \mathbf{f}_s\left(-\frac{t}{2}\right)\tau^-(s) = \mathbf{H}_\gamma \mathbf{M}_\tau(s). \quad (3.57)$$

Similarly, the higher-order moments equilibrium equation in the transverse direction is obtained by integrating in the thickness equation (3.51b) multiplied by $\hat{\mathbf{f}}_s(z)$:

$$\begin{aligned} \frac{d\mathbf{M}_\tau(s)}{ds} + \hat{\mathbf{f}}_s\left(\frac{t}{2}\right)\sigma^+(s) - \hat{\mathbf{f}}_s\left(-\frac{t}{2}\right)\sigma^-(s) \\ = \int_{-t/2}^{t/2} \frac{d\hat{\mathbf{f}}_s(z)}{dz} \sigma_z(s, z) dz. \end{aligned} \quad (3.58)$$

Considering equation (3.50) and defining $\mathbf{f}_\sigma(z)$ as the same functions used in the series expansion of the through-thickness strain (3.47c), $\mathbf{f}_\sigma(z) = \hat{\mathbf{f}}_s(z)$, equation (3.58) yields:

$$\frac{d\mathbf{M}_\tau(s)}{ds} + \hat{\mathbf{f}}_s\left(\frac{t}{2}\right)\sigma^+(s) - \hat{\mathbf{f}}_s\left(-\frac{t}{2}\right)\sigma^-(s) = \mathbf{H}_z \mathbf{M}_z(s). \quad (3.59)$$

Therefore, higher-order moments equilibrium is given by equations (3.57) and (3.59), which cannot be directly solved as in the case of the CBT forces and moment. The boundary conditions at both ends for these higher order moments may be obtained from the arbitrary boundary conditions, by integrating them according to the higher-order moments definition given in (3.52).

Constitutive law

The laminate is constituted by N_p plies. The 2D constitutive law of a ply p , with z varying from z_p^- to z_p^+ , can be expressed depending on the stiffness constants of the ply in the local coordinate system, Q_{ij}^p , with $i, j = 1, 3, 5$. The material is considered orthotropic in the local coordinate system, and then $Q_{15}^p = Q_{35}^p = 0$.

$$\sigma_s^p(s, z) = Q_{11}^p \varepsilon_s(s, z) + Q_{13}^p \varepsilon_z(s, z), \quad (3.60a)$$

$$\sigma_z^p(s, z) = Q_{13}^p \varepsilon_s(s, z) + Q_{33}^p \varepsilon_z(s, z), \quad (3.60b)$$

$$\tau_{sz}^p(s, z) = Q_{55}^p \gamma_{sz}(s, z). \quad (3.60c)$$

The stiffness constants Q_{ij}^p have to be calculated from the ply properties, considering the orientation of the ply and the bi-dimensional approximation. This 2D approximation is typically done by considering plane stress or plane strain in the ply, see 2.4.

Using the bi-dimensional constitutive law given in (3.60), the strains approximations given in (3.47) and the forces and moments definition given in (3.52), constitutive equations yield:

$$\begin{bmatrix} N(s) \\ M(s) \\ \mathbf{M}_s(s) \\ \mathbf{M}_z(s) \end{bmatrix} = \hat{\mathbf{K}}_\sigma \begin{bmatrix} e_N(s) \\ e_M(s) \\ \mathbf{e}_s(s) \\ \mathbf{e}_z(s) \end{bmatrix}, \quad (3.61a)$$

$$\begin{bmatrix} Q(s) \\ \mathbf{M}_\tau(s) \end{bmatrix} = \hat{\mathbf{K}}_\tau \begin{bmatrix} e_Q(s) \\ \mathbf{e}_\gamma(s) \end{bmatrix}, \quad (3.61b)$$

where $\hat{\mathbf{K}}_\sigma$ and $\hat{\mathbf{K}}_\tau$ are respectively the normal and shear stiffness matrices of the model. The components of the stiffness matrices $\hat{\mathbf{K}}_\sigma$ and $\hat{\mathbf{K}}_\tau$ are shown in [95] for the non-dimensional case, and they can be summarized as follows:

$$\hat{\mathbf{K}}_\sigma = \int_{-\frac{t}{2}}^{\frac{t}{2}} \begin{bmatrix} Q_{11}^p & Q_{11}^p z & Q_{11}^p \mathbf{f}_s^T(z) & Q_{13}^p \hat{\mathbf{f}}_s^T(z) \\ Q_{11}^p z & Q_{11}^p z^2 & Q_{11}^p z \mathbf{f}_s^T(z) & Q_{13}^p z \hat{\mathbf{f}}_s^T(z) \\ Q_{11}^p \mathbf{f}_s(z) & Q_{11}^p z \mathbf{f}_s(z) & Q_{11}^p \mathbf{f}_s(z) \mathbf{f}_s^T(z) & Q_{13}^p \mathbf{f}_s(z) \hat{\mathbf{f}}_s^T(z) \\ Q_{13}^p \hat{\mathbf{f}}_s(z) & Q_{13}^p z \hat{\mathbf{f}}_s(z) & Q_{13}^p \hat{\mathbf{f}}_s(z) \mathbf{f}_s^T(z) & Q_{33}^p \hat{\mathbf{f}}_s(z) \hat{\mathbf{f}}_s^T(z) \end{bmatrix} dz \quad (3.62a)$$

$$\hat{\mathbf{K}}_\tau = \int_{-\frac{t}{2}}^{\frac{t}{2}} Q_{55}^p \begin{bmatrix} 1 & \hat{\mathbf{f}}_s^T(z) \\ \hat{\mathbf{f}}_s(z) & \hat{\mathbf{f}}_s(z) \hat{\mathbf{f}}_s^T(z) \end{bmatrix} dz \quad (3.62b)$$

The compliance matrices can be defined by inverting the stiffness matrices, $\check{\mathbf{K}}_\sigma = \hat{\mathbf{K}}_\sigma^{-1}$ and $\check{\mathbf{K}}_\tau = \hat{\mathbf{K}}_\tau^{-1}$, so that decomposing the compliance matrices in several components as seen in [95], compliance equations yield:

$$\begin{aligned} \begin{bmatrix} e_N(s) \\ e_M(s) \\ \mathbf{e}_s(s) \\ \mathbf{e}_z(s) \end{bmatrix} &= \check{\mathbf{K}}_\sigma \begin{bmatrix} N(s) \\ M(s) \\ \mathbf{M}_s(s) \\ \mathbf{M}_z(s) \end{bmatrix} \\ &= \begin{bmatrix} \check{A}_{NN} & \check{A}_{NM} & \check{\mathbf{a}}_{Ns}^T & \check{\mathbf{b}}_{Nz}^T \\ \check{A}_{NM} & \check{A}_{MM} & \check{\mathbf{a}}_{Ms}^T & \check{\mathbf{b}}_{Mz}^T \\ \check{\mathbf{a}}_{Ns} & \check{\mathbf{a}}_{Ms} & \check{A}_{ss} & \check{\mathbf{B}}_{sz} \\ \check{\mathbf{b}}_{Nz} & \check{\mathbf{b}}_{Mz} & \check{\mathbf{B}}_{sz}^T & \check{D}_{zz} \end{bmatrix} \begin{bmatrix} N(s) \\ M(s) \\ \mathbf{M}_s(s) \\ \mathbf{M}_z(s) \end{bmatrix}, \end{aligned} \quad (3.63a)$$

$$\begin{bmatrix} e_Q(s) \\ \mathbf{e}_\gamma(s) \end{bmatrix} = \check{\mathbf{K}}_\tau \begin{bmatrix} Q(s) \\ \mathbf{M}_\tau(s) \end{bmatrix} = \begin{bmatrix} \check{C}_{QQ} & \check{\mathbf{c}}_{Q\tau}^T \\ \check{\mathbf{c}}_{Q\tau} & \check{\mathbf{C}}_{\tau\tau} \end{bmatrix} \begin{bmatrix} Q(s) \\ \mathbf{M}_\tau(s) \end{bmatrix}. \quad (3.63b)$$

Solution procedure

The solution procedure is similar to the one developed in [95] but including the distributed loads. First, substituting (3.57) in (3.59) the transverse higher-order moments yield:

$$\begin{aligned} \mathbf{M}_z(s) &= \mathbf{H}_z^{-1} \left(\mathbf{H}_\gamma^{-1} \left(\frac{d^2 \mathbf{M}_s(s)}{ds^2} + \mathbf{f}_s \left(\frac{t}{2} \right) \frac{d\tau^+(s)}{ds} - \mathbf{f}_s \left(-\frac{t}{2} \right) \frac{d\tau^-(s)}{ds} \right) \right. \\ &\quad \left. + \hat{\mathbf{f}}_s \left(\frac{t}{2} \right) \sigma^+(s) - \hat{\mathbf{f}}_s \left(-\frac{t}{2} \right) \sigma^-(s) \right). \end{aligned} \quad (3.64)$$

Introducing (3.63b) into (3.48e) longitudinal higher-order displacements yield:

$$\mathbf{H}_\gamma^T \mathbf{u}(s) = \check{\mathbf{C}}_{\tau\tau} \mathbf{M}_\tau(s) + \check{\mathbf{c}}_{Q\tau} Q(s) - \frac{d\mathbf{w}(s)}{ds}, \quad (3.65)$$

Substituting (3.63a) into (3.48d) and (3.48f), using (3.65) to eliminate the derivative of the longitudinal displacement $\mathbf{u}(s)$, using (3.57) to eliminate the higher-order shear moments $\mathbf{M}_\tau(s)$, and using equation (3.53b) to eliminate the derivative of the shear force $Q(s)$, the following differential equation may be obtained (see [95] and [96] for more details):

$$\begin{aligned} \frac{d^2 \mathbf{x}(s)}{ds^2} = & \mathbf{G}\mathbf{x}(s) + \mathbf{g}_N N(s) + \mathbf{g}_M M(s) \\ & + \mathbf{g}_{\sigma^+} \sigma^+(s) + \mathbf{g}_{\sigma^-} \sigma^-(s) + \mathbf{g}_{\tau^+} \frac{d\tau^+(s)}{ds} + \mathbf{g}_{\tau^-} \frac{d\tau^-(s)}{ds}, \end{aligned} \quad (3.66a)$$

$$\mathbf{x}(s) = \begin{bmatrix} \mathbf{M}_s(s) \\ \mathbf{w}(s) \end{bmatrix}, \quad (3.66b)$$

where the auxiliary matrices appearing in the previous equation (\mathbf{G} , \mathbf{g}_N , \mathbf{g}_M, \dots) are given in Appendix A.1.

The resolution of the previous equation is divided in two parts: obtaining a particular solution and solving the homogeneous equation. Notice that the axial force, the bending moment and the distributed loads affect only to the particular solution, which constitutes the regularized solution of the problem. This regularized solution coincides with the CLT solution. The homogeneous equation let us to calculate the perturbations over the regularized values so that the continuity conditions of stresses and displacements at the joint are satisfied.

Constant distributed loads case

Considering the straight beam under constant distributed loads $\sigma^+(s) = \sigma_0^+$, $\sigma^-(s) = \sigma_0^-$, $\tau^+(s) = \tau_0^+$ and $\tau^-(s) = \tau_0^-$ as a particular case, using equilibrium equations (3.53) and (3.54) and using the boundary conditions (3.55), the axial force, shear force and bending moment yield:

$$N(s) = N_0 - (\tau_0^+ - \tau_0^-)s, \quad (3.67a)$$

$$Q(s) = Q_0 - (\sigma_0^+ - \sigma_0^-)s, \quad (3.67b)$$

$$M(s) = M_0 + \left(Q_0 - \frac{t}{2}(\tau_0^+ + \tau_0^-) \right) s - (\sigma_0^+ - \sigma_0^-) \frac{s^2}{2}. \quad (3.67c)$$

Therefore, substituting (3.67) in (3.66a) the particular/regularized solution yields:

$$\mathbf{x}_{reg}(s) = \mathbf{q}_N N(s) + \mathbf{q}_M M(s) + \mathbf{q}_{\sigma^+} \sigma_0^+ + \mathbf{q}_{\sigma^-} \sigma_0^-, \quad (3.68)$$

where auxiliary vectors \mathbf{q}_N , \mathbf{q}_M , \mathbf{q}_{σ^+} and \mathbf{q}_{σ^-} are defined by:

$$\mathbf{q}_N = -\mathbf{G}^{-1} \mathbf{g}_N, \quad \mathbf{q}_M = -\mathbf{G}^{-1} \mathbf{g}_M, \quad (3.69a)$$

$$\mathbf{q}_{\sigma^+} = \mathbf{G}^{-1}(\mathbf{G}^{-1} \mathbf{g}_M - \mathbf{g}_{\sigma^+}), \quad \mathbf{q}_{\sigma^-} = -\mathbf{G}^{-1}(\mathbf{G}^{-1} \mathbf{g}_M + \mathbf{g}_{\sigma^-}). \quad (3.69b)$$

The derivative of $\mathbf{x}_{reg}(s)$, substituting (3.53a) and (3.54), yields:

$$\frac{d\mathbf{x}_{reg}(s)}{ds} = \mathbf{q}_Q Q(s) + \mathbf{q}_{\tau^+} \tau_0^+ + \mathbf{q}_{\tau^-} \tau_0^-, \quad (3.70)$$

where the auxiliary vectors are given by:

$$\mathbf{q}_Q = \mathbf{q}_M, \quad \mathbf{q}_{\tau^+} = -\mathbf{q}_N - \mathbf{q}_M \frac{t}{2}, \quad \mathbf{q}_{\tau^-} = \mathbf{q}_N - \mathbf{q}_M \frac{t}{2}. \quad (3.71)$$

The resolution of the homogeneous equation is analysed in section 3.7.

If a not constant distributed loads is applied, a similar procedure may be developed for obtaining the solution of the homogeneous equation.

Stresses calculation

The stresses calculation is developed in detail in [95]. In summary, the stresses calculation in the MBM is similar than the calculation in the model of order 1 developed in section 3.2. Once the vector $\mathbf{x}(s)$, given in (3.66b), has been calculated, the axial higher order moments $\mathbf{M}_s(s)$ are directly obtained as the first $n - 1$ components of $\mathbf{x}(s)$. Shear higher-order moments and transverse higher-order moments may be obtained from the equilibrium equations (3.57) and (3.59), respectively. Strains may be obtained by using the compliance equations (3.63). Once strains are obtained, stresses can be calculated in each ply by using the 2D constitutive equations (3.60).

Notwithstanding, only axial stress calculated with the aforementioned procedure results accurate. Therefore, similarly than in the CBT, the other two stresses (the shear stress and the transverse stress) are obtained from the axial stress by using the equilibrium equations (3.51).

In that way, stresses can be written as:

$$\sigma_\theta^p(s, z) = \mathbf{S}_s^p(z)^T \check{\mathbf{K}}_\sigma \mathbf{M}_T(s), \quad (3.72a)$$

$$\tau_{sz}^p(s, z) = \tau_{sz}^p(s, z_p^-) - \mathbf{S}_{sz}^p(z)^T \check{\mathbf{K}}_\sigma \frac{d\mathbf{M}_T(s)}{ds}, \quad (3.72b)$$

$$\sigma_z^p(s, z) = \sigma_z^p(s, z_p^-) - \frac{d\tau_{sz}^p(s, z_p^-)}{ds} (z - z_p^-) + \mathbf{S}_{z,2}^p(z)^T \check{\mathbf{K}}_\sigma \frac{d^2\mathbf{M}_T(s)}{ds^2}, \quad (3.72c)$$

where $\mathbf{M}_T(s)$ is a vector containing the axial and transverse moments:

$$\mathbf{M}_T(s) = \begin{bmatrix} N(s) \\ M(s) \\ \mathbf{M}_s(s) \\ \mathbf{M}_z(s) \end{bmatrix}, \quad (3.73)$$

and the shape vectors $\mathbf{S}_s^p(z)$ (defined by its components $(\mathbf{S}_s^p)_i(z)$ for $i = 0, 1, \dots, 2n - 1$), $\mathbf{S}_{sz}^p(z)$ and $\mathbf{S}_{z,2}^p(z)$ are given by:

$$(\mathbf{S}_s^p)_i(z) = Q_{11}^p z^i, \quad i = 0, 1, \dots, n, \quad (3.74a)$$

$$(\mathbf{S}_s^p)_{i+n-1}(z) = Q_{13}^p z^{i-2}, \quad i = 2, 3, \dots, n, \quad (3.74b)$$

$$\mathbf{S}_{sz}^p(z) = \int_{z_p^-}^z \mathbf{S}_s^p(z') dz', \quad (3.74c)$$

$$\mathbf{S}_{z,2}^p(z) = \int_{z_p^-}^z \mathbf{S}_{sz}^p(z') dz'. \quad (3.74d)$$

Notice that the shear stress and the transverse stress are obtained by integration of the equilibrium equations, which implies that boundary conditions for these stresses are required. In the case of the shear stress, $\tau_{sz}^p(s, z_p^-)$ is required at the bottom of each ply p , which is obtained by the corresponding value at the top of the previous ply $\tau_{sz}^p(s, z_p^-) = \tau_{sz}^{p-1}(s, z_{p-1}^+)$, beginning with a boundary condition for the first ply of $\tau_{sz}^1(s, -t/2) = \tau^-(s)$. The boundary condition $\tau_{sz}^{N_p}(s, t/2) = \tau^+(s)$ is automatically accomplished.

The same case is given in the transverse stress, where the boundary condition is obtained from the previous ply $\sigma_z^p(s, z_p^-) = \sigma_z^{p-1}(s, z_{p-1}^+)$ beginning with a boundary condition $\sigma_z^1(s, -t/2) = \sigma^-(s)$. The boundary condition $\sigma_z^{N_p}(s, t/2) = \sigma^+(s)$ is automatically accomplished.

3.4.2 Development of the MBM for curved beams

A curved beam with thickness t (considered non-dimensional with value $t = 2$) and length $L_k = R_k \Theta_k$ (where R_k is the mean radius and Θ_k is the angular length of the beam) is studied (see Figure 3.7). A local non-dimensional coordinate system s_k and z_k is used, similarly to that used for the straight beam. Notice that the only difference between the clockwise and the counter-clockwise curved beam lies in the direction of the z_k axis.

The beam is loaded under distributed transverse and shear loads in the positive boundary of z_k , $\sigma^+(s_k)$ and $\tau^+(s_k)$, and under distributed transverse and shear loads in the negative boundary of z_k , $\sigma^-(s_k)$ and $\tau^-(s_k)$. Arbitrary stresses boundary conditions are applied in $s_k = 0$, given by $\sigma_s^0(z_k)$ and $\tau_s^0(z_k)$, and in $s_k = L_k$, given by $\sigma_s^L(z_k)$ and $\tau_s^L(z_k)$. These stresses must be in equilibrium.

For the sake of simplicity, the index k indicating the component is suppressed in this section.

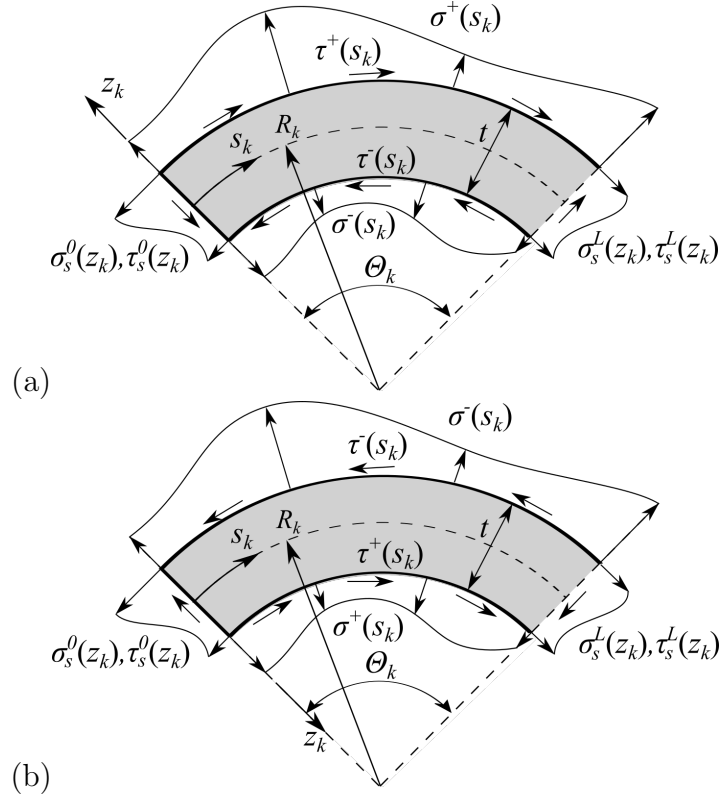


Figure 3.7: (a) Clockwise curved beam. (b) Counter-clockwise curved beam.

Displacements

The displacements approximation for this case is analogous to that made in the straight beam:

$$u_s(s, z) = u_o(s) + zu_1(s) + \mathbf{f}_s^T(z)\mathbf{u}(s), \quad (3.75a)$$

$$u_z(s, z) = w_1(s) + \mathbf{f}_z^T(z)\mathbf{w}(s), \quad (3.75b)$$

where vector $\mathbf{f}_s(z)$ contains the monomials with orders from 2 to n as given in (3.40c). Vector $\mathbf{f}_z(z)$ has to be obtained from the shear strain similarly as done in the straight beam model. The calculation of this vector can be found in [95], and its components $f_i^z(z)$, with $i = 2, 3, \dots, n$, are given by:

$$f_i^z(z) = z^{i-1} \pm \frac{i-1}{iR}z^i, \quad i = 2, 3, \dots, n. \quad (3.76)$$

When a symbol \pm or \mp is used in the present section, the upper symbol is used for the clockwise beam, and the lower symbol is used for the counter-clockwise beam.

Notice that the derivative of vector $\mathbf{f}_z(z)$ yields:

$$\frac{d\mathbf{f}_z(z)}{dz} = \frac{R \pm z}{R} \mathbf{H}_z \hat{\mathbf{f}}_s(z), \quad (3.77)$$

where matrix \mathbf{H}_z and vector $\hat{\mathbf{f}}_s(z)$ are the same than in the straight beam, given by equations (3.49).

Furthermore, according to (3.76), vector $\mathbf{f}_z(z)$ can be expressed depending on vector $\mathbf{f}_s(z)$ as follows:

$$\mathbf{f}_z(z) = \pm R (\mathbf{H}_s \mathbf{f}_s(z) + \mathbf{h}_M z), \quad (3.78)$$

where matrix \mathbf{H}_s is defined by its components H_{ij}^s , with $i, j = 2, 3, \dots, n$, and vector \mathbf{h}_M is defined by its components h_i^M , with $i = 2, 3, \dots, n$:

$$H_{ij}^s = \frac{(i-1)\delta_{ij}}{iR^2} \pm \frac{\delta_{(i-1)j}}{R}, \quad h_i^M = \pm \frac{\delta_{i2}}{R}. \quad (3.79)$$

Strains

Strains definitions in the local polar coordinate system are given by:

$$\varepsilon_s(s, z) = \frac{R}{R \pm z} \left(\frac{\partial u_s(s, z)}{\partial s} \pm \frac{u_z(s, z)}{R} \right), \quad (3.80a)$$

$$\gamma_{sz}(s, z) = \frac{R}{R \pm z} \left(\frac{R \pm z}{R} \frac{\partial u_s(s, z)}{\partial z} \mp \frac{u_s(s, z)}{R} + \frac{\partial u_z(s, z)}{\partial s} \right), \quad (3.80b)$$

$$\varepsilon_z(s, z) = \frac{\partial u_z(s, z)}{\partial z}. \quad (3.80c)$$

Substituting (3.75) in (3.80) and considering (3.77) and (3.78), strains can be written as:

$$\varepsilon_s(s, z) = \frac{R}{R \pm z} \left[e_N(s) + z e_M(s) + \mathbf{f}_s^T(z) \mathbf{e}_s(s) \right], \quad (3.81a)$$

$$\gamma_{sz}(s, z) = \frac{R}{R \pm z} \left[e_Q(s) + \mathbf{f}_z^T(z) \mathbf{e}_\gamma(s) \right], \quad (3.81b)$$

$$\varepsilon_z(s, z) = \frac{R \pm z}{R} \left[\hat{\mathbf{f}}_s^T(z) \mathbf{e}_z(s) \right], \quad (3.81c)$$

where $e_N(s)$, $e_M(s)$ and $e_Q(s)$ are the CBT 1D strain components, and $\mathbf{e}_s(s)$, $\mathbf{e}_\gamma(s)$ and $\mathbf{e}_z(s)$ are the higher-order 1D strain components, which are defined as:

$$e_N(s) = \frac{du_0(s)}{ds} \pm \frac{w_1(s)}{R}, \quad (3.82a)$$

$$e_M(s) = \frac{du_1(s)}{ds} + \mathbf{h}_M^T \mathbf{w}(s), \quad (3.82b)$$

$$e_Q(s) = u_1(s) \mp \frac{u_0(s)}{R} + \frac{dw_1(s)}{ds}, \quad (3.82c)$$

$$\mathbf{e}_s(s) = \frac{d\mathbf{u}(s)}{ds} + \mathbf{H}_s^T \mathbf{w}(s), \quad (3.82d)$$

$$\mathbf{e}_\gamma(s) = \frac{d\mathbf{w}(s)}{ds} + \mathbf{H}_\gamma^T \mathbf{u}(s), \quad (3.82e)$$

$$\mathbf{e}_z(s) = \mathbf{H}_z^T \mathbf{w}(s). \quad (3.82f)$$

Equilibrium

As in the straight beam case, the distributed loads appear only in the equilibrium equations, being the main difference with respect to the model developed in [95].

The 2D equilibrium equations expressed in the local polar coordinate system yield:

$$R \frac{\partial \sigma_s(s, z)}{\partial s} + \frac{1}{R \pm z} \frac{\partial}{\partial z} [(R \pm z)^2 \tau_{sz}(s, z)] = 0, \quad (3.83a)$$

$$\frac{\partial}{\partial z} [(R \pm z) \sigma_z(s, z)] + R \frac{\partial \tau_{sz}(s, z)}{\partial s} = \pm \sigma_s(s, z), \quad (3.83b)$$

The CBT forces and moment and the higher-order moments are defined, as in the straight beam, by equations (3.52). It is demonstrated in [95] that functions $\mathbf{f}_\tau(z)$ and $\mathbf{f}_\sigma(z)$ yield for the present case:

$$\mathbf{f}_\tau(z) = \mathbf{f}_z(z), \quad \mathbf{f}_\sigma(z) = \left(\frac{R \pm z}{R} \right)^2 \hat{\mathbf{f}}_s(z). \quad (3.84)$$

In that way, integrating the equilibrium equations (3.83) and also the first one of them multiplied by z , the CBT forces and moment equilibrium equations yield:

$$R \frac{dN(s)}{ds} \pm Q(s) + R^+ \tau^+(s) - R^- \tau^-(s) = 0, \quad (3.85a)$$

$$R \frac{dQ(s)}{ds} + R^+ \sigma^+(s) - R^- \sigma^-(s) = \pm N(s), \quad (3.85b)$$

$$\frac{dM(s)}{ds} + \frac{t}{2R} (R^+ \tau^+(s) + R^- \tau^-(s)) = Q(s). \quad (3.85c)$$

where R^+ is the radius in the positive boundary of z and R^- is the radius in the negative boundary of z , given by:

$$R^+ = R \pm \frac{t}{2}, \quad R^- = R \mp \frac{t}{2}. \quad (3.86)$$

The CBT forces, $N(s)$ and $Q(s)$, and moment, $M(s)$, are obtained directly by integrating equations (3.85) and introducing the boundary conditions given by equations (3.55).

Prescribed values of these CBT forces and moment in $s = L$ must be in equilibrium with the prescribed values in $s = 0$ and, therefore, boundary conditions in $s = L$ are automatically accomplished.

The higher-order moments equilibrium equation in direction s can be obtained by integrating equation (3.83a) multiplied by $\mathbf{f}_s(z)$, which yields:

$$\frac{d\mathbf{M}_s(s)}{ds} + \frac{R^+}{R} \mathbf{f}_s \left(\frac{t}{2} \right) \tau^+(s) - \frac{R^-}{R} \mathbf{f}_s \left(-\frac{t}{2} \right) \tau^-(s) = \mathbf{H}_\gamma \mathbf{M}_\tau(s). \quad (3.87)$$

Finally, the higher-order moments equilibrium equation in direction z can be obtained by integrating equation (3.83b) multiplied by $\mathbf{f}_z(z)$ and using properties (3.77) and (3.78), which yields:

$$\begin{aligned} \frac{d\mathbf{M}_\tau(s)}{ds} + \frac{R^+}{R} \mathbf{f}_z \left(\frac{t}{2} \right) \sigma^+(s) - \frac{R^-}{R} \mathbf{f}_z \left(-\frac{t}{2} \right) \sigma^-(s) \\ = \mathbf{H}_z \mathbf{M}_z(s) + \mathbf{H}_s \mathbf{M}_s(s) + \mathbf{h}_M M(s). \end{aligned} \quad (3.88)$$

Therefore, higher-order moments equilibrium is given by equations (3.87) and (3.88), which cannot be directly solved as in the case of the CBT forces and moment. The boundary conditions at both ends for these higher order moments may be obtained from the arbitrary boundary conditions, by integrating them according to the higher-order moments definition given in (3.52).

Constitutive law

As in the straight beam case, the 2D constitutive law for an individual ply is given by equations (3.60). Substituting in these equations the strains, given by (3.81), and integrating the equations in order to obtain the forces and moments (including the higher-order one), relations (3.61) are obtained. However, in this case the components of matrices $\hat{\mathbf{K}}_\sigma$ and $\hat{\mathbf{K}}_\tau$ are influenced by the curvature. Expressions of these matrices can be found in the Appendices of [95].

The compliance matrices can be defined by inverting the stiffness matrices, $\check{\mathbf{K}}_\sigma = \hat{\mathbf{K}}_\sigma^{-1}$ and $\check{\mathbf{K}}_\tau = \hat{\mathbf{K}}_\tau^{-1}$, so that decomposing the compliance matrices in several components as seen in [95], compliance equations yield (3.63).

Solution procedure

The solution procedure is analogous to the one developed in [95] but including the distributed loads. First, substituting (3.87) in (3.88) the transverse higher-order moments yield:

$$\begin{aligned} \mathbf{M}_z(s) = & \mathbf{H}_z^{-1} \left(\frac{R^+}{R} \mathbf{f}_z \left(\frac{t}{2} \right) \sigma^+(s) - \frac{R^-}{R} \mathbf{f}_z \left(-\frac{t}{2} \right) \sigma^-(s) \right. \\ & + \mathbf{H}_\gamma^{-1} \left(\frac{d^2 \mathbf{M}_s(s)}{ds^2} + \frac{R^+}{R} \mathbf{f}_s \left(\frac{t}{2} \right) \frac{d\tau^+(s)}{ds} - \frac{R^-}{R} \mathbf{f}_s \left(-\frac{t}{2} \right) \frac{d\tau^-(s)}{ds} \right) \\ & \left. - \mathbf{H}_s \mathbf{M}_s(s) - \mathbf{h}_M M(s) \right). \end{aligned} \quad (3.89)$$

Introducing (3.63b) into (3.82e) longitudinal higher-order displacements yield:

$$\mathbf{H}_\gamma^T \mathbf{u}(s) = \check{\mathbf{C}}_{\tau\tau} \mathbf{M}_\tau(s) + \check{\mathbf{c}}_{Q\tau} Q(s) - \frac{d\mathbf{w}(s)}{ds}, \quad (3.90)$$

Substituting (3.63a) into (3.82d) and (3.82f), using (3.90) to eliminate the derivative of the longitudinal displacement $\mathbf{u}(s)$, using (3.87) to eliminate the higher-order shear moments $\mathbf{M}_\tau(s)$, and using equation (3.85b) to eliminate the derivative of the shear force $Q(s)$, the following differential equation may be obtained (see [95] and [96] for more details):

$$\begin{aligned} \frac{d^2 \mathbf{x}(s)}{ds^2} = & \mathbf{G} \mathbf{x}(s) + \mathbf{g}_N N(s) + \mathbf{g}_M M(s) \\ & + \mathbf{g}_{\sigma^+} \sigma^+(s) + \mathbf{g}_{\sigma^-} \sigma^-(s) + \mathbf{g}_{\tau^+} \frac{d\tau^+(s)}{ds} + \mathbf{g}_{\tau^-} \frac{d\tau^-(s)}{ds}, \end{aligned} \quad (3.91)$$

where the matrices of the previous equation are given in Appendix A.2 and vector $\mathbf{x}(s)$ is defined in (3.66b).

The resolution of the previous equation is divided in two parts: obtaining a particular solution and solving the homogeneous equation. Notice that the axial force, the bending moment and the distributed loads affect only to the particular solution, which constitutes the regularized solution of the problem. This regularized solution converges to Ko & Jackson solution [4]

when the order increases. The homogeneous equation let us to calculate the perturbations over the regularized values so that the axial boundary conditions (the arbitrary boundary conditions) are satisfied.

Constant distributed loads case

Considering the curved beam loaded under constant distributed loads $\sigma^+(s) = \sigma_0^+$, $\sigma^-(s) = \sigma_0^-$, $\tau^+(s) = \tau_0^+$ and $\tau^-(s) = \tau_0^-$ as a particular case, using equilibrium equations (3.85) and using the boundary conditions (3.55), the axial force, shear force and bending moment can be written as:

$$N(s) = (N_0 \mp R^+ \sigma_0^+ \pm R^- \sigma_0^-) \cos \frac{s}{R} - (\pm Q_0 + R^+ \tau_0^+ - R^- \tau_0^-) \sin \frac{s}{R} \pm R^+ \sigma_0^+ \mp R^- \sigma_0^-, \quad (3.92a)$$

$$Q(s) = \pm(N_0 \mp R^+ \sigma_0^+ \pm R^- \sigma_0^-) \sin \frac{s}{R} \pm (\pm Q_0 + R^+ \tau_0^+ - R^- \tau_0^-) \cos \frac{s}{R} \mp R^+ \tau_0^+ \pm R^- \tau_0^-, \quad (3.92b)$$

$$M(s) = M_0 \pm R(N_0 \mp R^+ \sigma_0^+ \pm R^- \sigma_0^-) \left(1 - \cos \frac{s}{R}\right) \pm R(\pm Q_0 + R^+ \tau_0^+ - R^- \tau_0^-) \sin \frac{s}{R} \mp ((R^+)^2 \tau_0^+ - (R^-)^2 \tau_0^-) \frac{s}{R}. \quad (3.92c)$$

Therefore, substituting (3.92) in (3.91), the particular/regularized solution yields:

$$\mathbf{x}_{reg}(s) = \mathbf{q}_N N(s) + \mathbf{q}_M M(s) + \mathbf{q}_{\sigma^+} \sigma_0^+ + \mathbf{q}_{\sigma^-} \sigma_0^-, \quad (3.93)$$

where auxiliary vectors \mathbf{q}_N , \mathbf{q}_M , \mathbf{q}_{σ^+} and \mathbf{q}_{σ^-} are defined by:

$$\mathbf{q}_N = -(R^2 \mathbf{G} + \mathbf{I})^{-1} (R^2 \mathbf{g}_N \pm R \mathbf{G}^{-1} \mathbf{g}_M), \quad (3.94a)$$

$$\mathbf{q}_M = -\mathbf{G}^{-1} \mathbf{g}_M, \quad (3.94b)$$

$$\mathbf{q}_{\sigma^+} = -\mathbf{G}^{-1} \mathbf{g}_{\sigma^+} + (R^2 \mathbf{G} + \mathbf{I})^{-1} \mathbf{G}^{-1} (\mp \mathbf{g}_N + R \mathbf{g}_M) R^+, \quad (3.94c)$$

$$\mathbf{q}_{\sigma^-} = -\mathbf{G}^{-1} \mathbf{g}_{\sigma^-} + (R^2 \mathbf{G} + \mathbf{I})^{-1} \mathbf{G}^{-1} (\pm \mathbf{g}_N - R \mathbf{g}_M) R^-. \quad (3.94d)$$

The derivative of $\mathbf{x}_{reg}(s)$, substituting (3.85a) and (3.85c), yields:

$$\frac{d\mathbf{x}_{reg}(s)}{ds} = \mathbf{q}_Q Q(s) + \mathbf{q}_{\tau^+} \tau_0^+ + \mathbf{q}_{\tau^-} \tau_0^-, \quad (3.95)$$

where the auxiliary vectors are given by:

$$\mathbf{q}_Q = \mathbf{q}_M \mp \frac{\mathbf{q}_N}{R}, \quad (3.96a)$$

$$\mathbf{q}_{\tau^+} = \frac{R^+}{R} \left(-\mathbf{q}_N - \mathbf{q}_M \frac{t}{2} \right), \quad \mathbf{q}_{\tau^-} = \frac{R^-}{R} \left(\mathbf{q}_N - \mathbf{q}_M \frac{t}{2} \right). \quad (3.96b)$$

The resolution of the homogeneous equation is analysed in section 3.7.

If a non constant distributed loads is applied, a similar procedure may be developed for obtaining the solution of the homogeneous equation.

Stresses calculation

The stresses calculation is developed in detail in [95]. With a procedure analogous to the one employed in the straight beam case, once the vector $\mathbf{x}(s)$ given in (3.66b) has been calculated, the axial higher order moments $\mathbf{M}_s(s)$ are directly obtained as the first $n - 1$ components of $\mathbf{x}(s)$. Shear higher-order moments and transverse higher-order moments may be obtained from the equilibrium equations (3.87) and (3.88) respectively. Strains may be obtained by using the compliance equations (3.63). Once strains are obtained, circumferential stress can be calculated in each ply by using the 2D constitutive equations (3.60). Finally, the shear and through-thickness stresses are obtained by integration of the equilibrium equations (3.83). In that way, stresses can be written as:

$$\sigma_s^p(s, z) = \mathbf{S}_s^p(z)^T \check{\mathbf{K}}_\sigma \mathbf{M}_T(s), \quad (3.97a)$$

$$\tau_{sz}^p(s, z) = \tau_{sz}^p(s, z_p^-) \left(\frac{R \pm z_p^-}{R \pm z} \right)^2 - \mathbf{S}_{sz}^p(z)^T \check{\mathbf{K}}_\sigma \frac{d\mathbf{M}_T(s)}{ds}, \quad (3.97b)$$

$$\begin{aligned} \sigma_z^p(s, z) = & \frac{R \pm z_p^-}{R \pm z} \left(\sigma_z^p(s, z_p^-) \pm R \frac{d\tau_{sz}^p(s, z_p^-)}{ds} \left(\frac{R \pm z_p^-}{R \pm z} - 1 \right) \right) \\ & \pm \mathbf{S}_{z,1}^p(z)^T \check{\mathbf{K}}_\sigma \mathbf{M}_T(s) + \mathbf{S}_{z,2}^p(z)^T \check{\mathbf{K}}_\sigma \frac{d^2 \mathbf{M}_T(s)}{ds^2}, \end{aligned} \quad (3.97c)$$

where the vector $\mathbf{M}_T(s)$ is given in (3.73) and the shape vectors $\mathbf{S}_s^p(z)$ (given by its components $(\mathbf{S}_s^p)_i(z)$ for $i = 0, 1, \dots, 2n - 1$), $\mathbf{S}_{sz}^p(z)$, $\mathbf{S}_{z,1}^p(z)$ and $\mathbf{S}_{z,2}^p(z)$ are given by:

$$(\mathbf{S}_s^p)_i(z) = \frac{R}{R \pm z} Q_{11}^p z^i, \quad i = 0, 1, \dots, n, \quad (3.98a)$$

$$(\mathbf{S}_s^p)_{i+n-1}(z) = \frac{R \pm z}{R} Q_{13}^p z^{i-2}, \quad i = 2, 3, \dots, n, \quad (3.98b)$$

$$\mathbf{S}_{sz}^p(z) = \frac{R}{(R \pm z)^2} \int_{z_p^-}^z (R \pm z') \mathbf{S}_s^p(z') dz', \quad (3.98c)$$

$$\mathbf{S}_{z,1}^p(z) = \frac{1}{R \pm z} \int_{z_p^-}^z \mathbf{S}_s^p(z') dz', \quad (3.98d)$$

$$\mathbf{S}_{z,2}^p(z) = \frac{R}{R \pm z} \int_{z_p^-}^z \mathbf{S}_{sz}^p(z') dz'. \quad (3.98e)$$

Shear and through-thickness stresses have to be calculated iteratively as explained in the straight beam case, starting with the boundary conditions $\tau_{sz}^1(s, -t/2) = \tau^-(s)$ and $\sigma_z^1(s, -t/2) = \sigma^-(s)$. The boundary conditions $\tau_{sz}^{N_p}(s, t/2) = \tau^+(s)$ and $\sigma_z^{N_p}(s, t/2) = \sigma^+(s)$ are automatically accomplished.

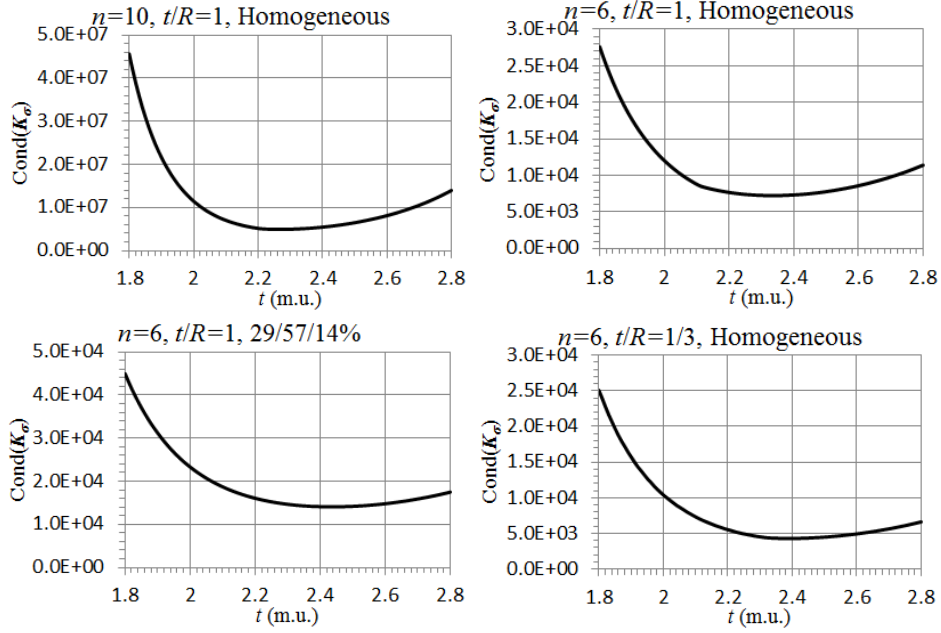
3.4.3 MBM numerical limitations

MBM let us to estimate the interlaminar and in-plane stresses in highly curved laminates obtaining very accurate results. Results are more accurate when using higher orders. However, the order of the model cannot indefinitely be increased in this model. The model order is limited in practice due to the need of inverting stiffness matrices $\hat{\mathbf{K}}_\sigma$ and $\hat{\mathbf{K}}_\tau$ to obtain the compliance matrices. Numerical inversion of the matrices is not accurate if the condition number of them is too high and when the model order is increased, the condition number of the matrix increases very fast, limiting the order to a maximum which depends on the thickness to mean radius ratio t/R and, in the dimensional case, on the thickness.

Considering the dimensional stiffness matrix $\hat{\mathbf{K}}_\sigma$ of a curved beam, the condition number has been evaluated for several thicknesses, stacking sequences and orders in a conventional CFRP, obtaining the condition numbers depending on the thickness depicted in Figure 3.8. Stiffness matrix $\hat{\mathbf{K}}_\tau$ have a similar thickness dependence of the condition number. However, it has not been depicted since matrix $\hat{\mathbf{K}}_\tau$ is smaller than $\hat{\mathbf{K}}_\sigma$, the condition number being lesser.

Notice that the condition number has an optimal value typically located in a thickness between 2 and 2.5. This is the reason why the problem has been adimensionalized with one half of the thickness, so that the non-dimensional thickness is $\bar{t} = 2$, trying to minimize the condition number in the thickness dependence.

Once the problem is expressed in a non-dimensional notation, the straight beam problem is limited (depending on the numerical software characteristics) by a maximum order of $n \sim 12$, while the curved beam limitation depends on the R/t ratio as seen in Table 3.1.

Figure 3.8: Condition number of $\hat{\mathbf{K}}_\sigma$ depending on the thickness.

R/t	0.55	0.6	0.8	1	1.2	1.5	2	3
n_{\max}	18	17	14	12	10	9	8	6
R/t	4	5	10	20	50	100	1000	...
n_{\max}	6	5	5	4	3	3	3	...

Table 3.1: Maximum order of the MBM depending on the R/t ratio.

3.5 Legendre polynomials based model (LPBM)

As shown previously, the condition number of the stiffness matrices $\hat{\mathbf{K}}_\sigma$ and $\hat{\mathbf{K}}_\tau$ in the MBM increases very fast when the order n increases and, as a consequence, the compliance matrices $\check{\mathbf{K}}_\sigma$ and $\check{\mathbf{K}}_\tau$ are obtained numerically with higher errors. This fact limits the order of the MBM to a maximum value in which errors in the calculation of the compliance matrix are not excessively high. The maximum order depends on the thickness to mean radius ratio t/R as shown in Table 3.1.

The increase of the condition number is due to the use of monomial functions in the series expansion. Monomial functions constitute a linearly independent base of functions in the domain of $z \in [-t/2, t/2]$ (or $\bar{z} \in [-1, 1]$)

for the non-dimensional case). However, this base is not an orthogonal base in this interval, this being the main cause of the high increase in the condition number of the stiffness matrices.

Hence, the solution to this limitation of the MBM is the use of orthogonal polynomials, $p_i(z)$, instead of monomials. The definition of the orthogonality in an interval $z \in [-t/2, t/2]$ establishes that the L^2 inner product of two different polynomials must be zero:

$$\int_{-t/2}^{t/2} p_i(z)p_j(z)dz = 0, \quad i \neq j. \quad (3.99)$$

Orthogonal polynomials have been widely studied by several authors [104, 105]. For the present case, the adequate polynomials are the Legendre polynomials, $p_i(\bar{z})$, which are orthogonal polynomials in $\bar{z} \in [-1, 1]$. Therefore, the model is being developed by using non-dimensional parameters.

Thereby, the LPBM is based on a series expansion of the non-dimensional displacements as follows:

$$\bar{u}_s(\bar{s}, \bar{z}) = \bar{u}_o(\bar{s}) + \bar{z}\bar{u}_1(\bar{s}) + \sum_{i=2}^n p_i(\bar{z})\bar{u}_i(\bar{s}), \quad (3.100a)$$

$$\bar{u}_z(\bar{s}, \bar{z}) = \bar{w}_1(\bar{s}) + \sum_{i=2}^n \bar{f}_i^z(\bar{z})\bar{w}_i(\bar{s}). \quad (3.100b)$$

where functions $\bar{f}_i^z(\bar{z})$ are determined by the number of terms in the series expansion of the shear strain, following a similar procedure to that used in the MBM.

For the sake of brevity, the bar indicating the non-dimensional parameters are not represented in the present section, since all the magnitudes used in the model are considered non-dimensional.

The theoretical basis of the LPBM are developed in [96]. The main features of the model are summarized in the present section.

3.5.1 Characteristics of the Legendre polynomials

Legendre polynomials, denoted $p_i(z)$ with $-1 \leq z \leq 1$, are defined by the Legendre's differential equation, which constitutes a Sturm–Liouville problem [106]:

$$\frac{d}{dz} \left[(1 - z^2) \frac{dp_i(z)}{dz} \right] + i(i + 1)p_i(z) = 0, \quad -1 < z < 1, \quad i = 0, 1, 2, \dots \quad (3.101)$$

These polynomials may be expressed as a summation of binomial expressions [107]. However, the easier way to obtain the polynomials consists in a three term recurrence relation, known as Bonnet's recursion formula, beginning with the known polynomials $p_0(z) = 1$ and $p_1(z) = z$:

$$p_i(z) = \frac{2i-1}{i} z p_{i-1}(z) - \frac{i-1}{i} p_{i-2}(z). \quad (3.102)$$

Legendre polynomials up to order 5 are depicted in Figure 3.9.

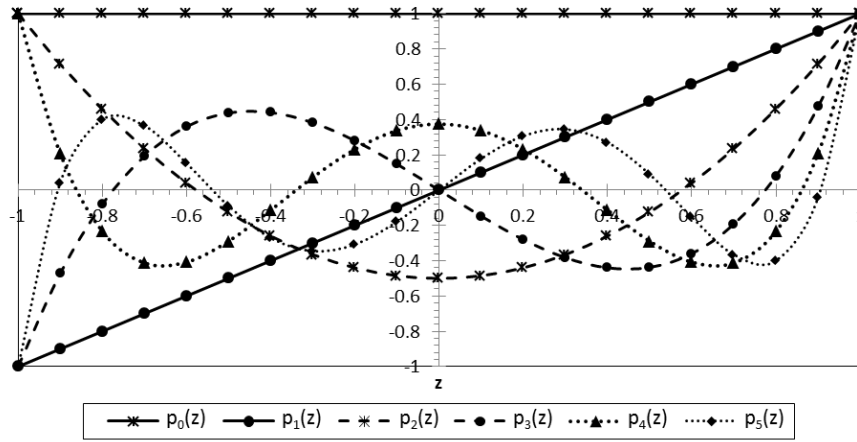


Figure 3.9: Legendre polynomials up to $i = 5$.

These polynomials, as commented previously, are orthogonal on the interval $-1 \leq z \leq 1$ with an unitary weighting function [104]:

$$\int_{-1}^1 p_i(z)p_j(z)dz = \frac{2}{2i+1}\delta_{ij}, \quad (3.103)$$

The integrals of the Legendre polynomials are calculated typically depending on the polynomials themselves by using the following expression:

$$(2i+1)p_i(z) = \frac{d}{dz} [p_{i+1}(z) - p_{i-1}(z)]. \quad (3.104)$$

The derivative of the polynomials are calculated by the next expression:

$$\frac{dp_i(z)}{dz} = (2(i-1)+1)p_{i-1}(z) + (2(i-3)+1)p_{i-3}(z) + (2(i-5)+1)p_{i-5}(z) + \dots \quad (3.105)$$

$$\mathbf{H}_z = \begin{bmatrix} 1 & 0 & 0 & 0 & 0 & \dots \\ 0 & 3 & 0 & 0 & 0 & \dots \\ 1 & 0 & 5 & 0 & 0 & \dots \\ 0 & 3 & 0 & 7 & 0 & \dots \\ 1 & 0 & 5 & 0 & 9 & \dots \\ \vdots & \vdots & \vdots & \vdots & \vdots & \ddots \end{bmatrix}. \quad (3.111b)$$

By using the property (3.102) the vectors of (3.107) are related by:

$$z\hat{\mathbf{f}}_s(z) = \mathbf{\Xi}_1 \mathbf{f}_s(z) + \mathbf{\Xi}_2 \hat{\mathbf{f}}_s(z), \quad (3.112)$$

where $\mathbf{\Xi}_1$ and $\mathbf{\Xi}_2$ are diagonal matrices defined as:

$$\Xi_{1,ij} = \frac{i}{2i-1} \delta_{ij}, \quad \Xi_{2,ij} = \frac{i-1}{2i-1} \delta_{ij}, \quad i, j = 2, 3, \dots, n. \quad (3.113)$$

3.5.2 Development of the LPBM for straight beams

A straight beam with thickness t (considered non-dimensional with value $t = 2$) and length L_k is studied (see Figure 3.6), in the same way as in the MBM. A local non-dimensional coordinate system s_k and z_k is used as defined previously.

The beam is loaded under distributed transverse and shear loads in the positive boundary of z_k , $\sigma^+(s_k)$ and $\tau^+(s_k)$, and under distributed transverse and shear loads in the negative boundary of z_k , $\sigma^-(s_k)$ and $\tau^-(s_k)$. Arbitrary stresses boundary conditions are applied at $s_k = 0$, given by $\sigma_s^0(z_k)$ and $\tau_s^0(z_k)$, and at $s_k = L_k$, given by $\sigma_s^L(z_k)$ and $\tau_s^L(z_k)$.

For the sake of simplicity, the index k indicating the component is suppressed in this section.

Displacements

The longitudinal and through-thickness displacements approximation of the straight beam is given by equations (3.100), where the axial displacements have been approximated by a series expansion by using Legendre polynomials. Introducing the matrix notation as in the MBM, the non-dimensional displacements can be written as:

$$u_s(s, z) = u_o(s) + zu_1(s) + \mathbf{f}_s^T(z) \mathbf{u}(s), \quad (3.114a)$$

$$u_z(s, z) = w_1(s) + \mathbf{f}_z^T(z) \mathbf{w}(s), \quad (3.114b)$$

where $\mathbf{f}_s(z)$ is given in equation (3.107a) and it can be demonstrated, following the same procedure employed in the straight beam case of the MBM, that $\mathbf{f}_z(z) = \hat{\mathbf{f}}_s(z)$, given in equation (3.107b).

Strains

By using the strain-displacement relations in Cartesian coordinates (3.42) and the Legendre polynomials properties (3.110), strains can be written as:

$$\varepsilon_s(s, z) = e_N(s) + ze_M(s) + \mathbf{f}_s^T(z)\mathbf{e}_s(s), \quad (3.115a)$$

$$\gamma_{sz}(s, z) = e_Q(s) + \hat{\mathbf{f}}_s^T(z)\mathbf{e}_\gamma(s), \quad (3.115b)$$

$$\varepsilon_z(s, z) = \hat{\mathbf{f}}_s^T(z)\mathbf{e}_z(s), \quad (3.115c)$$

where $e_N(s)$, $e_M(s)$ and $e_Q(s)$ are the non-dimensional CBT 1D strain components, and $\mathbf{e}_s(s)$, $\mathbf{e}_\gamma(s)$ and $\mathbf{e}_z(s)$ are the non-dimensional higher-order 1D strain components, which are defined by:

$$e_N(s) = \frac{du_0(s)}{ds}, \quad (3.116a)$$

$$e_M(s) = \frac{du_1(s)}{ds}, \quad (3.116b)$$

$$e_Q(s) = u_1(s) + \frac{dw_1(s)}{ds} + \mathbf{h}_Q^T \mathbf{u}(s), \quad (3.116c)$$

$$\mathbf{e}_s(s) = \frac{d\mathbf{u}(s)}{ds}, \quad (3.116d)$$

$$\mathbf{e}_\gamma(s) = \frac{d\mathbf{w}(s)}{ds} + \mathbf{H}_\gamma^T \mathbf{u}(s), \quad (3.116e)$$

$$\mathbf{e}_z(s) = \mathbf{H}_z^T \mathbf{w}(s), \quad (3.116f)$$

where for the present case of a straight beam $\mathbf{h}_Q = \boldsymbol{\rho}$. Notice that expressions (3.115) are the same than in the MBM but considering different matrices \mathbf{H}_γ and \mathbf{H}_z and considering a null vector $\boldsymbol{\rho}$ in the MBM case.

Equilibrium

The non-dimensional higher-order moments in the LPBM are defined as follows:

$$N(s) = \int_{-1}^1 \sigma_s(s, z) dz, \quad M(s) = \int_{-1}^1 \sigma_s(s, z) z dz, \quad (3.117a)$$

$$Q(s) = \int_{-1}^1 \tau_{sz}(s, z) dz, \quad (3.117b)$$

$$\mathbf{M}_s(s) = \int_{-1}^1 \sigma_s(s, z) \mathbf{f}_s(z) dz, \quad (3.117c)$$

$$\mathbf{M}_\tau(s) = \int_{-1}^1 \tau_{sz}(s, z) \mathbf{f}_\tau(z) dz, \quad (3.117d)$$

$$\mathbf{M}_z(s) = \int_{-1}^1 \sigma_z(s, z) \mathbf{f}_\sigma(z) dz. \quad (3.117e)$$

where it can be demonstrated with a similar procedure to that employed in the MBM that $\mathbf{f}_\tau(z) = \hat{\mathbf{f}}_s(z)$ and $\mathbf{f}_\sigma(z) = \hat{\mathbf{f}}_s(z)$.

Therefore, integrating the equilibrium equations (3.51), the forces and bending moment equilibrium equations yield as given in (3.53) and (3.54) considering the non-dimensional thickness $t = 2$, those equations being independent of the kind of model. The higher-order moments equilibrium equations yield:

$$\frac{d\mathbf{M}_s(s)}{ds} + \mathbf{f}_s(1) \tau^+(s) - \mathbf{f}_s(-1) \tau^-(s) = \mathbf{H}_\gamma \mathbf{M}_\tau(s) + \mathbf{h}_Q Q(s), \quad (3.118a)$$

$$\frac{d\mathbf{M}_\tau(s)}{ds} + \hat{\mathbf{f}}_s(1) \sigma^+(s) - \hat{\mathbf{f}}_s(-1) \sigma^-(s) = \mathbf{H}_z \mathbf{M}_z(s). \quad (3.118b)$$

Constitutive law

As in the straight beam case of the MBM, the 2D constitutive law for an individual ply is given by equations (3.60). Substituting in these equations the strains, given by (3.115), and integrating the equations in order to obtain the forces and moments (including the higher-order ones), relations (3.61) are obtained. However, in this case matrices $\hat{\mathbf{K}}_\sigma$ and $\hat{\mathbf{K}}_\tau$ are given by equations (3.62) using the functions $\mathbf{f}_s(z)$, $\hat{\mathbf{f}}_s(z)$ and $\hat{\mathbf{f}}_s(z)$ corresponding to the LPBM. Some integrals of these functions are solved in the Appendices of [96].

The compliance matrices can be defined by inverting the stiffness matrices, $\check{\mathbf{K}}_\sigma = \hat{\mathbf{K}}_\sigma^{-1}$ and $\check{\mathbf{K}}_\tau = \hat{\mathbf{K}}_\tau^{-1}$, so that decomposing the compliance matrices in several components as seen in [96], compliance equations yield (3.63).

Solution procedure

The solution procedure is similar to the one developed in the MBM. Introducing (3.63b) into (3.116e), longitudinal higher-order displacements yield:

$$\mathbf{H}_\gamma^T \mathbf{u}(s) = \check{\mathbf{C}}_{\tau\tau} \mathbf{M}_\tau(s) + \check{\mathbf{c}}_{Q\tau} Q(s) - \frac{d\mathbf{w}(s)}{ds}, \quad (3.119)$$

Substituting (3.63a) into (3.116d) and (3.116f), using (3.119) to eliminate the derivative of the longitudinal displacement $\mathbf{u}(s)$, using (3.118a) to eliminate the higher-order shear moments $\mathbf{M}_\tau(s)$, and using equation (3.53b) to eliminate the derivative of the shear force $Q(s)$, the following differential equation may be obtained (see [96] for more details):

$$\begin{aligned} \frac{d^2 \mathbf{x}(s)}{ds^2} = & \mathbf{G} \mathbf{x}(s) + \mathbf{g}_N N(s) + \mathbf{g}_M M(s) \\ & + \mathbf{g}_{\sigma^+} \sigma^+(s) + \mathbf{g}_{\sigma^-} \sigma^-(s) + \mathbf{g}_{\tau^+} \frac{d\tau^+(s)}{ds} + \mathbf{g}_{\tau^-} \frac{d\tau^-(s)}{ds}, \end{aligned} \quad (3.120)$$

where the auxiliary matrices employed in the previous equation are given in Appendix A.3 and vector $\mathbf{x}(s)$ is defined in (3.66b).

If a non constant distributed loads is applied, a similar procedure may be developed for obtaining the solution of the homogeneous equation.

Constant distributed loads case

Considering the straight beam loaded under constant distributed loads $\sigma^+(s) = \sigma_0^+$, $\sigma^-(s) = \sigma_0^-$, $\tau^+(s) = \tau_0^+$ and $\tau^-(s) = \tau_0^-$ as a particular case, using equilibrium equations (3.53) and (3.54) and using the boundary conditions (3.55), the axial force, shear force and bending moment yield (3.67).

Therefore, as the forces and the bending moment are the same as in the straight beam of the MBM, and the differential equation (3.120) is the same as in the MBM, using appropriate values of the auxiliary matrices (\mathbf{H}_γ , \mathbf{H}_z, \dots), the solution of this problem is the same than in the MBM, given by equations (3.68)-(3.71).

The resolution of the homogeneous equation is analysed in section 3.7.

Stresses calculation

With an analogous development to that carried out in the straight beam case of the MBM, once the vector $\mathbf{x}(s)$ given in (3.66b) has been calculated,

the axial higher order moments $\mathbf{M}_s(s)$ are directly obtained as the first $n-1$ components of $\mathbf{x}(s)$. Shear higher-order moments and transverse higher-order moments may be obtained from the equilibrium equations (3.118a) and (3.118b) respectively. Strains may be obtained by using the compliance equations (3.63). Once strains are obtained, circumferential stress can be calculated in each ply by using the 2D constitutive equations (3.60). Finally, the shear and through-thickness stresses are obtained by integration of the equilibrium equations (3.51). In that way, stresses yield:

$$\sigma_\theta^p(s, z) = \mathbf{S}_s^p(z)^T \check{\mathbf{K}}_\sigma \mathbf{M}_T(s), \quad (3.121a)$$

$$\tau_{sz}^p(s, z) = \tau_{sz}^p(s, z_p^-) - \mathbf{S}_{sz}^p(z)^T \check{\mathbf{K}}_\sigma \frac{d\mathbf{M}_T(s)}{ds}, \quad (3.121b)$$

$$\sigma_z^p(s, z) = \sigma_z^p(s, z_p^-) - \frac{d\tau_{sz}^p(s, z_p^-)}{ds} (z - z_p^-) + \mathbf{S}_{z,2}^p(z)^T \check{\mathbf{K}}_\sigma \frac{d^2\mathbf{M}_T(s)}{ds^2}, \quad (3.121c)$$

where the vector $\mathbf{M}_T(s)$ is given in (3.73) and the shape vectors $\mathbf{S}_s^p(z)$ (given by its components $(\mathbf{S}_s^p)_i(z)$ for $i = 0, 1, \dots, 2n-1$), $\mathbf{S}_{sz}^p(z)$ and $\mathbf{S}_{z,2}^p(z)$ are given by:

$$(\mathbf{S}_s^p)_i(z) = Q_{11}^p p_i(z), \quad i = 0, 1, \dots, n, \quad (3.122a)$$

$$(\mathbf{S}_s^p)_{i+n-1}(z) = Q_{13}^p p_{i-2}(z), \quad i = 2, 3, \dots, n, \quad (3.122b)$$

$$\mathbf{S}_{sz}^p(z) = \int_{z_p^-}^z \mathbf{S}_s^p(z') dz', \quad (3.122c)$$

$$\mathbf{S}_{z,2}^p(z) = \int_{z_p^-}^z \mathbf{S}_{sz}^p(z') dz'. \quad (3.122d)$$

Shear and through-thickness stresses have to be calculated iteratively as explained in the MBM, beginning with the boundary conditions $\tau_{sz}^1(s, -1) = \tau^-(s)$ and $\sigma_z^1(s, -1) = \sigma^-(s)$. The boundary conditions $\tau_{sz}^{N_p}(s, 1) = \tau^+(s)$ and $\sigma_z^{N_p}(s, 1) = \sigma^+(s)$ are automatically accomplished.

3.5.3 Development of the LPBM for curved beams

A curved beam with thickness t (considered non-dimensional with value $t = 2$) and length $L_k = R_k \Theta_k$ (where R_k is the mean radius and Θ_k is the angular length of the beam) is studied (see Figure 3.7). A local non-dimensional coordinate system s_k and z_k is used, defined as in the MBM. Notice that the difference of the clockwise and the counter-clockwise curved beam lies in the direction of the z_k axis.

The beam is loaded under distributed transverse and shear loads in the positive boundary of z_k , $\sigma^+(s_k)$ and $\tau^+(s_k)$, and under distributed transverse and shear loads in the negative boundary of z_k , $\sigma^-(s_k)$ and $\tau^-(s_k)$. Arbitrary stresses boundary conditions are applied at $s_k = 0$, given by $\sigma_s^0(z_k)$ and $\tau_s^0(z_k)$, and at $s_k = L_k$, given by $\sigma_s^L(z_k)$ and $\tau_s^L(z_k)$.

For the sake of simplicity, the index k indicating the component is not used in the model development.

The model development for a curved beam in the LPBM is detailed in [96]. Consequently, only the main equations of the model are shown below.

Displacements

The displacements in matrix notation are expressed by a series expansion according to equations (3.114). In the LPBM for a curved beam, functions $\mathbf{f}_z(z)$ yield:

$$\mathbf{f}_z(z) = \hat{\mathbf{f}}_s(z) \pm \frac{1}{R} \left(\Xi_2 \mathbf{f}_s(z) + \Xi_1 \hat{\mathbf{f}}_s(z) \right), \quad (3.123)$$

which accomplish property (3.77) and can be expressed also as follows:

$$\mathbf{f}_z(z) = \pm R (\mathbf{H}_s \mathbf{f}_s(z) + \mathbf{h}_M z + \mathbf{h}_N), \quad (3.124)$$

where matrix \mathbf{H}_s and vectors \mathbf{h}_N and \mathbf{h}_M are given by:

$$\mathbf{H}_s = \pm \frac{1}{R} \Upsilon + \frac{1}{R^2} (\Xi_2 + \Xi_1 \Upsilon \Upsilon), \quad (3.125a)$$

$$\mathbf{h}_M = \pm \frac{1}{R} \mathbf{v} + \frac{1}{R^2} \Xi_1 \Upsilon \mathbf{v}, \quad (3.125b)$$

$$\mathbf{h}_N = \frac{1}{R^2} \Xi_1 \mathbf{v}. \quad (3.125c)$$

Strains

Strains are given by:

$$\varepsilon_s(s, z) = \frac{R}{R \pm z} (e_N(s) + z e_M(s) + \mathbf{f}_s(z)^T \mathbf{e}_s(s)), \quad (3.126a)$$

$$\gamma_{sz}(s, z) = \frac{R}{R \pm z} (e_Q(s) + \mathbf{f}_z(z)^T \mathbf{e}_\gamma(s)), \quad (3.126b)$$

$$\varepsilon_z(s, z) = \frac{R \pm z}{R} \hat{\mathbf{f}}_s(z)^T \mathbf{e}_z(s), \quad (3.126c)$$

the components of the strains being defined as:

$$e_N(s) = \frac{du_0(s)}{ds} \pm \frac{w_1(s)}{R} + \mathbf{h}_N^T \mathbf{w}(s), \quad (3.127a)$$

$$e_M(s) = \frac{du_1(s)}{ds} + \mathbf{h}_M^T \mathbf{w}(s), \quad (3.127b)$$

$$e_Q(s) = u_1(s) \mp \frac{u_0(s)}{R} + \frac{dw_1(s)}{ds} + \mathbf{h}_Q^T \mathbf{u}(s), \quad (3.127c)$$

$$\mathbf{e}_s(s) = \frac{d\mathbf{u}(s)}{ds} + \mathbf{H}_s^T \mathbf{w}(s), \quad (3.127d)$$

$$\mathbf{e}_\gamma(s) = \frac{d\mathbf{w}(s)}{ds} + \mathbf{H}_\gamma^T \mathbf{u}(s), \quad (3.127e)$$

$$\mathbf{e}_z(s) = \mathbf{H}_z^T \mathbf{w}(s), \quad (3.127f)$$

where auxiliary vector \mathbf{h}_Q is given by:

$$\mathbf{h}_Q = \rho \mp \frac{1}{R} \mathbf{H}_\gamma \mathbf{\Xi}_2 \mathbf{v}. \quad (3.128)$$

Equilibrium

The forces, bending moment and higher-order moments are defined, as in the straight beam, by equations (3.117), by using functions $\mathbf{f}_\tau(z)$ and $\mathbf{f}_\sigma(z)$ given by equations (3.84) with the corresponding functions $\mathbf{f}_z(z)$ and $\hat{\mathbf{f}}_s(z)$ to the LPBM.

The equilibrium equations for the forces and the bending moment remain the same than in the MBM, given by (3.85) with a non-dimensional thickness of $t = 2$. The equilibrium equations for the higher-order moments yield:

$$\frac{d\mathbf{M}_s(s)}{ds} + \frac{R^+}{R} \tau^+(s) \mathbf{f}_s(1) - \frac{R^-}{R} \tau^-(s) \mathbf{f}_s(-1) = \mathbf{H}_\gamma \mathbf{M}_\tau(s) + \mathbf{h}_Q Q(s), \quad (3.129a)$$

$$\begin{aligned} \frac{d\mathbf{M}_\tau(s)}{ds} + \frac{R^+}{R} \sigma^+(s) \mathbf{f}_z(1) - \frac{R^-}{R} \sigma^-(s) \mathbf{f}_z(-1) \\ = \mathbf{H}_z \mathbf{M}_z(s) + \mathbf{H}_s \mathbf{M}_s(s) + \mathbf{h}_M M(s) + \mathbf{h}_N N(s). \end{aligned} \quad (3.129b)$$

Constitutive law

As in the straight beam case of the MBM, the 2D constitutive law for an individual ply is given by equations (3.60). Substituting in those equations

the strains, given by (3.115), and integrating the equations in order to obtain the forces and moments (including the higher-order ones), relations (3.61) are obtained. However, in this case components of matrices $\hat{\mathbf{K}}_\sigma$ and $\hat{\mathbf{K}}_\tau$ are different to those of the straight beam case due to the influence of the curvature. Expressions of these matrices can be found in [96].

The compliance matrices can be defined by inverting the stiffness matrices, $\check{\mathbf{K}}_\sigma = \hat{\mathbf{K}}_\sigma^{-1}$ and $\check{\mathbf{K}}_\tau = \hat{\mathbf{K}}_\tau^{-1}$, so that decomposing the compliance matrices in several components as seen in [96], compliance equations yield (3.63).

Solution procedure

Introducing (3.63b) into (3.127e) longitudinal higher-order displacements yield:

$$\mathbf{H}_\gamma^T \mathbf{u}(s) = \check{\mathbf{C}}_{\tau\tau} \mathbf{M}_\tau(s) + \check{\mathbf{c}}_{Q\tau} Q(s) - \frac{d\mathbf{w}(s)}{ds}, \quad (3.130)$$

Substituting (3.63a) into (3.127d) and (3.127f), using (3.130) to eliminate the derivative of the longitudinal displacement $\mathbf{u}(s)$, using (3.129a) to eliminate the higher-order shear moments $\mathbf{M}_\tau(s)$, and using equation (3.85b) to eliminate the derivative of the shear force $Q(s)$, the following differential equation is obtained:

$$\begin{aligned} \frac{d^2 \mathbf{x}(s)}{ds^2} = & \mathbf{G} \mathbf{x}(s) + \mathbf{g}_N N(s) + \mathbf{g}_M M(s) \\ & + \mathbf{g}_{\sigma^+} \sigma^+(s) + \mathbf{g}_{\sigma^-} \sigma^-(s) + \mathbf{g}_{\tau^+} \frac{d\tau^+(s)}{ds} + \mathbf{g}_{\tau^-} \frac{d\tau^-(s)}{ds}, \end{aligned} \quad (3.131)$$

where the matrices of the previous equation are given in Appendix A.4 and vector $\mathbf{x}(s)$ is defined in (3.66b).

Constant distributed loads case

Considering the curved beam loaded under constant distributed loads $\sigma^+(s) = \sigma_0^+$, $\sigma^-(s) = \sigma_0^-$, $\tau^+(s) = \tau_0^+$ and $\tau^-(s) = \tau_0^-$ as a particular case, using equilibrium equations (3.85) and using the boundary conditions (3.55), the axial force, shear force and bending moment yield (3.92).

Therefore, as the forces and the bending moment are the same than in the curved beam of the MBM, and the differential equation (3.131) is analogous to that in the MBM, the solution of this problem can be written as in the MBM, given by equations (3.93)-(3.96), but using the appropriate values of the auxiliary matrices (\mathbf{H}_γ , \mathbf{H}_z, \dots).

The resolution of the homogeneous equation is analysed in section 3.7.

If a not constant distributed loads is applied, a similar procedure may be developed for obtaining the solution of the homogeneous equation.

Stresses calculation

Stresses are obtained from the higher-order moments as follows:

$$\sigma_s^p(s, z) = \mathbf{S}_s^p(z)^T \check{\mathbf{K}}_\sigma \mathbf{M}_T(s), \quad (3.132a)$$

$$\tau_{sz}^p(s, z) = \tau_{sz}^p(s, z_p^-) \left(\frac{R \pm z_p^-}{R \pm z} \right)^2 - \mathbf{S}_{sz}^p(z)^T \check{\mathbf{K}}_\sigma \frac{d\mathbf{M}_T(s)}{ds}, \quad (3.132b)$$

$$\begin{aligned} \sigma_z^p(s, z) = & \frac{R \pm z_p^-}{R \pm z} \left(\sigma_z^p(s, z_p^-) \pm R \frac{d\tau_{sz}^p(s, z_p^-)}{ds} \left(\frac{R \pm z_p^-}{R \pm z} - 1 \right) \right) \\ & \pm \mathbf{S}_{z,1}^p(z)^T \check{\mathbf{K}}_\sigma \mathbf{M}_T(s) + \mathbf{S}_{z,2}^p(z)^T \check{\mathbf{K}}_\sigma \frac{d^2 \mathbf{M}_T(s)}{ds^2}, \end{aligned} \quad (3.132c)$$

where the vector $\mathbf{M}_T(s)$ is given in (3.73) and the shape vectors $\mathbf{S}_s^p(z)$ (given by its components $(\mathbf{S}_s^p)_i(z)$ for $i = 0, 1, \dots, 2n - 1$), $\mathbf{S}_{sz}^p(z)$, $\mathbf{S}_{z,1}^p(z)$ and $\mathbf{S}_{z,2}^p(z)$ are given by:

$$(\mathbf{S}_s^p)_i(z) = \frac{R}{R \pm z} Q_{11}^p p_i(z), \quad i = 0, 1, \dots, n, \quad (3.133a)$$

$$(\mathbf{S}_s^p)_{i+n-1}(z) = \frac{R \pm z}{R} Q_{13}^p p_{i-2}(z), \quad i = 2, 3, \dots, n, \quad (3.133b)$$

$$\mathbf{S}_{sz}^p(z) = \frac{R}{(R \pm z)^2} \int_{z_p^-}^z (R \pm z') \mathbf{S}_s^p(z') dz', \quad (3.133c)$$

$$\mathbf{S}_{z,1}^p(z) = \frac{1}{R \pm z} \int_{z_p^-}^z \mathbf{S}_s^p(z') dz', \quad (3.133d)$$

$$\mathbf{S}_{z,2}^p(z) = \frac{R}{R \pm z} \int_{z_p^-}^z \mathbf{S}_{sz}^p(z') dz'. \quad (3.133e)$$

Shear and through-thickness stresses have to be calculated iteratively as explained in the MBM, beginning with the boundary conditions $\tau_{sz}^1(s, -1) = \tau^-(s)$ and $\sigma_z^1(s, -1) = \sigma^-(s)$. The boundary conditions $\tau_{sz}^{N_p}(s, 1) = \tau^+(s)$ and $\sigma_z^{N_p}(s, 1) = \sigma^+(s)$ are automatically accomplished.

3.6 Resolution of the regularized problem by using the non-regularized models

Both non-regularized models, MBM and LPBM, have been developed following the same procedure. Therefore, both models are reduced to a set of differential equations that can be written in the same manner, using different constant vectors and matrices. In this way, e.g., the regularized values of vector $\mathbf{x}(s)$, defined in (3.66b), for constant distributed loads case are given by equation (3.68) for the straight beam in both MBM and LPBM, and (3.93) for the curved beam in both MBM and LPBM. If another kind of distributed load is given the particular solution have to be obtained in a similar way.

As described previously, once the regularized solution $\mathbf{x}_{reg}(s)$ has been obtained, regularized higher order moments, displacements, strains and stresses can be also obtained. In the present section, results of the aforementioned regularized solutions are compared for several orders with the regularized solution given by Ko & Jackson [4] in the case of null distributed loads, showing the convergence of the models when the order increases. Further comparisons may be found in [95, 108, 109]. The problem with constant distributed loads cannot be solved with Ko & Jackson's solution, then, it will be compared with finite elements solutions (for the non-regularized case) in a following section.

Both models, MBM and LPBM, are developed by a polynomial series expansion until an order n , and consequently, both models have almost the same accuracy for the same order, except when the MBM is used with any order above its limitation, given in Table 3.1. However, as it will be shown later, LPBM requires higher computational times, therefore for low orders (under the limit seen in Table 3.1) it is preferable to use the MBM and for higher orders it is preferable to use the LPBM. Hence, the results presented in this and the following sections are valid for both models while the order is under the limit shown in Table 3.1, and only for the LPBM for higher orders.

The model is applied to a L section forming 90° between the straight arms with a radius to thickness ratio of $R/t = 1.5$ at the corner. The material selected is a conventional UD-CFRP with a ply thickness of 0.2 mm and the ply properties summarized in Table 3.2. The stacking sequence chosen is a quasi-isotropic lay-up of 16 plies, defined by $[45,0,-45,90]_{2S}$.

The regularized solution depends only on the forces, bending moment and distributed loads. In the present section, stresses due to the forces and the bending moment will be analysed and compared with Ko & Jackson's

E_{11}	150 GPa	E_{22}	10 GPa	E_{33}	10 GPa
ν_{12}	0.3	ν_{13}	0.3	ν_{23}	0.3
G_{12}	6 GPa	G_{13}	6 GPa	G_{23}	3.85 GPa

Table 3.2: Ply properties for the numerical examples

solution. First, stresses due to an unitary bending moment, $M_0 = 1$ N, are depicted in Figure 3.10 by applying the non-regularized model for $n = 1, 2, 4$ and 8.

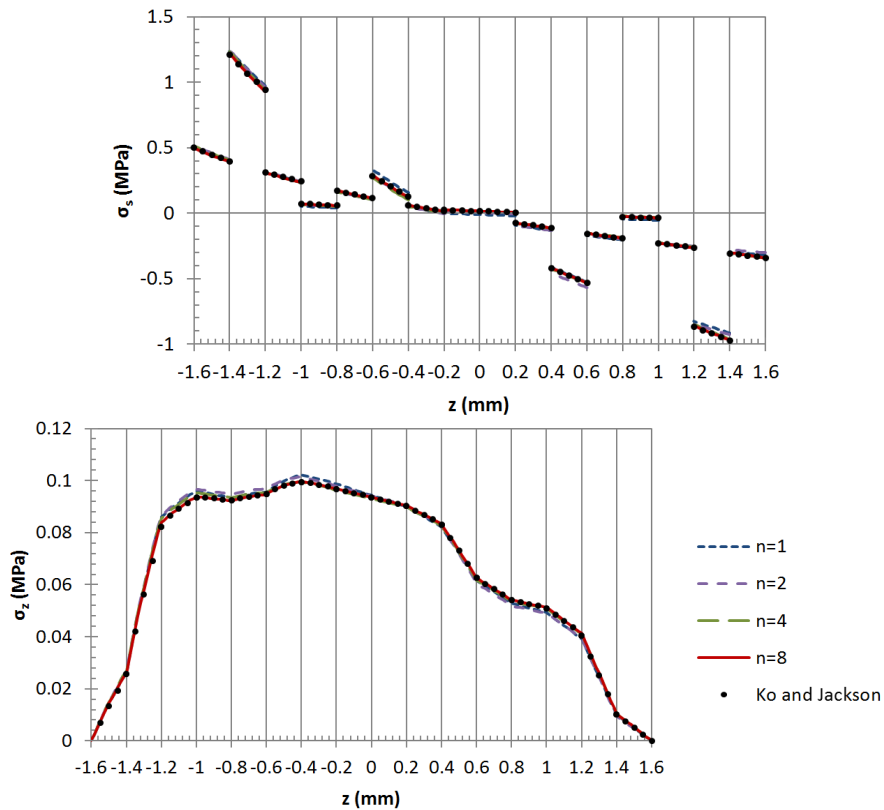


Figure 3.10: Regularized solution of the non-regularized models for the bending moment loading.

Notice that the shear stresses due to the bending moment are null, and they have not been depicted in Figure 3.10. Results of the model are very accurate for the regularized stresses due to the bending moment even for low orders, showing a fast convergence towards Ko and Jackson's solution.

Stresses due to an unitary axial force, $N_0 = 1$ N/mm, are depicted in Figure 3.11 by applying the non-regularized model for $n = 1, 3, 6$ and 12.

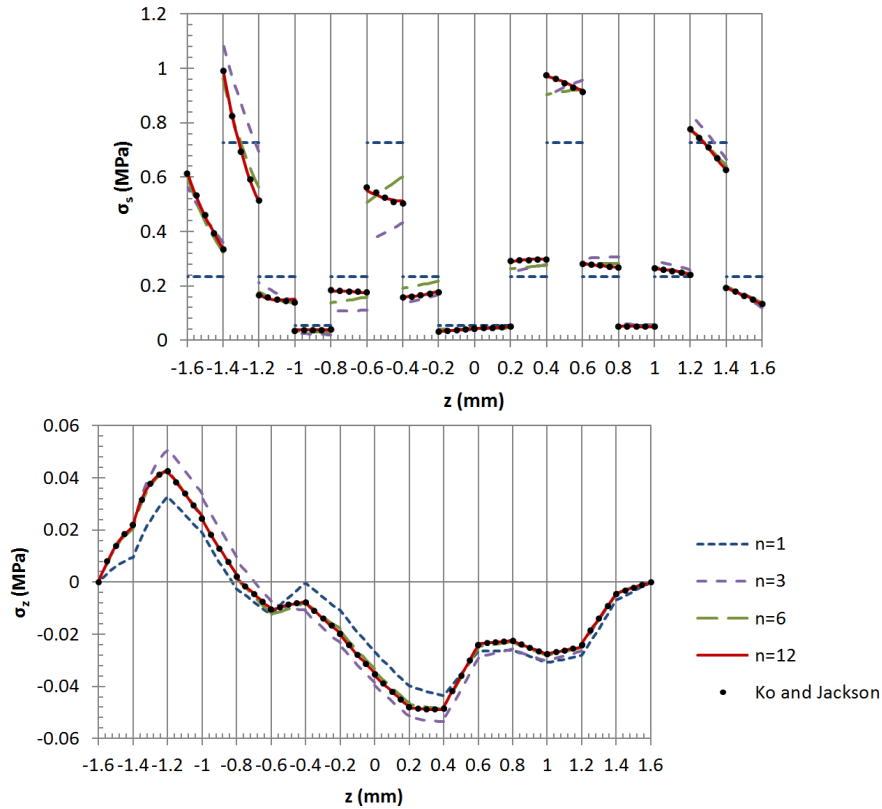


Figure 3.11: Regularized solution of the non-regularized models for the axial force loading.

Higher orders have been chosen for this case due to a lower convergence speed. Notice that the shear stresses due to the axial force are null, and they have not been depicted in Figure 3.11. For a given model order, stresses due to the axial force have the highest errors respect to the Ko & Jackson's solution, and a slower convergence. However, very accurate results may be obtained by using the maximum order of the MBM for the selected R/t ratio. Therefore, the maximum order of the MBM yields an accurate estimation of the regularized stresses, LPBM not being necessary in this case.

Stresses due to an unitary shear force, $Q_0 = 1$ N/mm, are depicted in Figure 3.12 by applying the non-regularized model for $n = 1, 2, 4$ and 8 . Notice that the axial and transverse stresses due to the axial force are null, and they have not been depicted in Figure 3.12. Errors of the shear stress due to the shear force are slightly higher than in the normal and through-the-thickness stresses due to the bending moment. However, results are still very accurate even using very low orders, presenting a very fast convergence

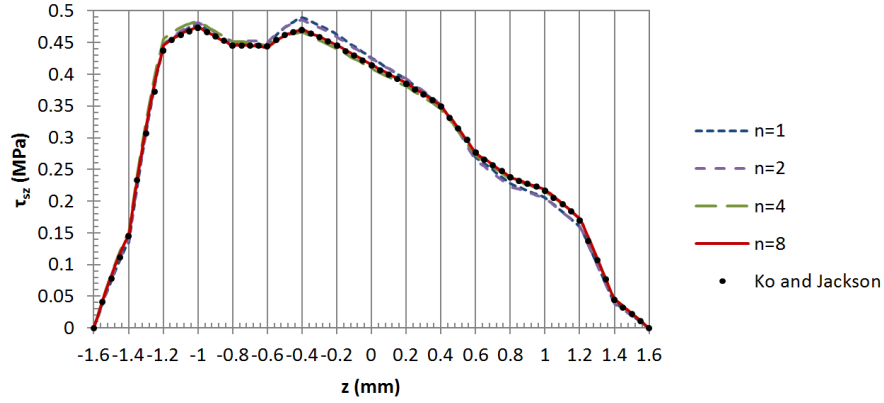


Figure 3.12: Regularized solution of the non-regularized models for the shear force loading.

towards Ko and Jackson's solution.

3.7 Resolution of the homogeneous problem

Non-regularized stresses and strains are determined by the superposition of the regularized values, analysed in the previous section, and the perturbations, calculated from the homogeneous equation. The homogeneous equation is determined by separating the solution vector, $\mathbf{x}(s)$, into its regularized value, $\mathbf{x}_{reg}(s)$, and the perturbations, $\hat{\mathbf{x}}(s)$, using $\mathbf{x}(s) = \mathbf{x}_{reg}(s) + \hat{\mathbf{x}}(s)$, yielding:

$$\frac{d^2 \hat{\mathbf{x}}(s)}{ds^2} = \mathbf{G} \hat{\mathbf{x}}(s). \quad (3.134)$$

The finite beam problem is defined by a (straight or curved) beam with non-dimensional length L , so that s varies from 0 to L . Boundary conditions in the through-the-thickness direction are given by the distributed loads, which are included in the regularized value. Equation 3.134 needs $4n - 4$ boundary conditions in the axial direction, while the number of components of vector $\hat{\mathbf{x}}(s)$ is $2n - 2$. These boundary conditions are determined by $2n - 2$ boundary conditions at $s = 0$ and $2n - 2$ boundary conditions at $s = L$. The boundary conditions in each end are expressed in displacements, in stresses or by a combination of both. Therefore, boundary conditions may be expressed with the pairs $(\mathbf{M}_s, \mathbf{M}_\tau)$, (\mathbf{u}, \mathbf{w}) , $(\mathbf{M}_s, \mathbf{w})$ or $(\mathbf{u}, \mathbf{M}_\tau)$ evaluated at $s = 0$ and $s = L$. When a joint between different components is given, an arbitrary stresses boundary condition is applied in the joint, so the pair

$(\mathbf{M}_s, \mathbf{M}_\tau)$ is used and it must be determined by imposing continuity of stresses and displacements at the joint between both components.

As seen in [95], matrix \mathbf{G} is decomposed in the eigenvalues matrix $\mathbf{\Lambda}$ and the eigenvectors matrix $\mathbf{\Phi}$, according to $\mathbf{G}\mathbf{\Phi} = \mathbf{\Phi}\mathbf{\Lambda}$, where $\mathbf{\Lambda}$ is a diagonal matrix with the eigenvalues λ_i ($i = 1, 2, \dots, 2n - 2$) in the diagonal, and $\mathbf{\Phi}$ is composed in its columns by the eigenvectors ϕ_i ($i = 1, 2, \dots, 2n - 2$). Notice that the eigenvalues and the components of the eigenvectors are, generally, complex numbers.

Equation 3.134 is solved using a change of variable of the form $\hat{\mathbf{x}}(s) = \mathbf{\Phi}\hat{\mathbf{y}}(s)$, so that the equation can be written as:

$$\frac{d^2\hat{\mathbf{y}}(s)}{ds^2} = \mathbf{\Lambda}\hat{\mathbf{y}}(s). \quad (3.135)$$

The solution of equation 3.135 is given by the following expression:

$$\hat{\mathbf{y}}(s) = \mathbf{Y}_0(s)\mathbf{c}_0 + \mathbf{Y}_L(s)\mathbf{c}_L, \quad (3.136)$$

where \mathbf{c}_0 and \mathbf{c}_L are vectors of constants to be determined by the boundary conditions and $\mathbf{Y}_0(s)$ and $\mathbf{Y}_L(s)$ are diagonal matrices, whose components are respectively $Y_{ij}^0(s)$ and $Y_{ij}^L(s)$, with $i, j = 1, \dots, 2n - 2$:

$$Y_{ij}^0(s) = \frac{\sinh\left((L-s)\sqrt{\lambda_i}\right)}{\sinh\left(L\sqrt{\lambda_i}\right)}\delta_{ij}, \quad Y_{ij}^L(s) = \frac{\sinh\left(s\sqrt{\lambda_i}\right)}{\sinh\left(L\sqrt{\lambda_i}\right)}\delta_{ij}. \quad (3.137)$$

Therefore, reverting the change of variable, vector $\hat{\mathbf{x}}(s)$ yields:

$$\hat{\mathbf{x}}(s) = \begin{bmatrix} \mathbf{X}_0(s) & \mathbf{X}_L(s) \end{bmatrix} \begin{bmatrix} \mathbf{c}_0 \\ \mathbf{c}_L \end{bmatrix}, \quad (3.138)$$

where matrices $\mathbf{X}_0(s)$ and $\mathbf{X}_L(s)$ are given by:

$$\mathbf{X}_0(s) = \mathbf{\Phi}\mathbf{Y}_0(s), \quad \mathbf{X}_L(s) = \mathbf{\Phi}\mathbf{Y}_L(s). \quad (3.139)$$

Matrix $\mathbf{X}_0(s)$ can be divided in the first $n - 1$ rows $\mathbf{X}_{s0}(s)$ and the last $n - 1$ rows $\mathbf{X}_{z0}(s)$. Similarly, matrix $\mathbf{X}_L(s)$ can be divided in the first $n - 1$ rows $\mathbf{X}_{sL}(s)$ and the last $n - 1$ rows $\mathbf{X}_{zL}(s)$. Considering this decomposition, circumferential higher-order moments and transverse displacements may be obtained by using the definition of vector $\hat{\mathbf{x}}(s)$ for the perturbation problem, yielding:

$$\begin{bmatrix} \hat{\mathbf{M}}_s(s) \\ \hat{\mathbf{w}}(s) \end{bmatrix} = \begin{bmatrix} \mathbf{X}_{s0}(s) & \mathbf{X}_{sL}(s) \\ \mathbf{X}_{z0}(s) & \mathbf{X}_{zL}(s) \end{bmatrix} \begin{bmatrix} \mathbf{c}_0 \\ \mathbf{c}_L \end{bmatrix}. \quad (3.140)$$

Shear higher-order moments may be also expressed depending on the unknowns \mathbf{c}_0 and \mathbf{c}_L by using equation (3.57) in the straight beams with the MBM, (3.118a) in the straight beams with the LPBM, (3.87) in the curved beams with the MBM or (3.129a) in the curved beams with the LPBM. Circumferential displacements are obtained by using equation (3.65). If those equations have to be used in the perturbations problem they have to be considered with null forces and bending moment and null distributed loads.

Therefore, any of the four pairs of boundary conditions $(\mathbf{M}_s, \mathbf{M}_\tau)$, (\mathbf{u}, \mathbf{w}) , $(\mathbf{M}_s, \mathbf{w})$ or $(\mathbf{u}, \mathbf{M}_\tau)$ may be applied at each end of the finite beam, obtaining the unknowns \mathbf{c}_0 and \mathbf{c}_L depending on those boundary conditions.

If a component of the problem under consideration is very long, stresses and strains are regularized in the central part of the component, so one end does not affect to the other end, being both non-regularized effects independent and separable. Therefore, when analysing the component from one side it can be considered as being semi-infinite, which consists in considering that stresses and strains tend to their regularized value in the semi-infinite direction, suppressing the unknowns associated to one end.

In this case, the solution of equation 3.135 is given by the following expression:

$$\hat{\mathbf{y}}(s) = \mathbf{Y}_0(s) \mathbf{c}_0, \quad (3.141)$$

where $\mathbf{Y}_0(s)$ is defined by its components $Y_{ij}^0(s)$, with $i, j = 1, \dots, 2n - 2$:

$$Y_{ij}^0(s) = \exp\left(\mp s \sqrt{\lambda_i}\right) \delta_{ij}, \quad (3.142)$$

with the \mp sign being positive if the beam is infinite in the negative s direction and viceversa.

Therefore, reverting the change of variable, vector $\hat{\mathbf{x}}(s)$ yields:

$$\hat{\mathbf{x}}(s) = \mathbf{X}_0(s) \mathbf{c}_0, \quad \mathbf{X}_0(s) = \Phi \mathbf{Y}_0(s). \quad (3.143)$$

In the present case, boundary conditions are applied at the unique existing end, obtaining the unknowns given in \mathbf{c}_0 .

3.8 Resolution of the joints between components

The beam section studied is supposed composed by N_c components included in the three kinds previously studied. If all the components are finite

beams, $(4n - 4)N_c$ unknown constants included in the vectors \mathbf{c}_0^k and \mathbf{c}_L^k ($k = 1, 2, \dots, N_c$) have to be determined by using the boundary conditions, where \mathbf{c}_0^k and \mathbf{c}_L^k are vectors \mathbf{c}_0 and \mathbf{c}_L , respectively, in the component k . If one or both end beams in the chain are approximated by semi-infinite, this or these beams have only $2n - 2$ unknown constants included in only one vector \mathbf{c}_0^k .

Boundary conditions at the ends of the chain are determined. They can be displacements or stresses boundary conditions (constituting $2n - 2$ equations as will be commented later) or they can be a semi-infinite approximation.

As stated in the previous section, boundary conditions at the joints of components are calculated by supposing an arbitrary stress boundary condition with the given axial and shear force and bending moment. This is equivalent to consider arbitrary values of $\mathbf{M}_s(s)$ and $\mathbf{M}_\tau(s)$ in the s coordinate. These arbitrary values are determined by imposing the continuity of the displacements and the stresses at the joint between both beams.

Therefore, in each component k the unknown constants are the arbitrary values of $\mathbf{M}_s(s)$ and $\mathbf{M}_\tau(s)$ at both ends: $\mathbf{M}_s^k(0)$, $\mathbf{M}_s^k(L)$, $\mathbf{M}_\tau^k(0)$ and $\mathbf{M}_\tau^k(L)$ or, in fact, the perturbations of them since the regularized values are known. By using equation (3.140) and equation (3.118a), which is common for all the components types:

$$\begin{bmatrix} \mathbf{c}_0^k \\ \mathbf{c}_L^k \end{bmatrix} = \begin{bmatrix} \mathbf{X}_{s0}^k(0) & \mathbf{X}_{sL}^k(0) \\ \mathbf{H}_\gamma^{-1} \frac{d\mathbf{X}_{s0}^k}{ds}(0) & \mathbf{H}_\gamma^{-1} \frac{d\mathbf{X}_{sL}^k}{ds}(0) \\ \mathbf{X}_{s0}^k(L) & \mathbf{X}_{sL}^k(L) \\ \mathbf{H}_\gamma^{-1} \frac{d\mathbf{X}_{s0}^k}{ds}(L) & \mathbf{H}_\gamma^{-1} \frac{d\mathbf{X}_{sL}^k}{ds}(L) \end{bmatrix}^{-1} \begin{bmatrix} \hat{\mathbf{M}}_s^k(0) \\ \hat{\mathbf{M}}_\tau^k(0) \\ \hat{\mathbf{M}}_s^k(L) \\ \hat{\mathbf{M}}_\tau^k(L) \end{bmatrix} = \begin{bmatrix} \Gamma_0^k \\ \Gamma_L^k \end{bmatrix} \begin{bmatrix} \hat{\mathbf{M}}_s^k(0) \\ \hat{\mathbf{M}}_\tau^k(0) \\ \hat{\mathbf{M}}_s^k(L) \\ \hat{\mathbf{M}}_\tau^k(L) \end{bmatrix}. \quad (3.144)$$

Notice that the distributed loads and the shear force are null in the perturbation problem as they are included only in the regularized problem.

For the semi-infinite beam, equation (3.144) can be written as follows:

$$\mathbf{c}_0^k = \begin{bmatrix} \mathbf{X}_{s0}^k(0) & \mathbf{X}_{sL}^k(0) \\ \mathbf{H}_\gamma^{-1} \frac{d\mathbf{X}_{s0}^k}{ds}(0) & \mathbf{H}_\gamma^{-1} \frac{d\mathbf{X}_{sL}^k}{ds}(0) \end{bmatrix}^{-1} \begin{bmatrix} \hat{\mathbf{M}}_s^k(0) \\ \hat{\mathbf{M}}_\tau^k(0) \end{bmatrix} = \Gamma_0^k \begin{bmatrix} \hat{\mathbf{M}}_s^k(0) \\ \hat{\mathbf{M}}_\tau^k(0) \end{bmatrix}. \quad (3.145)$$

3.8.1 Continuity of the circumferential stresses between components

The continuity of circumferential stresses between components k and $k - 1$ is imposed by equalling the higher-order moments:

$$\mathbf{M}_s^{k-1}(L) = \mathbf{M}_s^k(0). \quad (3.146)$$

Notice that the continuity is imposed using the non-regularized values, which includes the regularized values, which are known, and the perturbations, which depend on the unknowns \mathbf{c}_0^k and \mathbf{c}_L^k according to (3.144).

3.8.2 Continuity of the shear stresses between components

Continuity of the shear stresses in the joint between two adjacent beams they cannot be imposed term by term, since the definitions of these parameters depend on the mean radius and, therefore, shear higher-order moments are differently defined in beams with different curvature or direction (clockwise or counter-clockwise). Therefore, a change-of-basis matrix is required to impose the continuity in the shear stresses. It is recommended to change the basis for the curved beams and to express them in the basis of the straight beam. Therefore, if a joint between two curved beams is given, higher-order moments in both beams are expressed according to the straight beam and equalled, and if a joint between a curved beam and a straight one is given only the higher-order moments in the curved beam requires to change the basis and are equalled to those of the straight beam.

The definitions of the shear higher-order moments in the straight beam, $\bar{\mathbf{M}}_\tau(s)$, and for a curved beam of non-dimensional mean radius R , $\mathbf{M}_\tau(s)$, are given by:

$$\bar{Q}(s) = \int_{-1}^1 \tau_{sz}(s, z) dz, \quad \bar{\mathbf{M}}_\tau(s) = \int_{-1}^1 \hat{\mathbf{f}}_s(z) \tau_{sz}(s, z) dz, \quad (3.147a)$$

$$Q(s) = \int_{-1}^1 \tau_{sz}(s, z) dz, \quad \mathbf{M}_\tau(s) = \int_{-1}^1 \mathbf{f}_z(z) \tau_{sz}(s, z) dz. \quad (3.147b)$$

Notice that $\mathbf{f}_z(z)$ (which depends on the mean radius R) tends to $\hat{\mathbf{f}}_s(z)$ when $R \rightarrow \infty$. A change-of-basis matrix between the two definitions of shear moments is the same than a change-of-basis matrix between both functions $\mathbf{f}_z(z)$ and $\hat{\mathbf{f}}_s(z)$:

$$\begin{aligned} \begin{bmatrix} Q(s) \\ \mathbf{M}_\tau(s) \end{bmatrix} &\simeq \mathbf{K}_M \begin{bmatrix} \bar{Q}(s) \\ \bar{\mathbf{M}}_\tau(s) \end{bmatrix} = \begin{bmatrix} 1 & \mathbf{o}^T \\ \hat{\mathbf{k}}_o & \hat{\mathbf{K}}_M \end{bmatrix} \begin{bmatrix} \bar{Q}(s) \\ \bar{\mathbf{M}}_\tau(s) \end{bmatrix} \\ &\longrightarrow \begin{bmatrix} 1 \\ \mathbf{f}_z(z) \end{bmatrix} \simeq \mathbf{K}_M \begin{bmatrix} 1 \\ \hat{\mathbf{f}}_s(z) \end{bmatrix}. \end{aligned} \quad (3.148)$$

The matrix \mathbf{K}_M is calculated by using least squares in both sides of equation (3.148):

$$\frac{\partial}{\partial \mathbf{K}_M} \left(\int_{-1}^1 \left(\begin{bmatrix} 1 \\ \mathbf{f}_z(z) \end{bmatrix} - \mathbf{K}_M \begin{bmatrix} 1 \\ \hat{\mathbf{f}}_s(z) \end{bmatrix} \right)^2 dz \right) = 0, \quad (3.149)$$

where the derivative yields:

$$2 \int_{-1}^1 \left(\begin{bmatrix} 1 \\ \mathbf{f}_z(z) \end{bmatrix} - \mathbf{K}_M \begin{bmatrix} 1 \\ \hat{\mathbf{f}}_s(z) \end{bmatrix} \right) [1 \quad \hat{\mathbf{f}}_s(z)^T] dz = 0. \quad (3.150)$$

Considering that \mathbf{K}_M does not depend on z , it can be expressed as follows:

$$\mathbf{K}_M = \mathbf{B}_M \mathbf{A}_M^{-1}, \quad (3.151a)$$

$$\mathbf{A}_M = \int_{-1}^1 \begin{bmatrix} 1 \\ \hat{\mathbf{f}}_s(z) \end{bmatrix} [1 \quad \hat{\mathbf{f}}_s(z)] dz, \quad (3.151b)$$

$$\mathbf{B}_M = \int_{-1}^1 \begin{bmatrix} 1 \\ \mathbf{f}_z(z) \end{bmatrix} [1 \quad \hat{\mathbf{f}}_s(z)] dz. \quad (3.151c)$$

Therefore, continuity of shear stresses is imposed in a weak sense equalling the higher-order moments expressed in the common basis:

$$\bar{\mathbf{M}}_\tau^{k-1}(L) = \bar{\mathbf{M}}_\tau^k(0). \quad (3.152)$$

where $\bar{\mathbf{M}}_\tau^{k-1}(L)$ and $\bar{\mathbf{M}}_\tau^k(0)$ are obtained using (3.148).

3.8.3 Continuity of the circumferential displacements between components

To impose continuity, circumferential higher-order displacement vector have to be equalled between both components: $\mathbf{u}^{k-1}(L) = \mathbf{u}^k(0)$. Using equation (3.65) the equality can be written as:

$$\begin{aligned} -\frac{d\mathbf{w}^{k-1}}{ds}(L) + \check{\mathbf{C}}_{\tau\tau}^{k-1} \mathbf{M}_\tau^{k-1}(L) + \check{\mathbf{c}}_{Q\tau}^{k-1} Q^{k-1}(L) \\ = -\frac{d\mathbf{w}^k}{ds}(0) + \check{\mathbf{C}}_{\tau\tau}^k \mathbf{M}_\tau^k(0) + \check{\mathbf{c}}_{Q\tau}^k Q^k(0). \end{aligned} \quad (3.153)$$

Notice that matrices \mathbf{H}_γ do not depend on the typology of the component, so it has been cancelled at both sides of the previous equation.

Considering, for the sake of simplicity, the constant distributed loads case, the derivative of $\mathbf{w}(s)$ can be expressed depending on $\mathbf{M}_\tau(s)$ and $\mathbf{M}_s(s)$ by using the derivative of equation (3.140), equation (3.144), equation (3.95) and considering that the non-regularized value is the regularized value plus the perturbation, what results in:

$$\begin{aligned} \frac{d\mathbf{w}^k(s_k)}{ds} = & \begin{bmatrix} \frac{d\mathbf{X}_{z0}^k(s_k)}{ds} & \frac{d\mathbf{X}_{zL}^k(s_k)}{ds} \end{bmatrix} \begin{bmatrix} \Gamma_0^k \\ \Gamma_L^k \end{bmatrix} \left(\begin{bmatrix} \mathbf{M}_s^k(0) \\ \mathbf{M}_\tau^k(0) \\ \mathbf{M}_s^k(L) \\ \mathbf{M}_\tau^k(L) \end{bmatrix} - \begin{bmatrix} \mathbf{M}_{s,reg}^k(0) \\ \mathbf{M}_{\tau,reg}^k(0) \\ \mathbf{M}_{s,reg}^k(L) \\ \mathbf{M}_{\tau,reg}^k(L) \end{bmatrix} \right) \\ & + \mathbf{q}_{zQ}^k Q^k(s_k) + \mathbf{q}_{z\tau+}^k \tau_{0+}^k(s_k) + \mathbf{q}_{z\tau-}^k \tau_{0-}^k(s_k), \end{aligned} \quad (3.154)$$

where \mathbf{q}_{zQ}^k , $\mathbf{q}_{z\tau+}^k$ and $\mathbf{q}_{z\tau-}^k$ are respectively the last $n-1$ components of vectors \mathbf{q}_Q , $\mathbf{q}_{\tau+}$ and $\mathbf{q}_{\tau-}$ in the component k .

Considering equations (3.129a), (3.93) and (3.95), vectors $\mathbf{M}_{s,reg}^k(s_k)$ and $\mathbf{M}_{\tau,reg}^k(s_k)$ can be written as:

$$\begin{bmatrix} \mathbf{M}_{s,reg}^k(s_k) \\ \mathbf{M}_{\tau,reg}^k(s_k) \end{bmatrix} = \mathbf{K}_F \begin{bmatrix} N^k(s_k) \\ M^k(s_k) \\ Q^k(s_k) \end{bmatrix} + \mathbf{K}_\sigma \begin{bmatrix} \sigma_{0+}^k \\ \sigma_{0-}^k \\ \tau_{0+}^k \\ \tau_{0-}^k \end{bmatrix}, \quad (3.155a)$$

$$\mathbf{K}_F = \begin{bmatrix} \mathbf{q}_{sN}^k & \mathbf{q}_{sM}^k & \mathbf{o} \\ \mathbf{o} & \mathbf{o} & \mathbf{H}_\gamma^{-1}(\mathbf{q}_{sQ}^k - \mathbf{h}_Q^k) \end{bmatrix}, \quad (3.155b)$$

$$\mathbf{K}_\sigma = \begin{bmatrix} \mathbf{q}_{s\sigma+}^k & \mathbf{q}_{s\sigma-}^k & \mathbf{o} \\ \mathbf{o} & \mathbf{o} & \mathbf{H}_\gamma^{-1}(\mathbf{q}_{s\tau+}^k + \frac{R^+}{R} \mathbf{f}_s(1)) \quad \mathbf{H}_\gamma^{-1}(\mathbf{q}_{s\tau-}^k - \frac{R^-}{R} \mathbf{f}_s(-1)) \end{bmatrix}, \quad (3.155c)$$

where the constants σ_{0+}^k , σ_{0-}^k , τ_{0+}^k and τ_{0-}^k are the constant distributed loads σ_0^+ , σ_0^- , τ_0^+ and τ_0^- respectively in the component k .

Substituting (3.154), (3.155a) and (3.148) in (3.153) the continuity condition of the circumferential displacements is obtained:

$$\begin{aligned}
& \mathbf{K}_{sL}^{k-1} \begin{bmatrix} \bar{M}_s^{k-1}(0) \\ \bar{M}_\tau^{k-1}(0) \\ \bar{M}_s^{k-1}(L) \\ \bar{M}_\tau^{k-1}(L) \end{bmatrix} + \hat{\mathbf{K}}_{sL}^{k-1} \begin{bmatrix} N^{k-1}(0) \\ M^{k-1}(0) \\ Q^{k-1}(0) \\ N^{k-1}(L) \\ M^{k-1}(L) \\ Q^{k-1}(L) \end{bmatrix} + \hat{\mathbf{K}}_{sL}^{k-1} \begin{bmatrix} \sigma_{0+}^{k-1} \\ \sigma_{0-}^{k-1} \\ \tau_{0+}^{k-1} \\ \tau_{0-}^{k-1} \end{bmatrix} \\
&= \mathbf{K}_{s0}^k \begin{bmatrix} M_s^k(0) \\ \bar{M}_\tau^k(0) \\ M_s^k(L) \\ \bar{M}_\tau^k(L) \end{bmatrix} + \hat{\mathbf{K}}_{s0}^k \begin{bmatrix} N^k(0) \\ M^k(0) \\ Q^k(0) \\ N^k(L) \\ M^k(L) \\ Q^k(L) \end{bmatrix} + \hat{\mathbf{K}}_{s0}^k \begin{bmatrix} \sigma_{0+}^k \\ \sigma_{0-}^k \\ \tau_{0+}^k \\ \tau_{0-}^k \end{bmatrix}. \quad (3.156)
\end{aligned}$$

If one of the two adjacent beams is considered semi-infinite it affects to the corresponding side of the equal sign in equation (3.156). This is due to the dependence of equation (3.156) with the value of the higher-order moments at both ends $s_k = 0$ and $s_k = L_k$.

3.8.4 Continuity of the transverse displacements between components

As in the case of the shear moments, it is recommended to express the transverse displacement vector in the straight beam basis for imposing continuity of transverse displacements. The transverse displacements expressed in the straight beam basis and in the component own basis are given by:

$$u_z(s, z) = \bar{w}_1(s) + \hat{\mathbf{f}}_s^T(z) \bar{\mathbf{w}}(s), \quad u_z(s, z) = w_1(s) + \mathbf{f}_z^T(z) \mathbf{w}(s). \quad (3.157)$$

The continuity of displacements is imposed in a weak manner by using least squares. In the theoretical model $w_1(s)$ has been calculated independently of the rest of parameters, $w_1(s)$ being calculated once the rest of the problem has been solved, and, therefore, it is not considered in the least squares problem.

$$\frac{\partial}{\partial \bar{\mathbf{w}}} \left(\int_{-1}^1 \left(\hat{\mathbf{f}}_s^T(z) \bar{\mathbf{w}}(s) - \mathbf{f}_z^T(z) \mathbf{w}(s) \right)^2 dz \right) = 0. \quad (3.158)$$

The derivative yield:

$$\int_{-1}^1 \hat{\mathbf{f}}_s(z) \left(\hat{\mathbf{f}}_s^T(z) \bar{\mathbf{w}}(s) - \mathbf{f}_z^T(z) \mathbf{w}(s) \right) dz = 0. \quad (3.159)$$

Therefore, \mathbf{K}_w is obtained as following the same procedure used in the shear higher-order moments case:

$$\bar{\mathbf{w}}(s) = \mathbf{K}_w \mathbf{w}(s), \quad \mathbf{K}_w = \mathbf{A}_w^{-1} \mathbf{B}_w \quad (3.160a)$$

$$\mathbf{A}_w = \int_{-1}^1 \hat{\mathbf{f}}_s(z) \hat{\mathbf{f}}_s^T(z) dz, \quad \mathbf{B}_w = \int_{-1}^1 \hat{\mathbf{f}}_s(z) \mathbf{f}_z^T(z) dz. \quad (3.160b)$$

$$A_{w,ij} = \hat{A}_{L,i+1,j+1}, \quad i, j = 1, 2, \dots, n-1. \quad (3.160c)$$

$$B_{w,ij} = \hat{B}_{L,j+1,i+1}, \quad i, j = 1, 2, \dots, n-1. \quad (3.160d)$$

Equalling $\bar{\mathbf{w}}^{k-1}(L) = \bar{\mathbf{w}}^k(0)$, substituting equations (3.140), (3.144) and (3.93) and knowing that $\mathbf{X}_{z0}^k(L) = 0$ and $\mathbf{X}_{zL}^k(0) = 0$, the continuity of the transversal displacements is imposed with:

$$\begin{aligned} & \mathbf{K}_w^{k-1} \left(\mathbf{X}_{zL}^{k-1}(L) \Gamma_L^{k-1} \begin{bmatrix} \hat{M}_s^{k-1}(0) \\ \hat{M}_\tau^{k-1}(0) \\ \hat{M}_s^{k-1}(L) \\ \hat{M}_\tau^{k-1}(L) \end{bmatrix} + \begin{bmatrix} \mathbf{q}_{zN}^{k-1} & \mathbf{q}_{zM}^{k-1} \end{bmatrix} \begin{bmatrix} N^{k-1}(L) \\ M^{k-1}(L) \end{bmatrix} \right) \\ & = \mathbf{K}_w^k \left(\mathbf{X}_{z0}^k(0) \Gamma_0^k \begin{bmatrix} \hat{M}_s^k(0) \\ \hat{M}_\tau^k(0) \\ \hat{M}_s^k(L) \\ \hat{M}_\tau^k(L) \end{bmatrix} + \begin{bmatrix} \mathbf{q}_{zN}^k & \mathbf{q}_{zM}^k \end{bmatrix} \begin{bmatrix} N^k(0) \\ M^k(0) \end{bmatrix} \right). \quad (3.161) \end{aligned}$$

Separating the perturbations as the non-regularized value minus the regularized one, and using equations (3.155a) for the regularized values, the previous equation can be expressed as follows:

$$\begin{aligned}
 & \mathbf{K}_{zL}^{k-1} \begin{bmatrix} \mathbf{M}_s^{k-1}(0) \\ \bar{\mathbf{M}}_\tau^{k-1}(0) \\ \mathbf{M}_s^{k-1}(L) \\ \bar{\mathbf{M}}_\tau^{k-1}(L) \end{bmatrix} + \hat{\mathbf{K}}_{zL}^{k-1} \begin{bmatrix} N^{k-1}(0) \\ M^{k-1}(0) \\ Q^{k-1}(0) \\ N^{k-1}(L) \\ M^{k-1}(L) \\ Q^{k-1}(L) \end{bmatrix} + \hat{\mathbf{K}}_{zL}^{k-1} \begin{bmatrix} \sigma_{0+}^{k-1} \\ \sigma_{0-}^{k-1} \\ \tau_{0+}^{k-1} \\ \tau_{0-}^{k-1} \end{bmatrix} \\
 &= \mathbf{K}_{z0}^k \begin{bmatrix} \mathbf{M}_s^k(0) \\ \bar{\mathbf{M}}_\tau^k(0) \\ \mathbf{M}_s^k(L) \\ \bar{\mathbf{M}}_\tau^k(L) \end{bmatrix} + \hat{\mathbf{K}}_{z0}^k \begin{bmatrix} N^k(0) \\ M^k(0) \\ Q^k(0) \\ N^k(L) \\ M^k(L) \\ Q^k(L) \end{bmatrix} + \hat{\mathbf{K}}_{z0}^k \begin{bmatrix} \sigma_{0+}^k \\ \sigma_{0-}^k \\ \tau_{0+}^k \\ \tau_{0-}^k \end{bmatrix}. \quad (3.162)
 \end{aligned}$$

If one of the two adjacent beams is considered semi-infinite it affects to the corresponding side of the equal sign in equation (3.162).

3.8.5 Application of the boundary conditions and the continuity conditions

Each component has $4n - 4$ unknown variables given by the higher-order moments (radial and circumferential) at each end of the component, so $(4n - 4)N_c$ unknown variables are given. Continuity conditions of stresses, (3.146) and (3.152), allows the unknown variables to be reduced to $(2n - 2)(N_c + 1)$.

Boundary conditions at both ends of the chain of beams, which can be given in displacements or in stresses, provide $4n - 4$ equations, so $(2n - 2)(N_c - 1)$ additional equations are required. If one end component is considered semi-infinite, the number of unknowns in the component is reduced to $2n - 2$ unknowns. Therefore, if semi-infinite components are assumed at both ends $(2n - 2)(N_c - 1)$ additional equations are also required. These $(2n - 2)(N_c - 1)$ equations are given by the continuity conditions of the displacements, (3.156) and (3.162).

Notice that all the boundary conditions and continuity conditions are linear with the unknown variables, and, consequently, they can be solved easily as a problem of the form of $\mathbf{Ax} = \mathbf{b}$, where \mathbf{b} depends on the applied forces, bending moment and distributed loads. In the present case, vector \mathbf{x} includes all the circumferential higher-order moments $\mathbf{M}_s^k(0)$ and/or $\mathbf{M}_s^k(L)$, and all the shear higher-order moments expressed in the functions base of the straight beam $\bar{\mathbf{M}}_\tau^k(0)$ and/or $\bar{\mathbf{M}}_\tau^k(L)$. Notice also that the forces and the bending moment at the end of one component are the same than these at the beginning of the following component.

3.9 Results of the non-regularized models and validation by FEM

In the present section several geometries and loading states are analysed and compared with appropriate FE models to validate the semi-analytical model. First, a L-sectioned beam is analysed with two different loading states: a bending moment loading, similarly to a four-point bending test and a compression loading in one arm of the section. Finally, a joggle is analysed under tensile loading. The models can be also applied to other geometries including changes of curvature with constant thickness, such as Ω -shaped beams, C-shaped beams or corrugated laminates.

3.9.1 L-shaped beam under bending moment

The typical loading state associated to the unfolding failure is the bending moment of a corner. A L-shaped section loaded under a pure bending moment calculated with a regularized model has a constant stress distribution in the circumferential direction due to the constant value of the bending moment in that direction. However, the change of curvature due to the straight arms cause a non-constant stress distribution in the zone where the change of curvature takes place (see [14]).

For the numerical implementation, a material with ply properties of Table 3.2 is considered. The laminate considered is a quasi-isotropic laminate with stacking sequence $[45\ 0\ -45\ 90]_S$. The L-shaped section is determined by the thickness $t = 1.6$ mm and by the mean radius of the curved part $R = 2.4$ mm, see Figure 3.13. The applied load is $M_0 = 1$ Nm/m.

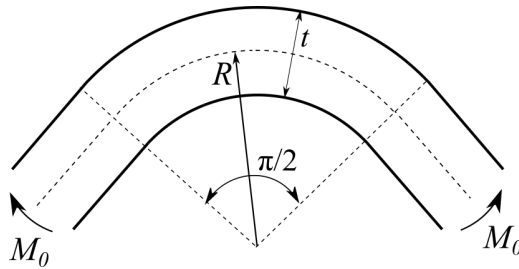


Figure 3.13: L-shaped beam under bending moment.

In the FE model, the straight arms are taken of length $L = 10$ mm, which has been considered long enough to avoid that the non-regularized effects of the end of the arms do no affect to the stresses distribution in the zone near

the change of curvature. Linear shell elements with four nodes have been used in the FE model with five elements per ply in the thickness direction. The ply properties are introduced considering a plane strain state. The hypotheses used for modelling the FE model are similar to the hypotheses employed in the semi-analytical model, and, consequently, similar solutions must be obtained.

The results of the maximum INS depending on the axial coordinate s by using the LPBM with an order of $n = 50$, Ko & Jackson's solution and the FEM results are depicted in Figure 3.14. The same solutions for the maximum/minimum ISS are depicted in Figure 3.15, where the Ko & Jackson's model solution has been suppressed as the regularized shear stress in the problem is null in the whole section.

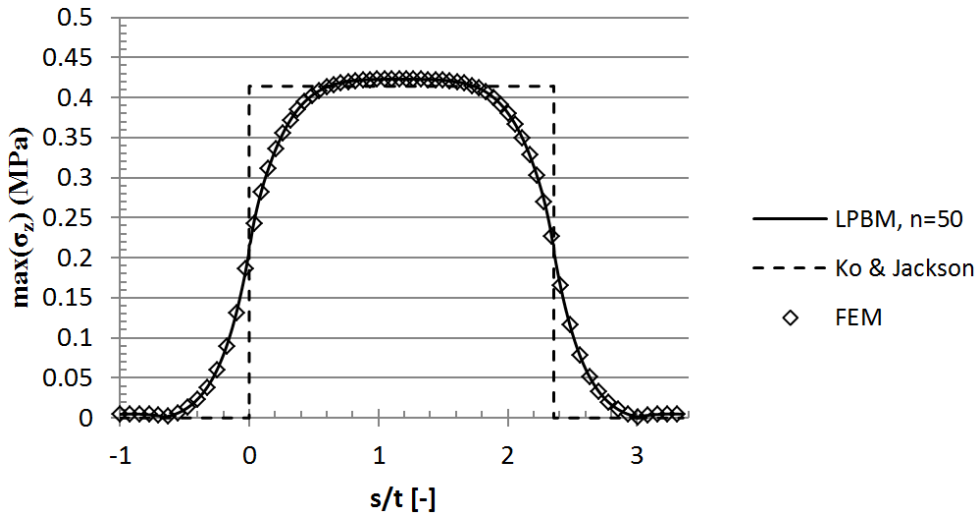


Figure 3.14: Maximum INS in the L-shaped beam under bending moment.

Notice that the FE model agrees well with the results of the LPBM, clearly showing the existence of the non-regularized effects due to the change of curvature and validating the non-regularized models developed in the present project.

The shear stresses appear even without the presence of a shear force due to the non-regularized effects in order to accomplish the equilibrium equations. These shear stresses present their maximum value in the change of curvature point, with a discontinuity in their derivative in the aforementioned section.

Notice that in the view of the obtained results, non-regularized models are not necessary to predict the unfolding failure in this case, as the maxi-

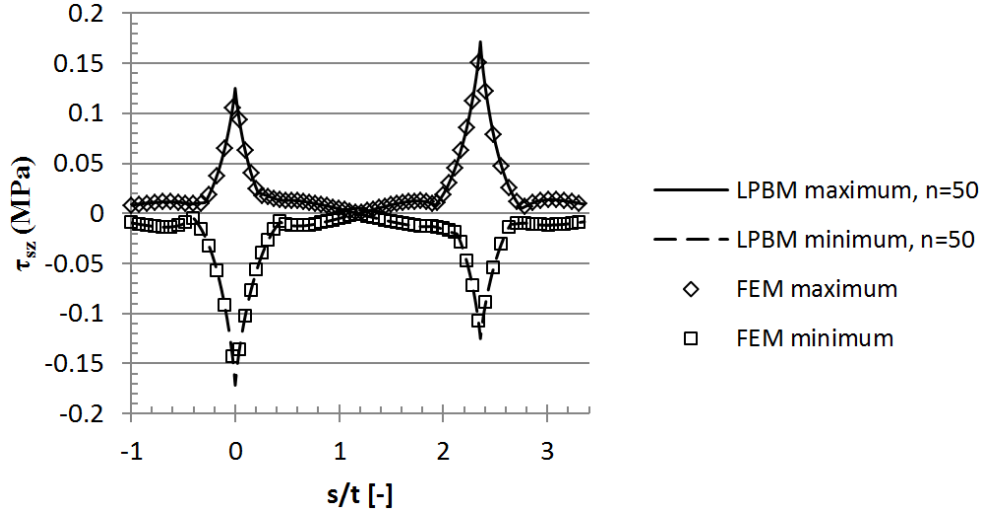


Figure 3.15: Maximum ISS in the L-shaped beam under bending moment.

imum value of the INS is predicted accurately by the regularized model given by Ko & Jackson. The reason is that the maximum regularized INS is constant in the whole curved beam. Notwithstanding, in a problem where the maximum INS is given near to a change of curvature non-regularized effects are more relevant, as in the case of a L-shaped beam under a compressive load shown in the next section.

3.9.2 L-shaped beam under a compressive load

A compressive loading in an arm of a L-shaped beam induces that the maximum bending moment is given at the change of curvature of the opposite arm. Therefore, the maximum INS is affected by the non-regularized effects and the use of a regularized model is not accurate in this kind of loading states.

For the numerical implementation, the same material, configuration and FE model characteristics are used, since the loading state is changed as depicted in Figure 3.16.

The results of the maximum INS depending on the axial coordinate s by using the LPBM with an order of $n = 50$, Ko & Jackson's solution and the FE model predictions are depicted in Figure 3.17. The results of the maximum/minimum ISS are depicted in Figure 3.18, where the maximum value of the Ko & Jackson's solution has been suppressed as the maximum value of the regularized shear stress in the problem is null in the whole beam.

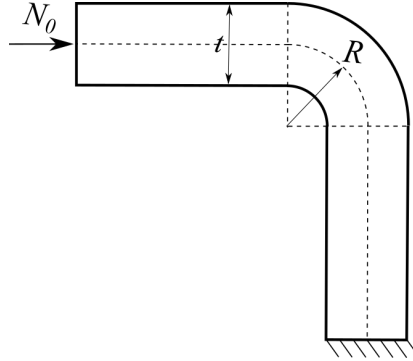


Figure 3.16: L-shaped beam under a compressive load.

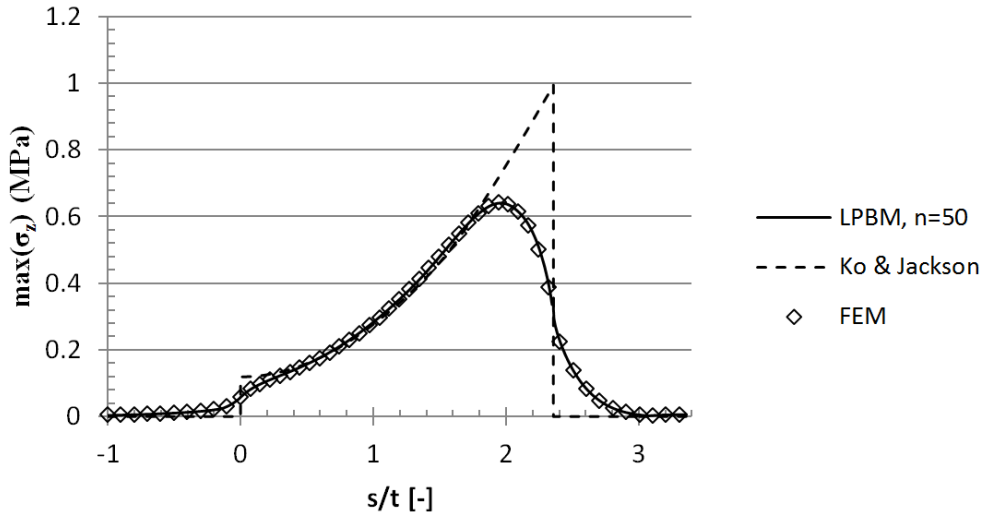


Figure 3.17: Maximum INS in the L-shaped beam under compressive load.

Notice that, as the bending problem analysed in the previous subsection, the FE model agrees well with the results of the LPBM. The maximum value of the INS in the present loading case is a 64% of the maximum value given by a regularized model. Consequently, regularized models are very conservative when the maximum INS is given near to a change of curvature. These results show the importance of considering the non-regularized effects in the calculation of the unfolding failure.

The regularized value of the ISS is very close to the non-regularized value, with small discrepancies near to the changes of curvature. In this case, the non-regularized effects for the ISS are not so important due to the

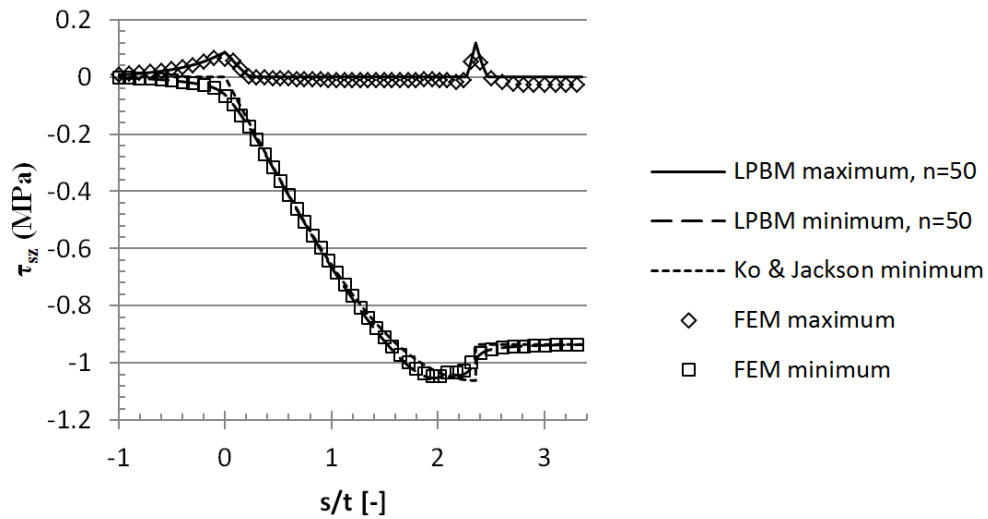


Figure 3.18: Maximum ISS in the L-shaped beam under compressive load.

presence of a dominant shear force.

3.9.3 Joggle under a tensile load

The joggle is a very common element in riveted or bolted joints between panels where the continuity of the surface is important from an aerodynamic point of view. This element has two curved parts, commonly having the same mean radius R . One of this curved parts is clockwise and the other one is counter-clockwise. Consequently, the joint between them constitutes a change of curvature even if they both have the same mean radius. However, a short straight part is usually located between both curved parts, see Figure 3.19.

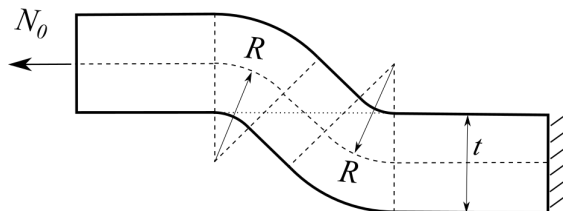


Figure 3.19: Joggle under a tensile load.

The importance of the non-regularized model in a joggle resides in the shortness of the curved elements and the high curvature, which implies that

the stresses cannot reach their regularized values in the zone between the changes of curvature. Furthermore, the importance of the non-regularized models is higher when the maximum of the regularized INS is located close to a change of curvature, as has been shown in the L-shaped beam.

The results of the maximum INS depending on the axial coordinate s by using the LPBM with an order of $n = 50$, the Ko & Jackson's solution and the FE model predictions are depicted in Figure 3.20. The same solutions for the maximum/minimum ISS are depicted in Figure 3.21, where the minimum value of the Ko & Jackson solution has been suppressed as the minimum value of the regularized shear stress in the problem is null in the whole beam.

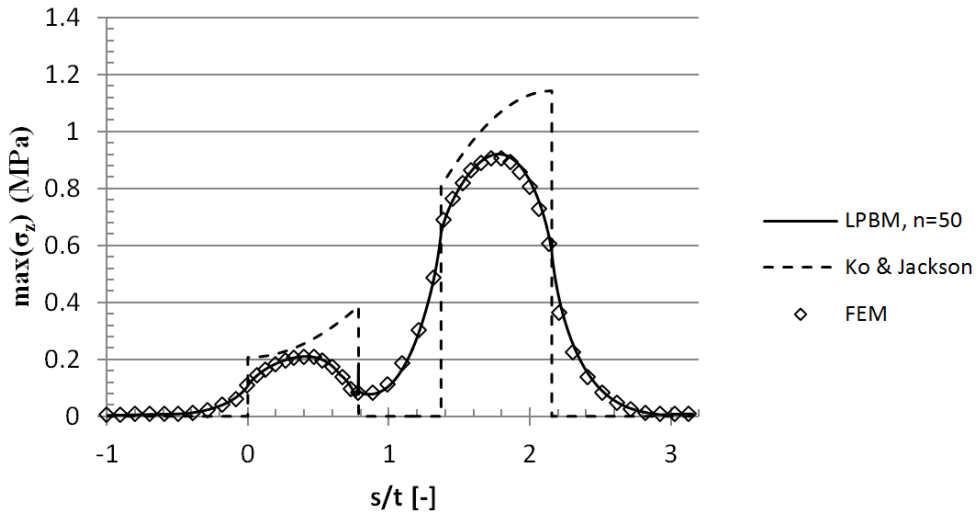


Figure 3.20: Maximum INS in the joggle under tensile load.

Again, FE results agrees with a very high accuracy with the results obtained with the LPBM.

Notice the symmetry of the regularized ISS respect to the geometrical center of the joggle due to the symmetry of the shear force. However, the non-regularized ISS is non-symmetric due to the effect of the bending moment, which is not symmetric. Notwithstanding, the maximum value of the ISS is similar with both regularized and non-regularized models.

Respect to the INS, the maximum value is the 80% of the maximum value given by the regularized model. Therefore, the use of a regularized model for estimating the unfolding failure is again very conservative. Furthermore, the results obtained considering the non-regularized effects show that the stresses do not reach the regularized value at any point of the curved parts

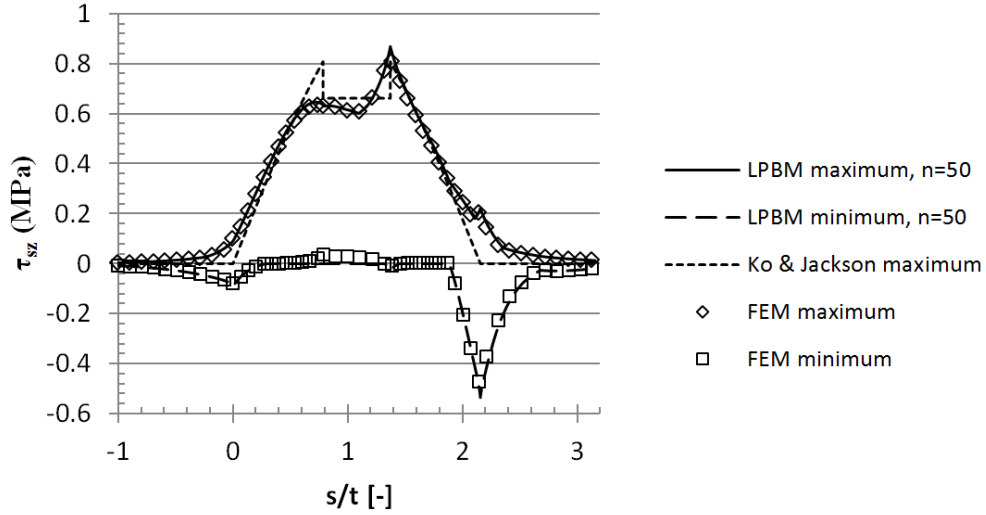


Figure 3.21: Maximum ISS in the joggle under tensile load.

due to the short length of these curved parts.

3.10 Numerical characteristics of the MBM and LPBM non regularized models

The MBM and the LPBM have been implemented in MatLab on a standard PC (Intel Core i3, 3.30 GHz). An analysis of the numerical characteristics of this model concerning the computational times and the errors (respect to a high enough order) has been carried out with the implemented methods.

The MBM has presented numerical limitations due to the very fast growth of the condition number of the stiffness matrix with the model order, which results in very high numerical errors when inverting the matrix. This limitation has been explained in the subsection 3.4.3, where a maximum order is deduced depending on the radius to thickness ratio R/t . This maximum order is summarized in Table 3.1.

The MBM has very low computational times which are shown in Figure 3.22(a) depending on the number of plies for a model order of $n = 9$, and in Figure 3.22(b) depending on the model order for a number of plies of $N_p = 8$. These computational times have been obtained for the bending problem studied in the subsection 3.9.1, which, with a relation $R/t = 1.5$, is limited to $n = 9$, changing the stacking sequence.

The LPBM has higher computational times than the MBM, which are shown in Figure 3.23(a) depending on the number of plies for a model order of $n = 20$, and in Figure 3.23(b) depending on the model order for a number of plies of $N_p = 1$.

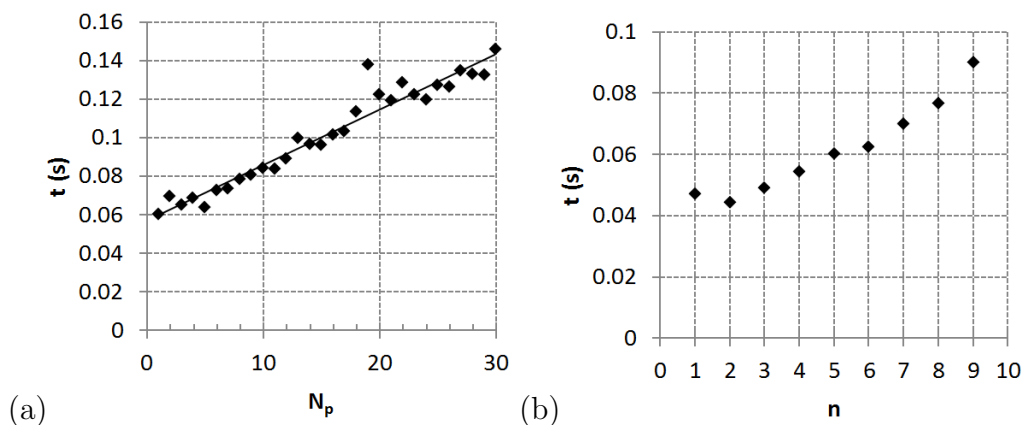


Figure 3.22: Computational times of the MBM. (a) Depending on N_p for $n = 9$. (b) Depending on n for $N_p = 8$.

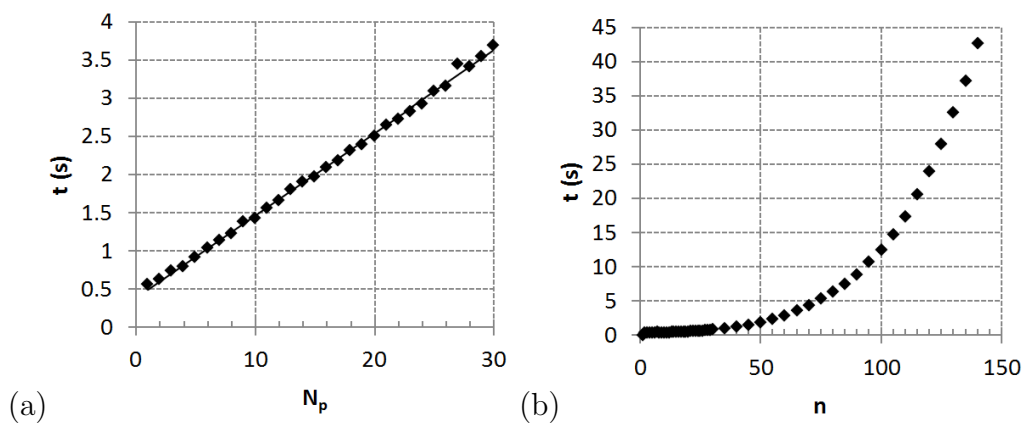


Figure 3.23: Computational times of the LPBM. (a) Depending on N_p for $n = 20$. (b) Depending on n for $N_p = 1$.

Every point of the Figures 3.22 and 3.23 have been obtained by evaluating 10 times the computational time and obtaining the mean value of them. The dependence with the number of plies of the computational times is linear, while the dependence with the model order is roughly exponential. The MBM has usually computational times in the order of 0.1 seconds,

while the LPBM for orders around 10 has computational times in the order of 1 second (10 times higher than the MBM) and for orders around 100 has computational times in the order of 10 seconds. The LPBM has higher computational times than the MBM due to the numerical integration by quadrature methods of the integrals without a known analytical solutions.

Numerical errors are similar in both models for the same order, and therefore, while an order lower than the maximum allowable order of the MBM is chosen it is convenient to choose the MBM for reducing the computational times. Notwithstanding, if a high accuracy is desired the LPBM has to be chosen with the corresponding higher model order.

The numerical errors are evaluated by considering as exact the solution of the model with a high enough order and comparing with models with lower orders. In that way, evaluating different geometries, loading states and stacking sequences (see [108]) the following estimation of the error ε in the maximum INS has been obtained:

$$\varepsilon = \frac{5t}{Rn^3}. \quad (3.163)$$

Therefore, the errors in the maximum INS decrease with a cubic order. Notice that the error of the maximum INS in the maximum order of the MBM are always between the 0.1% and the 0.5%, which is accurate enough for predicting the unfolding failure. However, errors at other points of the distribution different from the maximum, e.g., near to a change of curvature, can be much higher. Therefore, if the main interest of application of the model is to obtain an accurate stresses distribution and not only to predict the maximum, the LPBM is necessary.

3.11 Regularization distance

One parameter of importance when analysing a non-regularized problem is the regularization distance (RD). The RD is defined as the distance from the non-regularized focus necessary to reduce the perturbations of the non-regularized parameters to a 5% of its maximum value.

It can be considered that stresses and other parameters at points located at higher distances than the RD from all the non-regularized focuses are very close to their regularized values. Therefore, two non-regularized focuses distanced more than the summation of both RD associated to both focuses can be considered independent, and one of those focuses do not affect to the parameters in the closer area of the other focus.

That distance may be used to divide a section in several problems to analyse. E.g., in a L-shaped beam with a high R/t ratio the curved part

may be long enough so one change of curvature does not affect to the other one and, therefore, each change of curvature may be analysed independently considering the curved part as a semi-infinite beam. This is important in sections having many changes of curvature, where the complexity may be reduced by dividing the section in several chains of beams.

The perturbations have been obtained as a summation of exponential functions according to (3.136) and (3.137) (notice that the hyperbolic sine is equivalent to an exponential function). The decay rate of those functions are determined by the coefficients of the exponents of the exponentials, which, at the same time, are given by the square root of the eigenvalues λ_i of the matrix \mathbf{G} . Typically, the eigenvalues are complex numbers causing that the exponentials are damped oscillations. The decay rate is given only by the real part of the square root of λ_i , associated to the damping, the complex part being associated to the oscillations. Therefore, the decay rate of the perturbations may be approximated by the exponential with the coefficient in the exponent with a lower real part, $\sqrt{\lambda_{\min}}$:

$$\operatorname{Re} \left(\sqrt{\lambda_{\min}} \right) = \min_i \left(\operatorname{Re} \left(\sqrt{\lambda_i} \right) \right). \quad (3.164)$$

Notice that the coefficient with a lower real part of $\sqrt{\lambda_{\min}}$ does not necessarily coincide with the eigenvalue λ_i with the minimum real part, as the coefficient is defined as the square root of the eigenvalue and the real part of the square root of λ_i depends also on the imaginary part of λ_i .

Therefore, the regularization distance, L_{reg} may be approximated by the value of s where the exponential associated to $\sqrt{\lambda_{\min}}$ has declined to the 5% of its maximum value (which is given in $s = 0$):

$$e^{-\operatorname{Re}(\sqrt{\lambda_{\min}})L_{\text{reg}}\frac{2}{t}} \simeq 0.05, \quad (3.165)$$

where the inverse of one half of the thickness has been added in the expression to consider the dimensional value of the regularization distance L_{reg} instead of the non-dimensional ones used in the development of the MBM and the LPBM.

Hence, the approximation of the RD yields:

$$L_{\text{reg}} \simeq \frac{3t}{2 \operatorname{Re} \left(\sqrt{\lambda_{\min}} \right)}. \quad (3.166)$$

Equation (3.166) may be used to obtain the RD numerically by using the LPBM with a model order high enough. However, a closed-form equation is desired to evaluate the RD before running the non-regularized model. This closed-form equation may be obtained by approximating $\sqrt{\lambda_{\min}}$ by the

corresponding parameter in a model with order $n = 2$, since generally the eigenvalues associated to higher orders are lower. A model with order $n = 2$ applied to a homogeneous material has two eigenvalues which are given by the following expressions:

$$\lambda_{1,2} = \frac{3(Q_{11}Q_{33} - Q_{13}^2)}{2Q_{11}Q_{55}} \pm \frac{3}{2} \sqrt{\frac{(Q_{13}^2 - Q_{11}Q_{33})(Q_{13}^2 - Q_{11}Q_{33} + 20Q_{55}^2)}{Q_{11}^2Q_{55}^2}}. \quad (3.167)$$

For a composite material the corresponding eigenvalues may be approximated by equation (3.167) by considering the homogeneous equivalent material and calculating the corresponding stiffnesses Q_{ij} . The eigenvalue with the minimum real part is obtained by choosing the minus sign in equation (3.167):

$$\lambda_{\min} = \frac{3(Q_{11}Q_{33} - Q_{13}^2)}{2Q_{11}Q_{55}} - \frac{3}{2} \sqrt{\frac{(Q_{13}^2 - Q_{11}Q_{33})(Q_{13}^2 - Q_{11}Q_{33} + 20Q_{55}^2)}{Q_{11}^2Q_{55}^2}}. \quad (3.168)$$

Notice that the eigenvalue λ_{\min} is highly influenced by the parameter Q_{55} , the RD being highly influenced by the shear stiffness of the material.

Summarizing, the RD may be evaluated by equation (3.166) calculating numerically $\sqrt{\lambda_{\min}}$ by using an order high enough in the LPBM. Notwithstanding, $\sqrt{\lambda_{\min}}$ can be approximated by using the homogeneous equivalent material and using equation (3.168) for a quick estimation of the RD.

Considering a single-ply laminate with ply properties given in Table 3.2 and changing the orientation of the ply, the square root of the eigenvalue whose square root has the minimum real part is depicted in the complex plane in Figure 3.24 for the approximation given in equation (3.168), a straight beam and a curved beam with $R = t$.

The 0° ply and the 90° ply cases are marked in the Figure. The eigenvalue square root in low orientations has a null imaginary part until an orientation between 45° and 55° where the imaginary part becomes not null. Notice a discontinuity in the curved beam case when the imaginary part becomes not null. That discontinuity is due to a change in the eigenvalue with the minimum real part in its square root.

The RD yields as depicted in Figure 3.25, where a discontinuity in the slope is observed when the imaginary part of $\sqrt{\lambda_{\min}}$ becomes not null.

Therefore, the approximation results slightly anti-conservative, specially in the straight beam case. Furthermore, it can be observed that the RD are, for the present material properties and a single-ply laminate, delimited

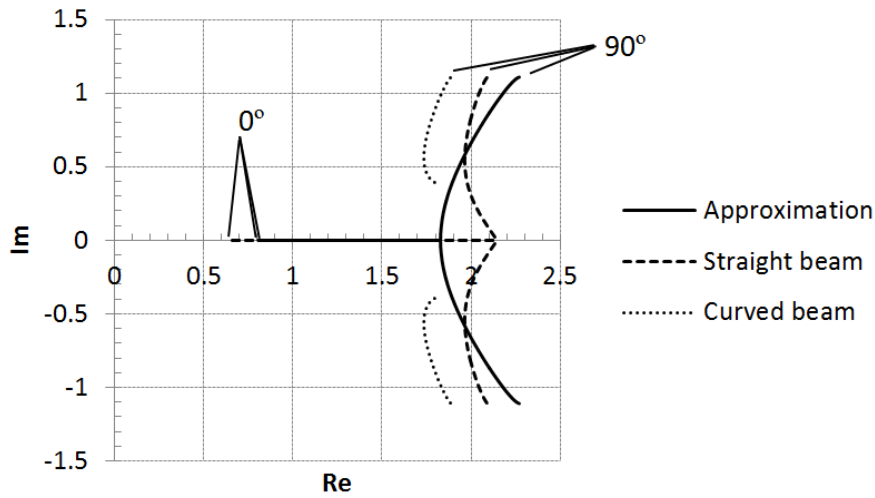


Figure 3.24: Complex plane representation of $\sqrt{\lambda_{\min}}$.

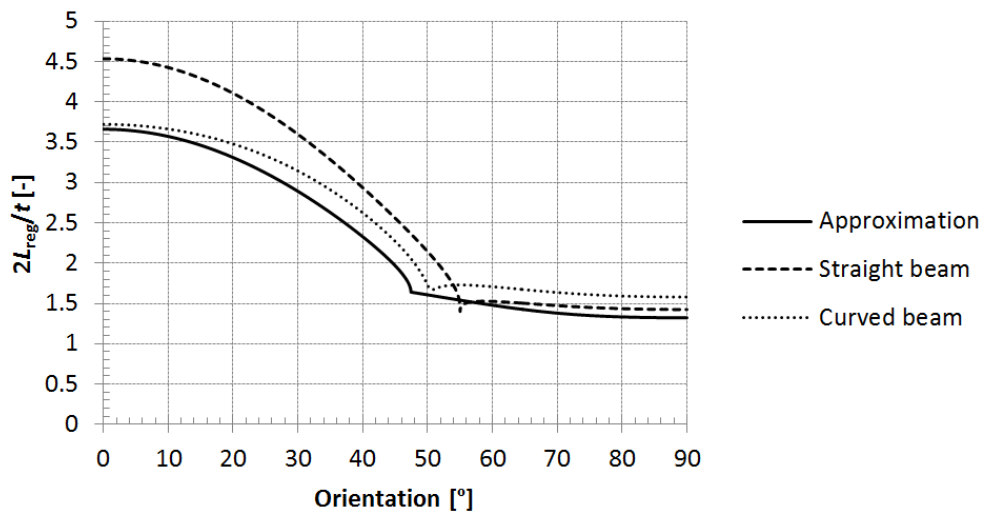


Figure 3.25: Regularization distances for a single-ply laminate depending on the orientation.

between a value of $0.65t$ and $2.25t$. In the case of a composite laminate these values may change and it is necessary to evaluate each stacking sequence independently.

3.12 Off-topic applications of the non regularized models

The MBM and LPBM have been applied in the previous sections to composite sections loaded by end forces and bending moments including changes of curvature, in order to predict the effect of these changes of curvature on the stresses distribution. However, these models may be applied to many others applications [110]. In particular, in the present section, the models are applied to evaluate stresses at joints between beams with different material properties, to determine non-regularized effects at the vicinity of an embedment and to analyse the three point bending test.

3.12.1 Joint of beams with different material properties

In a joint of two materials a discontinuity in the material properties takes place, which, due to the different Poisson contractions of the materials, causes the appearance of a singular stress field. This kind of problem may be analysed using the models developed in section 3.8 by considering two components and introducing different material properties in each component.

As a numerical example, two homogeneous isotropic materials are considered with different Young modulus and the same Poisson coefficients, with the material properties shown in Table 3.3.

Material 1	E_1	100 GPa	ν_1	0.3
Material 2	E_2	10 GPa	ν_2	0.3

Table 3.3: Material properties for the numerical examples

The two beams made with different materials are considered perfectly bonded at a flat surface as shown in Figure 3.26. Both beams are of constant thickness t . Furthermore, a tensile load N_0 is acting perpendicular to the joint surface.

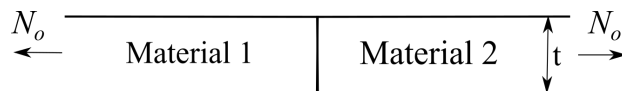


Figure 3.26: Joint of two beams with different material properties, axially loaded.

For comparison reasons, the problem has been implemented in a FE software. Quadratic bi-dimensional elements with a plane strain assumption have been used, where a variable mesh size has been used concentrating the elements near to the free edges and near to the joint section.

Figure 3.27 shows the distribution of the axial stress σ_s at the joint section obtained by using the LPBM with $n = 500$, which has required a computational time of 50 seconds, and compared with the FE results.

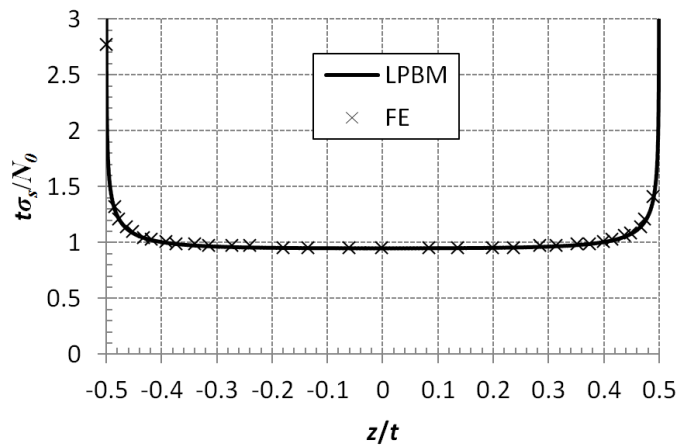


Figure 3.27: Axial stress at the joint of two different materials.

The LPBM, as the FEM or any model based on series expansion with polynomials, cannot predict an infinite value of the stresses at the singular point. However, the tendency is clearly captured, observing both tendencies to an infinite value in the free edges. The LPBM obtains a similar distribution to the FEM. Far away from the joint section the distribution of stresses tends to a constant value, it being the regularized value.

Figure 3.28(a) shows the shear stress τ_{sz} and Figure 3.28(b) shows the through-thickness stress σ_z in the joint section obtained by using the LPBM with $n = 500$ and compared with the FE results. The through-thickness stress is different at both sides, as this stress is not continuous in the axial direction s , so the stress at both sides, corresponding to both materials, is depicted.

The stiffer material is tensioned in the through-thickness direction, while the softer material is compressed. For the present material properties, the through-thickness stress is in the same order than the mean value of the axial stress. The normal through-thickness stress is not singular in the free edges. Notwithstanding, it has an infinite slope changing sharply from 0 to a finite value. The shear stress is singular similarly than the axial stress,

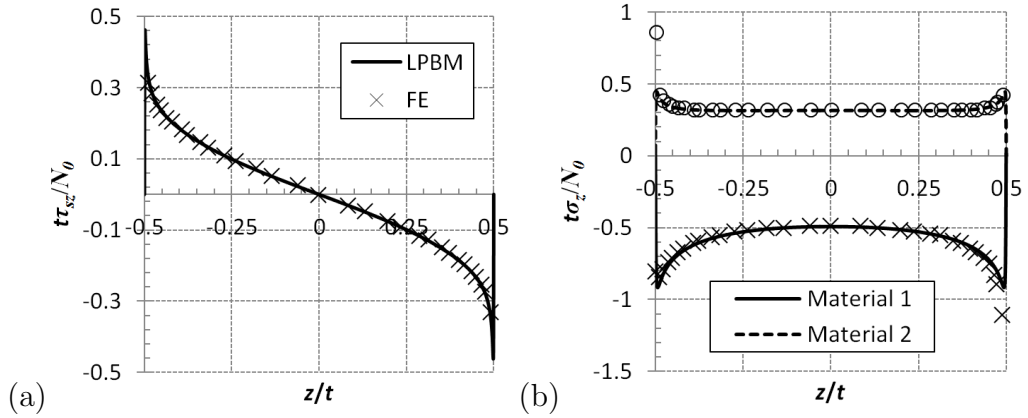


Figure 3.28: Stresses in the joint of two different materials. (a) Shear stress. (b) Through-thickness stress in both sides.

however, it is neither captured by the LPBM nor by the FE model. A high agreement is observed between the LPBM and the FEM results.

3.12.2 Non-regularized effects due to the boundary conditions

The way in which the load is applied may introduce also non-regularized effects. According to the Saint-Venant principle, at sufficiently large distances from load the way of application of two equivalent loads do not affect to the stress distribution. However, the way in which the load is applied affects to the nearest zone in the form of non-regularized effects.

If boundary conditions are prescribed stresses, this kind of non-regularized effects may be calculated. Analogously, prescribed displacements may introduce non-regularized effects over the stress distribution.

As a numerical example, a straight semi-infinite beam embedded, that is, with null transverse and longitudinal displacements at the end, is considered. It is loaded under a tensile load N_0 , and it is constituted by a homogeneous isotropic material with $E = 100$ GPa and $\nu = 0.3$.

For comparison reasons, the problem has been implemented in a FEM software. Quadratic bi-dimensional elements with a plane strain assumption have been used, where a variable mesh size has been used concentrating the elements near to the free edge in the thickness direction and near to the constrained section.

Figure 3.29 shows the axial stress σ_s in the embedment section obtained by using the LPBM with $n = 500$, which has required a computational time

of 25 seconds, and by using a FE model.

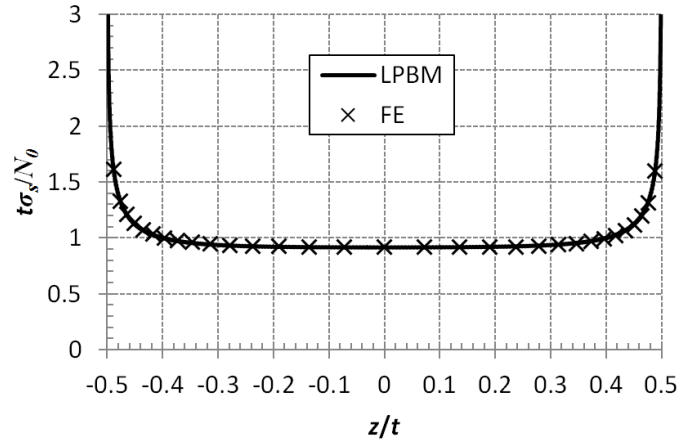


Figure 3.29: Axial stress in an embedment under tensile load.

The stress distribution obtained in Figure 3.29 is very similar to the stress distribution obtained in Figure 3.27 as the embedment is analogous to a joint with a material with an infinite stiffness. The singular behaviour of the stress is clearly captured with the model, and results have a high agreement with the FE results.

Figure 3.30(a) shows the shear stress τ_{sz} and Figure 3.30(b) shows the through-thickness stress σ_z in the embedment section obtained by using the LPBM with $n = 500$ and the FEM.

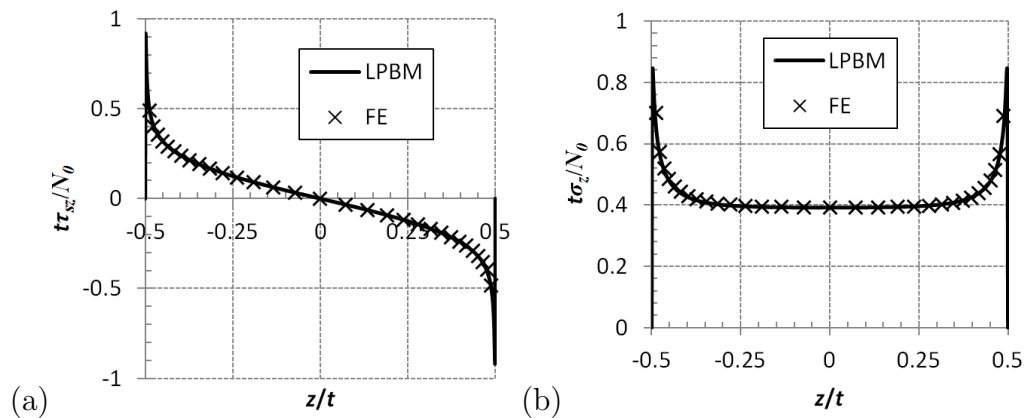


Figure 3.30: Stresses in an embedment under tensile load. (a) Shear stress. (b) Through-thickness stress.

Shear and through-thickness stresses have more pronounced distributions than in the case of the joint with a different material. Shear stress and through-thickness normal stress have a singular value at the free edge, and both have a high agreement with FE results.

Another numerical example is analysed by using a pure bending moment load M_0 instead of the tensile load. Figure 3.31 shows the axial stresses σ_s in the embedment section obtained by using the LPBM with $n = 500$ with the mentioned bending moment, which has required a computational time of 25 seconds, and by using a FE model.

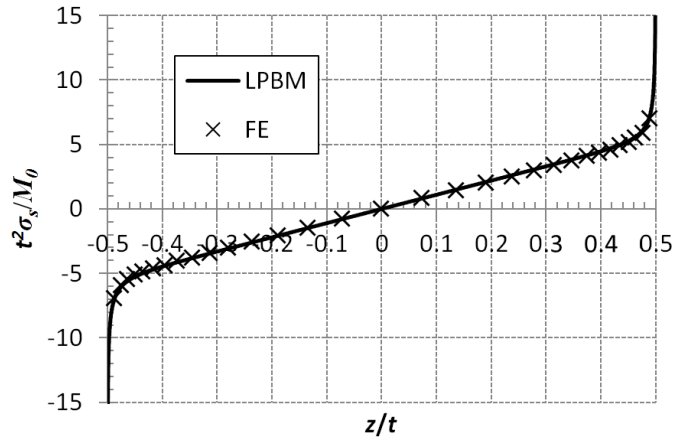


Figure 3.31: Axial stress in an embedment under bending moment.

A singular behaviour in the axial stresses distribution is again observed, with axial stresses tending to infinite in the free edges in the embedment section. A high agreement with the FE results is again observed.

Figure 3.32(a) shows the shear stresses τ_{sz} and Figure 3.32(b) shows the through-thickness stresses σ_z in the embedment section obtained by using the LPBM with $n = 500$ and the FEM.

In the present case the shear stresses tend to infinite in the free edge. Respect to the through-thickness stress, a tensile zone and a compressive zone is observed in difference with the tensile load case. A high agreement with the FE results is again observed.

3.12.3 Non-regularized effects due to punctual loads

The last off-topic application analysed is the effect of punctual loads over the stress distribution. Theotokoglou and Sideridis [111] showed that near to a punctual load in flat laminates the stress distribution is distorted and the

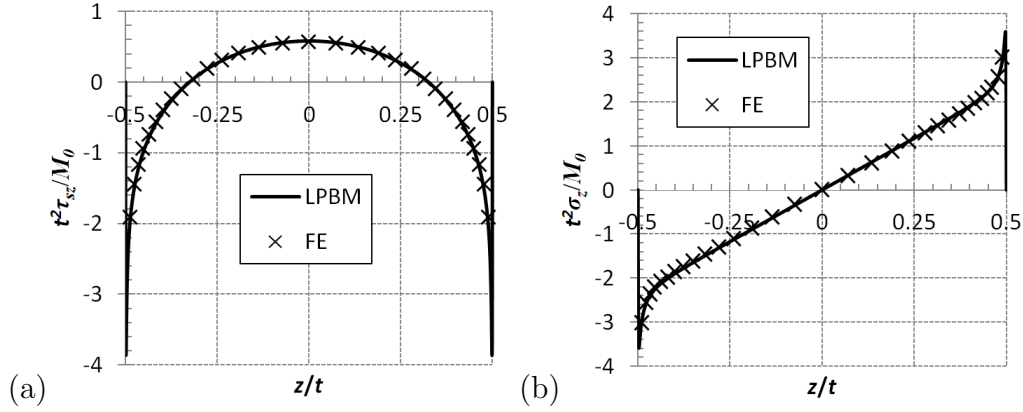


Figure 3.32: Stresses in an embedment under bending moment. (a) Shear stress. (b) Through-thickness stress.

typical lineal distribution of axial stresses is not obtained. In particular, a three-point bending test is analysed. The stress distribution in a three-point bending test has been analysed by Makeev et al. [78].

The model developed can predict the effect of a punctual load by considering a external pressure modelled as a Dirac delta and obtaining the regularized expression from equation (3.131). However, the resolution of the regularized value in that case is not easy. As an alternative, by using the developed regularized solution, the punctual load is approximated by a very short straight component with a very high constant pressure whose resultant is the applied load.

For the numerical example, the three-point bending test depicted in Figure 3.33 is considered with $P = 1$ N/mm, $L = 2.5$ mm and an eight-ply laminate with stacking sequence $[45,0,-45,90]_{2S}$, a thickness per ply of 0.2 mm and the ply properties of table 3.2.

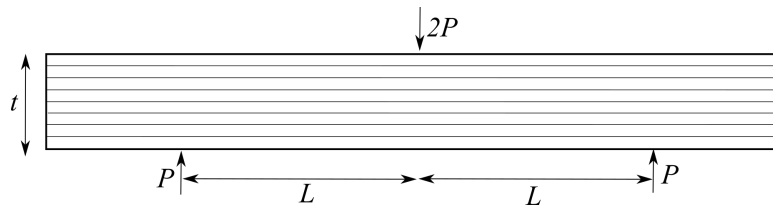


Figure 3.33: Three-point bending test configuration.

All loads are approximated as applied in a length $\delta = 0.05$ mm as a pressure with the resultant force given in Figure 3.33.

The numerical example in the non-regularized case is evaluated by using the LPBM with an order of $n = 100$, which has required a computational time of 30 seconds.

The regularized solution of the present problem consists in a linear distribution of axial stresses in the thickness, which increases or decreases linearly with the s coordinate according to the bending moment. The regularized shear stress has a quadratic distribution in the thickness.

The axial stresses in the top face of the top ply of Figure 3.33 and in the bottom face of the bottom ply of Figure 3.33 depending on the s coordinate are depicted in Figure 3.34 in parallel with their regularized values.

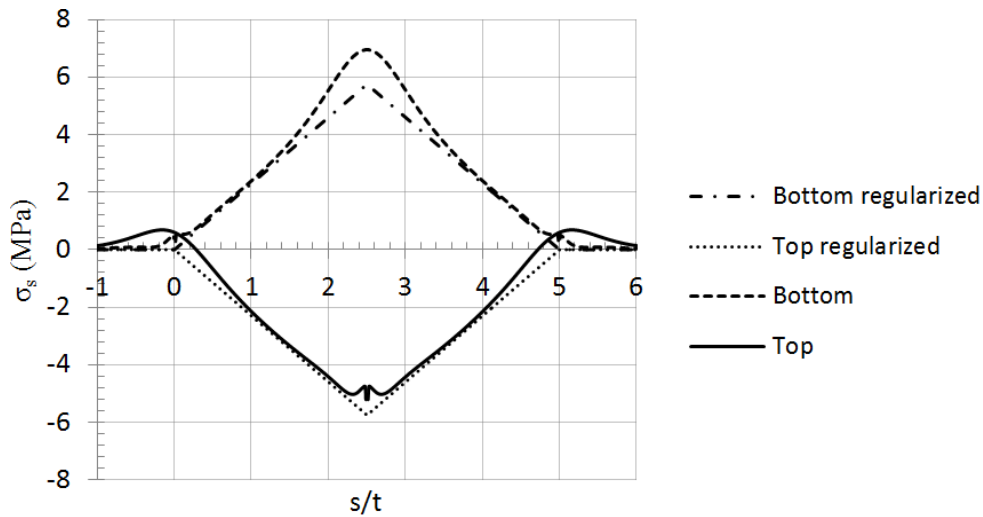


Figure 3.34: Axial stress in the top and bottom of a three-point bending test sample.

The maximum of the axial stress in the bottom ply is a 15% higher than the one predicted by a regularized model, and similarly for the top face in the compression zone. This is due to the non-regularized effect of the punctual load, which changes the distribution of the axial stress near to the section of the load application. Far from the load application points, the axial stress tends to its regularized value.

The maximum and minimum values of the shear stress depending on the s coordinate is depicted in Figure 3.35.

The shear stress presents a singularity at the load application points, tendency which is captured by the non-regularized model. Far away from the load application points, the shear stress tend to its regularized value, which is typically used for the calculation of the interlaminar shear strength

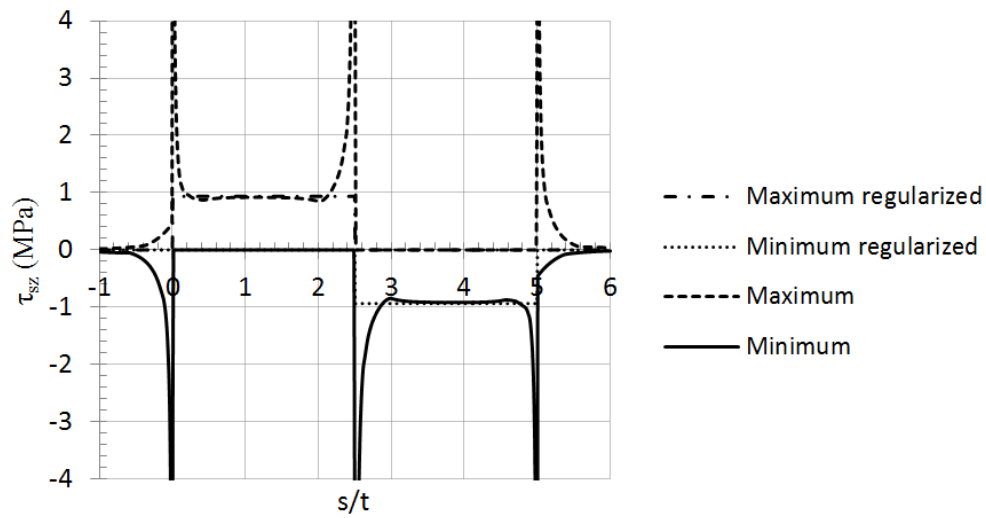


Figure 3.35: Shear stress in a three-point bending test.

when this kind of test is used for characterization of the material.

Chapter 4

Three-dimensional models for evaluating interlaminar stresses

The unfolding failure is typically calculated, from an analytical point of view, by using bi-dimensional (2D) approximations as those presented in Chapter 3, considering in most cases a plane stress or a plane strain approximation, although other generalized plane assumptions may give better results. When a more complex geometry is given, or loads are not constant in the width direction, finite elements models are typically used for calculating the stresses in the curved laminates. By using finite elements models some three-dimensional (3D) effects appearing in curved laminates may be obtained, such as the free-edge effects, the torsion due to the $\pm 45^\circ$ plies or the anticlastic effect.

In the present Chapter, two kinds of 3D models are developed. These 3D models are developed for a singly curved composite laminate loaded under pure bending moment. The pure bending moment case has been chosen because the failure is generally given in zones of the laminate where the bending moment is the predominant load.

The first model developed consists in considering the regularized zone of the laminate, far away from the free-edges in the width direction and far away from a change of curvature in the curved direction. Thus, stresses and strains are considered to depend only on the interlaminar coordinate, which reduces considerably the complexity of the problem expressing the partial derivatives as absolute derivatives with respect to a single coordinate. Spencer et al. [97] developed a similar model, only applied to determining the residual stresses due to a homogeneous temperature change in the laminate. The present regularized model is an extension of this model to consider also the loads acting over the laminate. Several authors have developed approximated models in a 3D stresses state for estimating the stresses due

to the bending moment, as Chiang [112] or Wu and Chi [113]. Notice that this first model is not actually a 3D model while only one coordinate is considered, but the whole 3D stresses state is obtained and 3D effects such as the torsion are considered.

The second model is considered regularized only in the circumferential direction, so the effect of the finite width and the free-edge effects are obtained. This model is developed following the same procedure used for the MBM or the LPBM, considering an approximation of the displacements based on a series expansion. The difference with the MBM and the LPBM is that this novel model is made in a different plane and that all 3D stress components are considered, and not only the stress components contained in a 2D plane. The non-regularized effect in the circumferential direction may be obtained by the MBM or the LPBM, and, consequently, it has not been considered in this model. A combination of both non-regularized effects may be obtained by developing a whole non-regularized 3D model in both directions, whose basis are given with the present 3D non-regularized model. However, this whole non-regularized model is not developed here for the sake of brevity, being a future development of the work presented here.

Therefore, since Chapter 3 is based on a 2D elasticity problem with a 2D constitutive equation, developing a 2D model for obtaining the stresses and strains, while the present Chapter is based on a 3D elasticity problem with all the components of stresses and strains. The basis for solving that 3D problem with a 3D model are presented, but only a 1D model is developed in a first instance and a 2D model including the width direction is finally developed based on an extension of the LPBM.

Both 3D problems will be solved considering residual strains due to the manufacturing process (assumed that they are only due to the homogeneous change of temperature in the curing cycle). The effects of the manufacturing process over the residual stresses in a laminate was summarized by Wisnom et al. [55]. The three most important mechanisms generating these residual stresses are:

- Differential thermal expansion. The thermal expansion coefficient of the matrix is much higher than the corresponding coefficient in the fibre. This implies a different thermal expansion coefficient in unidirectional plies between the fibre direction and the perpendicular ones. Therefore, in a laminate with plies having different orientations, the free deformation of each ply is constrained by the deformation of the other plies and, hence, residual stresses appear. Accordingly, in the cooling after the curing process, the fibre direction of the plies is compressed and the in-plane perpendicular direction is tensioned.

- Cure shrinkage. The polymers have a chemical shrink during the curing process, causing also residual stresses when they cannot flow to compensate this shrinkage. Depending on the resin, this residual stresses may be even in the same order than the residual stresses due to the differential thermal expansion.
- Interaction between the tooling and the laminate. Mainly due to the different thermal expansion coefficients of the tools respect to those of the composite laminate.

The aim of the present work is not to estimate these manufacturing process effects (see Kravchenko et al. [114, 115]), but to consider them in the model and in the stress calculation. In that way, these mechanisms due to the manufacturing process are introduced in the analytical model as residual strains ε_{ij}^{MP} . In the case of the thermal expansion in the cooling from the curing temperature the residual strains, in the orthotropic ply axes, may be expressed as follows:

$$\varepsilon_i^{MP} = \alpha_i \Delta T, \quad i = 1, 2, 3, \quad (4.1)$$

where ΔT is the homogeneous change of temperature in the laminate and α_i are the thermal expansion coefficients in the orthotropic axes of a ply.

These residual strains and, consequently, the associated residual stresses, are not generally considered in the analysis of the unfolding problem as in flat laminates they affect more significantly to the in-plane stresses and not to the interlaminar stresses. However, when the laminate is highly curved residual interlaminar stresses may be also significant, reaching in several cases a high percentage of the strength in that direction (see [56]).

4.1 3D model with double regularization for singly-curved beams under bending moment and residual strains

This model, named 3Ddr in the following, is developed in order to obtain regularized stresses and strains in a curved composite laminate with only one curvature radius, which is considered constant. The model is obtained considering that the regularized stresses and strains in the laminate depend only on the radial coordinate. This hypothesis is only valid in several cases such as a bending problem, a torsion problem or a spatially uniform change of temperature. Therefore, the solution obtained is not valid when the shell

is under non-membrane axial or shear forces, and is not accurate near the free-edges or near to a change of curvature. The solutions is also valid for composite pipes. The geometry considered is depicted in Figure 4.1.

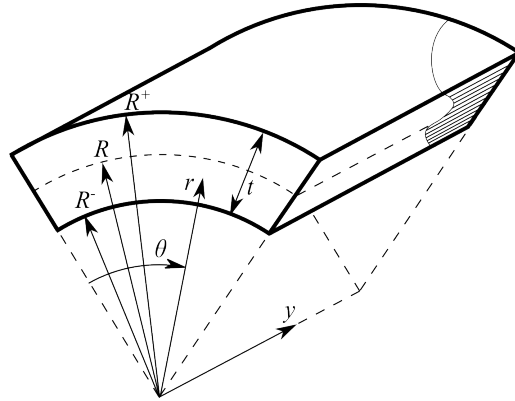


Figure 4.1: Geometry of the studied problem and parameters definition.

A cylindrical coordinate system is used as shown in Figure 4.1, where θ is the curvilinear coordinate, r is the radial coordinate and y is the axial coordinate. The hollow-cylinder-shaped laminate has a mean radius R and a thickness t , which define the inner radius R^- and the outer radius R^+ .

The displacements will generally depend on the three coordinates, where $u(r, \theta, y)$ is the circumferential displacement, $v(r, \theta, y)$ is the axial displacement and $w(r, \theta, y)$ is the radial displacement. However, these displacements are conditioned to cause only r -dependant strains. Therefore, the distribution of the displacements under the condition of strains depending only on the radial coordinate has to be determined. This is carried out by using the compatibility equations, which can be expressed depending on the strains.

The most common residual strains are those caused by a spatially constant temperature increment, ΔT . These residual strains are typically given in the curing process when cooling from the curing temperature. This case can be modelled with the thermal expansion coefficients α_i , with $i = 1, 2, 3$, where the residual strains yield as equation (4.1). Notice that the thermal expansion coefficients are considered to be constant with the temperature.

It is important to determine accurately the residual strains in order to predict in an accurate way the springback and the residual stresses in the component. Residual stresses are given when the component cannot deform freely, which is typically due to the stacking sequence of the laminate, but it can also be due to other geometrical restrictions, such as the curvature of the laminate.

4.1.1 Theoretical development

Strains

The first step in the development of the model is to determine the through-the-thickness distribution of the strains. This distribution is obtained by using the compatibility equations, which expressed in the cylindrical coordinate system are given by:

$$r^2 \frac{\partial^2 \varepsilon_\theta}{\partial y^2} + \frac{\partial^2 \varepsilon_y}{\partial \theta^2} + r \frac{\partial \varepsilon_y}{\partial r} - r \frac{\partial^2 \gamma_{\theta y}}{\partial \theta \partial y} - \frac{1}{r} \frac{\partial \gamma_{ry}}{\partial y} = 0, \quad (4.2a)$$

$$\frac{\partial}{\partial r} \left(r^2 \frac{\partial \varepsilon_\theta}{\partial r} \right) + \frac{\partial^2 \varepsilon_r}{\partial \theta^2} - r \frac{\partial \varepsilon_r}{\partial r} - \frac{\partial^2 (r \gamma_{r\theta})}{\partial \theta \partial r} = 0, \quad (4.2b)$$

$$\frac{\partial^2 \varepsilon_y}{\partial r^2} + \frac{\partial^2 \varepsilon_r}{\partial y^2} - \frac{\partial^2 \gamma_{ry}}{\partial y \partial r} = 0, \quad (4.2c)$$

$$2r \frac{\partial^2 (r \varepsilon_\theta)}{\partial y \partial r} - 2r \frac{\partial \varepsilon_r}{\partial y} + \frac{\partial^2 \gamma_{ry}}{\partial \theta^2} - r \frac{\partial^2 \gamma_{r\theta}}{\partial \theta \partial y} - \frac{\partial^2 (r \gamma_{\theta y})}{\partial \theta \partial r} = 0, \quad (4.2d)$$

$$2r \frac{\partial^2 (\varepsilon_y / r)}{\partial \theta \partial r} + r \frac{\partial^2 \gamma_{r\theta}}{\partial y^2} - r^2 \frac{\partial^2 (\gamma_{\theta y} / r)}{\partial y \partial r} - \frac{\partial^2 \gamma_{ry}}{\partial \theta \partial y} = 0, \quad (4.2e)$$

$$2 \frac{\partial^2 \varepsilon_r}{\partial \theta \partial y} + r \frac{\partial}{\partial r} \left(\frac{1}{r} \frac{\partial (r \gamma_{\theta y})}{\partial r} \right) - r \frac{\partial^2 (\gamma_{ry} / r)}{\partial \theta \partial r} - \frac{1}{r} \frac{\partial^2 (r^2 \gamma_{r\theta})}{\partial y \partial r} = 0, \quad (4.2f)$$

where ε_θ is the circumferential strain, ε_r is the radial strain, ε_y is the axial strain, $\gamma_{r\theta}$ is the interlaminar shear strain associated to the circumferential direction, γ_{ry} is the interlaminar shear strain associated to the axial direction, and $\gamma_{\theta y}$ is the in-plane shear strain.

In the problem under consideration, the strains only depend on the radial coordinate. Therefore, equations (4.2) can be reduced to the following four equations:

$$\frac{d\varepsilon_y(r)}{dr} = 0, \quad (4.3a)$$

$$\frac{d}{dr} \left(r^2 \frac{d\varepsilon_\theta(r)}{dr} \right) - r \frac{d\varepsilon_r(r)}{dr} = 0, \quad (4.3b)$$

$$\frac{d^2 \varepsilon_y(r)}{dr^2} = 0, \quad (4.3c)$$

$$\frac{d}{dr} \left(\frac{1}{r} \frac{d(r \gamma_{\theta y}(r))}{dr} \right) = 0. \quad (4.3d)$$

Equation (4.3c) is automatically accomplished by equation (4.3a), and it is obviated. Notice that the interlaminar shear strains, $\gamma_{ry}(r)$ and $\gamma_{r\theta}(r)$, do

not appear in equations (4.3), so they are not affected by the compatibility equations.

The axial strain, $\varepsilon_y(r)$, has to be constant in the thickness in accordance with equation (4.3a). Therefore, it can be defined from the mean line axial strain, ε_y^0 , as follows:

$$\varepsilon_y(r) = \varepsilon_y^0. \quad (4.4)$$

Equation (4.3d) establishes the condition for the in-plane shear strain, which, integrating the equation, can be expressed depending on the auxiliary in-plane shear constants, $\gamma_{\theta y}^0$ and $\gamma_{y\theta}^0$:

$$\gamma_{\theta y}(r) = \frac{r}{R}\gamma_{\theta y}^0 + \frac{R}{r}\gamma_{y\theta}^0. \quad (4.5)$$

Finally, the circumferential and radial strains are related according to equation (4.3b). Integrating the equation, these strains can be expressed as functions of the radial displacement, $w_o(r)$, and the auxiliary circumferential constant, ε_θ^0 , as follows:

$$\varepsilon_\theta(r) = \varepsilon_\theta^0 + \frac{w_o(r)}{r}, \quad (4.6a)$$

$$\varepsilon_r(r) = \frac{dw_o(r)}{dr}. \quad (4.6b)$$

Therefore, according to the compatibility equations, strains can be expressed depending only on four constants (ε_y^0 , $\gamma_{\theta y}^0$, $\gamma_{y\theta}^0$ and ε_θ^0) and three functions ($\gamma_{ry}(r)$, $\gamma_{r\theta}(r)$ and $w_o(r)$).

Equilibrium equations

The three-dimensional stress tensor in the cylindrical coordinate system is defined by its components: the circumferential stress σ_θ , the radial stress σ_r , the axial stress σ_y , the interlaminar shear stress associated to the axial direction τ_{ry} , the interlaminar shear stress associated to the circumferential direction $\tau_{r\theta}$ and the in-plane shear stress $\tau_{\theta y}$.

The equilibrium equations for the previously defined stresses are given by the following equations:

$$\frac{\partial \sigma_\theta}{\partial \theta} + r \frac{\partial \tau_{\theta y}}{\partial y} + \frac{1}{r} \frac{\partial (r^2 \tau_{r\theta})}{\partial r} = 0, \quad (4.7a)$$

$$\frac{\partial \tau_{\theta y}}{\partial \theta} + r \frac{\partial \sigma_y}{\partial y} + \frac{\partial (r \tau_{ry})}{\partial r} = 0, \quad (4.7b)$$

$$\frac{\partial \tau_{r\theta}}{\partial \theta} + r \frac{\partial \tau_{ry}}{\partial y} + \frac{\partial (r\sigma_r)}{\partial r} = \sigma_\theta. \quad (4.7c)$$

Considering that the stresses only depend on the radial coordinate, equilibrium equations can be written as:

$$\frac{d(r^2 \tau_{r\theta}(r))}{dr} = 0, \quad (4.8a)$$

$$\frac{d(r \tau_{ry}(r))}{dr} = 0, \quad (4.8b)$$

$$\frac{d(r \sigma_r(r))}{dr} = \sigma_\theta(r). \quad (4.8c)$$

Constitutive law

The constitutive law of a generic ply in the orthotropic axes is defined by the following relation:

$$\begin{bmatrix} \sigma_{11}(r) \\ \sigma_{22}(r) \\ \sigma_{33}(r) \\ \sigma_{23}(r) \\ \sigma_{13}(r) \\ \sigma_{12}(r) \end{bmatrix} = \begin{bmatrix} C_{11} & C_{12} & C_{13} & 0 & 0 & 0 \\ C_{12} & C_{22} & C_{23} & 0 & 0 & 0 \\ C_{13} & C_{23} & C_{33} & 0 & 0 & 0 \\ 0 & 0 & 0 & C_{44} & 0 & 0 \\ 0 & 0 & 0 & 0 & C_{55} & 0 \\ 0 & 0 & 0 & 0 & 0 & C_{66} \end{bmatrix} \begin{bmatrix} \varepsilon_{11}(r) - \varepsilon_1^{MP} \\ \varepsilon_{22}(r) - \varepsilon_2^{MP} \\ \varepsilon_{33}(r) - \varepsilon_3^{MP} \\ \varepsilon_{23}(r) \\ \varepsilon_{13}(r) \\ \varepsilon_{12}(r) \end{bmatrix}, \quad (4.9)$$

where σ_{ij} (with $i, j = 1, 2, 3$) are the stresses in the orthotropic coordinate system, ε_{ij} (with $i, j = 1, 2, 3$) are the strains in the orthotropic coordinate system, C_{ij} (with $i, j = 1, 2, \dots, 6$) are the orthotropic stiffnesses of the ply and ε_i^{MP} (with $i = 1, 2, 3$) are the residual strains induced during the manufacturing process. Notice that residual strains are constant in the thickness.

The constitutive law given by equation (4.9) has to be rotated around axis x_3 (which coincides at each point with the radial coordinate axis r) in order to obtain the constitutive law expressed in the cylindrical coordinate system. Proceeding as commented, the constitutive law of a ply p can be written as:

$$\begin{bmatrix} \sigma_\theta^p(r) \\ \sigma_y^p(r) \\ \sigma_r^p(r) \\ \tau_{ry}^p(r) \\ \tau_{r\theta}^p(r) \\ \tau_{\theta y}^p(r) \end{bmatrix} = \begin{bmatrix} \bar{C}_{11}^p & \bar{C}_{12}^p & \bar{C}_{13}^p & 0 & 0 & \bar{C}_{16}^p \\ \bar{C}_{12}^p & \bar{C}_{22}^p & \bar{C}_{23}^p & 0 & 0 & \bar{C}_{26}^p \\ \bar{C}_{13}^p & \bar{C}_{23}^p & \bar{C}_{33}^p & 0 & 0 & \bar{C}_{36}^p \\ 0 & 0 & 0 & \bar{C}_{44}^p & \bar{C}_{45}^p & 0 \\ 0 & 0 & 0 & \bar{C}_{45}^p & \bar{C}_{55}^p & 0 \\ \bar{C}_{16}^p & \bar{C}_{26}^p & \bar{C}_{36}^p & 0 & 0 & \bar{C}_{66}^p \end{bmatrix} \begin{bmatrix} \varepsilon_\theta(r) - \Delta \varepsilon_\theta^p \\ \varepsilon_y(r) - \Delta \varepsilon_y^p \\ \varepsilon_r(r) - \Delta \varepsilon_r^p \\ \gamma_{ry}(r) \\ \gamma_{r\theta}(r) \\ \gamma_{\theta y}(r) - \Delta \gamma_{\theta y}^p \end{bmatrix}, \quad (4.10)$$

where \bar{C}_{ij}^p (with $i, j = 1, 2, \dots, 6$) are the stiffnesses of the ply p expressed in the cylindrical coordinate system, $\Delta\varepsilon_\theta^p$ is the residual strain of the ply p in the circumferential direction, $\Delta\varepsilon_y^p$ is the residual strain of the ply p in the axial direction, $\Delta\varepsilon_r^p$ is the residual strain of the ply p in the radial direction and $\Delta\gamma_{\theta y}^p$ is the residual shear in-plane strain of the ply p . Notice that plies may be differently oriented and, therefore, stresses have been marked with a superscript p indicating in which ply they are calculated.

Resolution of the interlaminar shear strains

The interlaminar shear strain functions, $\gamma_{ry}(r)$ and $\gamma_{r\theta}(r)$, can be easily determined by combining the corresponding equilibrium equations with the constitutive law. Hence, substituting the interlaminar shear constitutive equations of (4.10) in the equilibrium equations (4.8a) and (4.8b) they yield:

$$\bar{C}_{44}^p \frac{d(r\gamma_{ry}(r))}{dr} + \bar{C}_{45}^p \frac{d(r\gamma_{r\theta}(r))}{dr} = 0, \quad (4.11a)$$

$$\bar{C}_{45}^p \frac{d(r^2\gamma_{ry}(r))}{dr} + \bar{C}_{55}^p \frac{d(r^2\gamma_{r\theta}(r))}{dr} = 0. \quad (4.11b)$$

The solution of the differential equations system (4.11) yield:

$$\gamma_{ry}(r) = \frac{R_p^-}{\zeta_{45}^p r} \left(\bar{C}_{55}^p \eta_1^p - \bar{C}_{45}^p \frac{R_p^-}{r} \eta_2^p \right), \quad (4.12a)$$

$$\gamma_{r\theta}(r) = \frac{R_p^-}{\zeta_{45}^p r} \left(-\bar{C}_{45}^p \eta_1^p + \bar{C}_{44}^p \frac{R_p^-}{r} \eta_2^p \right), \quad (4.12b)$$

where R_p^- is the lowest radius of ply p (which constitutes the interface between ply p and ply $p-1$) and, equivalently, R_p^+ is the highest radius of ply p . η_1^p and η_2^p are the integration constants in ply p , and ζ_{45}^p is defined by:

$$\zeta_{45}^p = \bar{C}_{44}^p \bar{C}_{55}^p - (\bar{C}_{45}^p)^2. \quad (4.13)$$

Substituting equations (4.12) into the corresponding constitutive equations of (4.10), interlaminar shear stresses yield:

$$\tau_{ry}^p(r) = \frac{R_p^-}{r} \eta_1^p, \quad (4.14a)$$

$$\tau_{r\theta}^p(r) = \left(\frac{R_p^-}{r} \right)^2 \eta_2^p. \quad (4.14b)$$

Equations (4.14) may also be obtained by integrating directly equations (4.8a) and (4.8b). In view of (4.14), there are a total of $2N_p$ integration

constants, η_1^p and η_2^p , with $p = 1, 2, \dots, N_p$, where N_p is the total number of plies. An amount of $(2N_p - 2)$ equations can be obtained by using the equilibrium between plies, which establish the continuity of the interlaminar stresses in the interfaces. The other two equations can be obtained by applying a boundary condition of the interlaminar stresses in the inner or in the outer radius of the laminate. If a boundary condition for one of the through-thickness shear stresses is applied on the inner or outer radius, the other boundary condition in the opposite radius is automatically satisfied due to the equilibrium equations.

In the present model, a boundary condition of a null value of both shear interlaminar stresses in the inner radius is considered, which implies a null value of both interlaminar stresses in the outer radius. With these conditions, the integration constants yield $\eta_1^p = \eta_2^p = 0$ for every ply p , and, therefore, interlaminar shear stresses and strains are null in the whole thickness.

Resolution of the radial displacements

The radial displacements can be determined by the radial equilibrium equation. Substituting the constitutive law (4.10) into the equilibrium equation (4.8c) it yields:

$$\begin{aligned} \bar{C}_{13}^p \frac{d(r\varepsilon_\theta(r))}{dr} + \bar{C}_{23}^p \frac{d(r\varepsilon_y(r))}{dr} + \bar{C}_{33}^p \frac{d(r\varepsilon_r(r))}{dr} + \bar{C}_{36}^p \frac{d(r\gamma_{\theta y}(r))}{dr} = \\ \bar{C}_{11}^p \varepsilon_\theta(r) + \bar{C}_{12}^p \varepsilon_y(r) + \bar{C}_{13}^p \varepsilon_r(r) + \bar{C}_{16}^p \gamma_{\theta y}(r) + \delta_3^p - \delta_1^p, \end{aligned} \quad (4.15)$$

where:

$$\delta_i^p = \bar{C}_{1i}^p \Delta \varepsilon_\theta^p + \bar{C}_{2i}^p \Delta \varepsilon_y^p + \bar{C}_{3i}^p \Delta \varepsilon_r^p + \bar{C}_{6i}^p \Delta \gamma_{\theta y}^p, \quad i = 1, 2, 3, 6. \quad (4.16)$$

Notice that $\bar{C}_{ij}^p = \bar{C}_{ji}^p$.

Substituting the strains from equations (4.4), (4.5) and (4.6) into equation (4.15):

$$\begin{aligned} \bar{C}_{33}^p r \frac{d}{dr} \left(r \frac{dw_o(r)}{dr} \right) - \bar{C}_{11}^p w_o(r) = \\ h_1^p \gamma_{\theta y}^0 \frac{r^2}{R} + [h_2^p \varepsilon_\theta^0 + h_3^p \varepsilon_y^0 + \delta_3^p - \delta_1^p] r + \bar{C}_{16}^p R \gamma_{y\theta}^0, \end{aligned} \quad (4.17)$$

where the auxiliary parameters h_1^p , h_2^p and h_3^p are defined as:

$$h_1^p = \bar{C}_{16}^p - 2\bar{C}_{36}^p, \quad h_2^p = \bar{C}_{11}^p - \bar{C}_{13}^p, \quad h_3^p = \bar{C}_{12}^p - \bar{C}_{23}^p. \quad (4.18)$$

Equation (4.17) can be integrated by, first, obtaining a particular solution and, second, solving the homogeneous equation. Therefore, integrating equation (4.17) the radial displacement yields:

$$w_0(r) = -h_4^p R \gamma_{y\theta}^0 + r (h_5^p \varepsilon_\theta^0 + h_6^p \varepsilon_y^0 + h_7^p) + \frac{r^2}{R} h_8^p \gamma_{\theta y}^0 + \frac{\xi_1^p r^{\kappa^p}}{\bar{C}_{13}^p + \kappa^p \bar{C}_{33}^p} + \frac{\xi_2^p r^{-\kappa^p}}{\bar{C}_{13}^p - \kappa^p \bar{C}_{33}^p}, \quad (4.19)$$

where ξ_1^p and ξ_2^p are two integration constants introduced by the homogeneous equation, which depend on the ply p .

In (4.19), the parameter κ^p , establishing the radial dependence of the radial displacement, is defined as:

$$\kappa^p = \sqrt{\frac{\bar{C}_{11}^p}{\bar{C}_{33}^p}}, \quad (4.20)$$

and the auxiliary parameters are defined as:

$$h_4^p = \frac{\bar{C}_{16}^p}{\bar{C}_{11}^p}, \quad h_5^p = \frac{\bar{C}_{11}^p - \bar{C}_{13}^p}{\bar{C}_{33}^p - \bar{C}_{11}^p}, \quad h_6^p = \frac{\bar{C}_{12}^p - \bar{C}_{23}^p}{\bar{C}_{33}^p - \bar{C}_{11}^p}, \quad (4.21a)$$

$$h_7^p = \frac{\delta_3^p - \delta_1^p}{\bar{C}_{33}^p - \bar{C}_{11}^p}, \quad h_8^p = \frac{\bar{C}_{16}^p - 2\bar{C}_{36}^p}{4\bar{C}_{33}^p - \bar{C}_{11}^p}. \quad (4.21b)$$

The particular solution of (4.19) is not valid in plies with $\kappa^p = 1$ or with $\kappa^p = 2$. These cases are considered in a following subsection. The particular solution is not valid when $\kappa^p = 0$ either, but this is not a realistic case, and it is not studied.

Notice that κ^p reminds the Lekhnitskii's parameter given in equation (3.10a) relating the circumferential and the radial stiffnesses. However, it is not exactly the same, coinciding only when the Lekhnitskii's equations are applied considering a plane strain assumption.

The ply integration constants ξ_1^p and ξ_2^p constitute a set of $2N_p$ unknown variables. These variables are determined by imposing the continuity of $w_1(r)$ and $\sigma_r(r)$ between plies, which implies a total of $2N_p - 2$ equations, and by imposing the boundary conditions of $\sigma_r(r)$ in both radial boundaries, R^- and R^+ . These boundary conditions are usually applied with a null

value, but they can also have another value, which will cause membrane forces, N_θ , which are defined as:

$$N_\theta = \int_{R^-}^{R^+} \sigma_\theta(r) dr. \quad (4.22)$$

Substituting the equilibrium equation (4.8c) into (4.22), the membrane forces yield:

$$N_\theta = \int_{R^-}^{R^+} \frac{d(r\sigma_r(r))}{dr} dr = R^+ p^+ - R^- p^-. \quad (4.23)$$

Once the continuity between plies and the boundary conditions have been imposed, the unknown variables ξ_1^p and ξ_2^p are determined depending on the strain constant parameters ε_θ^0 , ε_y^0 , $\gamma_{\theta y}^0$ and $\gamma_{y\theta}^0$. These strain parameters define the circumferential strain, the axial strain and torsional strains, which can be fixed as inputs in the problem, or they can be calculated from the applied loads to the laminate. The calculation from applied loads is studied in a following section. In this last case, the unknown variables ξ_1^p and ξ_2^p are determined jointly with the strain constant parameters ε_θ^0 , ε_y^0 , $\gamma_{\theta y}^0$ and $\gamma_{y\theta}^0$.

Strains and stresses calculation

In order to apply the equilibrium equations of the radial stress, σ_r , between plies, it is necessary to obtain its closed-form equation. In this way, stresses expressions can be obtained from the strains expressions. Strains expressions can be obtained by substituting the radial displacement, $w_0(r)$, given in equation (4.19), into equations (4.6), which yield:

$$\varepsilon_\theta(r) = -\frac{R}{r} h_4^p \gamma_{y\theta}^0 + (1 + h_5^p) \varepsilon_\theta^0 + h_6^p \varepsilon_y^0 + h_7^p + \frac{r}{R} h_8^p \gamma_{\theta y}^0 + \frac{\xi_1^p r^{\kappa^p - 1}}{\bar{C}_{13}^p + \kappa^p \bar{C}_{33}^p} + \frac{\xi_2^p r^{-\kappa^p - 1}}{\bar{C}_{13}^p - \kappa^p \bar{C}_{33}^p}, \quad (4.24a)$$

$$\varepsilon_r(r) = h_5^p \varepsilon_\theta^0 + h_6^p \varepsilon_y^0 + h_7^p + 2 \frac{r}{R} h_8^p \gamma_{\theta y}^0 + \frac{\kappa^p \xi_1^p r^{\kappa^p - 1}}{\bar{C}_{13}^p + \kappa^p \bar{C}_{33}^p} - \frac{\kappa^p \xi_2^p r^{-\kappa^p - 1}}{\bar{C}_{13}^p - \kappa^p \bar{C}_{33}^p}. \quad (4.24b)$$

Substituting the strains given in equations (4.24), (4.4) and (4.5) into the constitutive law (4.10), the stresses can be written as:

$$\sigma_\theta^p(r) = H_{11}^p \varepsilon_\theta^0 + H_{12}^p \varepsilon_y^0 + \frac{R}{r} H_{13}^p \gamma_{y\theta}^0 + H_{14}^p \gamma_{\theta y}^0 \frac{r}{R} + H_{15}^p \xi_1^p r^{\kappa^p - 1} + H_{16}^p \xi_2^p r^{-\kappa^p - 1} + H_{17}^p, \quad (4.25a)$$

$$\sigma_y^p(r) = H_{21}^p \varepsilon_\theta^0 + H_{22}^p \varepsilon_y^0 + \frac{R}{r} H_{23}^p \gamma_{y\theta}^0 + H_{24}^p \gamma_{\theta y}^0 \frac{r}{R} + H_{25}^p \xi_1^p r^{\kappa^p-1} + H_{26}^p \xi_2^p r^{-\kappa^p-1} + H_{27}^p, \quad (4.25b)$$

$$\sigma_r^p(r) = H_{31}^p \varepsilon_\theta^0 + H_{32}^p \varepsilon_y^0 + \frac{R}{r} H_{33}^p \gamma_{y\theta}^0 + H_{34}^p \gamma_{\theta y}^0 \frac{r}{R} + H_{35}^p \xi_1^p r^{\kappa^p-1} + H_{36}^p \xi_2^p r^{-\kappa^p-1} + H_{37}^p, \quad (4.25c)$$

$$\tau_{\theta y}^p(r) = H_{61}^p \varepsilon_\theta^0 + H_{62}^p \varepsilon_y^0 + \frac{R}{r} H_{63}^p \gamma_{y\theta}^0 + H_{64}^p \gamma_{\theta y}^0 \frac{r}{R} + H_{65}^p \xi_1^p r^{\kappa^p-1} + H_{66}^p \xi_2^p r^{-\kappa^p-1} + H_{67}^p, \quad (4.25d)$$

where the auxiliary ply constants H_{ij}^p , with $i = 1, 2, 3, 6$ and $j = 1, 2, \dots, 7$, are defined as follows:

$$H_{i1}^p = \bar{C}_{i1}^p + (\bar{C}_{i1}^p + \bar{C}_{i3}^p) h_5^p, \quad i = 1, 2, 3, 6, \quad (4.26a)$$

$$H_{i2}^p = \bar{C}_{i2}^p + (\bar{C}_{i1}^p + \bar{C}_{i3}^p) h_6^p, \quad i = 1, 2, 3, 6, \quad (4.26b)$$

$$H_{i3}^p = \bar{C}_{i6}^p - \bar{C}_{i1}^p h_4^p, \quad i = 1, 2, 3, 6, \quad (4.26c)$$

$$H_{i4}^p = \bar{C}_{i6}^p + (\bar{C}_{i1}^p + 2\bar{C}_{i3}^p) h_8^p, \quad i = 1, 2, 3, 6, \quad (4.26d)$$

$$H_{i5}^p = \frac{\bar{C}_{i1}^p + \kappa^p \bar{C}_{i3}^p}{\bar{C}_{13}^p + \kappa^p \bar{C}_{33}^p}, \quad H_{i6}^p = \frac{\bar{C}_{i1}^p - \kappa^p \bar{C}_{i3}^p}{\bar{C}_{13}^p - \kappa^p \bar{C}_{33}^p}, \quad i = 1, 2, 3, 6, \quad (4.26e)$$

$$H_{i7}^p = (\bar{C}_{i1}^p + \bar{C}_{i3}^p) h_7^p - \delta_i^p, \quad i = 1, 2, 3, 6, \quad (4.26f)$$

Therefore, equation (4.25c) is used to apply the continuity of the transversal stresses between plies, in the same way than equation (4.19) is used to apply the continuity of the radial displacements.

Displacements calculation

The displacement field is defined by its components: the circumferential displacement $u(r, \theta, y)$, the axial displacement $v(r, \theta, y)$ and the radial displacement $w(r, \theta, y)$. Displacements are obtained by integrating the displacement/strain relations, which can be expressed in cylindrical coordinates as:

$$\varepsilon_\theta(r) = \frac{1}{r} \frac{\partial u(r, \theta, y)}{\partial \theta} + \frac{w(r, \theta, y)}{r}, \quad \varepsilon_y(r) = \frac{\partial v(r, \theta, y)}{\partial y}, \quad \varepsilon_r(r) = \frac{\partial w(r, \theta, y)}{\partial r}, \quad (4.27a)$$

$$\gamma_{\theta y}(r) = \frac{\partial u(r, \theta, y)}{\partial y} + \frac{1}{r} \frac{\partial v(r, \theta, y)}{\partial \theta}, \quad \gamma_{ry}(r) = \frac{\partial w(r, \theta, y)}{\partial y} + \frac{\partial v(r, \theta, y)}{\partial r}, \quad (4.27b)$$

$$\gamma_{r\theta}(r) = \frac{\partial u(r, \theta, y)}{\partial r} - \frac{u(r, \theta, y)}{r} + \frac{1}{r} \frac{\partial w(r, \theta, y)}{\partial \theta}. \quad (4.27c)$$

Therefore, by introducing (4.4), (4.5), (4.6) and the null values of the interlaminar shear strains ($\gamma_{r\theta} = \gamma_{ry} = 0$) into equations (4.27), and integrating the equations, displacements (cancelling the rigid solid motion that appears) are given by:

$$u(r, \theta, y) = y \frac{r}{R} \gamma_{\theta y}^0 + \theta r \varepsilon_{\theta}^0, \quad (4.28a)$$

$$v(r, \theta, y) = y \varepsilon_y^0 + R \theta \gamma_{y\theta}^0, \quad (4.28b)$$

$$w(r, \theta, y) = w_0(r). \quad (4.28c)$$

Hence, ε_{θ}^0 is associated to a normal circumferential deformation, ε_y^0 is associated to a normal axial deformation, $\gamma_{\theta y}^0$ is associated to a torsional deformation and $\gamma_{y\theta}^0$ is associated to an in-plane shear deformation in the width direction, as depicted in Figure 4.2.

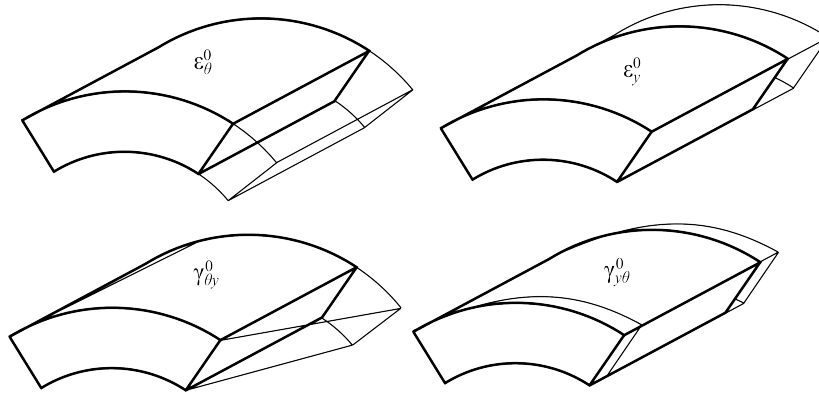


Figure 4.2: Deformations associated to the strain constant parameters.

4.1.2 Loads application and boundary conditions

The forces and moments in the laminate are firstly defined for a general loading state depending on the two in-plane coordinates, θ and y . After that, the non-dependence of these forces and moments with both in-plane coordinates is considered, in order to obtain their values from the applied loads.

Once the values of the forces and moments have been obtained, a system of linear equations is developed in order to determine the strain constant parameters, ε_{θ}^0 , ε_y^0 , $\gamma_{\theta y}^0$ and $\gamma_{y\theta}^0$, and the integration constants of the radial displacement, ξ_1^p and ξ_2^p , depending on these loads.

Equilibrium of forces and moments

The forces and moments in a cylindrical shell for a general loading state are defined by the following expressions [116, chap. 1]:

$$N_\theta(\theta, y) = \int_{R^-}^{R^+} \sigma_\theta(r, \theta, y) dr, \quad M_\theta(\theta, y) = \int_{R^-}^{R^+} (r - R) \sigma_\theta(r, \theta, y) dr, \quad (4.29a)$$

$$N_{\theta y}(\theta, y) = \int_{R^-}^{R^+} \tau_{\theta y}(r, \theta, y) dr, \quad M_{\theta y}(\theta, y) = \int_{R^-}^{R^+} (r - R) \tau_{\theta y}(r, \theta, y) dr, \quad (4.29b)$$

$$N_y(\theta, y) = \int_{R^-}^{R^+} \frac{r}{R} \sigma_y(r, \theta, y) dr, \quad M_y(\theta, y) = \int_{R^-}^{R^+} \frac{r}{R} (r - R) \sigma_y(r, \theta, y) dr, \quad (4.29c)$$

$$N_{y\theta}(\theta, y) = \int_{R^-}^{R^+} \frac{r}{R} \tau_{\theta y}(r, \theta, y) dr, \quad M_{y\theta}(\theta, y) = \int_{R^-}^{R^+} \frac{r}{R} (r - R) \tau_{\theta y}(r, \theta, y) dr, \quad (4.29d)$$

$$Q_\theta(\theta, y) = \int_{R^-}^{R^+} \tau_{r\theta}(r, \theta, y) dr, \quad Q_y(\theta, y) = \int_{R^-}^{R^+} \frac{r}{R} \tau_{ry}(r, \theta, y) dr, \quad (4.29e)$$

where N_θ , as defined previously, is the membrane force or the circumferential force, M_θ is the circumferential moment, N_y is the axial force, M_y is the axial moment, Q_θ is the circumferential shear force, Q_y is the axial shear force, $N_{\theta y}$ is the in-plane shear force associated to the circumferential direction, $N_{y\theta}$ is the in-plane shear force associated to the axial direction, $M_{\theta y}$ is the torsional moment associated to the circumferential direction and $M_{y\theta}$ is the torsional moment associated to the axial direction. Notice that forces and moments are defined per unit width due to the shell assumption.

Notice that torsional moment associated to the circumferential direction and the in-plane shear forces are related by the following equation:

$$M_{\theta y}(\theta, y) = R(N_{y\theta}(\theta, y) - N_{\theta y}(\theta, y)). \quad (4.30)$$

The equilibrium equations of forces can be obtained by integrating equations (4.7) in the thickness and considering the value of normal interlaminar stresses and the null value of shear interlaminar stresses in the radial boundaries, yielding:

$$\frac{\partial N_\theta(\theta, y)}{\partial \theta} + R \frac{\partial N_{y\theta}(\theta, y)}{\partial y} + Q_\theta(\theta, y) = 0, \quad (4.31a)$$

$$\frac{\partial N_{\theta y}(\theta, y)}{\partial \theta} + R \frac{\partial N_y(\theta, y)}{\partial y} = 0, \quad (4.31b)$$

$$\frac{\partial Q_\theta(\theta, y)}{\partial \theta} + R \frac{\partial Q_y(\theta, y)}{\partial y} + R^+ p^+ - R^- p^- = N_\theta(\theta, y). \quad (4.31c)$$

The equilibrium equations of moments can be obtained by integrating equations (4.7a) and (4.7b) in the thickness multiplied by $(r - R)$ and considering a null value of shear interlaminar stresses in the radial boundaries. These equilibrium equations yield:

$$\frac{\partial M_\theta(\theta, y)}{\partial \theta} + R \frac{\partial M_{y\theta}(\theta, y)}{\partial y} = R Q_\theta(\theta, y), \quad (4.32a)$$

$$\frac{\partial M_{\theta y}(\theta, y)}{\partial \theta} + R \frac{\partial M_y(\theta, y)}{\partial y} = R Q_y(\theta, y). \quad (4.32b)$$

Suppressing $M_{\theta y}(\theta, y)$ by substituting (4.30) in (4.32b):

$$\frac{\partial N_{y\theta}(\theta, y)}{\partial \theta} - \frac{\partial N_{\theta y}(\theta, y)}{\partial \theta} + \frac{\partial M_y(\theta, y)}{\partial y} = Q_y(\theta, y). \quad (4.33)$$

Considering that the zone under study is far enough from the free edges and the changes of curvature and under a loading state for which stresses do not depend on θ and y , then the forces and moments neither depend on θ nor on y . Substituting these conditions in equations (4.31c) and (4.32) the circumferential and axial shear forces, Q_θ and Q_y , are null and the circumferential force, N_θ , is given by the membrane forces (4.23). The absence of the shear forces was previously demonstrated with the absence of the interlaminar shear stresses, $\tau_{r\theta}$ and τ_{ry} . However, these conditions are not sufficient to solve the problem.

In that way, to get the conditions to solve the problem it is necessary to consider the non-dependence with each coordinate independently of the other. Hence, considering only the non-dependence of the forces and moments with the y -direction, equations (4.31) and (4.32a) yield:

$$\frac{dN_\theta(\theta)}{d\theta} + Q_\theta(\theta) = 0, \quad \frac{dQ_\theta(\theta)}{d\theta} + R^+ p^+ - R^- p^- = N_\theta(\theta), \quad (4.34a)$$

$$\frac{dN_{\theta y}(\theta)}{d\theta} = 0, \quad (4.34b)$$

$$\frac{dM_\theta(\theta)}{d\theta} = R Q_\theta(\theta). \quad (4.34c)$$

Notice that $Q_\theta(\theta)$ is null and $N_\theta(\theta)$ is given by the membrane forces in the zone far enough from the free edges and the changes of curvature. However, equation (4.34a) implies a sinusoidal variation of these forces plus the membrane force, so taking into account that far enough from the free

edges and the changes of curvatures in the θ -direction they have to be equal to the membrane value, implies that $Q_\theta(\theta) = 0$ and $N_\theta(\theta)$ is given by the membrane forces (4.23). Substituting the null value of $Q_\theta(\theta)$ in equation (4.34c) it implies that $M_\theta(\theta)$ is constant, so that $M_\theta(\theta) = M_0$ with M_0 being the applied bending moment at the θ boundary. Equation (4.34b) implies also a constant value of $N_{\theta y}(\theta) = P_0$, with P_0 being the applied in-plane shear force in the circumferential direction at the θ boundary.

Notice that M_0 and P_0 are not respectively the total applied bending moment and in-plane shear force divided between the width of the specimen in the axial direction. This is due to the consideration of being far enough from the free edges in the y -direction. Near to the free edges the distribution may be different so $M_\theta(\theta)$ and $N_{\theta y}(\theta)$ are not constant in the whole width. However, when the width is much higher than the thickness $M_\theta(\theta)$ and $N_{\theta y}(\theta)$ can be approximated by the total applied bending moment and in-plane shear force divided by the width.

If a closed cylinder is calculated (a pipe), the values of M_0 and P_0 may not be easy to obtain. However, in this case the displacements have to take the same value at $\theta = 0$ and at $\theta = 2\pi$. Introducing this condition into (4.28) the two equations of M_0 and P_0 can be substituted by null values of ε_θ^0 and $\gamma_{y\theta}^0$.

In the same way, considering only the non-dependence of the forces and moments with the θ -direction, equations (4.31a), (4.31b) and (4.32a) yield:

$$\frac{dN_y(y)}{dy} = 0, \quad (4.35a)$$

$$R \frac{dN_{y\theta}(y)}{dy} + Q_\theta(y) = 0, \quad \frac{dM_{y\theta}(y)}{dy} = Q_\theta(y). \quad (4.35b)$$

Equation (4.35a) implies a constant value of the axial force, $N_y(y) = N_0$, where N_0 is the applied axial load. On the other side, equations (4.35b) imply, suppressing $Q_\theta(y)$ by substituting one equation in the other, a constant value of $M_{y\theta}(y) + RN_{y\theta}(y) = T_0$, where T_0 is the applied torsional moment.

Therefore, in the studied zone where stresses and strains depend only on the radial coordinate, the four remaining equations to close the problem and determining the strain constant parameters, ε_θ^0 , ε_y^0 , $\gamma_{\theta y}^0$ and $\gamma_{y\theta}^0$, are given by the applied loads $M_\theta = M_0$, $N_y = N_0$, $N_{\theta y} = P_0$ and $M_{y\theta} + RN_{y\theta} = T_0$.

The forces and moments not included in the previous conditions, such as the membrane force (N_θ) or the axial moment (M_y), are not inputs of the problems as they are results of other loads or effects, such as the pressure or the anticlastic effect combined with the curvature, and they are calculated from the input loads.

Application of the external loads

To apply the external loads equation it is necessary to integrate equations (4.25) accordingly to the forces and moments definitions. Therefore, substituting the circumferential stress (4.25a) into the definition of the circumferential bending moment (4.29a) and considering that $M_\theta = M_0$, the applied bending moment per unit of width can be written as:

$$M_0 = \sum_{p=1}^{N_p} \int_{R_p^-}^{R_p^+} (r - R) \sigma_\theta^p(r) dr = \sum_{p=1}^{N_p} (K_{1p}^M \varepsilon_\theta^0 + K_{2p}^M \varepsilon_y^0 + K_{3p}^M \gamma_{y\theta}^0 + K_{4p}^M \gamma_{\theta y}^0 + K_{5p}^M \xi_1^p + K_{6p}^M \xi_2^p + K_{7p}^M), \quad (4.36)$$

where the auxiliary ply constants K_{jp}^M (with $j = 1, 2, \dots, 7$ and $p = 1, 2, \dots, N_p$) are defined as follows:

$$K_{jp}^M = H_{1j}^p \frac{R_p^+ - R_p^-}{2} (R_p^+ + R_p^- - 2R), \quad j = 1, 2, 7, \quad (4.37a)$$

$$K_{3p}^M = H_{13}^p R \left(R_p^+ - R_p^- - R \log \left(\frac{R_p^+}{R_p^-} \right) \right), \quad (4.37b)$$

$$K_{4p}^M = H_{14}^p \left(\frac{(R_p^+)^3 - (R_p^-)^3}{3R} - \frac{(R_p^+)^2 - (R_p^-)^2}{2} \right), \quad (4.37c)$$

$$K_{5p}^M = H_{15}^p \left(\frac{(R_p^+)^{\kappa^p+1} - (R_p^-)^{\kappa^p+1}}{\kappa^p + 1} - R \frac{(R_p^+)^{\kappa^p} - (R_p^-)^{\kappa^p}}{\kappa^p} \right), \quad (4.37d)$$

$$K_{6p}^M = H_{16}^p \left(\frac{(R_p^+)^{1-\kappa^p} - (R_p^-)^{1-\kappa^p}}{1 - \kappa^p} + R \frac{(R_p^+)^{-\kappa^p} - (R_p^-)^{-\kappa^p}}{\kappa^p} \right). \quad (4.37e)$$

Substituting the axial stress (4.25b) into the definition of the axial force (4.29c) and considering that $N_y = N_0$, the applied axial force per unit of length can be written as:

$$N_0 = \sum_{p=1}^{N_p} \int_{R_p^-}^{R_p^+} \frac{r}{R} \sigma_y^p(r) dr = \sum_{p=1}^{N_p} (K_{1p}^N \varepsilon_\theta^0 + K_{2p}^N \varepsilon_y^0 + K_{3p}^N \gamma_{y\theta}^0 + K_{4p}^N \gamma_{\theta y}^0 + K_{5p}^N \xi_1^p + K_{6p}^N \xi_2^p + K_{7p}^N), \quad (4.38)$$

where the auxiliary ply constants K_{jp}^N (with $j = 1, 2, \dots, 7$ and $p = 1, 2, \dots, N_p$) are defined as follows:

$$K_{jp}^N = H_{2j}^p \frac{(R_p^+)^2 - (R_p^-)^2}{2R}, \quad j = 1, 2, 7, \quad (4.39a)$$

$$K_{3p}^N = H_{23}^p (R_p^+ - R_p^-), \quad K_{4p}^N = H_{24}^p \frac{(R_p^+)^3 - (R_p^-)^3}{3R^2}, \quad (4.39b)$$

$$K_{5p}^N = H_{25}^p \frac{(R_p^+)^{\kappa^p+1} - (R_p^-)^{\kappa^p+1}}{(\kappa^p + 1)R}, \quad K_{6p}^N = H_{26}^p \frac{(R_p^+)^{1-\kappa^p} - (R_p^-)^{1-\kappa^p}}{(1 - \kappa^p)R}. \quad (4.39c)$$

Substituting the in-plane shear stress (4.25d) into the definition of the in-plane shear force associated to the circumferential direction (4.29b) and considering that $N_{\theta y} = P_0$, the applied in-plane shear force per unit of length can be written as:

$$P_0 = \sum_{p=1}^{N_p} \int_{R_p^-}^{R_p^+} \tau_{\theta y}^p(r) dr = \sum_{p=1}^{N_p} (K_{1p}^P \varepsilon_{\theta}^0 + K_{2p}^P \varepsilon_y^0 + K_{3p}^P \gamma_{y\theta}^0 + K_{4p}^P \gamma_{\theta y}^0 + K_{5p}^P \xi_1^p + K_{6p}^P \xi_2^p + K_{7p}^P), \quad (4.40)$$

where the auxiliary ply constants K_{jp}^P (with $j = 1, 2, \dots, 7$ and $p = 1, 2, \dots, N_p$) are defined as follows:

$$K_{jp}^P = H_{6j}^p (R_p^+ - R_p^-), \quad j = 1, 2, 7, \quad (4.41a)$$

$$K_{3p}^P = H_{63}^p R \log \left(\frac{R_p^+}{R_p^-} \right), \quad K_{4p}^P = H_{64}^p \frac{(R_p^+)^2 - (R_p^-)^2}{2R}, \quad (4.41b)$$

$$K_{5p}^P = H_{65}^p \frac{(R_p^+)^{\kappa^p} - (R_p^-)^{\kappa^p}}{\kappa^p}, \quad K_{6p}^P = -H_{66}^p \frac{(R_p^+)^{-\kappa^p} - (R_p^-)^{-\kappa^p}}{\kappa^p}. \quad (4.41c)$$

Finally, substituting the in-plane shear stress (4.25d) into the definition of the in-plane shear moment and force associated to the axial direction (4.29d) and considering that $M_{y\theta} + RN_{y\theta} = T_0$, the applied torsional moment per unit of length can be written as:

$$T_0 = \sum_{p=1}^{N_p} \int_{R_p^-}^{R_p^+} \frac{r^2}{R} \tau_{\theta y}^p(r) dr = \sum_{p=1}^{N_p} (K_{1p}^T \varepsilon_{\theta}^0 + K_{2p}^T \varepsilon_y^0 + K_{3p}^T \gamma_{y\theta}^0 + K_{4p}^T \gamma_{\theta y}^0 + K_{5p}^T \xi_1^p + K_{6p}^T \xi_2^p + K_{7p}^T), \quad (4.42)$$

where the auxiliary ply constants K_{jp}^T (with $j = 1, 2, \dots, 7$ and $p = 1, 2, \dots, N_p$) are defined as follows:

$$K_{jp}^T = H_{6j}^p \frac{(R_p^+)^3 - (R_p^-)^3}{3R}, \quad j = 1, 2, 7, \quad (4.43a)$$

$$K_{3p}^T = H_{63}^p \frac{(R_p^+)^2 - (R_p^-)^2}{2}, \quad K_{4p}^T = H_{64}^p \frac{(R_p^+)^4 - (R_p^-)^4}{4R^2}, \quad (4.43b)$$

$$K_{5p}^T = H_{65}^p \frac{(R_p^+)^{\kappa^p+2} - (R_p^-)^{\kappa^p+2}}{(\kappa^p + 2)R}, \quad K_{6p}^T = H_{66}^p \frac{(R_p^+)^{2-\kappa^p} - (R_p^-)^{2-\kappa^p}}{(2 - \kappa^p)R}. \quad (4.43c)$$

Summary of the problem resolution procedure

The problem developed in the present section is constituted by a set of $(4 + 2N_p)$ unknown variables. These unknown variables are divided in four strain constant parameters ε_{θ}^0 , ε_y^0 , $\gamma_{\theta y}^0$ and $\gamma_{y\theta}^0$, and in $2N_p$ ply constants ξ_1^p and ξ_2^p (with $p = 1, 2, \dots, N_p$).

The problem is then closed by using $(4+2N_p)$ equations. These equations are also divided in two groups. The first group is constituted by the $2N_p$ ply equations, which are subdivided in $N_p - 1$ equations of compatibility of radial displacements between plies by using equation (4.19), $N_p - 1$ equations of equilibrium of the radial stress between plies by using equation (4.25c), and two boundary conditions applied to the first ply with $\sigma_r^{p=1}(R^-) = p^-$ and to the last ply with $\sigma_r^{p=N_p}(R^+) = p^+$. The second group of equations is constituted by the four applied loads, which involve the whole laminate, given by equations (4.36), (4.38), (4.40) and (4.42).

Notice that the last group of equations may be substituted by other equations if the boundary conditions require it, e.g., in a pipe it is necessary to change equations (4.36) and (4.40) by the imposition of $\varepsilon_{\theta}^0 = 0$ and $\gamma_{y\theta}^0 = 0$, or in the case that the axial deformation is avoided by the embedding of the axial ends equation (4.38) has to be substituted by the imposition of $\varepsilon_y^0 = 0$.

The $(4 + 2N_p)$ set of equations constitutes a linear system of equations of the $(4 + 2N_p)$ unknown variables, which can be numerically implemented as a matrix inversion problem of the form $Ax = b$, where x includes all the unknown variables. Notice that all the residual strains parameters and the applied loads are included in vector b .

Once the unknown variables have been obtained, stresses and displacements can be easily evaluated by using equations (4.25) and (4.28) respectively. The evaluation of the radial displacement requires also the use of equation (4.19). Furthermore, strains can be also evaluated by using equations (4.4), (4.5) and (4.24).

The terms of the aforementioned matrix have been obtained in the present model, depending on ply parameters. However, those parameters cannot be calculated for matrices having certain combinations of elastic properties, the particular cases being developed in the following section.

4.1.3 Particular cases

There are three particular cases where the solution of the equation (4.17) is not the equation (4.19). These three particular cases are given in plies p with $\kappa^p = 0$, $\kappa^p = 1$ or $\kappa^p = 2$. The first particular case, $\kappa^p = 0$, is not a realistic configuration, as it implies a null value of the circumferential stiffness of the ply or an infinite value of the radial stiffness. The second particular case, $\kappa^p = 1$, is very typical in common laminates, as it implies the same circumferential stiffness than radial stiffness, $\bar{C}_{11}^p = \bar{C}_{33}^p$, which is typically occurring in UD plies with the fibre oriented in the axial direction. The third case, $\kappa^p = 2$, is not usual but possible, and it implies $\bar{C}_{11}^p = 4\bar{C}_{33}^p$.

Hence, the case $\kappa^p = 0$ is not being developed in the present document. The other two particular cases are studied in the following subsections.

Problem resolution in a ply p with $\bar{C}_{11}^p = \bar{C}_{33}^p$

The case of a ply with $\bar{C}_{11}^p = \bar{C}_{33}^p$ has singularities in the developed solution of the problem, so it needs to be independently analysed. This is, for example, the case of a 90° ply (defining the 0° direction as the ply with the fibres in the θ direction). Consequently, this particular case has a high importance.

In this case the solution of equation (4.17) yields:

$$w_0(r) = -h_4^p R \gamma_{y\theta}^0 + r \log(r) (h_5^p \varepsilon_\theta^0 + h_6^p \varepsilon_y^0 + h_7^p) + \frac{r^2}{R} h_8^p \gamma_{\theta y}^0 + \frac{\xi_1^p r}{\bar{C}_{13}^p + \bar{C}_{11}^p} + \frac{\xi_2^p r^{-1}}{\bar{C}_{13}^p - \bar{C}_{11}^p}, \quad (4.44)$$

where h_4^p and h_8^p remains as in the general ply case accordingly to (4.21), and h_5^p , h_6^p and h_7^p yield for this ply p :

$$h_5^p = \frac{\bar{C}_{11}^p - \bar{C}_{13}^p}{2\bar{C}_{11}^p}, \quad h_6^p = \frac{\bar{C}_{12}^p - \bar{C}_{23}^p}{2\bar{C}_{11}^p}, \quad h_7^p = \frac{\delta_3^p - \delta_1^p}{2\bar{C}_{11}^p}. \quad (4.45)$$

Therefore, substituting (4.44) into (4.6) the circumferential and radial strains can be written as:

$$\varepsilon_\theta(r) = -h_4^p \frac{R}{r} \gamma_{y\theta}^0 + \varepsilon_\theta^0 + (h_5^p \varepsilon_\theta^0 + h_6^p \varepsilon_y^0 + h_7^p) \log(r) + \frac{r}{R} h_8^p \gamma_{\theta y}^0 + \frac{\xi_1^p}{\bar{C}_{13}^p + \bar{C}_{11}^p} + \frac{\xi_2^p r^{-2}}{\bar{C}_{13}^p - \bar{C}_{11}^p}, \quad (4.46a)$$

$$\varepsilon_r(r) = (h_5^p \varepsilon_\theta^0 + h_6^p \varepsilon_y^0 + h_7^p)(1 + \log(r)) + 2 \frac{r}{R} h_8^p \gamma_{\theta y}^0 + \frac{\xi_1^p}{\bar{C}_{13}^p + \bar{C}_{11}^p} - \frac{\xi_2^p r^{-2}}{\bar{C}_{13}^p - \bar{C}_{11}^p}. \quad (4.46b)$$

Substituting the strains given in equations (4.46), (4.4) and (4.5) into the constitutive law (4.10), the stresses can be written as:

$$\sigma_\theta^p(r) = (H_{11}^p + G_{11}^p \log(r)) \varepsilon_\theta^0 + (H_{12}^p + G_{12}^p \log(r)) \varepsilon_y^0 + H_{13}^p \frac{R}{r} \gamma_{y\theta}^0 + H_{14}^p \frac{r}{R} \gamma_{\theta y}^0 + H_{15}^p \xi_1^p + H_{16}^p \xi_2^p r^{-2} + H_{17}^p + G_{17}^p \log(r), \quad (4.47a)$$

$$\sigma_y^p(r) = (H_{21}^p + G_{21}^p \log(r)) \varepsilon_\theta^0 + (H_{22}^p + G_{22}^p \log(r)) \varepsilon_y^0 + H_{23}^p \frac{R}{r} \gamma_{y\theta}^0 + H_{24}^p \frac{r}{R} \gamma_{\theta y}^0 + H_{25}^p \xi_1^p + H_{26}^p \xi_2^p r^{-2} + H_{27}^p + G_{27}^p \log(r), \quad (4.47b)$$

$$\sigma_r^p(r) = (H_{31}^p + G_{31}^p \log(r)) \varepsilon_\theta^0 + (H_{32}^p + G_{32}^p \log(r)) \varepsilon_y^0 + H_{33}^p \frac{R}{r} \gamma_{y\theta}^0 + H_{34}^p \frac{r}{R} \gamma_{\theta y}^0 + H_{35}^p \xi_1^p + H_{36}^p \xi_2^p r^{-2} + H_{37}^p + G_{37}^p \log(r), \quad (4.47c)$$

$$\begin{aligned} \tau_{\theta y}^p(r) = & (H_{61}^p + G_{61}^p \log(r))\varepsilon_{\theta}^0 + (H_{62}^p + G_{62}^p \log(r))\varepsilon_y^0 + \\ & H_{63}^p \frac{R}{r} \gamma_{y\theta}^0 + H_{64}^p \frac{r}{R} \gamma_{\theta y}^0 + H_{65}^p \xi_1^p + H_{66}^p \xi_2^p r^{-2} + H_{67}^p + G_{67}^p \log(r), \end{aligned} \quad (4.47d)$$

where the auxiliary ply constants H_{ij}^p , with $i = 1, 2, 3, 6$ and $j = 3, 4, 5, 6$ remain as in the general ply case, according to (4.26), and the auxiliary ply constants H_{ij}^p and G_{ij}^p , with $i = 1, 2, 3, 6$ and $j = 1, 2, 7$, are defined as follows:

$$H_{i1}^p = \bar{C}_{i1}^p + \bar{C}_{i3}^p h_5^p, \quad G_{i1}^p = (\bar{C}_{i1}^p + \bar{C}_{i3}^p) h_5^p, \quad i = 1, 2, 3, 6, \quad (4.48a)$$

$$H_{i2}^p = \bar{C}_{i2}^p + \bar{C}_{i3}^p h_6^p, \quad G_{i2}^p = (\bar{C}_{i1}^p + \bar{C}_{i3}^p) h_6^p, \quad i = 1, 2, 3, 6, \quad (4.48b)$$

$$H_{i7}^p = \bar{C}_{i3}^p h_7^p - \delta_i^p, \quad G_{i7}^p = (\bar{C}_{i1}^p + \bar{C}_{i3}^p) h_7^p, \quad i = 1, 2, 3, 6. \quad (4.48c)$$

Therefore, when the present ply is involved in an equation of continuity of the radial displacement, equation (4.44) must be used instead of (4.19), and when the present ply is involved in an equation of continuity of the radial stress, equation (4.47c) must be used instead of (4.25c).

In the total forces equations (4.36), (4.38), (4.40) and (4.42), the present ply p is included with the following parameters K_{jp}^M , K_{jp}^N , K_{jp}^P and K_{jp}^T (with $j = 1, 2, 7$ and p given by the present ply):

$$\begin{aligned} K_{jp}^M = & G_{1j}^p (R (R_p^+ (1 - \log R_p^+) - R_p^- (1 - \log R_p^-)) + \\ & \frac{(R_p^+)^2}{2} \left(\log R_p^+ - \frac{1}{2} \right) - \frac{(R_p^-)^2}{2} \left(\log R_p^- - \frac{1}{2} \right)) + \\ & H_{1j}^p \frac{R_p^+ - R_p^-}{2} (R_p^+ + R_p^- - 2R), \quad j = 1, 2, 7, \end{aligned} \quad (4.49a)$$

$$\begin{aligned} K_{jp}^N = & \left(H_{2j}^p - \frac{G_{2j}^p}{2} \right) \frac{(R_p^+)^2 - (R_p^-)^2}{2R} + \\ & \frac{G_{2j}^p}{2R} ((R_p^+)^2 \log R_p^+ - (R_p^-)^2 \log R_p^-), \quad j = 1, 2, 7, \end{aligned} \quad (4.49b)$$

$$\begin{aligned} K_{jp}^P = & (H_{6j}^p - G_{6j}^p) (R_p^+ - R_p^-) + \\ & G_{6j}^p (R_p^+ \log R_p^+ - R_p^- \log R_p^-), \quad j = 1, 2, 7, \end{aligned} \quad (4.49c)$$

$$K_{jp}^T = \left(H_{6j}^p - \frac{G_{6j}^p}{3} \right) \frac{(R_p^+)^3 - (R_p^-)^3}{3R} + \frac{G_{6j}^p}{3R} \left((R_p^+)^3 \log R_p^+ - (R_p^-)^3 \log R_p^- \right), \quad j = 1, 2, 7, \quad (4.49d)$$

and parameters K_{6p}^M and K_{6p}^N are given by:

$$K_{6p}^M = H_{16}^p \left(\log \left(\frac{R_p^+}{R_p^-} \right) + R \frac{(R_p^+)^{-\kappa^p} - (R_p^-)^{-\kappa^p}}{\kappa^p} \right), \quad (4.50a)$$

$$K_{6p}^N = \frac{H_{26}^p}{R} \log \left(\frac{R_p^+}{R_p^-} \right). \quad (4.50b)$$

Parameters K_{jp}^M and K_{jp}^N , with $j = 3, 4, 5$, and K_{jp}^P and K_{jp}^T , with $j = 3, 4, 5, 6$, remain as in equations (4.37), (4.39), (4.41) and (4.43), respectively.

Problem resolution in a ply p with $C_{11}^p = 4C_{33}^p$

The case of a ply with $\bar{C}_{11}^p = 4\bar{C}_{33}^p$ is not common, but is possible. In this case, the solution of equation (4.17) can be written as:

$$w_0(r) = -h_4^p R \gamma_{y\theta}^0 + r \left(h_5^p \varepsilon_\theta^0 + h_6^p \varepsilon_y^0 + h_7^p \right) + \frac{r^2}{R} \log(r) h_8^p \gamma_{\theta y}^0 + \frac{\xi_1^p r^2}{\bar{C}_{13}^p + 2\bar{C}_{33}^p} + \frac{\xi_2^p r^{-2}}{\bar{C}_{13}^p - 2\bar{C}_{33}^p}, \quad (4.51)$$

where h_4^p , h_5^p , h_6^p and h_7^p remain as in the general ply case, accordingly to (4.21), and h_8^p yields for this ply p :

$$h_8^p = \frac{\bar{C}_{16}^p - 2\bar{C}_{36}^p}{4\bar{C}_{33}^p}. \quad (4.52)$$

Therefore, substituting (4.51) into (4.6) the circumferential and radial strains can be written as:

$$\varepsilon_\theta(r) = -h_4^p \frac{R}{r} \gamma_{y\theta}^0 + (1 + h_5^p) \varepsilon_\theta^0 + h_6^p \varepsilon_y^0 + h_7^p + \frac{r}{R} \log(r) h_8^p \gamma_{\theta y}^0 + \frac{\xi_1^p r}{\bar{C}_{13}^p + 2\bar{C}_{33}^p} + \frac{\xi_2^p r^{-3}}{\bar{C}_{13}^p - 2\bar{C}_{33}^p}, \quad (4.53a)$$

$$\varepsilon_r(r) = h_5^p \varepsilon_\theta^0 + h_6^p \varepsilon_y^0 + h_7^p + \frac{r}{R} (1 + 2 \log(r)) h_8^p \gamma_{\theta y}^0 + \frac{2\xi_1^p r}{\bar{C}_{13}^p + 2\bar{C}_{33}^p} - \frac{2\xi_2^p r^{-3}}{\bar{C}_{13}^p - 2\bar{C}_{33}^p}. \quad (4.53b)$$

Substituting the strains given in equations (4.53), (4.4) and (4.5) into the constitutive law (4.10), the stresses can be written as:

$$\begin{aligned} \sigma_\theta^p(r) = & H_{11}^p \varepsilon_\theta^0 + H_{12}^p \varepsilon_y^0 + H_{13}^p \frac{R}{r} \gamma_{y\theta}^0 + \\ & (H_{14}^p + G_{14}^p \log(r)) \frac{r}{R} \gamma_{\theta y}^0 + H_{15}^p \xi_1^p r + H_{16}^p \xi_2^p r^{-3} + H_{17}^p, \end{aligned} \quad (4.54a)$$

$$\begin{aligned} \sigma_y^p(r) = & H_{21}^p \varepsilon_\theta^0 + H_{22}^p \varepsilon_y^0 + H_{23}^p \frac{R}{r} \gamma_{y\theta}^0 + \\ & (H_{24}^p + G_{24}^p \log(r)) \frac{r}{R} \gamma_{\theta y}^0 + H_{25}^p \xi_1^p r + H_{26}^p \xi_2^p r^{-3} + H_{27}^p, \end{aligned} \quad (4.54b)$$

$$\begin{aligned} \sigma_r^p(r) = & H_{31}^p \varepsilon_\theta^0 + H_{32}^p \varepsilon_y^0 + H_{33}^p \frac{R}{r} \gamma_{y\theta}^0 + \\ & (H_{34}^p + G_{34}^p \log(r)) \frac{r}{R} \gamma_{\theta y}^0 + H_{35}^p \xi_1^p r + H_{36}^p \xi_2^p r^{-3} + H_{37}^p, \end{aligned} \quad (4.54c)$$

$$\begin{aligned} \tau_{\theta y}^p(r) = & H_{61}^p \varepsilon_\theta^0 + H_{62}^p \varepsilon_y^0 + H_{63}^p \frac{R}{r} \gamma_{y\theta}^0 + \\ & (H_{64}^p + G_{64}^p \log(r)) \frac{r}{R} \gamma_{\theta y}^0 + H_{65}^p \xi_1^p r + H_{66}^p \xi_2^p r^{-3} + H_{67}^p, \end{aligned} \quad (4.54d)$$

where the auxiliary ply constants H_{ij}^p , with $i = 1, 2, 3, 6$ and $j = 1, 2, 3, 5, 6, 7$ remain as in the general ply case according to (4.26), and the auxiliary ply constants H_{ij}^p and G_{ij}^p , with $i = 1, 2, 3, 6$ and $j = 4$, are defined as follows:

$$H_{i4}^p = \bar{C}_{i6}^p + \bar{C}_{i3}^p h_8^p, \quad G_{i4}^p = (\bar{C}_{i1}^p + 2\bar{C}_{i3}^p) h_8^p, \quad i = 1, 2, 3, 6. \quad (4.55a)$$

Therefore, when the present ply is involved in an equation of continuity of the radial displacement, equation (4.51) must be used instead of (4.19), and when the present ply is involved in an equation of continuity of the radial stress, equation (4.54c) must be used instead of (4.25c).

In the total forces equations (4.36), (4.38), (4.40) and (4.42), the present ply p is included with the following parameters K_{jp}^M , K_{jp}^N , K_{jp}^P and K_{jp}^T (with $j = 4$ and p given by the present ply):

$$K_{4p}^M = G_{14}^p \left(\frac{(R_p^+)^2}{2} \left(\frac{1}{2} - \log R_p^+ \right) - \frac{(R_p^-)^2}{2} \left(\frac{1}{2} - \log R_p^- \right) + \frac{(R_p^+)^3}{3R} \left(\log R_p^+ - \frac{1}{3} \right) - \frac{(R_p^-)^3}{3R} \left(\log R_p^- - \frac{1}{3} \right) \right) + H_{14}^p \left(\frac{(R_p^+)^3 - (R_p^-)^3}{3R} - \frac{(R_p^+)^2 - (R_p^-)^2}{2} \right), \quad (4.56a)$$

$$K_{4p}^N = \left(H_{24}^p - \frac{G_{24}^p}{3} \right) \frac{(R_p^+)^3 - (R_p^-)^3}{3R^2} + \frac{G_{24}^p}{3R^2} \left((R_p^+)^3 \log R_p^+ - (R_p^-)^3 \log R_p^- \right), \quad (4.56b)$$

$$K_{4p}^P = \left(H_{64}^p - \frac{G_{64}^p}{2} \right) \frac{(R_p^+)^2 - (R_p^-)^2}{2R} + \frac{G_{64}^p}{2R} \left((R_p^+)^2 \log R_p^+ - (R_p^-)^2 \log R_p^- \right), \quad (4.56c)$$

$$K_{4p}^T = \left(H_{64}^p - \frac{G_{64}^p}{4} \right) \frac{(R_p^+)^4 - (R_p^-)^4}{4R^2} + \frac{G_{64}^p}{4R^2} \left((R_p^+)^4 \log R_p^+ - (R_p^-)^4 \log R_p^- \right), \quad (4.56d)$$

and parameter K_{6p}^T is given by:

$$K_{6p}^T = \frac{H_{66}^p}{R} \log \left(\frac{R_p^+}{R_p^-} \right). \quad (4.57)$$

Parameters K_{jp}^M , K_{jp}^N and K_{jp}^P , with $j = 1, 2, 3, 5, 6, 7$, and K_{jp}^T , with $j = 1, 2, 3, 5, 7$, remain as in equations (4.37), (4.39), (4.41) and (4.43), respectively.

4.2 Analysis of the effect of residual stresses in the unfolding failure

UD plies of composite laminates have different thermal expansion coefficients in the fibre direction and the in-plane direction perpendicular to the fibre, due to the different expansion coefficient between the matrix and the fibre. When a laminate with different orientations of the plies is manufactured the free expansion of the plies is constrained by the plies with a different orientation, causing the appearance of in-plane residual stresses. This kind of residual stresses are well-known and correctly calculated for the flat laminates, which typically raise during the cooling after the curing process. However, when the laminate is curved the existence of axial stresses,

σ_θ , causes the apparition of interlaminar stresses to fulfil the equilibrium equation (4.8c).

In this way, a temperature change induces the apparition of interlaminar stresses in a curved laminate. These interlaminar stresses can be tensile or compressive, depending on the stacking sequence, respectively anticipating or delaying the unfolding failure. When the temperature change is higher the residual stresses are higher too. Therefore, residual stresses depend on the service temperature. When the service temperature is lower, residual stresses are higher.

4.2.1 Homogeneous anisotropic materials

At mesoscopic scale, composite materials are not homogeneous as each ply is oriented in a different direction. However, an individual ply, or a laminate with all the plies oriented in the same direction, can be approximated as homogeneous and orthotropic. In a homogeneous material there are no differences in the coefficients of thermal expansion between plies. Therefore, by using the previous explanation about the differences in these coefficients, the non-existence of the mentioned residual stresses becomes reasonable. However, the curvature may induce residual stresses in many cases, even in homogeneous materials.

An orthotropic material is considered in this section as an example of anisotropic material. When the material orthotropic directions are coincident with the θ and y axes, it can shrink or expand freely in those directions without inducing residual stresses. However, when the orthotropic axes are oriented in other directions the curvature constrains the thermal expansion and residual stresses appear.

In this section the model is applied to a shell with a mean radius equal to the thickness: $R = t = 1$ mm. The stiffness properties and the coefficients of thermal expansion, expressed in the orthotropic axes, are given in Table 4.1.

Table 4.1: Material properties

E_{11} (MPa)	150	ν_{12}	0.3	G_{12} (MPa)	4.8	α_{11} (K ⁻¹)	$-1 \cdot 10^{-6}$
E_{22} (MPa)	10	ν_{13}	0.3	G_{13} (MPa)	4.8	α_{22} (K ⁻¹)	$3 \cdot 10^{-5}$
E_{33} (MPa)	10	ν_{23}	0.3	G_{23} (MPa)	4.8	α_{33} (K ⁻¹)	$3 \cdot 10^{-5}$

Considering that the 0° direction is defined by the direction 1 of the material being coincident with the θ axis, a material with 45° of orientation under a temperature decrement of 160°C presents the residual stresses (calculated according to the regularized solution developed in the previous

section) depicted in Figure 4.3. These stresses expressed in the material axes are depicted in Figure 4.4.

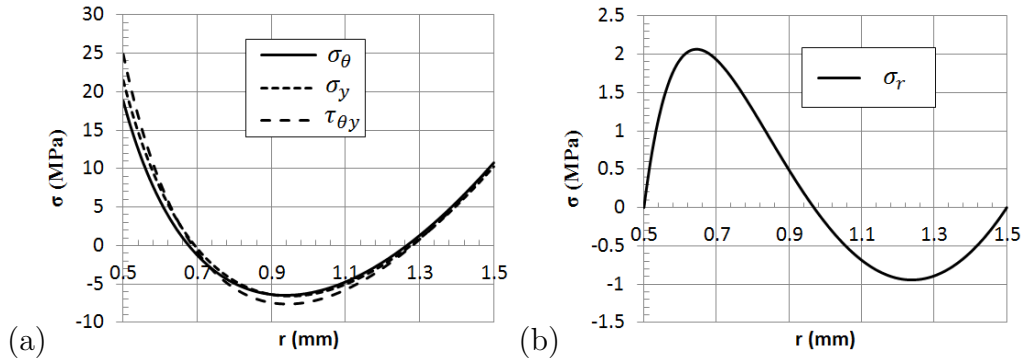


Figure 4.3: Residual stresses in a 45° single ply laminate with $\Delta T = -160^\circ\text{C}$. (a) Circumferential, axial and shear stresses. (b) Interlaminar normal stress.

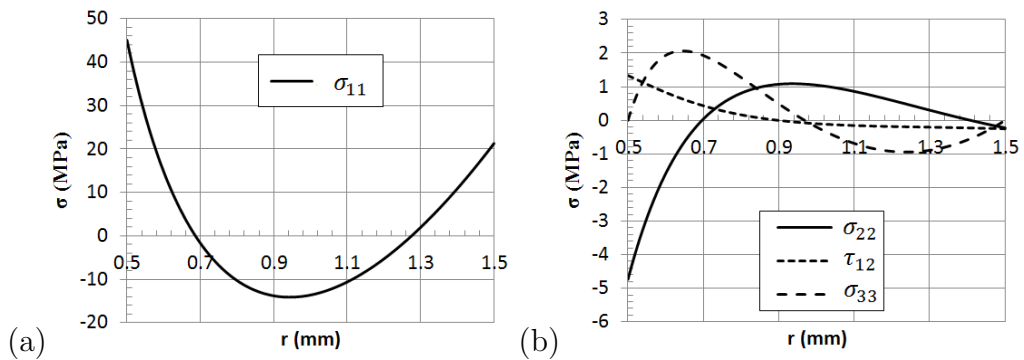


Figure 4.4: Residual stresses in a 45° single ply laminate with $\Delta T = -160^\circ\text{C}$ expressed in the material axes. (a) Stress in the fibre direction. (b) Stresses in the orthotropic matrix directions and shear stress.

In Figure 4.4, it can be observed that the highest stresses are given in the stiffest direction of the material (direction 1). The depicted residual stresses represent the thermal stresses due to the curvature.

Considering a typical strength in the radial direction of the material of approximately 50 MPa, and considering that the unfolding failure is typically given for radius smaller than the mean radius, the thermal stresses in the given configuration represent a 4% of the total failure load.

Figure 4.5 shows the maximum radial stress appearing in a homogeneous curved sample under a temperature decrement of 160°C , depending on the

orientation of the material. It can be observed that the maximum radial stress for the present case is given for approximately 38° . Furthermore, directions 0° and 90° have null residual stresses, since they are able to deform freely.

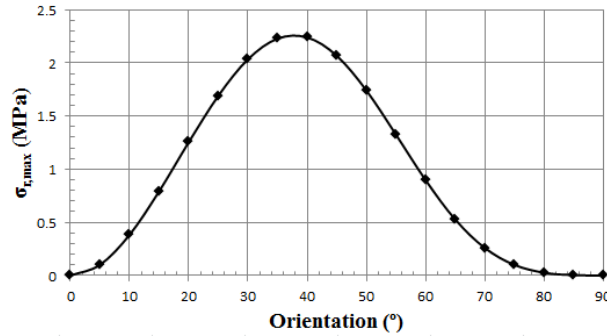


Figure 4.5: Maximum radial stress for $\Delta T = -160^\circ\text{C}$ depending on the orientation of the single ply laminate.

4.2.2 Composite laminates

In the case of a composite laminate, the different thermal expansion coefficients in the same direction of each ply due to their different orientations induces significant residual in-plane stresses, and according to (4.8c) interlaminar stresses too.

As an example of application of the model to calculate the regularized thermal stresses, let us consider the material properties of Table 4.1 and two different stacking sequences given by $[45, 0, -45, 90]_S$ and $[45, 90, -45, 0]_S$. In these cases, Figure 4.6 shows the radial stresses obtained when applying a temperature decrement $\Delta T = -160^\circ\text{C}$.

In a composite laminate, fibres have very low (or even negative) expansion coefficients, and therefore, the plies have very small expansion coefficients in direction 1, the expansion coefficient being higher in direction 2. As a consequence, referring to the circumferential stresses, the 0° plies are compressed in the circumferential direction while the 90° plies are tensioned in the same direction. By using equation (4.8c), the presence of compressed plies implies a decrease of the interlaminar stress when the radial coordinate increases, and, on the contrary, the presence of tensioned plies implies an increase of the interlaminar stress when the radial coordinate increases. Hence, when the 0° plies are outer, in the stacking sequence, than the 90° plies, the inner plies are compressed in the through-the-thickness direction

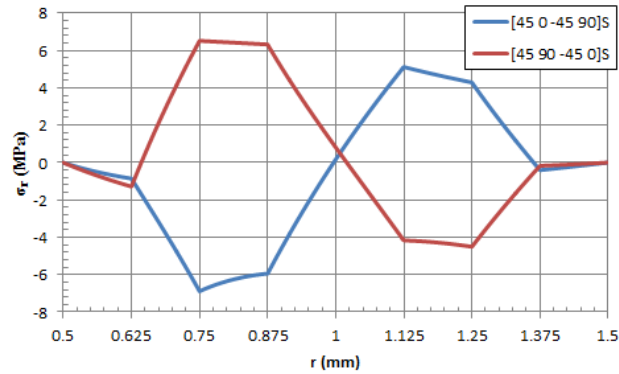


Figure 4.6: Radial stresses due to the temperature increment in different stacking sequences.

and the outer plies are tensioned, as can be seen in Figure 4.6. Inversely, when the 90° plies are outer than the 0° plies the inner plies are tensioned in the through-the-thickness direction and the outer plies are compressed.

The unfolding failure is given in these curved beams when the component is under a bending moment that induces an opening of the curvature. Under this load state the maximum of the radial stresses is located in the inner part. Therefore, from the residual stresses point of view, it is optimal to locate the 0° plies outer than the 90° plies in the stacking sequence. This configuration is optimal also when considering the stresses distributions due to the bending moment, residual stresses reinforcing this optimization criterion.

Furthermore, considering an interlaminar strength with a value of approximately 50 MPa with the selected material properties, the residual stresses in the case of the $[45, 90, -45, 0]_S$ stacking sequence anticipates a 12% the unfolding failure, and in the case of the $[45, 0, -45, 90]_S$ stacking sequence it improves a 12%, considering the given geometry with $t = R$.

The interlaminar stresses are lower when the relation t_l/R decreases, t_l being the thickness of a ply. This parameter can decrease in two cases, when the number of plies increases maintaining the t/R relation, or when the mean radius increases maintaining the number of plies and the ply thickness. Figure 4.7 shows the decrement of the interlaminar normal stresses in both cases respect to the interlaminar normal stresses depicted in Figure 4.6.

Hence, the effect of the residual stresses is specially important in thin laminates (with a small number of plies) and in laminates with a small mean radius respect to the thickness.

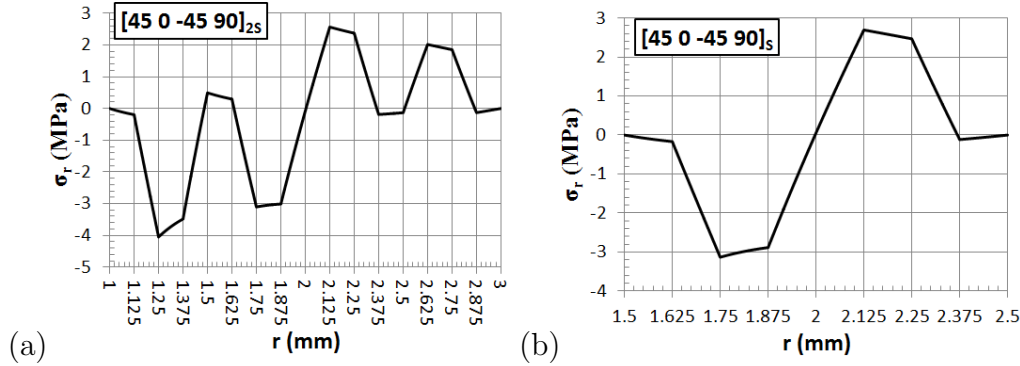


Figure 4.7: Radial stresses due to the temperature increment in different geometries. (a) Increment of the number of plies. (b) Increment of the mean radius.

4.2.3 Finite elements comparison

The solution obtained with the model has been compared with results of a FE model. The FEM is carried out by considering a 135° curved hollow cylinder, so that the stresses may be observed far enough from the free edge in the θ direction, and with a width $W = 10t$, so that the stresses may be observed far enough from the free edge in the y direction. The solid model has been meshed with 10 quadratic elements in the thickness, a high accuracy being obtained for the interlaminar stresses.

Figure 4.8 shows in continuous line the solution of the model for the material of Table 4.1 with $R = 2t$ and an individual ply of 45° , and in asterisks the numerical solution by using the FE model and obtaining the stresses far enough from the boundaries.

The analytical model constitutes the exact solution of the regularized stresses, and the FEM results show a good agreement with that solution. The small differences seen in Figure 4.8 are mainly due to numerical errors and slight non-regularized effects.

4.3 Analysis of the three-dimensional effects over the unfolding failure

The regularized 3D model developed can be also applied to the calculation of regularized stresses due to a bending moment M_0 , an in-plane shear force P_0 , a torsional moment T_0 and an axial force N_0 . In the present Chapter, the bending moment case, M_0 , is analysed since it is the typical load

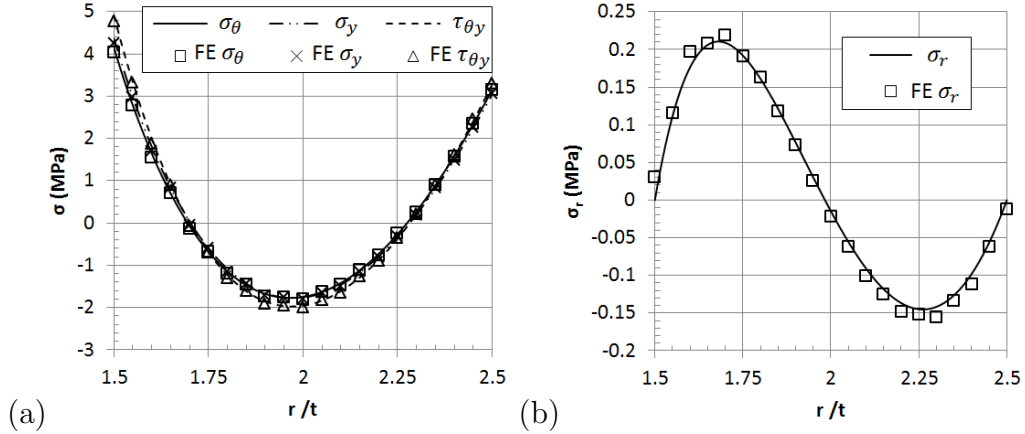


Figure 4.8: Validation of the model (continuous line) with finite elements results (asterisks) in the homogeneous case of 45° . (a) In-plane stresses. (b) Interlaminar stresses.

in the unfolding failure. This load state is given, for instance, in the ILTS test, consisting in a four-point bending test on a L-sectioned beam.

The load state associated to a bending moment M_0 has been widely analysed with 2D regularized models, it being typically calculated with the Lekhnitskii's equations (see [19], Chapter 3) or with the Ko and Jackson's equations [4]. It can be also calculated with the non-regularized models developed in Chapter 3. In the present section, the solution of the model applied for several stacking sequences is being compared with the exact regularized model given in [4] to analyse the accuracy of the 2D approximation, typically used in the calculation of the unfolding failure.

4.3.1 Homogeneous anisotropic materials

In the homogeneous anisotropic material the solution of the 2D regularized problem given by Ko and Jackson [4] coincides with the one given by Lekhnitskii et al. [19].

The regularized 3D model developed, when applied to the pure bending moment case, includes several important hypothesis regarding the forces and moments. It assumes that the forces and moments reach their regularized values, which are the inputs of the model, and those regularized values are determined by the free boundaries at the ends in the y direction and a bending moment applied uniformly at the ends of the θ direction (it is considered uniform only when it is regularized in the y direction, as it has actually different values at the free edge). This model is equivalent to a

free torsion model, the beam can torsion freely while $T_0 = 0$ due to the boundary condition of null $\tau_{\theta y}$ at the free edges along the width. The axial force is considered also null, $N_0 = 0$, due to the boundary condition of null σ_y at the free edges in the width as well as the applied in-plane shear force is considered null also, $P_0 = 0$.

A second model has been considered as a constrained model. In this model the torsion is constrained and an uniform bending moment is applied at the ends along θ (the condition of $T_0 = 0$ used is substituted by $\gamma_{\theta y}^0 = 0$, which implies a null torsion). Hence, 3D deformations are constrained in this model. As a consequence, this model is not realistic for the ILTS four-point bending test [3].

Considering an orthotropic material with properties given in Table 4.1 and varying the orientation angle in a single-ply laminate, for a geometry determined by $t = R = 1$ mm and a load of $M_0 = -1$ Nm/m, the evolution of the maximum regularized radial stress as a function of the orientation angle is depicted in Figure 4.9.

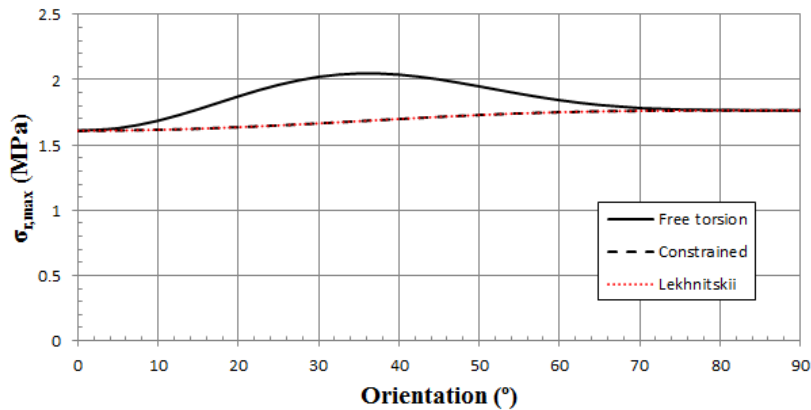


Figure 4.9: Maximum radial stress for $M_0 = -1$ Nm/m depending on the orientation of the single ply laminate.

It can be seen that using a 2D model for the homogeneous material returns similar results to the 3D constrained model. However, in a more realistic model where the beam can freely torsion, the maximum radial stress is significantly higher than that given by the 2D model. Therefore, a 2D model is not accurate for this kind of configuration. The difference between the 3D model and the 2D model is maximum around 35° for the given material properties, and it is null in the 0° and 90° single ply laminates.

Considering the case with a maximum difference, given by an orientation of 35° , all the stresses in the regularized beam calculated with both 3D

models are depicted in Figure 4.10.

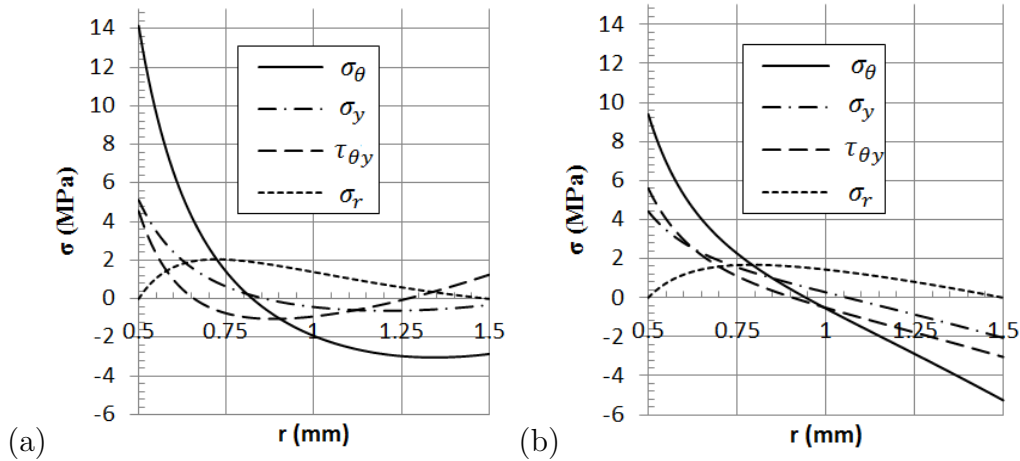


Figure 4.10: Stresses in a 35° single ply laminate under $M_0 = -1$ Nm/m for (a) the free torsion model and (b) the constrained model.

The stresses calculated with the free torsion model present high differences with the ones calculated with the constrained model (which are similar to those of the 2D models since the 3D deformations are constrained). Specially, the differences are very high in the maximum values of the circumferential and the radial stress, affecting significantly to the failure prediction.

4.3.2 Composite laminates

The 2D models for composite laminates are typically obtained by assuming a plane strain or plane stress state. Plane stress is not a realistic state because a null stress state in the y direction does not fulfil the compatibility equations, causing discontinuities in the displacements along the transversal direction. However, in the same way, a null strain state in the y direction, when the laminate has any ply with an orientation different to 0° and 90° , causes discontinuities in the radial shear stress associated to the y direction, τ_{ry} , and then it is neither physically possible.

Therefore, it is expected that a 3D model can return more accurate results than the 2D models, as a 3D model accomplish the continuity in the displacements and in the shear stress τ_{ry} . For this reason, the constrained 3D model yields more accurate results than the 2D model in the laminate case.

If a typical laminate with plies oriented at 0° , $\pm 45^\circ$ and 90° is considered, it is expected to obtain higher errors in a 2D model when the number of

$\pm 45^\circ$ plies increases and when the asymmetry of the stacking sequence is higher.

Although not shown here, it has been observed that, generally, the differences between the 2D model and the 3D model decrease when the number of plies increase, as the stacking sequence causes a more homogeneous material. Consequently, the 2D model is less accurate when it is applied to thin laminates or less quasi-isotropic laminates.

An interesting 3D effect is the difference between plies of 45° and -45° when both kind of plies are given in the same stacking sequence. In a 2D model the stiffnesses of a 45° ply are the same than the stiffnesses of a -45° ply and, therefore, the stresses are not affected by the sign of the orientation. Consequently, when a ply of 45° is adjacent to a ply of -45° the circumferential stresses are continuous. However, due to the torsion, in a 3D model when a ply of 45° is adjacent to a ply of -45° , circumferential stresses are not continuous across the interface. This effect can be seen in Figure 4.11, where a stacking sequence $[45 -45 -45 45]$ has been used. In this Figure the free torsion model presents discontinuities in the circumferential stress, while the constrained model presents a continuous distribution.

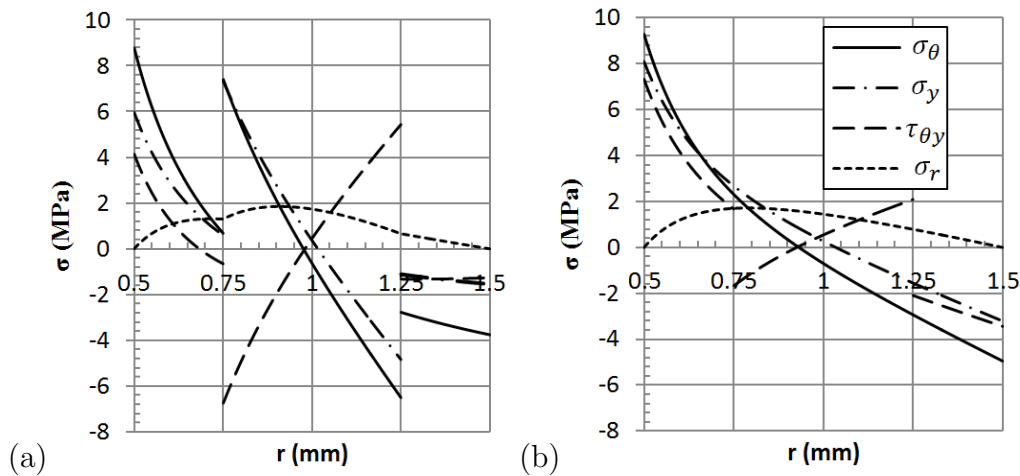


Figure 4.11: Differences between 45° plies and -45° plies when both are used in a laminate, showed in a $[45 -45 -45 45]$ stacking sequence. (a) Free torsion model, (b) Constrained model.

4.3.3 Finite elements comparison

The solution of the model has been compared with FE results for the case of the bending moment. A curved beam with the material given in

Table 4.1 has been used with a single-ply configuration of orientation 45° , 1 mm thickness, a mean radius of 2 mm, a total angle of 300° and a width in the y direction of 10 mm. A -10 Nmm total bending moment has been applied. Considering the 10 mm width, a bending moment per width of $M_0 = -1$ Nmm/mm is given. The solid has been meshed with 10 quadratic elements in the thickness, so a high accuracy is obtained for the interlaminar stresses. By comparing the finite elements results obtained with the free torsion model and with the constrained model, Figure 4.12 is obtained.

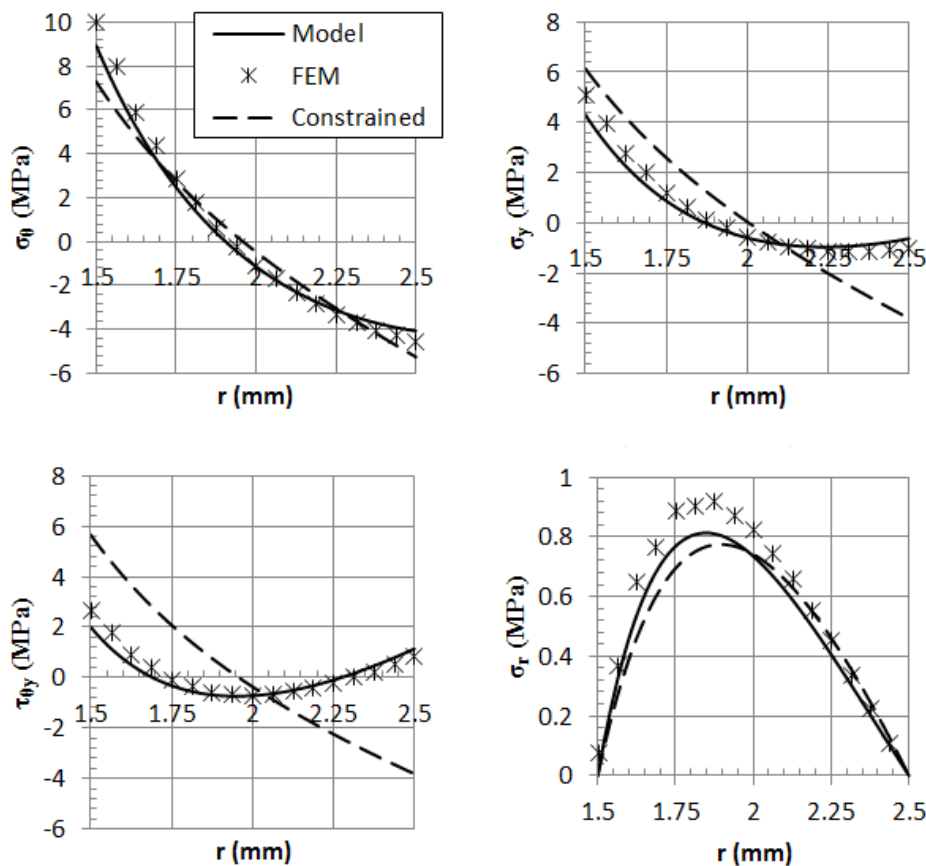


Figure 4.12: Validation of the models (continuous and discontinuous lines) by using $M_0 = -1$ N with finite elements results (asterisks) in the homogeneous case of 45° .

Small differences (about a 10%) are observed between the solution of the free torsion 3D model and the FE results in all the stress components. These differences are due to the finite width of the specimen in the FE model. The finite width in the y direction induces a stress state of plane stress in the

boundary, causing the bending moment in the edges to be smaller than the bending moment in the center of the beam. The bending moment, M_0 [N], has been calculated from the total moment, M_T [Nmm], and from the width, W [mm], as $M_0 = M_T/W$, supposing that it is homogeneously distributed. Actually, due to the edge effect we have that the regularized bending moment is calculated as $M_0 = k_W M_T/W$, where the parameter k_W depends mainly on the W/t ratio although it depends also on the stacking sequence, the material properties, the R/t ratio, etc. It can be deduced that $k_W \rightarrow 1$ when $W/t \rightarrow \infty$.

Therefore, the edge effects causes that the maximum value of M_0 is higher than M_T/W . Using a FE model for the present problem a value of $k_W = 1.2$ has been obtained. Therefore, by using a $M_0 = 1.2$ N bending moment, Figure 4.13 is obtained.

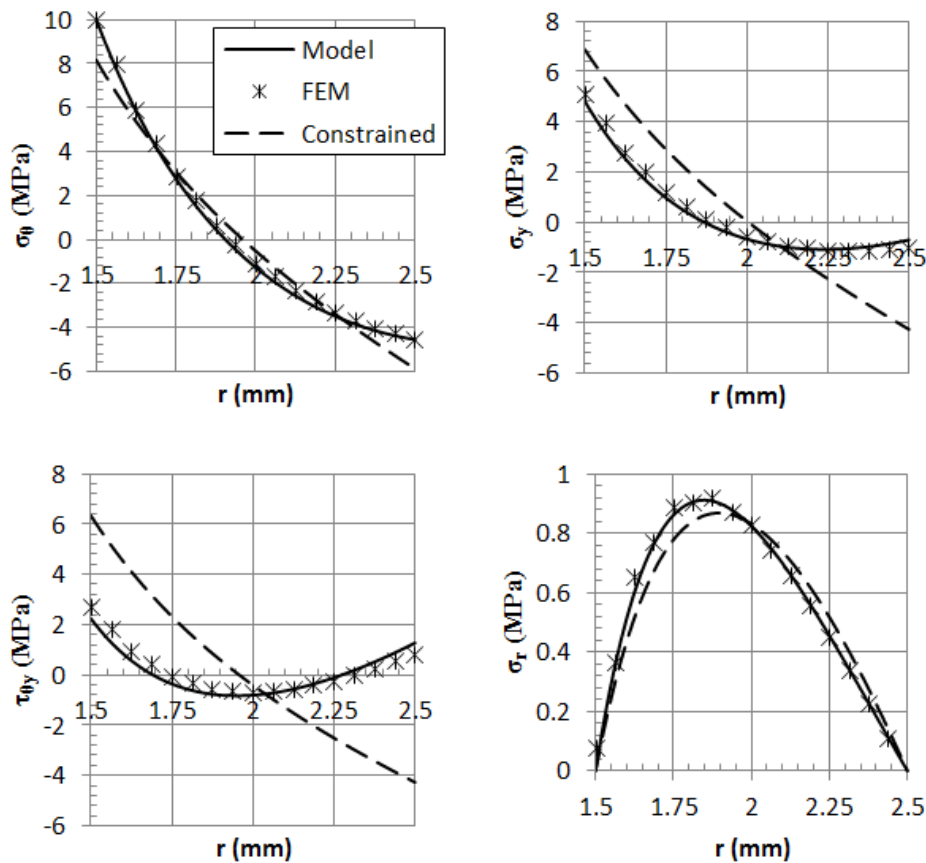


Figure 4.13: Validation of the models (continuous and discontinuous lines) by using $M_0 = -1.2$ N and comparing with FE results (asterisks) in the homogeneous case of 45° .

Considering the right value of the parameter k_W and, therefore, the right value of the bending moment per unit of length in the inner part of the sample M_0 , the differences between the finite element results and the free torsion 3D model are considerably reduced. The free torsion model results are very accurate compared with the finite elements model, as no kind of displacement constraint has been imposed in the finite elements model. However, the constrained model (which has similar characteristics to a 2D model) is less accurate in this case due to the torsion induced by the orientation of the ply.

The importance of considering the effect of the finite width by the parameter k_W in the bending moment calculation has been showed. The analytical calculation of k_W is necessary for an accurate calculation of the stress components, the regularized 3D model not being satisfactory at that point. This effect is calculated by using the non-regularized model developed in the following section.

4.4 Three-dimensional non-regularized models

The finite width of the specimens combined with the anticlastic effect may cause that the value of the regularized bending moment in the inner part of the sample M_0 is different to the total bending moment divided by the width M_T/W . This effect can be corrected using a factor k_W so that M_0 may be obtained from the total applied bending moment as follows:

$$M_0 = k_W \frac{M_T}{W}. \quad (4.58)$$

In order to obtain the bending moment distribution in the width in a more accurate way and to calculate the free-edge effects, an extension of the MBM and the LPBM to a 3D problem is developed in the present chapter. This extension may be carried out either with a series expansion in z of the displacements, and, consequently, the parameters of the problem depend on s and y , or with a double series expansion in z and y , and, consequently, parameters of the problem depend on s . A whole 3D model should be expanded in both z and y , to obtain uni-dimensional differential equations which have to be solved following a similar procedure as in the original LPBM and MBM.

To simplify the model, considering that the interesting loading state for the unfolding problem is the bending problem, a s non-dependant problem is considered in the strains and stresses, so that the non-regularized problem is

considered only in the y direction. In that way, a 3D model is used to solve a 2D problem as depicted in Figure 4.14. Therefore, the problem is expanded only in the z direction since the solution in s is regularized and may be determined. Consequently, the final differential equation only depends on y .

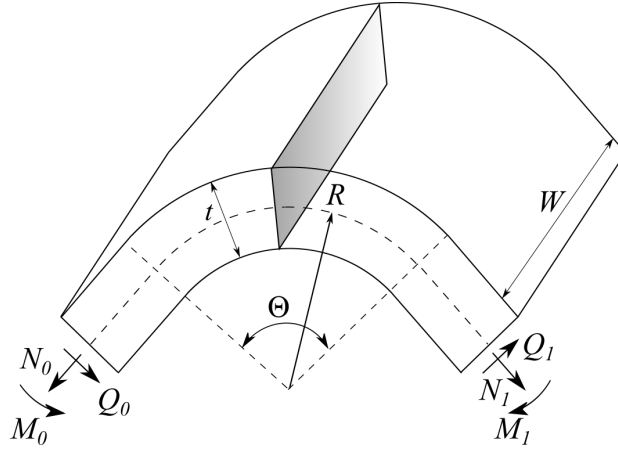


Figure 4.14: Section studied with the 3D model.

The calculation of the non-regularized problem in the y direction let us to estimate not only the finite width effect, but also the free edge effect in the through-the-width direction.

The model is developed first for flat laminates as a simpler model, and it is subsequently extended to the curved laminate problem. For the sake of brevity, only the LPBM is developed, while a similar development may be carried out for the MBM. Therefore, displacements and lengths are considered non-dimensionalized with one half of the thickness, $t/2$, including the through-the-width coordinate y and the respective length W .

Using the concept of the LPBM, the theoretical basis of the 3D non-regularized model developed with a series expansion in the z coordinate with Legendre polynomials is given by the following:

$$u_s(s, y, z) = u_0(s, y) + zu_1(s, y) + \sum_{i=2}^n p_i(z)u_i(s, y), \quad (4.59a)$$

$$u_y(s, y, z) = v_0(s, y) + zv_1(s, y) + \sum_{i=2}^n f_i^y(z)v_i(s, y), \quad (4.59b)$$

$$u_z(s, y, z) = w_1(s, y) + \sum_{i=2}^n f_i^z(z)w_i(s, y). \quad (4.59c)$$

where $p_i(z)$ is the Legendre polynomial of order i , and $f_i^y(z)$ and $f_i^z(z)$ are functions to be determined. As explained previously, this model can be used considering the regularization in s -direction so that unknown parameters depend only on the y coordinate.

Notice that, if no regularization is given in the s -direction, the displacements components depends then on both coordinates s and y . Therefore, the final system of differential equations of the model will be with partial derivatives and, therefore, it will not be as easy to solve as in the LPBM. In order to obtain absolute derivatives in the final system of differential equations, a double series expansion may be used:

$$u_s(s, y, z) = \sum_{i=0}^n \sum_{j=0}^m p_i(z) p_j(y) u_{ji}(s), \quad (4.60a)$$

$$u_y(s, y, z) = \sum_{i=1}^n \sum_{j=1}^m f_i^y(z) g_j^y(y) v_{ji}(s), \quad (4.60b)$$

$$u_z(s, y, z) = \sum_{i=1}^n \sum_{j=1}^m f_i^z(z) g_j^z(y) w_{ji}(s). \quad (4.60c)$$

where $g_j^y(y)$ and $g_j^z(y)$ are functions to be determined. This series expansion of displacements requires a higher number of displacements components, and, therefore, the model will require a higher number of higher-order moments in the stresses side. Furthermore, it needs to differentiate orders n and m in directions z and y , respectively.

For the development of a whole three-dimensional model it is recommendable to use the approximation given by equations (4.60). However, the model developed in the present section, as commented previously, considers a s non-dependant problem in the stresses and strains, which is given only in some particular cases such as the bending problem. Therefore, in the present section approximation (4.59) is used since the behaviour in direction s may be calculated, thus, suppressing this coordinate from the differential equation of the model. Notice that, although the model is only valid for a particular case, it is associated to the dominant load in the unfolding problem.

4.4.1 Development of the 3D non-regularized model in flat laminates

The non-regularized model is first developed for the flat laminates as a simpler case. In this case the free-edge effects have been widely studied

for some kinds of stacking sequences and the results can be compared with numerical and analytical solutions.

Displacements and strains distributions

Strains and stresses are considered non-dependant with the s coordinate, which causes a given dependence of the displacements with the aforementioned coordinate. The terms of the strains could be obtained by using the compatibility equations, as in the regularized 3D model. However, in the present section the displacements are obtained by integrating the strain equations since the resolution from compatibility equations is complexer in a three-dimensional case. Notwithstanding, the same result may be obtained with the compatibility equations.

Therefore, considering the axial strain, $\varepsilon_s(y, z)$, which only depends on the coordinates y and z , and integrating the respective strain-displacement relation, yields:

$$\varepsilon_s(y, z) = \frac{\partial u_s(s, y, z)}{\partial s} \longrightarrow u_s(s, y, z) = u_s^A(y, z) + \varepsilon_s(y, z)s. \quad (4.61)$$

where $u_s^A(y, z)$ and $\varepsilon_s(y, z)$ are auxiliary functions due to the integration.

Considering also the transverse strain, $\varepsilon_y(y, z)$, and the interlaminar strain, $\varepsilon_z(y, z)$, and integrating the respective strain-displacement relations yields:

$$\varepsilon_y(y, z) = \frac{\partial u_y(s, y, z)}{\partial y} \longrightarrow u_y(s, y, z) = u_y^0(y, z) + u_y^A(s, z), \quad (4.62a)$$

$$\varepsilon_z(y, z) = \frac{\partial u_z(s, y, z)}{\partial z} \longrightarrow u_z(s, y, z) = u_z^0(y, z) + u_z^A(s, y), \quad (4.62b)$$

where $u_y^0(y, z)$, $u_y^A(s, z)$, $u_z^0(y, z)$ and $u_z^A(s, y)$ are auxiliary functions due to the integration.

Considering now the shear strain $\gamma_{yz}(y, z)$, and using (4.62), yields:

$$\begin{aligned} \gamma_{yz}(y, z) &= \frac{\partial u_y(s, y, z)}{\partial z} + \frac{\partial u_z(s, y, z)}{\partial y} = \\ &= \frac{\partial u_y^0(y, z)}{\partial z} + \frac{\partial u_z^0(y, z)}{\partial y} + \frac{\partial u_y^A(s, z)}{\partial z} + \frac{\partial u_z^A(s, y)}{\partial y}. \end{aligned} \quad (4.63)$$

Since the right term of equation (4.63) cannot depend on s , the auxiliary functions $u_y^A(s, z)$ and $u_z^A(s, y)$ can be written as:

$$u_y^A(s, z) = u_y^B(s) - z\xi_A(s), \quad (4.64a)$$

$$u_z^A(s, y) = u_z^B(s) + y\xi_A(s), \quad (4.64b)$$

where $u_y^B(s)$, $u_z^B(s)$ and $\xi_A(x)$ are auxiliary functions.

Considering now the shear strain $\gamma_{sy}(y, z)$, and using (4.61), (4.62a) and (4.64a), yields:

$$\begin{aligned} \gamma_{sy}(y, z) &= \frac{\partial u_s(s, y, z)}{\partial y} + \frac{\partial u_y(s, y, z)}{\partial s} = \\ &= \frac{\partial u_s^A(y, z)}{\partial y} + s \frac{\partial \varepsilon_s(y, z)}{\partial y} + \frac{du_y^B(s)}{ds} - z \frac{d\xi_A(s)}{ds}. \end{aligned} \quad (4.65)$$

Since the right term of equation (4.65) cannot depend on s , the auxiliary functions $\varepsilon_s(y, z)$, $u_y^B(s)$ and $\xi_A(s)$ are given by:

$$\varepsilon_s(y, z) = \varepsilon_s^A(z) + y\kappa_y^0 + yz\xi_B, \quad (4.66a)$$

$$u_y^B(s) = s\phi_z - \frac{s^2}{2}\kappa_y^0, \quad (4.66b)$$

$$\xi_A(s) = s\kappa_{yz}^0 + \frac{s^2}{2}\xi_B, \quad (4.66c)$$

where ξ_B is an auxiliary constant, $\varepsilon_s^A(z)$ is an auxiliary function, κ_y^0 is the curvature in the y direction associated to the axial strain $\varepsilon_s(y, z)$, ϕ_z is the rigid body rotation around z axis and κ_{yz}^0 is the mean line torsional curvature.

Finally, considering the shear strain $\gamma_{sz}(y, z)$, and using (4.61), (4.62b), (4.64b), (4.66a) and (4.66c), yields:

$$\begin{aligned} \gamma_{sz}(y, z) &= \frac{\partial u_s(s, y, z)}{\partial z} + \frac{\partial u_z(s, y, z)}{\partial s} = \\ &= \frac{\partial u_s^A(y, z)}{\partial z} + y\kappa_{yz}^0 + s \frac{d\varepsilon_s^A(z)}{dz} + 2sy\xi_B + \frac{du_z^B(s)}{ds}. \end{aligned} \quad (4.67)$$

Since the right term of equation (4.67) cannot depend on s , the auxiliary constant ξ_B and the auxiliary functions $\varepsilon_s^A(z)$ and $u_z^B(s)$ are given by:

$$\varepsilon_s^A(z) = \varepsilon_s^0 + z\kappa_z^0, \quad (4.68a)$$

$$u_z^B(s) = s\phi_y - \frac{s^2}{2}\kappa_z^0, \quad (4.68b)$$

$$\xi_B = 0, \quad (4.68c)$$

where ε_s^0 is the mean line axial strain, κ_z^0 is the curvature in the z direction associated to the axial strain $\varepsilon_s(y, z)$ and ϕ_y is the rigid body rotation around the axis y .

Furthermore, the following definition is considered, which allows a simpler expression of the strains to be obtained:

$$u_s^A(y, z) = u_s^0(y, z) - y\phi_z - z\phi_y. \quad (4.69)$$

Therefore, substituting (4.64), (4.66), (4.68) and (4.69) in (4.61) and (4.62) the displacements can be written as:

$$u_s(s, y, z) = u_s^0(y, z) + s\varepsilon_s^0 + sz\kappa_z^0 + sy\kappa_y^0 - y\phi_z - z\phi_y, \quad (4.70a)$$

$$u_y(s, y, z) = u_y^0(y, z) + s\phi_z - \frac{s^2}{2}\kappa_y^0 - sz\kappa_{yz}^0, \quad (4.70b)$$

$$u_z(s, y, z) = u_z^0(y, z) + s\phi_y - \frac{s^2}{2}\kappa_z^0 + sy\kappa_{yz}^0. \quad (4.70c)$$

Substituting in the strains definitions, strains can be written as:

$$\varepsilon_s(y, z) = \varepsilon_s^0 + z\kappa_z^0 + y\kappa_y^0, \quad (4.71a)$$

$$\varepsilon_y(y, z) = \frac{\partial u_y^0(y, z)}{\partial y}, \quad \varepsilon_z(y, z) = \frac{\partial u_z^0(y, z)}{\partial z}, \quad (4.71b)$$

$$\gamma_{yz}(y, z) = \frac{\partial u_y^0(y, z)}{\partial z} + \frac{\partial u_z^0(y, z)}{\partial y}, \quad (4.71c)$$

$$\gamma_{sy}(y, z) = \frac{\partial u_s^0(y, z)}{\partial y} - z\kappa_{yz}^0, \quad (4.71d)$$

$$\gamma_{sz}(y, z) = \frac{\partial u_s^0(y, z)}{\partial z} + y\kappa_{yz}^0. \quad (4.71e)$$

Notice that the rigid body rotations, ϕ_y and ϕ_z , do not affect to the strains.

Displacements approximation

Displacements are approximated by using a series expansion according to (4.59). However, under the assumption of non-dependence of the strains and stresses with the axial coordinate s , displacements have been simplified to equations (4.70). Therefore, in the present model, the auxiliary functions $u_s^0(y, z)$, $u_y^0(y, z)$ and $u_z^0(y, z)$ have been approximated by a series expansion in the z -coordinate:

$$u_s^0(y, z) = u_0(y) + zu_1(y) + \sum_{i=2}^n p_i(z)u_i(y), \quad (4.72a)$$

$$u_y^0(y, z) = v_0(y) + zv_1(y) + \sum_{i=2}^n f_i^y(z)v_i(y), \quad (4.72b)$$

$$u_z^0(y, z) = w_1(y) + \sum_{i=2}^n f_i^z(z)w_i(y). \quad (4.72c)$$

Using the matrix notation introduced in Chapter 3 the series expansion can be expressed as follows:

$$u_s^0(y, z) = u_0(y) + zu_1(y) + \mathbf{f}_s^T(z)\mathbf{u}(y), \quad (4.73a)$$

$$u_y^0(y, z) = v_0(y) + zv_1(y) + \mathbf{f}_y^T(z)\mathbf{v}(y), \quad (4.73b)$$

$$u_z^0(y, z) = w_1(y) + \mathbf{f}_z^T(z)\mathbf{w}(y). \quad (4.73c)$$

Functions $\mathbf{f}_s(z)$, according to the LPBM, are defined by the Legendre polynomials. Function $\mathbf{f}_z(z)$ was defined in the LPBM as $\mathbf{f}_z(z) = \hat{\mathbf{f}}_s(z)$. Function $\mathbf{f}_y(z)$ is defined by the shear strains, which for the straight laminate yield $\mathbf{f}_y(z) = \mathbf{f}_s(z)$.

Strains

After substituting (4.73) in the strains equations (4.71), and considering the properties of the derivatives of the Legendre polynomials vectors exposed in Chapter 3, the strains components can be written as:

$$\varepsilon_s(y, z) = e_N^s(y) + ze_M^s(y), \quad (4.74a)$$

$$\varepsilon_y(y, z) = e_N^y(y) + ze_M^y(y) + \mathbf{f}_s^T(z)\mathbf{e}_y(y), \quad (4.74b)$$

$$\gamma_{sy}(y, z) = e_N^{sy}(y) + ze_M^{sy}(y) + \mathbf{f}_s^T(z)\mathbf{e}_{sy}(y), \quad (4.74c)$$

$$\gamma_{yz}(y, z) = e_Q^{yz}(y) + \hat{\mathbf{f}}_s^T(z)\mathbf{e}_{yz}(y), \quad (4.74d)$$

$$\gamma_{sz}(y, z) = e_Q^{sz}(y) + \hat{\mathbf{f}}_s^T(z) \mathbf{e}_{sz}(y). \quad (4.74e)$$

$$\varepsilon_z(y, z) = \hat{\mathbf{f}}_s^T(z) \mathbf{e}_z(y), \quad (4.74f)$$

where $e_N^s(y)$, $e_M^s(y)$, $e_N^y(y)$, $e_M^y(y)$, $e_N^{sy}(y)$, $e_M^{sy}(y)$, $e_Q^{yz}(y)$ and $e_Q^{sz}(y)$ are the non-dimensional first-order 1D strain components, and $\mathbf{e}_y(y)$, $\mathbf{e}_{sy}(y)$, $\mathbf{e}_{yz}(y)$, $\mathbf{e}_{sz}(y)$ and $\mathbf{e}_z(y)$ are the non-dimensional higher-order 1D strain components, which are defined as:

$$e_N^s(y) = \varepsilon_s^0 + y\kappa_y^0, \quad e_M^s(y) = \kappa_z^0, \quad (4.75a)$$

$$e_N^y(y) = \frac{dv_0(y)}{dy}, \quad e_M^y(y) = \frac{dv_1(y)}{dy}, \quad \mathbf{e}_y(y) = \frac{d\mathbf{v}(y)}{dy}, \quad (4.75b)$$

$$e_N^{sy}(y) = \frac{du_0(y)}{dy}, \quad e_M^{sy}(y) = \frac{du_1(y)}{dy} - \kappa_{yz}^0, \quad \mathbf{e}_{sy}(y) = \frac{d\mathbf{u}(y)}{dy}, \quad (4.75c)$$

$$e_Q^{yz}(y) = v_1(y) + \frac{dw_1(y)}{dy} + \mathbf{h}_Q^T \mathbf{v}(y), \quad \mathbf{e}_{yz}(y) = \mathbf{H}_\gamma^T \mathbf{v}(y) + \frac{d\mathbf{w}(y)}{dy}, \quad (4.75d)$$

$$e_Q^{sz}(y) = u_1(y) + y\kappa_{yz}^0 + \mathbf{h}_Q^T \mathbf{u}(y), \quad \mathbf{e}_{sz}(y) = \mathbf{H}_\gamma^T \mathbf{u}(y), \quad (4.75e)$$

$$\mathbf{e}_z(y) = \mathbf{H}_z^T \mathbf{w}(y). \quad (4.75f)$$

Notice that the constant matrices \mathbf{H}_γ and \mathbf{H}_z and vector \mathbf{h}_Q are defined in Chapter 3 in the development of the LPBM (see (3.111) and $\mathbf{h}_Q = \boldsymbol{\rho}$ for the flat laminate case).

Equilibrium

The classical shell forces and moments in a flat laminate are defined as follows:

$$N_s(y) = \int_{-1}^1 \sigma_s(y, z) dz, \quad M_s(y) = \int_{-1}^1 \sigma_s(y, z) z dz, \quad (4.76a)$$

$$N_y(y) = \int_{-1}^1 \sigma_y(y, z) dz, \quad M_y(y) = \int_{-1}^1 \sigma_y(y, z) z dz, \quad (4.76b)$$

$$N_{sy}(y) = \int_{-1}^1 \tau_{sy}(y, z) dz, \quad M_{sy}(y) = \int_{-1}^1 \tau_{sy}(y, z) z dz, \quad (4.76c)$$

$$Q_s(y) = \int_{-1}^1 \tau_{sz}(y, z) dz, \quad Q_y(y) = \int_{-1}^1 \tau_{yz}(y, z) dz. \quad (4.76d)$$

The higher-order moments are defined as follows:

$$\mathbf{M}_y(y) = \int_{-1}^1 \sigma_y(y, z) \mathbf{f}_s(z) dz, \quad (4.77a)$$

$$\mathbf{M}_{sy}(y) = \int_{-1}^1 \tau_{sy}(y, z) \mathbf{f}_s(z) dz, \quad (4.77b)$$

$$\mathbf{M}_{sz}(y) = \int_{-1}^1 \tau_{sz}(y, z) \hat{\mathbf{f}}_s(z) dz, \quad (4.77c)$$

$$\mathbf{M}_{yz}(y) = \int_{-1}^1 \tau_{yz}(y, z) \hat{\mathbf{f}}_s(z) dz, \quad (4.77d)$$

$$\mathbf{M}_z(y) = \int_{-1}^1 \sigma_z(y, z) \hat{\mathbf{f}}_s(z) dz. \quad (4.77e)$$

Notice that the higher-order moments associated to $\sigma_s(y, z)$ have not been defined as they are not needed in the constitutive law, due to the absence of higher-order components in the expression of $\varepsilon_s(y, z)$ in (4.74a).

The elasticity equilibrium equations in a 3D Cartesian coordinate system, simplified considering the non-dependence of the stresses with s , are given by the following equations:

$$\frac{\partial \tau_{sy}(y, z)}{\partial y} + \frac{\partial \tau_{sz}(y, z)}{\partial z} = 0, \quad (4.78a)$$

$$\frac{\partial \sigma_y(y, z)}{\partial y} + \frac{\partial \tau_{yz}(y, z)}{\partial z} = 0, \quad (4.78b)$$

$$\frac{\partial \tau_{yz}(y, z)}{\partial y} + \frac{\partial \sigma_z(y, z)}{\partial z} = 0. \quad (4.78c)$$

The forces equilibrium equations are obtained by integrating equations (4.78) in the thickness and the first-order moment equilibrium equations are obtained by integrating equations (4.78a) and (4.78b) multiplied by z in the thickness. If null values of σ_z , τ_{sz} and τ_{yz} are prescribed in both thickness boundaries, the aforementioned equation may be written as:

$$\frac{dN_{sy}(y)}{dy} = 0, \quad \frac{dN_y(y)}{dy} = 0, \quad \frac{dQ_y(y)}{dy} = 0, \quad \frac{dM_y(y)}{dy} = Q_y(y), \quad (4.79a)$$

$$\frac{dM_{sy}(y)}{dy} = Q_s(y). \quad (4.79b)$$

Considering that the edges in the y direction are free and, therefore, prescribing null values of $\sigma_y(y, z)$, $\tau_{sy}(y, z)$ and $\tau_{yz}(y, z)$ in the width boundaries, equations (4.79a) imply null values of $N_{sy}(y)$, $N_y(y)$, $Q_y(y)$ and $M_y(y)$. Hence, only equation (4.79b) needs to be considered in the following.

The higher-order moments equilibrium equations are obtained integrating equations (4.78a) and (4.78b) multiplied by $\mathbf{f}_s(z)$ and integrating equation (4.78c) multiplied by $\hat{\mathbf{f}}_s(z)$, yielding:

$$\frac{d\mathbf{M}_{sy}(y)}{dy} = \mathbf{H}_\gamma \mathbf{M}_{sz}(y) + \mathbf{h}_Q Q_s(y), \quad (4.80a)$$

$$\frac{d\mathbf{M}_y(y)}{dy} = \mathbf{H}_\gamma \mathbf{M}_{yz}(y) + \mathbf{h}_Q Q_y(y) = \mathbf{H}_\gamma \mathbf{M}_{yz}(y), \quad (4.80b)$$

$$\frac{d\mathbf{M}_{yz}(y)}{dy} = \mathbf{H}_z \mathbf{M}_z(y). \quad (4.80c)$$

Constitutive law

As in Chapter 3, the laminate is considered constituted by N_p plies. The 3D constitutive law of a ply p , with z varying from z_p^- to z_p^+ , can be expressed depending on the stiffness matrix of the ply expressed in the ply orthotropic coordinate system, C_{ij}^p , with $i, j = 1, 2, \dots, 6$, according to equations (4.9). Rotating the stiffness matrix to the global system (s, y, z), the following stiffness matrix is obtained:

$$\begin{bmatrix} \sigma_s^p(y, z) \\ \sigma_y^p(y, z) \\ \sigma_z^p(y, z) \\ \tau_{yz}^p(y, z) \\ \tau_{sz}^p(y, z) \\ \tau_{sy}^p(y, z) \end{bmatrix} = \begin{bmatrix} \bar{C}_{11}^p & \bar{C}_{12}^p & \bar{C}_{13}^p & 0 & 0 & \bar{C}_{16}^p \\ \bar{C}_{12}^p & \bar{C}_{22}^p & \bar{C}_{23}^p & 0 & 0 & \bar{C}_{26}^p \\ \bar{C}_{13}^p & \bar{C}_{23}^p & \bar{C}_{33}^p & 0 & 0 & \bar{C}_{36}^p \\ 0 & 0 & 0 & \bar{C}_{44}^p & \bar{C}_{45}^p & 0 \\ 0 & 0 & 0 & \bar{C}_{45}^p & \bar{C}_{55}^p & 0 \\ \bar{C}_{16}^p & \bar{C}_{26}^p & \bar{C}_{36}^p & 0 & 0 & \bar{C}_{66}^p \end{bmatrix} \begin{bmatrix} \varepsilon_s(y, z) - \Delta \varepsilon_s^p \\ \varepsilon_y(y, z) - \Delta \varepsilon_y^p \\ \varepsilon_z(y, z) - \Delta \varepsilon_z^p \\ \gamma_{yz}(y, z) \\ \gamma_{sz}(y, z) \\ \gamma_{sy}(y, z) - \Delta \gamma_{sy}^p \end{bmatrix}, \quad (4.81)$$

where \bar{C}_{ij}^p , with $i, j = 1, 2, \dots, 6$, are the stiffness constants in the global coordinate system and $\Delta \varepsilon_{ij}^p$, with $i, j = s, y, z$, are the residual strains due to the manufacturing process ($\Delta \gamma_{sy}^p = 2\Delta \varepsilon_{sy}^p$).

Using the three-dimensional constitutive law given in (4.81), the strains approximations given in (4.74) and the forces and moments definition given in (4.76) and (4.77), constitutive equations yield:

$$\begin{bmatrix} N_s(y) \\ M_s(y) \\ N_y(y) \\ M_y(y) \\ \mathbf{M}_y(y) \\ N_{sy}(y) \\ M_{sy}(y) \\ \mathbf{M}_{sy}(y) \\ M_z(y) \end{bmatrix} + \begin{bmatrix} N_s^\varepsilon \\ M_s^\varepsilon \\ N_y^\varepsilon \\ M_y^\varepsilon \\ \mathbf{M}_y^\varepsilon \\ N_{sy}^\varepsilon \\ M_{sy}^\varepsilon \\ \mathbf{M}_{sy}^\varepsilon \\ M_z^\varepsilon \end{bmatrix} = \mathbf{K}_\sigma \begin{bmatrix} e_N^s(y) \\ e_M^s(y) \\ e_N^y(y) \\ e_M^y(y) \\ \mathbf{e}_y(y) \\ e_N^{sy}(y) \\ e_M^{sy}(y) \\ \mathbf{e}_{sy}(y) \\ e_z(y) \end{bmatrix}, \quad (4.82a)$$

$$\begin{bmatrix} Q_y(y) \\ \mathbf{M}_{yz}(y) \\ Q_s(y) \\ \mathbf{M}_{sz}(y) \end{bmatrix} = \mathbf{K}_\tau \begin{bmatrix} e_Q^{yz}(y) \\ \mathbf{e}_{yz}(y) \\ e_Q^{sz}(y) \\ \mathbf{e}_{sz}(y) \end{bmatrix}, \quad (4.82b)$$

where N_{ij}^ε , M_{ij}^ε and $\mathbf{M}_{ij}^\varepsilon$ are the residual forces, moments and higher-order moments due to the manufacturing process, and \mathbf{K}_σ and \mathbf{K}_τ are respectively the normal and shear stiffness matrices of the model.

The components of the stiffness matrices \mathbf{K}_σ and \mathbf{K}_τ are shown in Appendix B.1.

The residual forces, moments and higher-order moments due to the manufacturing process are calculated as follows:

$$N_s^\varepsilon = \sum_{p=1}^{N_p} (z_p^+ - z_p^-) \Delta \sigma_s^p, \quad M_s^\varepsilon = \sum_{p=1}^{N_p} \frac{1}{2} ((z_p^+)^2 - (z_p^-)^2) \Delta \sigma_s^p, \quad (4.83a)$$

$$N_y^\varepsilon = \sum_{p=1}^{N_p} (z_p^+ - z_p^-) \Delta \sigma_y^p, \quad M_y^\varepsilon = \sum_{p=1}^{N_p} \frac{1}{2} ((z_p^+)^2 - (z_p^-)^2) \Delta \sigma_y^p, \quad (4.83b)$$

$$N_{sy}^\varepsilon = \sum_{p=1}^{N_p} (z_p^+ - z_p^-) \Delta \tau_{sy}^p, \quad M_{sy}^\varepsilon = \sum_{p=1}^{N_p} \frac{1}{2} ((z_p^+)^2 - (z_p^-)^2) \Delta \tau_{sy}^p, \quad (4.83c)$$

$$\mathbf{M}_y^\varepsilon = \sum_{p=1}^{N_p} \left(\Delta \sigma_y^p \int_{z_p^-}^{z_p^+} \mathbf{f}_s(z) dz \right), \quad (4.83d)$$

$$\mathbf{M}_{sy}^\varepsilon = \sum_{p=1}^{N_p} \left(\Delta \tau_{sy}^p \int_{z_p^-}^{z_p^+} \mathbf{f}_s(z) dz \right), \quad (4.83e)$$

$$\mathbf{M}_z^\varepsilon = \sum_{p=1}^{N_p} \left(\Delta\sigma_z^p \int_{z_p^-}^{z_p^+} \hat{\mathbf{f}}_s(z) dz \right), \quad (4.83f)$$

where $\Delta\sigma_s^p$, $\Delta\sigma_y^p$, $\Delta\sigma_z^p$ and $\Delta\tau_{sy}^p$ are calculated from the following expressions:

$$\begin{bmatrix} \Delta\sigma_s^p \\ \Delta\sigma_y^p \\ \Delta\sigma_z^p \\ \Delta\tau_{sy}^p \end{bmatrix} = \begin{bmatrix} \bar{C}_{11}^p & \bar{C}_{12}^p & \bar{C}_{13}^p & \bar{C}_{16}^p \\ \bar{C}_{12}^p & \bar{C}_{22}^p & \bar{C}_{23}^p & \bar{C}_{26}^p \\ \bar{C}_{13}^p & \bar{C}_{23}^p & \bar{C}_{33}^p & \bar{C}_{36}^p \\ \bar{C}_{16}^p & \bar{C}_{26}^p & \bar{C}_{36}^p & \bar{C}_{66}^p \end{bmatrix} \begin{bmatrix} \Delta\varepsilon_s^p \\ \Delta\varepsilon_y^p \\ \Delta\varepsilon_z^p \\ \Delta\gamma_{sy}^p \end{bmatrix}. \quad (4.84)$$

According to (4.75a), the dependency of $e_N(y)$ and $e_M(y)$ with the coordinate y is fixed depending only on three constants. Therefore, the two first equations of (4.82a) are not needed for the development of the final differential equation, it being only used for the calculation of the axial force and the axial bending moment. After extracting the two first equations, and, rearranging, equations (4.82a) may be expressed as follows:

$$\begin{bmatrix} N_y(y) \\ M_y(y) \\ \mathbf{M}_y(y) \\ N_{sy}(y) \\ M_{sy}(y) \\ \mathbf{M}_{sy}(y) \\ M_z(y) \end{bmatrix} + \begin{bmatrix} N_y^\varepsilon \\ M_y^\varepsilon \\ \mathbf{M}_y^\varepsilon \\ N_{sy}^\varepsilon \\ M_{sy}^\varepsilon \\ \mathbf{M}_{sy}^\varepsilon \\ M_z^\varepsilon \end{bmatrix} = \mathbf{K}_\sigma^A \begin{bmatrix} e_N^y(y) \\ e_M^y(y) \\ \mathbf{e}_y(y) \\ e_N^{sy}(y) \\ e_M^{sy}(y) \\ \mathbf{e}_{sy}(y) \\ e_z(y) \end{bmatrix} + \mathbf{K}_\sigma^B \begin{bmatrix} e_N^s(y) \\ e_M^s(y) \end{bmatrix}, \quad (4.85)$$

where matrices \mathbf{K}_σ^A and \mathbf{K}_σ^B are defined in Appendix B.1.

Equations (4.85) and (4.82b) may be inverted yielding the following compliance equations:

$$\begin{bmatrix} e_N^y(y) \\ e_M^y(y) \\ \mathbf{e}_y(y) \\ e_N^{sy}(y) \\ e_M^{sy}(y) \\ \mathbf{e}_{sy}(y) \\ e_z(y) \end{bmatrix} = \tilde{\mathbf{K}}_\sigma^A \begin{bmatrix} N_y(y) - N_y^\varepsilon \\ M_y(y) - M_y^\varepsilon \\ \mathbf{M}_y(y) - \mathbf{M}_y^\varepsilon \\ N_{sy}(y) - N_{sy}^\varepsilon \\ M_{sy}(y) - M_{sy}^\varepsilon \\ \mathbf{M}_{sy}(y) - \mathbf{M}_{sy}^\varepsilon \\ M_z(y) - M_z^\varepsilon \end{bmatrix} - \tilde{\mathbf{K}}_\sigma^B \begin{bmatrix} e_N^s(y) \\ e_M^s(y) \end{bmatrix}, \quad (4.86a)$$

$$\begin{bmatrix} e_Q^{yz}(y) \\ \mathbf{e}_{yz}(y) \\ e_Q^{sz}(y) \\ \mathbf{e}_{sz}(y) \end{bmatrix} = \tilde{\mathbf{K}}_\tau \begin{bmatrix} Q_y(y) \\ \mathbf{M}_{yz}(y) \\ Q_s(y) \\ \mathbf{M}_{sz}(y) \end{bmatrix}, \quad (4.86b)$$

where $\check{K}_\sigma^A = (K_\sigma^A)^{-1}$, $\check{K}_\sigma^B = (K_\sigma^A)^{-1}K_\sigma^B$ and $\check{K}_\tau = K_\tau^{-1}$, and their components are denominated as follows:

$$\check{K}_\sigma^A = \begin{bmatrix} \check{A}_{22} & \check{B}_{22} & (\check{k}_{22}^A)^T & \check{A}_{26} & \check{B}_{26} & (\check{k}_{26}^A)^T & (\check{k}_{23}^A)^T \\ \check{B}_{22} & \check{D}_{22} & (\check{k}_{22}^B)^T & \check{B}_{26} & \check{D}_{26} & (\check{k}_{26}^B)^T & (\check{k}_{23}^B)^T \\ \check{k}_{22}^A & \check{k}_{22}^B & \check{K}_{22}^\sigma & \check{k}_{26}^A & \check{k}_{26}^B & \check{K}_{26}^\sigma & \check{K}_{23}^\sigma \\ \check{A}_{26} & \check{A}_{26} & (\check{k}_{26}^A)^T & \check{A}_{66} & \check{B}_{66} & (\check{k}_{66}^A)^T & (\check{k}_{36}^A)^T \\ \check{B}_{26} & \check{B}_{26} & (\check{k}_{26}^B)^T & \check{B}_{66} & \check{D}_{66} & (\check{k}_{66}^B)^T & (\check{k}_{36}^B)^T \\ \check{k}_{26}^A & \check{k}_{26}^B & \check{K}_{26}^\sigma & \check{k}_{66}^A & \check{k}_{66}^B & \check{K}_{66}^\sigma & \check{K}_{36}^\sigma \\ \check{k}_{23}^A & \check{k}_{23}^B & (\check{K}_{23}^\sigma)^T & \check{k}_{36}^A & \check{k}_{36}^B & (\check{K}_{36}^\sigma)^T & \check{K}_{33}^\sigma \end{bmatrix}, \quad (4.87a)$$

$$\check{K}_\sigma^B = \begin{bmatrix} \check{A}_{12} & \check{B}_{12} \\ \check{B}_{12} & \check{D}_{12} \\ \check{k}_{12}^A & \check{k}_{12}^B \\ \check{A}_{16} & \check{B}_{16} \\ \check{B}_{16} & \check{D}_{16} \\ \check{k}_{16}^A & \check{k}_{16}^B \\ \check{k}_{13}^A & \check{k}_{13}^B \end{bmatrix}, \quad (4.87b)$$

$$\check{K}_\tau = \begin{bmatrix} \check{A}_{44} & (\check{k}_{44}^C)^T & \check{A}_{45} & (\check{k}_{45}^C)^T \\ \check{k}_{44}^C & \check{K}_{44}^\tau & \check{k}_{45}^C & \check{K}_{45}^\tau \\ \check{A}_{45} & (\check{k}_{45}^C)^T & \check{A}_{55} & (\check{k}_{55}^C)^T \\ \check{k}_{45}^C & \check{K}_{45}^\tau & \check{k}_{55}^C & \check{K}_{55}^\tau \end{bmatrix}. \quad (4.87c)$$

Solution procedure

The solution is obtained by jointly solving the strain-displacements equations, the constitutive law and the equilibrium equations. Deriving equation (4.86b), considering the null value of Q_y and introducing equations (4.80a), (4.80b), (4.79b), (4.75d) and (4.75e), the shear compliance equations can be written as:

$$\begin{bmatrix} \frac{dv_1(y)}{dy} + \frac{d^2w_1(y)}{dy^2} + \mathbf{h}_Q^T \frac{dv(y)}{dy} \\ \mathbf{H}_\gamma^T \frac{dv(y)}{dy} + \frac{d^2w(y)}{dy^2} \\ \frac{du_1(y)}{dy} + \kappa_{yz}^0 + \mathbf{h}_Q^T \frac{du(y)}{dy} \\ \mathbf{H}_\gamma^T \frac{du(y)}{dy} \end{bmatrix} = \check{K}_\tau \begin{bmatrix} 0 \\ \mathbf{H}_\gamma^{-1} \frac{d^2M_y(y)}{dy^2} \\ \frac{d^2M_{sy}(y)}{dy^2} \\ \mathbf{H}_\gamma^{-1} \left(\frac{d^2M_{sy}(y)}{dy^2} - \mathbf{h}_Q \frac{d^2M_{sy}(y)}{dy^2} \right) \end{bmatrix}. \quad (4.88)$$

The in-plane displacements components $\mathbf{v}(y)$, $u_1(y)$ and $\mathbf{u}(y)$ may be obtained from equation (4.88) as follows:

$$\frac{d\mathbf{v}(y)}{dy} = \mathbf{H}_{11}^Q \frac{d^2 \mathbf{M}_y(y)}{dy^2} + \mathbf{H}_{12}^Q \frac{d^2 M_{sy}(y)}{dy^2} + \mathbf{H}_{13}^Q \frac{d^2 \mathbf{M}_{sy}(y)}{dy^2} - (\mathbf{H}_\gamma^T)^{-1} \frac{d^2 \mathbf{w}(y)}{dy^2}, \quad (4.89a)$$

$$\frac{du_1(y)}{dy} = \mathbf{H}_{21}^Q \frac{d^2 \mathbf{M}_y(y)}{dy^2} + H_{22}^Q \frac{d^2 M_{sy}(y)}{dy^2} + \mathbf{H}_{23}^Q \frac{d^2 \mathbf{M}_{sy}(y)}{dy^2} - \kappa_{yz}^0, \quad (4.89b)$$

$$\frac{d\mathbf{u}(y)}{dy} = \mathbf{H}_{31}^Q \frac{d^2 \mathbf{M}_y(y)}{dy^2} + \mathbf{H}_{32}^Q \frac{d^2 M_{sy}(y)}{dy^2} + \mathbf{H}_{33}^Q \frac{d^2 \mathbf{M}_{sy}(y)}{dy^2}, \quad (4.89c)$$

where the auxiliary matrices are defined in Appendix B.2.

Considering that $N_y(y)$, $M_y(y)$ and $N_{sy}(y)$ are null, and substituting the strains from equations (4.75b), (4.75c) and (4.75f), the equations of (4.86a) associated to $\mathbf{e}_y(y)$, $e_M^{sy}(y)$, $\mathbf{e}_{sy}(y)$ and $\mathbf{e}_z(y)$ yield:

$$\begin{bmatrix} \frac{d\mathbf{v}(y)}{dy} \\ \frac{du_1(y)}{dy} - \kappa_{yz}^0 \\ \frac{d\mathbf{u}(y)}{dy} \\ \mathbf{H}_z^T \mathbf{w}(y) \end{bmatrix} = \begin{bmatrix} \check{\mathbf{K}}_{22}^\sigma & \check{\mathbf{k}}_{26}^B & \check{\mathbf{K}}_{26}^\sigma & \check{\mathbf{K}}_{23}^\sigma \\ (\check{\mathbf{k}}_{26}^B)^T & \check{D}_{66} & (\check{\mathbf{k}}_{66}^B)^T & (\check{\mathbf{k}}_{36}^B)^T \\ \check{\mathbf{K}}_{26}^\sigma & \check{\mathbf{k}}_{66}^B & \check{\mathbf{K}}_{66}^\sigma & \check{\mathbf{K}}_{36}^\sigma \\ (\check{\mathbf{K}}_{23}^\sigma)^T & \check{\mathbf{k}}_{36}^B & (\check{\mathbf{K}}_{36}^\sigma)^T & \check{\mathbf{K}}_{33}^\sigma \end{bmatrix} \begin{bmatrix} M_y(y) \\ M_{sy}(y) \\ \mathbf{M}_{sy}(y) \\ M_z(y) \end{bmatrix} - \begin{bmatrix} \check{\mathbf{k}}_{12}^A & \check{\mathbf{k}}_{12}^B \\ \check{B}_{16} & \check{D}_{16} \\ \check{\mathbf{k}}_{16}^A & \check{\mathbf{k}}_{16}^B \\ \check{\mathbf{k}}_{13}^A & \check{\mathbf{k}}_{13}^B \end{bmatrix} \begin{bmatrix} e_N^s(y) \\ e_M^s(y) \end{bmatrix} - \mathbf{H}_\varepsilon, \quad (4.90)$$

where the auxiliary vector \mathbf{H}_ε is defined in Appendix B.2.

Substituting equations (4.89), (4.75a) and (4.80) into equations (4.90), the differential equation of the model is given by:

$$\frac{d^2 \mathbf{x}(y)}{dy^2} = \mathbf{G} \mathbf{x}(y) + \mathbf{G}_c \mathbf{v}(y) + \mathbf{g}_\varepsilon, \quad (4.91a)$$

$$\mathbf{x}(y) = \begin{bmatrix} M_y(y) \\ M_{sy}(y) \\ \mathbf{M}_{sy}(y) \\ \mathbf{w}(y) \end{bmatrix}, \quad \mathbf{v}(y) = \begin{bmatrix} \kappa_{yz}^0 \\ \varepsilon_s^0 + y\kappa_y^0 \\ \kappa_z^0 \end{bmatrix}, \quad (4.91b)$$

where matrices \mathbf{G} and \mathbf{G}_c and vector \mathbf{g}_ε are defined in Appendix B.2.

As described in Chapter 3 for the MBM and LPBM, the differential equation (4.91a) can be solved by obtaining a particular solution (the regularized

solution) and the solution of the homogeneous equation. The regularized solution is given by:

$$\mathbf{x}_{reg}(y) = -\mathbf{G}^{-1}\mathbf{G}_c\mathbf{v}(y) - \mathbf{G}^{-1}\mathbf{G}_\varepsilon. \quad (4.92)$$

Non-regularized stresses and strains are determined by the superposition of their regularized values, given in equation (4.92), and the perturbations, calculated from the homogeneous equation. The homogeneous equation is determined by separating the solution vector, $\mathbf{x}(y)$, into its regularized value, $\mathbf{x}_{reg}(y)$, and the perturbations, $\hat{\mathbf{x}}(y)$. Therefore, the homogeneous equation is obtained with the variable change $\mathbf{x}(y) = \mathbf{x}_{reg}(y) + \hat{\mathbf{x}}(y)$, and the differential equation results in:

$$\frac{d^2\hat{\mathbf{x}}(y)}{dy^2} = \mathbf{G}\hat{\mathbf{x}}(y). \quad (4.93)$$

Equation (4.93) is solved as an eigenvalue problem as described in the MBM and the LPBM of Chapter 3 and imposing the boundary conditions associated to the free edge $\mathbf{M}_y(y) = 0$, $M_{sy}(y) = 0$, $\mathbf{M}_{sy}(y) = 0$ and $\mathbf{M}_{yz}(y) = 0$ in $y = 0$ and in $y = W$.

Stresses calculation

With an analogous development to that employed in the straight beam case of the MBM and the LPBM, once the vector $\mathbf{x}(y)$ given in (4.91b) has been calculated, the moment and higher order moments $M_{sy}(y)$, $\mathbf{M}_y(y)$ and $\mathbf{M}_{sy}(y)$ are directly obtained as the corresponding components of $\mathbf{x}(y)$. Shear higher-order moments and transverse higher-order moments are obtained from the equilibrium equations (4.80). Strains are obtained by using the compliance equations (4.86). Once strains are obtained, the axial, transverse and in-plane shear stress are calculated for each ply by using the 3D constitutive equations (4.81):

$$\sigma_s^p(y, z) = \mathbf{S}_s^p(z)^T \left(\tilde{\mathbf{K}}_\sigma^A \mathbf{M}_T(y) - \tilde{\mathbf{K}}_\sigma^B \begin{bmatrix} \varepsilon_s^0 + y\kappa_y^0 \\ \kappa_z^0 \end{bmatrix} \right) + Q_{11}^p(\varepsilon_s^0 + y\kappa_y^0 + z\kappa_z^0), \quad (4.94a)$$

$$\sigma_y^p(y, z) = \mathbf{S}_y^p(z)^T \left(\tilde{\mathbf{K}}_\sigma^A \mathbf{M}_T(y) - \tilde{\mathbf{K}}_\sigma^B \begin{bmatrix} \varepsilon_s^0 + y\kappa_y^0 \\ \kappa_z^0 \end{bmatrix} \right) + Q_{12}^p(\varepsilon_s^0 + y\kappa_y^0 + z\kappa_z^0), \quad (4.94b)$$

$$\tau_{sy}^p(y, z) = \mathbf{S}_{sy}^p(z)^T \left(\check{\mathbf{K}}_{\sigma}^A \mathbf{M}_T(y) - \check{\mathbf{K}}_{\sigma}^B \begin{bmatrix} \varepsilon_s^0 + y\kappa_y^0 \\ \kappa_z^0 \end{bmatrix} \right) + Q_{16}^p(\varepsilon_s^0 + y\kappa_y^0 + z\kappa_z^0), \quad (4.94c)$$

where the vector $\mathbf{M}_T(y)$ is defined as follows:

$$\mathbf{M}_T(y) = \begin{bmatrix} N_y(y) - N_y^{\varepsilon} \\ M_y(y) - M_y^{\varepsilon} \\ \mathbf{M}_y(y) - \mathbf{M}_y^{\varepsilon} \\ N_{sy}(y) - N_{sy}^{\varepsilon} \\ M_{sy}(y) - M_{sy}^{\varepsilon} \\ \mathbf{M}_{sy}(y) - \mathbf{M}_{sy}^{\varepsilon} \\ M_z(y) - M_z^{\varepsilon} \end{bmatrix}, \quad (4.95)$$

and the shape vectors $\mathbf{S}_s^p(z)$, $\mathbf{S}_y^p(z)$ and $\mathbf{S}_{sy}^p(z)$, defined by their components $(\mathbf{S}_s^p)_i(z)$, $(\mathbf{S}_y^p)_i(z)$ and $(\mathbf{S}_{sy}^p)_i(z)$ respectively for $i = 0, 1, \dots, 3n$, are given by:

$$(\mathbf{S}_s^p)_i(z) = Q_{12}^p p_i(z), \quad (\mathbf{S}_s^p)_{i+n+1}(z) = Q_{16}^p p_i(z), \quad i = 0, 1, \dots, n, \quad (4.96a)$$

$$(\mathbf{S}_s^p)_{i+2n}(z) = Q_{13}^p p_{i-2}(z), \quad i = 2, 3, \dots, n, \quad (4.96b)$$

$$(\mathbf{S}_y^p)_i(z) = Q_{22}^p p_i(z), \quad (\mathbf{S}_y^p)_{i+n+1}(z) = Q_{26}^p p_i(z), \quad i = 0, 1, \dots, n, \quad (4.96c)$$

$$(\mathbf{S}_y^p)_{i+2n}(z) = Q_{23}^p p_{i-2}(z), \quad i = 2, 3, \dots, n, \quad (4.96d)$$

$$(\mathbf{S}_{sy}^p)_i(z) = Q_{26}^p p_i(z), \quad (\mathbf{S}_{sy}^p)_{i+n+1}(z) = Q_{66}^p p_i(z), \quad i = 0, 1, \dots, n, \quad (4.96e)$$

$$(\mathbf{S}_{sy}^p)_{i+2n}(z) = Q_{36}^p p_{i-2}(z), \quad i = 2, 3, \dots, n. \quad (4.96f)$$

Finally, the out-of-plane shear and through-thickness stresses are obtained by integration of the equilibrium equations (4.78):

$$\tau_{sz}^p(y, z) = \tau_{sz}^p(y, z_p^-) - \mathbf{S}_{sz}^p(z)^T \left(\check{\mathbf{K}}_{\sigma}^A \frac{d\mathbf{M}_T(y)}{dy} - \check{\mathbf{K}}_{\sigma}^B \begin{bmatrix} \kappa_y^0 \\ 0 \end{bmatrix} \right) - Q_{16}^p \kappa_y^0 (z - z_p^-), \quad (4.97a)$$

$$\tau_{yz}^p(y, z) = \tau_{yz}^p(y, z_p^-) - \mathbf{S}_{yz}^p(z)^T \left(\check{\mathbf{K}}_\sigma^A \frac{d\mathbf{M}_T(y)}{dy} - \check{\mathbf{K}}_\sigma^B \begin{bmatrix} \kappa_y^0 \\ 0 \end{bmatrix} \right) + Q_{12}^p \kappa_y^0 (z - z_p^-), \quad (4.97b)$$

$$\sigma_z^p(y, z) = \sigma_z^p(y, z_p^-) - \frac{d\tau_{sz}^p(y, z_p^-)}{dy} (z - z_p^-) + \mathbf{S}_{z,2}^p(z)^T \check{\mathbf{K}}_\sigma^A \frac{d^2 \mathbf{M}_T(y)}{dy^2}, \quad (4.97c)$$

and the shape vectors:

$$\mathbf{S}_{sz}^p(z) = \int_{z_p^-}^z \mathbf{S}_{sy}^p(z') dz', \quad (4.98a)$$

$$\mathbf{S}_{yz}^p(z) = \int_{z_p^-}^z \mathbf{S}_y^p(z') dz', \quad (4.98b)$$

$$\mathbf{S}_{z,2}^p(z) = \int_{z_p^-}^z \mathbf{S}_{yz}^p(z') dz'. \quad (4.98c)$$

Out-of-plane shear and through-thickness stresses have to be calculated recursively ply by ply as in the MBM and the LPBM, starting with the boundary conditions $\tau_{sz}^1(y, -1) = \tau_{yz}^1(y, -1) = \sigma_z^1(y, -1) = 0$. In the successive layers, continuity with the previous layers is imposed. The boundary conditions $\tau_{sz}^{N_p}(y, 1) = \tau_{yz}^{N_p}(y, 1) = \sigma_z^{N_p}(y, 1) = 0$ are automatically accomplished.

Loads application

The solution of the model and, consequently, the stress components, have been expressed depending on the mean line strains ε_s^0 , κ_y^0 , κ_z^0 and κ_{yz}^0 . However, the inputs of the problem are usually the loads applied to the laminate, which are given as an axial force N_0 , a bending moment M_0 , an in-plane bending moment P_0 and a torsional moment T_0 . These total forces and moments are obtained by integrating in the width the corresponding distributed forces and moments as follows:

$$N_0 = \int_0^W N_s(y) dy, \quad (4.99a)$$

$$M_0 = \int_0^W M_s(y) dy, \quad (4.99b)$$

$$P_0 = \int_0^W \left(y - \frac{W}{2} \right) N_s(y) dy, \quad (4.99c)$$

$$T_0 = \int_0^W (M_{sy}(y) - yQ_s(y)) dy. \quad (4.99d)$$

4.4.2 Development of the 3D non-regularized model in curved laminates

The non-regularized model applied to curved laminates constitutes a more complex case than the flat laminates model since the anticlastic effect, combined with the curvature, constrains several kinds of deformations.

Displacements and strains distributions

As in the flat laminate case, strains and stresses are considered non-dependant on the s coordinate, what enforces a given dependence of the displacements with the aforementioned coordinate. As in the regularized 3D model, the terms of the strains may be obtained by using the compatibility equations. However, in the present section the displacements are being obtained by integrating the strain equations as in the flat laminate case.

Therefore, considering the transverse strain, $\varepsilon_y(y, z)$, and the interlaminar strain, $\varepsilon_z(y, z)$, and integrating their respective strain-displacement relations, it yields:

$$\varepsilon_y(y, z) = \frac{\partial u_y(s, y, z)}{\partial y} \longrightarrow u_y(s, y, z) = u_y^0(y, z) + u_y^A(s, z), \quad (4.100a)$$

$$\varepsilon_z(y, z) = \frac{\partial u_z(s, y, z)}{\partial z} \longrightarrow u_z(s, y, z) = u_z^0(y, z) + u_z^A(s, y), \quad (4.100b)$$

where $u_y^0(y, z)$, $u_y^A(s, z)$, $u_z^0(y, z)$ and $u_z^A(s, y)$ are auxiliary functions due to the integration.

Considering now the shear strain $\gamma_{yz}(y, z)$, and substituting (4.100), yields:

$$\begin{aligned} \gamma_{yz}(y, z) &= \frac{\partial u_y(s, y, z)}{\partial z} + \frac{\partial u_z(s, y, z)}{\partial y} = \\ &= \frac{\partial u_y^0(y, z)}{\partial z} + \frac{\partial u_z^0(y, z)}{\partial y} + \frac{\partial u_y^A(s, z)}{\partial z} + \frac{\partial u_z^A(s, y)}{\partial y}. \end{aligned} \quad (4.101)$$

Since the right term of equation (4.101) cannot depend on s , the auxiliary functions $u_y^A(s, z)$ and $u_z^A(s, y)$ can be written as:

$$u_y^A(s, z) = u_y^B(s) - (z + R)\xi_A(s), \quad (4.102a)$$

$$u_z^A(s, y) = u_z^B(s) + y\xi_A(s), \quad (4.102b)$$

where $u_y^B(s)$, $u_z^B(s)$ and $\xi_A(s)$ are auxiliary functions.

Substituting (4.100a) and (4.102a) in the shear strain $\gamma_{sy}(y, z)$ yields:

$$\begin{aligned} \gamma_{sy}(y, z) &= \frac{\partial u_s(s, y, z)}{\partial y} + \frac{R}{R+z} \frac{\partial u_y(s, y, z)}{\partial s} = \\ &= \frac{\partial u_s(s, y, z)}{\partial y} + \frac{R}{R+z} \left(\frac{du_y^B(s)}{ds} - (z+R) \frac{d\xi_A(s)}{ds} \right). \end{aligned} \quad (4.103)$$

Since the right term of equation (4.103) cannot depend on s , the displacement $u_s(s, y, z)$ can be written as:

$$u_s(s, y, z) = u_s^A(y, z) + u_s^B(s, z) - \frac{Ry}{R+z} \frac{du_y^B(s)}{ds} + Ry \frac{d\xi_A(s)}{ds}, \quad (4.104)$$

where $u_s^A(y, z)$ and $u_s^B(s, z)$ are auxiliary functions due to the integration.

Considering now the axial strain, $\varepsilon_s(y, z)$, which depends only on the coordinates y and z , and substituting (4.104), (4.100b) and (4.102b), the following expression can be obtained:

$$\begin{aligned} \varepsilon_s(y, z) &= \frac{R}{R+z} \left(\frac{\partial u_s(s, y, z)}{\partial s} + \frac{u_z(s, y, z)}{R} \right) = \frac{R}{R+z} \left(\frac{\partial u_s^B(s, z)}{\partial s} - \right. \\ &\quad \left. \frac{Ry}{R+z} \frac{d^2 u_y^B(s)}{ds^2} + Ry \frac{d^2 \xi_A(s)}{ds^2} + \frac{u_z^0(y, z) + u_z^B(s) + y \xi_A(s)}{R} \right). \end{aligned} \quad (4.105)$$

Since the right term of equation (4.105) cannot depend on s , the auxiliary functions $u_s^B(s, z)$, $u_y^B(s)$, $u_z^B(s)$ and $\xi_A(s)$ can be written as:

$$u_s^B(s, z) = s u_s^C(z) + \xi_B(s), \quad (4.106a)$$

$$u_y^B(s) = s \gamma_{sy}^0 - \frac{s^2}{2} k_y^0, \quad (4.106b)$$

$$u_z^B(s) = -R \frac{d\xi_B(s)}{ds}, \quad (4.106c)$$

$$\xi_A(s) = \phi_s \cos \frac{s}{R} + \phi_z \sin \frac{s}{R}, \quad (4.106d)$$

where $u_s^C(z)$ and $\xi_B(s)$ are auxiliary functions due to the integration, γ_{sy}^0 is the mean line in-plane shear strain, k_y^0 is the mean line curvature associated to the y direction and ϕ_s and ϕ_z are rigid body rotations.

Finally, considering the shear strain $\gamma_{sz}(y, z)$ and substituting (4.104), (4.100b), (4.102b) and (4.106), it yields:

$$\begin{aligned} \gamma_{sz}(y, z) = & \frac{R}{R+z} \left(\frac{R+z}{R} \frac{\partial u_s(s, y, z)}{\partial z} - \frac{u_s(s, y, z)}{R} + \frac{\partial u_z(s, y, z)}{\partial s} \right) = \\ & \frac{R}{R+z} \left(\frac{R+z}{R} \frac{\partial u_s^A(y, z)}{\partial z} + \frac{R+z}{R} s \frac{du_s^C(z)}{dz} + \right. \\ & \left. \frac{2y}{R+z} (\gamma_{sy}^0 - sk_y^0) - \frac{u_s^0(y, z) + su_s^C(z) + \xi_B(s)}{R} - R \frac{d^2 \xi_B(s)}{ds^2} \right). \end{aligned} \quad (4.107)$$

Since the right term of equation (4.107) cannot depend on s , the auxiliary constant k_y^0 and the auxiliary functions $u_s^B(z)$ and $\xi_B(s)$ can be written as:

$$u_s^C(z) = \frac{R+z}{R} \varepsilon_s^0, \quad (4.108a)$$

$$\xi_B(s) = U_X \cos \frac{s}{R} + U_Z \sin \frac{s}{R}, \quad (4.108b)$$

$$k_y^0 = 0, \quad (4.108c)$$

where ε_s^0 is the mean line axial strain and U_X and U_Z are the rigid body displacements in the (s, z) plane.

Furthermore, for the sake of simplicity, the following definition is considered in order to obtain a simpler expression of the strain components:

$$u_s^A(y, z) = u_s^0(y, z) + \frac{Ry}{R+z} \gamma_{sy}^0. \quad (4.109)$$

Therefore, substituting (4.102), (4.106), (4.108) and (4.109) in (4.100) and (4.104) the displacements can be written as:

$$\begin{aligned} u_s(s, y, z) = & u_s^0(y, z) + s \frac{R+z}{R} \varepsilon_s^0 + U_X \cos \frac{s}{R} + U_Z \sin \frac{s}{R} - \\ & y \phi_s \sin \frac{s}{R} + y \phi_z \cos \frac{s}{R}, \end{aligned} \quad (4.110a)$$

$$u_y(s, y, z) = u_y^0(y, z) + s \gamma_{sy}^0 - (z+R) \left(\phi_s \cos \frac{s}{R} + \phi_z \sin \frac{s}{R} \right), \quad (4.110b)$$

$$\begin{aligned} u_z(s, y, z) = & u_z^0(y, z) + U_X \sin \frac{s}{R} - U_Z \cos \frac{s}{R} + \\ & y \phi_s \cos \frac{s}{R} + y \phi_z \sin \frac{s}{R}. \end{aligned} \quad (4.110c)$$

Substituting in the strains definitions, strains components can be written as:

$$\varepsilon_s(y, z) = \varepsilon_s^0 + \frac{u_z^0(y, z)}{R + z}, \quad (4.111a)$$

$$\varepsilon_y(y, z) = \frac{\partial u_y^0(y, z)}{\partial y}, \quad \varepsilon_z(y, z) = \frac{\partial u_z^0(y, z)}{\partial z}, \quad (4.111b)$$

$$\gamma_{yz}(y, z) = \frac{\partial u_y^0(y, z)}{\partial z} + \frac{\partial u_z^0(y, z)}{\partial y}, \quad (4.111c)$$

$$\gamma_{sy}(y, z) = \frac{\partial u_s^0(y, z)}{\partial y} + \frac{R}{R + z} \gamma_{sy}^0, \quad (4.111d)$$

$$\gamma_{sz}(y, z) = \frac{\partial u_s^0(y, z)}{\partial z} - \frac{u_s^0(y, z)}{R + z}. \quad (4.111e)$$

Displacements approximation

Displacements are approximated by using a series expansion according to (4.59). However, under the assumption of non-dependence of the strains and stresses with the axial coordinate s , displacements have been simplified to equations (4.110). Therefore, in the present model, the auxiliary functions $u_s^0(y, z)$, $u_y^0(y, z)$ and $u_z^0(y, z)$ have been approximated by a series expansion in the z -coordinate:

$$u_s^0(y, z) = u_0(y) + zu_1(y) + \sum_{i=2}^n p_i(z)u_i(y), \quad (4.112a)$$

$$u_y^0(y, z) = v_0(y) + zv_1(y) + \sum_{i=2}^n f_i^y(z)v_i(y), \quad (4.112b)$$

$$u_z^0(y, z) = w_1(y) + \sum_{i=2}^n f_i^z(z)w_i(y). \quad (4.112c)$$

Using the matrix notation developed in Chapter 3 the series expansion is expressed as follows:

$$u_s^0(y, z) = u_0(y) + zu_1(y) + \mathbf{f}_s^T(z)\mathbf{u}(y), \quad (4.113a)$$

$$u_y^0(y, z) = v_0(y) + zv_1(y) + \mathbf{f}_y^T(z)\mathbf{v}(y), \quad (4.113b)$$

$$u_z^0(y, z) = w_1(y) + \mathbf{f}_z^T(z)\mathbf{w}(y). \quad (4.113c)$$

Functions $\mathbf{f}_s(z)$, according to the LPBM, are defined by the Legendre polynomials. Function $\mathbf{f}_z(z)$ was defined in the LPBM according to equation (3.124). Function $\mathbf{f}_y(z)$ is defined by the shear strain $\gamma_{yz}(y, z)$. Substituting (4.113) in equation (4.111c):

$$\gamma_{yz}(y, z) = v_1(y) + \frac{dw_1(y)}{dy} + \frac{d\mathbf{f}_y^T(z)}{dz}\mathbf{v}(y) + \mathbf{f}_z^T(z)\frac{d\mathbf{w}(y)}{dy}. \quad (4.114)$$

According to the LPBM, it is desirable to express the shear strain in the following way:

$$\gamma_{yz}(y, z) = e_Q^{yz}(y) + \mathbf{f}_z^T(z)\mathbf{e}_{yz}(y). \quad (4.115a)$$

$$\mathbf{e}_{yz}(y) = \mathbf{H}_\gamma^T\mathbf{v}(y) + \frac{d\mathbf{w}(y)}{dy}. \quad (4.115b)$$

Hence, substituting (4.114) in (4.115), the strain component $e_Q^{yz}(y)$ and function $\mathbf{f}_y(z)$ yield:

$$e_Q^{yz}(y) = v_1(y) + \frac{dw_1(y)}{dy} + \frac{\mathbf{A}^T}{R}\mathbf{v}(y), \quad (4.116a)$$

$$\mathbf{f}_z^T(z) = \left(\frac{d\mathbf{f}_y^T(z)}{dz} - \frac{\mathbf{A}^T}{R} \right) (\mathbf{H}_\gamma^{-1})^T \longrightarrow \frac{d\mathbf{f}_y(z)}{dz} = \mathbf{H}_\gamma\mathbf{f}_z(z) + \frac{\mathbf{A}}{R}. \quad (4.116b)$$

Where \mathbf{A} is a constant vector to be determined. According to [96], function $\mathbf{f}_z(z)$ may be expressed as follows:

$$\mathbf{H}_\gamma\mathbf{f}_z(z) = (z + R)\frac{d\mathbf{f}_s(z)}{dz} - \mathbf{f}_s(z) - R\mathbf{h}_Q. \quad (4.117)$$

Substituting (4.117) in (4.116b):

$$\frac{d\mathbf{f}_y(z)}{dz} = \frac{1}{R} \left((z + R)\frac{d\mathbf{f}_s(z)}{dz} - \mathbf{f}_s(z) - R\mathbf{h}_Q + \mathbf{A} \right). \quad (4.118)$$

Integrating equation (4.118), function $\mathbf{f}_y(z)$ yields:

$$\mathbf{f}_y(z) = \mathbf{f}_s(z) + \frac{1}{R} \left(\int z \frac{d\mathbf{f}_s(z)}{dz} dz - \int \mathbf{f}_s(z) dz + (\mathbf{A} - R\mathbf{h}_Q)z + \mathbf{B} \right), \quad (4.119)$$

where \mathbf{B} is an integration constant vector to be determined.

Using integration by parts over the first integral of equation (4.119) function $\mathbf{f}_y(z)$ yields:

$$\mathbf{f}_y(z) = \mathbf{f}_s(z) + \frac{1}{R} \left(z \mathbf{f}_s(z) - 2 \int \mathbf{f}_s(z) dz + (\mathbf{A} - R \mathbf{h}_Q) z + \mathbf{B} \right). \quad (4.120)$$

To simplify (4.120), it is necessary to define other shifted vector $\check{\mathbf{f}}_s(z)$ analogous to the previously defined vectors $\hat{\mathbf{f}}_s(z)$ and $\hat{\hat{\mathbf{f}}}_s(z)$ as follows:

$$\check{\mathbf{f}}_s^T(z) = [p_3(z) \quad p_4(z) \quad p_5(z) \quad \dots \quad p_{n+1}(z)]. \quad (4.121)$$

Vector $\check{\mathbf{f}}_s(z)$ accomplishes the following properties:

$$z \mathbf{f}_s(z) = \check{\Xi}_1 \check{\mathbf{f}}_s(z) + \check{\Xi}_2 \hat{\mathbf{f}}_s(z), \quad (4.122a)$$

$$\frac{d\check{\mathbf{f}}_s(z)}{dz} = \mathbf{H}_y \mathbf{f}_s(z) + 3\rho z + \check{\rho}, \quad (4.122b)$$

$$\mathbf{f}_s(z) = \Upsilon \check{\mathbf{f}}_s(z) + \frac{1}{2}(3z^2 - 1)\mathbf{v}, \quad (4.122c)$$

where matrices $\check{\Xi}_1$ and $\check{\Xi}_2$ are defined by their components $\check{\Xi}_{1,ij}$ and $\check{\Xi}_{2,ij}$ respectively as follows:

$$\check{\Xi}_{1,ij} = \frac{i+2}{2i+3} \delta_{ij}, \quad \check{\Xi}_{2,ij} = \frac{i+1}{2i+3} \delta_{ij}, \quad i, j = 1, 2, \dots, n-1, \quad (4.123)$$

and matrix \mathbf{H}_y and vector $\check{\rho}$ are defined as follows:

$$\check{\rho} = \begin{bmatrix} 1 \\ 0 \\ 1 \\ 0 \\ 1 \\ \dots \end{bmatrix}, \quad \mathbf{H}_y = \begin{bmatrix} 5 & 0 & 0 & 0 & 0 & \dots \\ 0 & 7 & 0 & 0 & 0 & \dots \\ 5 & 0 & 9 & 0 & 0 & \dots \\ 0 & 7 & 0 & 11 & 0 & \dots \\ 5 & 0 & 9 & 0 & 13 & \dots \\ \dots & \dots & \dots & \dots & \dots & \dots \end{bmatrix}. \quad (4.124)$$

The previous matrices and vectors may be obtained easily from those used in the bi-dimensional LPBM by using the following expressions:

$$\check{\Xi}_1 = (3\Xi_1 - \Xi_2)^{-1}(2\Xi_1 - \Xi_2), \quad \check{\Xi}_2 = (3\Xi_1 - \Xi_2)^{-1}\Xi_1, \quad (4.125a)$$

$$\check{\rho} = \Upsilon \rho + \mathbf{v}, \quad (4.125b)$$

$$\mathbf{H}_y = \mathbf{H}_\gamma(3\Xi_1 - \Xi_2). \quad (4.125c)$$

Furthermore, matrices \mathbf{H}_y , $\check{\check{\mathbf{E}}}_1$ and $\check{\check{\mathbf{E}}}_2$ accomplish the following relations:

$$\check{\check{\mathbf{E}}}_1 + \check{\check{\mathbf{E}}}_2 = \mathbf{I}, \quad (4.126a)$$

$$\mathbf{H}_y^{-1} = (\check{\check{\mathbf{E}}}_1 - \check{\check{\mathbf{E}}}_2)(\mathbf{I} - \Upsilon\Upsilon), \quad (4.126b)$$

$$\mathbf{H}_y^{-1}\boldsymbol{\rho} = (\check{\check{\mathbf{E}}}_1 - \check{\check{\mathbf{E}}}_2)\Upsilon\mathbf{v}. \quad (4.126c)$$

Therefore, by using the property (4.122b), the integral inside equation (4.120) yield:

$$\int \mathbf{f}_s(z)dz = \mathbf{H}_y^{-1} \left(\check{\check{\mathbf{f}}}_s(z) - 3\rho \frac{z^2}{2} - \check{\check{\rho}}z \right). \quad (4.127)$$

Substituting (4.122a) and (4.127) in (4.120), function $\mathbf{f}_y(z)$ can be written as:

$$\mathbf{f}_y(z) = \mathbf{f}_s(z) + \frac{1}{R} \left(\check{\check{\mathbf{E}}}_1 \check{\check{\mathbf{f}}}_s(z) + \check{\check{\mathbf{E}}}_2 \hat{\mathbf{f}}_s(z) - \mathbf{H}_y^{-1} (2\check{\check{\mathbf{f}}}_s(z) - 3\rho z^2 - 2\check{\check{\rho}}z) + (\mathbf{A} - R\mathbf{h}_Q)z + \mathbf{B} \right). \quad (4.128)$$

Substituting (4.126b) in (4.128) yields:

$$\mathbf{f}_y(z) = \mathbf{f}_s(z) + \frac{1}{R} \left((2\check{\check{\mathbf{E}}}_2 - \check{\check{\mathbf{E}}}_1) \check{\check{\mathbf{f}}}_s(z) + \check{\check{\mathbf{E}}}_2 \hat{\mathbf{f}}_s(z) + 2(\check{\check{\mathbf{E}}}_1 - \check{\check{\mathbf{E}}}_2)\Upsilon\Upsilon \check{\check{\mathbf{f}}}_s(z) + \mathbf{H}_y^{-1} (3\rho z^2 + 2\check{\check{\rho}}z) + (\mathbf{A} - R\mathbf{h}_Q)z + \mathbf{B} \right). \quad (4.129)$$

Substituting (3.108) in (4.122c) yields:

$$\Upsilon\Upsilon \check{\check{\mathbf{f}}}_s(z) = \hat{\mathbf{f}}_s(z) - \frac{1}{2}(3z^2 - 1)\Upsilon\mathbf{v} - \mathbf{v}z. \quad (4.130)$$

Substituting (4.130) in (4.129) and considering (4.126b) and (4.126c) yields:

$$\mathbf{f}_y(z) = \mathbf{f}_s(z) + \frac{1}{R} \left((2\check{\check{\mathbf{E}}}_2 - \check{\check{\mathbf{E}}}_1) \check{\check{\mathbf{f}}}_s(z) + (2\check{\check{\mathbf{E}}}_1 - \check{\check{\mathbf{E}}}_2) \hat{\mathbf{f}}_s(z) - (\check{\check{\mathbf{E}}}_1 - \check{\check{\mathbf{E}}}_2) (2\mathbf{v}z - \Upsilon\mathbf{v} - (\mathbf{I} - \Upsilon\Upsilon)2\check{\check{\rho}}z) + (\mathbf{A} - R\mathbf{h}_Q)z + \mathbf{B} \right). \quad (4.131)$$

Substituting (4.125b) in (4.131) and considering that $\Upsilon\check{\check{\rho}} = \rho$ yields:

$$\mathbf{f}_y(z) = \mathbf{f}_s(z) + \frac{1}{R} \left((2\check{\Xi}_2 - \check{\Xi}_1)\check{\mathbf{f}}_s(z) + (2\check{\Xi}_1 - \check{\Xi}_2)\hat{\mathbf{f}}_s(z) + (\check{\Xi}_1 - \check{\Xi}_2)\Upsilon\mathbf{v} + (\mathbf{A} - R\mathbf{h}_Q)z + \mathbf{B} \right). \quad (4.132)$$

Applying the condition of same value in $z = 1$ of the polynomials contained in vector $\mathbf{f}_y(z)$, vectors \mathbf{A} and \mathbf{B} yield:

$$\mathbf{A} = R\mathbf{h}_Q, \quad (4.133a)$$

$$\mathbf{B} = -(\check{\Xi}_1 - \check{\Xi}_2)\Upsilon\mathbf{v} = -\mathbf{H}_y^{-1}\boldsymbol{\rho}. \quad (4.133b)$$

Therefore, functions $\mathbf{f}_y(z)$ are obtained as:

$$\mathbf{f}_y(z) = \mathbf{f}_s(z) + \frac{1}{R} \left((2\check{\Xi}_2 - \check{\Xi}_1)\check{\mathbf{f}}_s(z) + (2\check{\Xi}_1 - \check{\Xi}_2)\hat{\mathbf{f}}_s(z) \right). \quad (4.134)$$

Consequently, the components $f_i^y(z)$, with $i = 2, 3, \dots, n$, of vector $\mathbf{f}_y(z)$ are defined as:

$$f_{i+1}^y(z) = p_{i+1}(z) + \frac{1}{R} \frac{ip_{i+2}(z) + (i+3)p_i(z)}{2i+3}. \quad (4.135)$$

The derivative of vector $\mathbf{f}_y(z)$, in accordance with equations (4.116b) and (4.133a), can be written as:

$$\frac{d\mathbf{f}_y(z)}{dz} = \mathbf{H}_\gamma \mathbf{f}_z(z) + \mathbf{h}_Q. \quad (4.136)$$

Strains

Substituting (4.113) in the strains equations (4.111) and considering the properties of the derivatives of the Legendre polynomials vectors exposed in Chapter 3, strain components can be written as:

$$\varepsilon_s(y, z) = \varepsilon_s^0 + \frac{R}{R+z} \left(e_N^s(y) + ze_M^s(y) + \mathbf{f}_s^T(z)\mathbf{e}_s(y) \right), \quad (4.137a)$$

$$\varepsilon_y(y, z) = e_N^y(y) + ze_M^y(y) + \mathbf{f}_y^T(z)\mathbf{e}_y(y), \quad (4.137b)$$

$$\gamma_{sy}(y, z) = \frac{R}{R+z}\gamma_{sy}^0 + e_N^{ys}(y) + ze_M^{ys}(y) + \mathbf{f}_s^T(z)\mathbf{e}_{ys}(y), \quad (4.137c)$$

$$\gamma_{yz}(y, z) = e_Q^{yz}(y) + \mathbf{f}_z^T(z)\mathbf{e}_{yz}(y), \quad (4.137d)$$

$$\gamma_{sz}(y, z) = \frac{R}{R+z} (e_Q^{sz}(y) + \mathbf{f}_z^T(z) \mathbf{e}_{sz}(y)), \quad (4.137e)$$

$$\varepsilon_z(y, z) = \frac{R+z}{R} \hat{\mathbf{f}}_s^T(z) \mathbf{e}_z(y), \quad (4.137f)$$

where $e_N^s(y)$, $e_M^s(y)$, $e_N^y(y)$, $e_M^y(y)$, $e_N^{ys}(y)$, $e_M^{ys}(y)$, $e_Q^{yz}(y)$ and $e_Q^{sz}(y)$ are the non-dimensional first-order 1D strain components, and $\mathbf{e}_s(y)$, $\mathbf{e}_y(y)$, $\mathbf{e}_{ys}(y)$, $\mathbf{e}_{yz}(y)$, $\mathbf{e}_{sz}(y)$ and $\mathbf{e}_z(y)$ are the non-dimensional higher-order 1D strain components, which are defined by:

$$e_N^s(y) = \frac{w_1(y)}{R} + \mathbf{h}_N^T \mathbf{w}(y), \quad e_M^s(y) = \mathbf{h}_M^T \mathbf{w}(y), \quad (4.138a)$$

$$\mathbf{e}_s(y) = \mathbf{H}_s^T \mathbf{w}(y), \quad (4.138b)$$

$$e_N^y(y) = \frac{dv_0(y)}{dy}, \quad e_M^y(y) = \frac{dv_1(y)}{dy}, \quad \mathbf{e}_y(y) = \frac{d\mathbf{v}(y)}{dy}, \quad (4.138c)$$

$$e_N^{ys}(y) = \frac{du_0(y)}{dy}, \quad e_M^{ys}(y) = \frac{du_1(y)}{dy}, \quad \mathbf{e}_{ys}(y) = \frac{d\mathbf{u}(y)}{dy}, \quad (4.138d)$$

$$e_Q^{yz}(y) = v_1(y) + \frac{dw_1(y)}{dy} + \mathbf{h}_Q^T \mathbf{v}(y), \quad \mathbf{e}_{yz}(y) = \mathbf{H}_\gamma^T \mathbf{v}(y) + \frac{d\mathbf{w}(y)}{dy}, \quad (4.138e)$$

$$e_Q^{sz}(y) = u_1(y) - \frac{u_0(y)}{R} + \mathbf{h}_Q^T \mathbf{u}(y), \quad \mathbf{e}_{sz}(y) = \mathbf{H}_\gamma^T \mathbf{u}(y), \quad (4.138f)$$

$$\mathbf{e}_z(y) = \mathbf{H}_z^T \mathbf{w}(y). \quad (4.138g)$$

Notice that the constant matrices \mathbf{H}_s , \mathbf{H}_γ and \mathbf{H}_z and vectors \mathbf{h}_N , \mathbf{h}_M and \mathbf{h}_Q are defined in Chapter 3 in the development of the LPBM (see (3.111), (3.125) and (3.128)). The curved case includes also the higher-order 1D strain component in the axial strain, $\mathbf{e}_s(y)$, which were not needed in the flat laminate.

Equilibrium

The forces and moments in a cylindrical shell for a general loading state are defined in [116, chap. 1], which are shown in equations (4.29). For the present case, in which forces and moments do not depend on the circumferential coordinate s , definition of forces and moments may be reduced as follows:

$$N_s(y) = \int_{-1}^1 \sigma_s(y, z) dz, \quad M_s(y) = \int_{-1}^1 \sigma_s(y, z) z dz, \quad (4.139a)$$

$$N_y(y) = \int_{-1}^1 \frac{z+R}{R} \sigma_y(y, z) dz, \quad M_y(y) = \int_{-1}^1 \frac{z+R}{R} \sigma_y(y, z) z dz, \quad (4.139b)$$

$$N_{ys}(y) = \int_{-1}^1 \frac{z+R}{R} \tau_{sy}(y, z) dz, \quad M_{ys}(y) = \int_{-1}^1 \frac{z+R}{R} \tau_{sy}(y, z) z dz, \quad (4.139c)$$

$$Q_s(y) = \int_{-1}^1 \tau_{sz}(y, z) dz, \quad Q_y(y) = \int_{-1}^1 \frac{z+R}{R} \tau_{yz}(y, z) dz. \quad (4.139d)$$

The higher-order moments are defined as follows:

$$\mathbf{M}_s(y) = \int_{-1}^1 \sigma_s(y, z) \mathbf{f}_s(z) dz, \quad (4.140a)$$

$$\mathbf{M}_y(y) = \int_{-1}^1 \frac{z+R}{R} \sigma_y(y, z) \mathbf{f}_y(z) dz, \quad (4.140b)$$

$$\mathbf{M}_{ys}(y) = \int_{-1}^1 \frac{z+R}{R} \tau_{sy}(y, z) \mathbf{f}_s(z) dz, \quad (4.140c)$$

$$\mathbf{M}_{sz}(y) = \int_{-1}^1 \tau_{sz}(y, z) \mathbf{f}_z(z) dz, \quad (4.140d)$$

$$\mathbf{M}_{yz}(y) = \int_{-1}^1 \frac{z+R}{R} \tau_{yz}(y, z) \mathbf{f}_z(z) dz, \quad (4.140e)$$

$$\mathbf{M}_z(y) = \int_{-1}^1 \left(\frac{z+R}{R} \right)^2 \sigma_z(y, z) \hat{\mathbf{f}}_s(z) dz. \quad (4.140f)$$

The 3D elasticity equilibrium equations for a cylindrical coordinate system, and considering the non-dependence of the stresses with s , are given by the following equations:

$$(z+R) \frac{\partial \tau_{sy}(y, z)}{\partial y} + \frac{1}{(z+R)} \frac{\partial}{\partial z} [(z+R)^2 \tau_{sz}(y, z)] = 0, \quad (4.141a)$$

$$(z+R) \frac{\partial \sigma_y(y, z)}{\partial y} + \frac{\partial}{\partial z} [(z+R) \tau_{yz}(y, z)] = 0, \quad (4.141b)$$

$$(z+R) \frac{\partial \tau_{yz}(y, z)}{\partial y} + \frac{\partial}{\partial z} [(z+R) \sigma_z(y, z)] = \sigma_s(y, z). \quad (4.141c)$$

The forces equilibrium equations are obtained by integrating equations (4.141) in the thickness and the first-order moment equilibrium equations are obtained by integrating equations (4.141a) and (4.141b) multiplied by z in the thickness. Null values of σ_z , τ_{sz} and τ_{yz} are prescribed in both thickness boundaries $z = \pm 1$.

$$R \frac{dN_{ys}(y)}{dy} + Q_s(y) = 0, \quad (4.142a)$$

$$\frac{dN_y(y)}{dy} = 0, \quad (4.142b)$$

$$R \frac{dQ_y(y)}{dy} = N_s(y), \quad (4.142c)$$

$$\frac{dM_{ys}(y)}{dy} = Q_s(y), \quad (4.142d)$$

$$\frac{dM_y(y)}{dy} = Q_y(y). \quad (4.142e)$$

Considering that the edges in the y direction are free and, therefore, considering null prescribed values of σ_y , τ_{sy} and τ_{yz} in the width boundaries ($y = 0$ and $y = W$), equation (4.79b) implies a null value of $N_y(y) = 0$. Furthermore, substituting (4.142d) in (4.142a) and considering also the boundary conditions in y , the following relation is obtained:

$$RN_{ys}(y) + M_{ys}(y) = 0. \quad (4.143)$$

Substituting (4.142e) in (4.142c) yields:

$$N_s(y) = R \frac{d^2 M_y(y)}{dy^2}. \quad (4.144)$$

The higher-order moments equilibrium equations are obtained integrating equations (4.78a) and (4.78b) multiplied by $\mathbf{f}_s(z)$ and integrating equation (4.78c) multiplied by $\hat{\mathbf{f}}_s(z)$, yielding:

$$\frac{d\mathbf{M}_{ys}(y)}{dy} = \mathbf{H}_\gamma \mathbf{M}_{sz}(y) + \mathbf{h}_Q Q_s(y), \quad (4.145a)$$

$$\frac{d\mathbf{M}_y(y)}{dy} = \mathbf{H}_\gamma \mathbf{M}_{yz}(y) + \mathbf{h}_Q Q_y(y), \quad (4.145b)$$

$$\frac{d\mathbf{M}_{yz}(y)}{dy} = \mathbf{H}_z \mathbf{M}_z(y) + \mathbf{H}_s \mathbf{M}_s(y) + \mathbf{h}_M M_s(y) + \mathbf{h}_N N_s(y). \quad (4.145c)$$

Constitutive law

The constitutive law of the plies is considered in the same way as in the development of the model of the flat laminate. Therefore, the constitutive law expressed in the (s, y, z) coordinate system is given by equation (4.81), including also the manufacturing process residual strains.

Using the three-dimensional constitutive law given in (4.81), the strains approximations given in (4.74) and the forces and moments definition given in (4.139) and (4.140), constitutive equations yield:

$$\begin{bmatrix} N_s(y) \\ M_s(y) \\ \mathbf{M}_s(y) \\ N_y(y) \\ M_y(y) \\ \mathbf{M}_y(y) \\ N_{ys}(y) \\ M_{ys}(y) \\ \mathbf{M}_{ys}(y) \\ M_z(y) \end{bmatrix} + \begin{bmatrix} N_s^\varepsilon \\ M_s^\varepsilon \\ \mathbf{M}_s^\varepsilon \\ N_y^\varepsilon \\ M_y^\varepsilon \\ \mathbf{M}_y^\varepsilon \\ N_{ys}^\varepsilon \\ M_{ys}^\varepsilon \\ \mathbf{M}_{ys}^\varepsilon \\ M_z^\varepsilon \end{bmatrix} = \mathbf{K}_\sigma \begin{bmatrix} e_N^s(y) \\ e_M^s(y) \\ \mathbf{e}_s(y) \\ e_N^y(y) \\ e_M^y(y) \\ \mathbf{e}_y(y) \\ e_N^{ys}(y) \\ e_M^{ys}(y) \\ \mathbf{e}_{ys}(y) \\ e_z(y) \end{bmatrix} + \mathbf{K}_{\varepsilon\gamma} \begin{bmatrix} \varepsilon_s^0 \\ \gamma_{sy}^0 \end{bmatrix}, \quad (4.146a)$$

$$\begin{bmatrix} Q_y(y) \\ \mathbf{M}_{yz}(y) \\ Q_s(y) \\ \mathbf{M}_{sz}(y) \end{bmatrix} = \mathbf{K}_\tau \begin{bmatrix} e_Q^{yz}(y) \\ \mathbf{e}_{yz}(y) \\ e_Q^{sz}(y) \\ \mathbf{e}_{sz}(y) \end{bmatrix}, \quad (4.146b)$$

where N_{ij}^ε , M_{ij}^ε and $\mathbf{M}_{ij}^\varepsilon$ are the residual forces, moments and higher-order moments due to the manufacturing process, \mathbf{K}_σ and \mathbf{K}_τ are respectively the normal and shear stiffness matrices of the model, and $\mathbf{K}_{\varepsilon\gamma}$ is the stiffness matrix associated to the mean line strains ε_s^0 and γ_{sy}^0 .

The components of the stiffness matrices \mathbf{K}_σ , \mathbf{K}_τ and $\mathbf{K}_{\varepsilon\gamma}$ are shown in Appendix B.3.

The residual forces, moments and higher-order moments due to the manufacturing process are calculated as follows:

$$N_s^\varepsilon = \sum_{p=1}^{N_p} (z_p^+ - z_p^-) \Delta\sigma_s^p, \quad M_s^\varepsilon = \sum_{p=1}^{N_p} \frac{1}{2} ((z_p^+)^2 - (z_p^-)^2) \Delta\sigma_s^p, \quad (4.147a)$$

$$N_y^\varepsilon = \sum_{p=1}^{N_p} \left(\Delta\sigma_y^p \int_{z_p^-}^{z_p^+} \frac{z+R}{R} dz \right), \quad M_y^\varepsilon = \sum_{p=1}^{N_p} \left(\Delta\sigma_y^p \int_{z_p^-}^{z_p^+} \frac{z+R}{R} z dz \right), \quad (4.147b)$$

$$N_{ys}^\varepsilon = \sum_{p=1}^{N_p} \left(\Delta\tau_{sy}^p \int_{z_p^-}^{z_p^+} \frac{z+R}{R} dz \right), \quad M_{ys}^\varepsilon = \sum_{p=1}^{N_p} \left(\Delta\tau_{sy}^p \int_{z_p^-}^{z_p^+} \frac{z+R}{R} z dz \right), \quad (4.147c)$$

$$M_s^\varepsilon = \sum_{p=1}^{N_p} \left(\Delta\sigma_s^p \int_{z_p^-}^{z_p^+} \mathbf{f}_s(z) dz \right), \quad (4.147d)$$

$$M_y^\varepsilon = \sum_{p=1}^{N_p} \left(\Delta\sigma_y^p \int_{z_p^-}^{z_p^+} \frac{z+R}{R} \mathbf{f}_y(z) dz \right), \quad (4.147e)$$

$$M_{ys}^\varepsilon = \sum_{p=1}^{N_p} \left(\Delta\tau_{sy}^p \int_{z_p^-}^{z_p^+} \frac{z+R}{R} \mathbf{f}_s(z) dz \right), \quad (4.147f)$$

$$M_z^\varepsilon = \sum_{p=1}^{N_p} \left(\Delta\sigma_z^p \int_{z_p^-}^{z_p^+} \left(\frac{z+R}{R} \right)^2 \hat{\mathbf{f}}_s(z) dz \right), \quad (4.147g)$$

where $\Delta\sigma_s^p$, $\Delta\sigma_y^p$, $\Delta\sigma_z^p$ and $\Delta\tau_{sy}^p$ are calculated from equations (4.84).

Equations (4.146a) and (4.146b) can be inverted yielding the following compliance equations:

$$\begin{bmatrix} e_N^s(y) \\ e_M^s(y) \\ \mathbf{e}_s(y) \\ e_N^y(y) \\ e_M^y(y) \\ \mathbf{e}_y(y) \\ e_N^{ys}(y) \\ e_M^{ys}(y) \\ \mathbf{e}_{ys}(y) \\ e_z(y) \end{bmatrix} = \check{\mathbf{K}}_\sigma \begin{bmatrix} N_s(y) \\ M_s(y) \\ \mathbf{M}_s(y) \\ N_y(y) \\ M_y(y) \\ \mathbf{M}_y(y) \\ N_{ys}(y) \\ M_{ys}(y) \\ \mathbf{M}_{ys}(y) \\ M_z(y) \end{bmatrix} - \check{\mathbf{k}}_\varepsilon + \check{\mathbf{K}}_{\varepsilon\gamma} \begin{bmatrix} \varepsilon_s^0 \\ \gamma_{sy}^0 \end{bmatrix}, \quad (4.148a)$$

$$\begin{bmatrix} e_Q^{yz}(y) \\ \mathbf{e}_{yz}(y) \\ e_Q^{sz}(y) \\ \mathbf{e}_{sz}(y) \end{bmatrix} = \check{\mathbf{K}}_\tau \begin{bmatrix} Q_y(y) \\ \mathbf{M}_{yz}(y) \\ Q_s(y) \\ \mathbf{M}_{sz}(y) \end{bmatrix}, \quad (4.148b)$$

where $\check{\mathbf{K}}_\sigma = (\mathbf{K}_\sigma)^{-1}$, $\check{\mathbf{K}}_{\varepsilon\gamma} = -(\mathbf{K}_\sigma)^{-1} \mathbf{K}_{\varepsilon\gamma}$ and $\check{\mathbf{K}}_\tau = \mathbf{K}_\tau^{-1}$. The components of matrices $\check{\mathbf{K}}_\sigma$, $\check{\mathbf{K}}_{\varepsilon\gamma}$ and $\check{\mathbf{K}}_\tau$ are denominated following the same rules used for defining the components of matrices \mathbf{K}_σ , $\mathbf{K}_{\varepsilon\gamma}$ and \mathbf{K}_τ respectively. Therefore, expressions shown in Appendix B.3 for the components

of \mathbf{K}_σ , $\mathbf{K}_{\varepsilon\gamma}$ and \mathbf{K}_τ can be used for calculating $\check{\mathbf{K}}_\sigma$, $\check{\mathbf{K}}_{\varepsilon\gamma}$ and $\check{\mathbf{K}}_\tau$. The matrix $\check{\mathbf{k}}_\varepsilon$ is defined as follows:

$$\check{\mathbf{k}}_\varepsilon = \begin{bmatrix} \check{k}_1^\varepsilon \\ \check{k}_2^\varepsilon \\ \check{\mathbf{k}}_3^\varepsilon \\ \check{k}_4^\varepsilon \\ \check{k}_5^\varepsilon \\ \check{\mathbf{k}}_6^\varepsilon \\ \check{k}_7^\varepsilon \\ \check{k}_8^\varepsilon \\ \check{\mathbf{k}}_9^\varepsilon \\ \check{k}_z^\varepsilon \end{bmatrix} = \check{\mathbf{K}}_\sigma \begin{bmatrix} N_s^\varepsilon \\ M_s^\varepsilon \\ \mathbf{M}_s^\varepsilon \\ N_y^\varepsilon \\ M_y^\varepsilon \\ \mathbf{M}_y^\varepsilon \\ N_{ys}^\varepsilon \\ M_{ys}^\varepsilon \\ \mathbf{M}_{ys}^\varepsilon \\ M_z^\varepsilon \end{bmatrix}. \quad (4.149)$$

Solution procedure

The solution is obtained by solving jointly the strain-displacements equations, the constitutive law and the equilibrium equations. Deriving equation (4.148b) and introducing equations (4.142a), (4.142e), (4.145a), (4.145b), (4.138e) and (4.138f) the shear compliance equations yield:

$$\begin{bmatrix} \frac{dv_1(y)}{dy} + \frac{d^2w_1(y)}{dy^2} + \mathbf{h}_Q^T \frac{d\mathbf{v}(y)}{dy} \\ \mathbf{H}_\gamma^T \frac{d\mathbf{v}(y)}{dy} + \frac{d^2\mathbf{w}(y)}{dy^2} \\ \frac{du_1(y)}{dy} - \frac{1}{R} \frac{du_0(y)}{dy} + \mathbf{h}_Q^T \frac{d\mathbf{u}(y)}{dy} \\ \mathbf{H}_\gamma^T \frac{d\mathbf{u}(y)}{dy} \end{bmatrix} = \check{\mathbf{K}}_\tau \begin{bmatrix} \frac{d^2M_y(y)}{dy^2} \\ \mathbf{H}_\gamma^{-1} \left(\frac{d^2M_y(y)}{dy^2} - \mathbf{h}_Q \frac{d^2M_y(y)}{dy^2} \right) \\ \frac{d^2M_{ys}(y)}{dy^2} \\ \mathbf{H}_\gamma^{-1} \left(\frac{d^2M_{ys}(y)}{dy^2} - \mathbf{h}_Q \frac{d^2M_{ys}(y)}{dy^2} \right) \end{bmatrix}. \quad (4.150)$$

Therefore, the in-plane displacements components may be obtained from equation (4.150) as follows:

$$\begin{aligned} \frac{dv_1(y)}{dy} = & H_{00}^Q \frac{d^2M_y(y)}{dy^2} + \mathbf{H}_{01}^Q \frac{d^2\mathbf{M}_y(y)}{dy^2} + H_{02}^Q \frac{d^2M_{ys}(y)}{dy^2} + \\ & \mathbf{H}_{03}^Q \frac{d^2\mathbf{M}_{ys}(y)}{dy^2} - \frac{d^2w_1(y)}{dy^2} + \mathbf{h}_Q^T (\mathbf{H}_\gamma^T)^{-1} \frac{d^2\mathbf{w}(y)}{dy^2}, \end{aligned} \quad (4.151a)$$

$$\begin{aligned} \frac{d\mathbf{v}(y)}{dy} = & \mathbf{H}_{10}^Q \frac{d^2M_y(y)}{dy^2} + \mathbf{H}_{11}^Q \frac{d^2\mathbf{M}_y(y)}{dy^2} + \mathbf{H}_{12}^Q \frac{d^2M_{ys}(y)}{dy^2} + \\ & \mathbf{H}_{13}^Q \frac{d^2\mathbf{M}_{ys}(y)}{dy^2} - (\mathbf{H}_\gamma^T)^{-1} \frac{d^2\mathbf{w}(y)}{dy^2}, \end{aligned} \quad (4.151b)$$

$$\frac{du_1(y)}{dy} - \frac{1}{R} \frac{du_0(y)}{dy} = H_{20}^Q \frac{d^2 M_y(y)}{dy^2} + \mathbf{H}_{21}^Q \frac{d^2 \mathbf{M}_y(y)}{dy^2} + H_{22}^Q \frac{d^2 M_{ys}(y)}{dy^2} + \mathbf{H}_{23}^Q \frac{d^2 \mathbf{M}_{ys}(y)}{dy^2}, \quad (4.151c)$$

$$\frac{d\mathbf{u}(y)}{dy} = \mathbf{H}_{30}^Q \frac{d^2 M_y(y)}{dy^2} + \mathbf{H}_{31}^Q \frac{d^2 \mathbf{M}_y(y)}{dy^2} + \mathbf{H}_{32}^Q \frac{d^2 M_{ys}(y)}{dy^2} + \mathbf{H}_{33}^Q \frac{d^2 \mathbf{M}_{ys}(y)}{dy^2}, \quad (4.151d)$$

where the auxiliary matrices are defined in Appendix B.4.

Substituting the equilibrium equations (4.142), (4.143), (4.144) and (4.145), taking into account the null value of $N_y(y) = 0$ and the strain components definition (4.138) in equation (4.148a), the compliance equations yield:

$$\begin{bmatrix} \frac{w_1(y)}{R} + \mathbf{h}_N^T \mathbf{w}(y) \\ \mathbf{h}_M^T \mathbf{w}(y) \\ \mathbf{H}_s^T \mathbf{w}(y) \\ \frac{dv_0(y)}{dy} \\ \frac{dv_1(y)}{dy} \\ \frac{d\mathbf{v}(y)}{dy} \\ \frac{du_0(y)}{dy} \\ \frac{du_1(y)}{dy} \\ \frac{d\mathbf{u}(y)}{dy} \\ \mathbf{H}_z^T \mathbf{w}(y) \end{bmatrix} = \check{\mathbf{K}}_A \begin{bmatrix} M_s(y) \\ \mathbf{M}_s(y) \\ \frac{d^2 M_y(y)}{dy^2} \\ M_y(y) \\ \frac{d^2 \mathbf{M}_y(y)}{dy^2} \\ \mathbf{M}_y(y) \\ M_{ys}(y) \\ \mathbf{M}_{ys}(y) \end{bmatrix} - \check{\mathbf{k}}_\varepsilon + \check{\mathbf{K}}_{\varepsilon\gamma} \begin{bmatrix} \varepsilon_s^0 \\ \gamma_{sy}^0 \end{bmatrix}, \quad (4.152)$$

where the matrix $\check{\mathbf{K}}_A$ is defined in Appendix B.4.

The system of equations (4.152) can be rearranged and expressed as follows, in order to obtain the axial bending and higher-order moments:

$$\begin{bmatrix} M_s(y) \\ \mathbf{M}_s(y) \end{bmatrix} = \check{\mathbf{K}}_B \begin{bmatrix} \frac{d^2 M_y(y)}{dy^2} \\ M_y(y) \\ \frac{d^2 \mathbf{M}_y(y)}{dy^2} \\ \mathbf{M}_y(y) \\ M_{ys}(y) \\ \mathbf{M}_{ys}(y) \\ \mathbf{w}(y) \end{bmatrix} + \check{\mathbf{K}}_C \begin{bmatrix} \varepsilon_s^0 \\ \gamma_{sy}^0 \end{bmatrix} + \check{\mathbf{K}}_D, \quad (4.153)$$

where the matrices $\check{\mathbf{K}}_B$ and $\check{\mathbf{K}}_C$ and the vector $\check{\mathbf{K}}_D$ are defined in Appendix B.4.

Substituting (4.153) and (4.151) in (4.152) the following system of differential equations is obtained:

$$\frac{d^2 \mathbf{x}(y)}{dy^2} = \mathbf{G} \mathbf{x}(y) + \mathbf{G}_c \mathbf{v}(y) + \mathbf{g}_\varepsilon, \quad (4.154a)$$

$$\mathbf{x}(y) = \begin{bmatrix} M_y(y) \\ \mathbf{M}_y(y) \\ M_{ys}(y) \\ \mathbf{M}_{ys}(y) \\ w_1(y) \\ \mathbf{w}(y) \end{bmatrix}, \quad \mathbf{v}(y) = \begin{bmatrix} \varepsilon_s^0 \\ \gamma_{sy}^0 \end{bmatrix}, \quad (4.154b)$$

where matrices \mathbf{G} and \mathbf{G}_c and vector \mathbf{g}_ε are defined in Appendix B.4.

As in the flat laminate case, the system of differential equations (4.154a) may be solved by obtaining a particular solution (the regularized solution) and the solution of the homogeneous equation. The regularized solution yields:

$$\mathbf{x}_{reg}(y) = -\mathbf{G}^{-1} \mathbf{G}_c \mathbf{v}(y) - \mathbf{G}^{-1} \mathbf{G}_\varepsilon. \quad (4.155)$$

Non-regularized stresses and strains are determined by the superposition of their regularized values, given by equation (4.155), and the perturbations, calculated from the homogeneous equation. The homogeneous equation is determined by separating the solution vector, $\mathbf{x}(y)$, into its regularized value, $\mathbf{x}_{reg}(y)$, and the perturbation, $\hat{\mathbf{x}}(y)$. Therefore, the homogeneous equation is obtained by doing the variable change $\mathbf{x}(y) = \mathbf{x}_{reg}(y) + \hat{\mathbf{x}}(y)$, and the equation yields:

$$\frac{d^2 \hat{\mathbf{x}}(y)}{dy^2} = \mathbf{G} \hat{\mathbf{x}}(y). \quad (4.156)$$

Equation (4.156) is solved as an eigenvalue problem, as in the flat laminate case, and imposing the boundary conditions of the free edge $M_y(y) = 0$, $\mathbf{M}_y(y) = 0$, $M_{ys}(y) = 0$, $\mathbf{M}_{ys}(y) = 0$, $Q_y(y) = 0$ and $\mathbf{M}_{yz}(y) = 0$ in $y = 0$ and $y = W$.

Stresses calculation

With a similar procedure to that made in the flat laminate case, once the vector $\mathbf{x}(y)$ given in (4.154b) has been calculated, the moments and higher order moments $M_y(y)$, $M_{ys}(y)$, $\mathbf{M}_y(y)$ and $\mathbf{M}_{ys}(y)$ are directly obtained as

the corresponding components of $\mathbf{x}(y)$. Shear higher-order moments and transverse higher-order moments are obtained from the equilibrium equations (4.145), and the axial higher-order moments are obtained from equation (4.153). Strains may be obtained by using the compliance equations (4.148). However, in the present procedure, compliance equations (4.152) (considering the strain components definition (4.138)) are used instead of equations (4.148). Once strains are obtained, the axial, transverse and in-plane shear stresses are calculated for each ply by using the 3D constitutive equations (4.81):

$$\sigma_s^p(y, z) = \mathbf{S}_s^p(z)^T \left(\check{\mathbf{K}}_\sigma^A \mathbf{M}_T(y) - \check{\mathbf{k}}_\varepsilon + \check{\mathbf{K}}_{\varepsilon\gamma} \begin{bmatrix} \varepsilon_s^0 \\ \gamma_{sy}^0 \end{bmatrix} \right) + Q_{11}^p \varepsilon_s^0 + Q_{16}^p \frac{R}{R+z} \gamma_{sy}^0, \quad (4.157a)$$

$$\sigma_y^p(y, z) = \mathbf{S}_y^p(z)^T \left(\check{\mathbf{K}}_\sigma^A \mathbf{M}_T(y) - \check{\mathbf{k}}_\varepsilon + \check{\mathbf{K}}_{\varepsilon\gamma} \begin{bmatrix} \varepsilon_s^0 \\ \gamma_{sy}^0 \end{bmatrix} \right) + Q_{12}^p \varepsilon_s^0 + Q_{26}^p \frac{R}{R+z} \gamma_{sy}^0, \quad (4.157b)$$

$$\tau_{sy}^p(y, z) = \mathbf{S}_{sy}^p(z)^T \left(\check{\mathbf{K}}_\sigma^A \mathbf{M}_T(y) - \check{\mathbf{k}}_\varepsilon + \check{\mathbf{K}}_{\varepsilon\gamma} \begin{bmatrix} \varepsilon_s^0 \\ \gamma_{sy}^0 \end{bmatrix} \right) + Q_{16}^p \varepsilon_s^0 + Q_{66}^p \frac{R}{R+z} \gamma_{sy}^0, \quad (4.157c)$$

where the vector $\mathbf{M}_T(y)$ is defined as follows:

$$\mathbf{M}_T(y) = \begin{bmatrix} M_s(y) \\ \mathbf{M}_s(y) \\ \frac{d^2 M_y(y)}{dy^2} \\ M_y(y) \\ \frac{d^2 M_{ys}(y)}{dy^2} \\ \mathbf{M}_y(y) \\ M_{ys}(y) \\ \mathbf{M}_{ys}(y) \end{bmatrix}, \quad (4.158)$$

and the shape vectors $\mathbf{S}_s^p(z)$, $\mathbf{S}_y^p(z)$ and $\mathbf{S}_{sy}^p(z)$, defined by their components $(\mathbf{S}_s^p)_i(z)$, $(\mathbf{S}_y^p)_i(z)$ and $(\mathbf{S}_{sy}^p)_i(z)$ respectively for $i = 0, 1, \dots, 4n + 1$, are given by:

$$\left(\mathbf{S}_s^p\right)_i(z) = Q_{11}^p \frac{R}{R+z} p_i(z), \quad \left(\mathbf{S}_s^p\right)_{i+n+1}(z) = Q_{12}^p f_i^y(z), \quad i = 0, 1, \dots, n, \quad (4.159a)$$

$$\left(\mathbf{S}_s^p\right)_{i+2n+2}(z) = Q_{16}^p p_i(z), \quad i = 0, 1, \dots, n, \quad (4.159b)$$

$$\left(\mathbf{S}_s^p\right)_{i+3n+1}(z) = Q_{13}^p \frac{R+z}{R} p_{i-2}(z), \quad i = 2, 3, \dots, n, \quad (4.159c)$$

$$\left(\mathbf{S}_y^p\right)_i(z) = Q_{12}^p \frac{R}{R+z} p_i(z), \quad \left(\mathbf{S}_y^p\right)_{i+n+1}(z) = Q_{22}^p f_i^y(z), \quad i = 0, 1, \dots, n, \quad (4.159d)$$

$$\left(\mathbf{S}_y^p\right)_{i+2n+2}(z) = Q_{26}^p p_i(z), \quad i = 0, 1, \dots, n, \quad (4.159e)$$

$$\left(\mathbf{S}_y^p\right)_{i+3n+1}(z) = Q_{23}^p \frac{R+z}{R} p_{i-2}(z), \quad i = 2, 3, \dots, n, \quad (4.159f)$$

$$\left(\mathbf{S}_{sy}^p\right)_i(z) = Q_{16}^p \frac{R}{R+z} p_i(z), \quad \left(\mathbf{S}_{sy}^p\right)_{i+n+1}(z) = Q_{26}^p f_i^y(z), \quad i = 0, 1, \dots, n, \quad (4.159g)$$

$$\left(\mathbf{S}_{sy}^p\right)_{i+2n+2}(z) = Q_{66}^p p_i(z), \quad i = 0, 1, \dots, n, \quad (4.159h)$$

$$\left(\mathbf{S}_{sy}^p\right)_{i+3n+1}(z) = Q_{36}^p \frac{R+z}{R} p_{i-2}(z), \quad i = 2, 3, \dots, n. \quad (4.159i)$$

Finally, the out-of-plane shear and through-thickness stresses are obtained by integration of the equilibrium equations (4.141):

$$\tau_{sz}^p(y, z) = \tau_{sz}^p(y, z_p^-) \left(\frac{R+z_p^-}{R+z} \right)^2 - \mathbf{S}_{sz}^p(z)^T \tilde{\mathbf{K}}_\sigma^A \frac{d\mathbf{M}_T(y)}{dy}, \quad (4.160a)$$

$$\tau_{yz}^p(y, z) = \tau_{yz}^p(y, z_p^-) \frac{R+z_p^-}{R+z} - \mathbf{S}_{yz}^p(z)^T \tilde{\mathbf{K}}_\sigma^A \frac{d\mathbf{M}_T(y)}{dy}, \quad (4.160b)$$

$$\begin{aligned} \sigma_z^p(y, z) &= \sigma_z^p(y, z_p^-) \frac{R+z_p^-}{R+z} - \frac{d\tau_{sz}^p(y, z_p^-)}{dy} (z-z_p^-) \frac{R+z_p^-}{R+z} + \\ &\mathbf{S}_{z,1}^p(z)^T \left(\tilde{\mathbf{K}}_\sigma^A \mathbf{M}_T(y) - \check{\mathbf{k}}_\varepsilon + \tilde{\mathbf{K}}_{\varepsilon\gamma} \begin{bmatrix} \varepsilon_s^0 \\ \gamma_{sy}^0 \end{bmatrix} \right) + Q_{11}^p \varepsilon_s^0 (z-z_p^-) + \\ &Q_{16}^p \gamma_{sy}^0 \frac{R}{R+z} \log \left(\frac{R+z}{R+z_p^-} \right) + \mathbf{S}_{z,2}^p(z)^T \tilde{\mathbf{K}}_\sigma^A \frac{d^2 \mathbf{M}_T(y)}{dy^2}, \end{aligned} \quad (4.160c)$$

and the shape vectors:

$$\mathbf{S}_{sz}^p(z) = \frac{1}{(z+R)^2} \int_{z_p^-}^z (z+R)^2 \mathbf{S}_{sy}^p(z') dz', \quad (4.161a)$$

$$\mathbf{S}_{yz}^p(z) = \frac{1}{z+R} \int_{z_p^-}^z (z+R) \mathbf{S}_y^p(z') dz', \quad (4.161b)$$

$$\mathbf{S}_{z,1}^p(z) = \frac{1}{z+R} \int_{z_p^-}^z \mathbf{S}_s^p(z') dz'. \quad (4.161c)$$

$$\mathbf{S}_{z,2}^p(z) = \frac{1}{z+R} \int_{z_p^-}^z (z+R) \mathbf{S}_{yz}^p(z') dz'. \quad (4.161d)$$

Out-of-plane shear and through-thickness stresses have to be calculated recursively ply-by-ply as in the MBM and the LPBM, starting with the boundary conditions $\tau_{sz}^1(y, -1) = \tau_{yz}^1(y, -1) = \sigma_z^1(y, -1) = 0$. In the successive layers, continuity with the previous layers is imposed. The boundary conditions $\tau_{sz}^{N_p}(y, 1) = \tau_{yz}^{N_p}(y, 1) = \sigma_z^{N_p}(y, 1) = 0$ are automatically accomplished.

Loads application

The solution of the model and the stresses have been developed depending on the mean line strains ε_s^0 and γ_{sy}^0 . However, the inputs of the problem are usually the loads applied to the laminate, which are given as a bending moment M_0 and an in-plane shear force P_0 . These loads are obtained by integrating in the width the corresponding distributed forces and moments as follows:

$$M_0 = \int_0^W M_s(y) dy, \quad (4.162a)$$

$$P_0 = \int_0^W N_{sy}(y) dy, \quad (4.162b)$$

where the force $N_{sy}(y)$ is defined as follows:

$$N_{sy}(y) = \int_{-1}^1 \tau_{sy}(y, z) dz. \quad (4.163)$$

4.5 Applications of the 3D non-regularized models

The three-dimensional non-regularized models developed in section 4.4 are an expansion of the LPBM to analyse some three-dimensional effects in the problem under study but reduced to a s non-dependant model. For this reason, only s -regularized problems under a bending moment M_0 or a shear in-plane load P_0 may be calculated. Notwithstanding, the applications of these novel models let us to calculate the non-regularized effects given in the y direction.

First, in the curved laminates, the 3D non regularized model let us to calculate the effect of the finite width, which introduces non-regularized effects due to the curvature. The curvature prevents the free deformation of the laminate due to the anticlastic effect, introducing a through-the-width bending moment $M_y(y)$. However, this bending moment $M_y(y)$ has to vanish along the free boundaries at the width ends, so non-regularized effects are introduced near to these free boundaries in order to accomplish the boundary condition. These non-regularized effects affect also to the bending moment distribution in the width $M_s(y)$ due to M_0 . This distribution is usually considered uniform with a value $M_s(y) = M_0/W$. However, the non-regularized effects change the distribution inducing a maximum of the regularized bending moment higher than M_0/W , and causing the calculation of the unfolding failure by considering the constant distribution assumption to become non conservative.

Another effect which may be calculated with the present non-regularized models is the free-edge effect. The residual stresses and the through-the-width stresses due to the loads have to accomplish the stress-free boundary conditions along the boundaries in the width ends, causing also non-regularized effects traditionally known as free-edge effects.

Finally, other three-dimensional effects which have already been obtained by the regularized solution given in section 4.1 may be obtained also with the present model, such as the torsion of the laminate or the manufacturing process residual stresses (which now may be obtained also including the free-edge effects). These effects are not shown in the present section as they have been studied previously and they are associated to the regularized 3D stress distribution.

4.5.1 Through-the-width distributions

The curvature constrains the free deformation of a curved laminate due to the anticlastic effect, introducing a through-the-width moment $M_y(y)$.

The null boundary conditions of this moment along the free-edge induce non-regularized effects which affect also to the other stresses.

As a numerical example, laminates with the material properties of Table 4.1, a ply thickness of 0.2 mm, a mean radius $R = t$ and a width $W = 10t$ are considered loaded under a bending moment M_0 . The stacking sequences considered are $[45,-45,90,0]_S$ and $[45,0,-45,90]_S$.

The distributed axial moment (bending moment) and force depending on the y coordinate are depicted in Figure 4.15 for both laminates by using the present non-regularized model with $n = 50$ and compared with the regularized values.

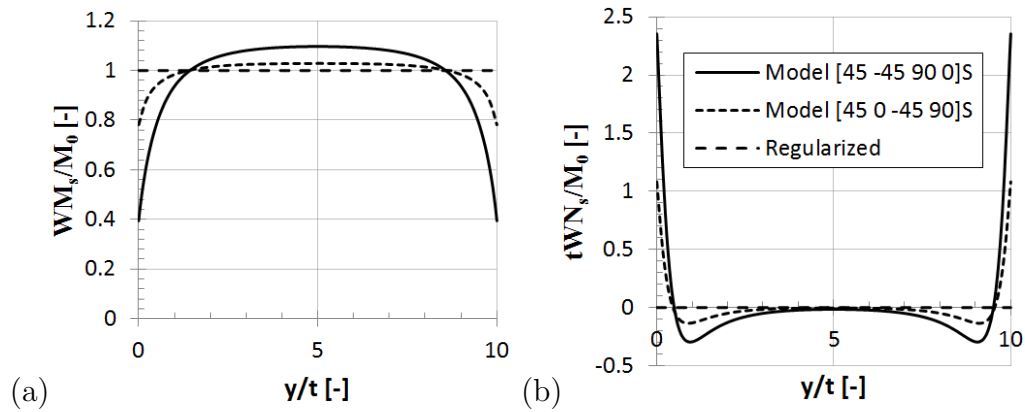


Figure 4.15: Distributed forces and moments distribution through the width: (a) bending moment $M_s(y)$, (b) axial force $N_s(y)$.

The regularized value of $N_s(y)$ is a null value, as no axial force is applied. The regularized value of the bending moment is M_0/W . Both regularized values coincide with their respective mean values of the non-regularized distribution along the width.

Notice that a non uniform distribution of the bending moment $M_s(y)$ is obtained, due to the non-regularized effects, causing that the maximum is higher than the average value given by a regularized model. In particular, for the laminate $[45,-45,90,0]_S$ the maximum of the bending moment is a 10% higher than the one predicted by a regularized model. The laminate $[45,0,-45,90]_S$ presents a similar distribution but the maximum value is closer to the regularized value. If the width is increased, as the mean value of the distribution is the regularized value and the regularization distance does not depend on the width, the maximum non-regularized value tends to the regularized value.

The distributed axial force $N_s(y)$ tends to the regularized null value in

the center of the specimen, reaching its maximum value at the free ends. The maximum value is higher in the $[45,-45,90,0]_s$ stacking sequence than in the $[45,0,-45,90]_s$ stacking sequence.

The distributed anticlastic bending moment and torsional moment depending on the y coordinate are depicted in Figure 4.16 for both laminates by using the present non-regularized model with $n = 50$ and compared with their respective regularized values. In this case the regularized values are different for each stacking sequence.

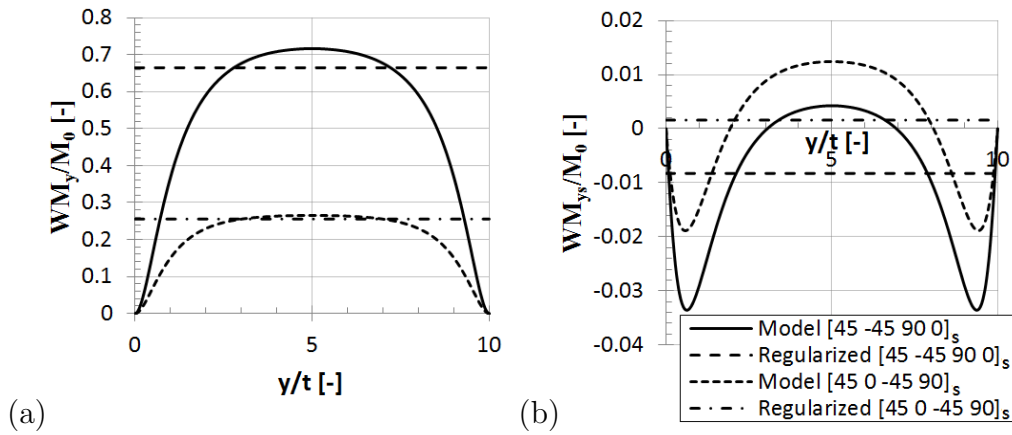


Figure 4.16: Distributed forces and moments distribution through the width: (a) anticlastic bending moment $M_y(y)$, (b) torsional moment $M_{y_s}(y)$.

The anticlastic bending moment $M_y(y)$ has a similar distribution to that of the axial bending moment $M_s(y)$ but with null values at the free edges. The moment tend to the regularized value far enough from the free edge. As can be seen in Figure 4.16b, the torsional moment distribution is significantly deviated from its regularized value. Notwithstanding, its mean value is equal to the regularized value.

The finite width effect is given also in flat laminates. However, the distributions in a flat laminate are less pronounced than in the curved laminate when a bending moment load is applied, not being included here for the sake of brevity.

4.5.2 Free-edge effects

The free-edge effects are given for any kind of geometry near the free edges of a composite laminate. Due to the different properties in the different directions of the plies and to the stacking sequence with plies in different

directions, the compatibility and equilibrium in the free edges implies a stress concentration with theoretically infinite stresses.

The non-regularized model developed in section 4.4 is based in polynomials, so it cannot predict infinite stresses. However, it can predict the tendency of the stresses within a high enough model order.

The free-edge effects are analysed first as a numerical example in a flat laminate with a cross-ply laminate $[0,90]_S$, where the shape of the stress distribution has been extensively studied and approximated in the literature (see Mittelstedt and Becker [68]). Considering the ply properties of table 4.1, a width $W = 10t$ and an axial load per unit of width N_0 in the s direction, the INS obtained in the interface between a 0° and a 90° ply is depicted in Figure 4.17. The stress distribution has been obtained by using the non-regularized model with $n = 50$.

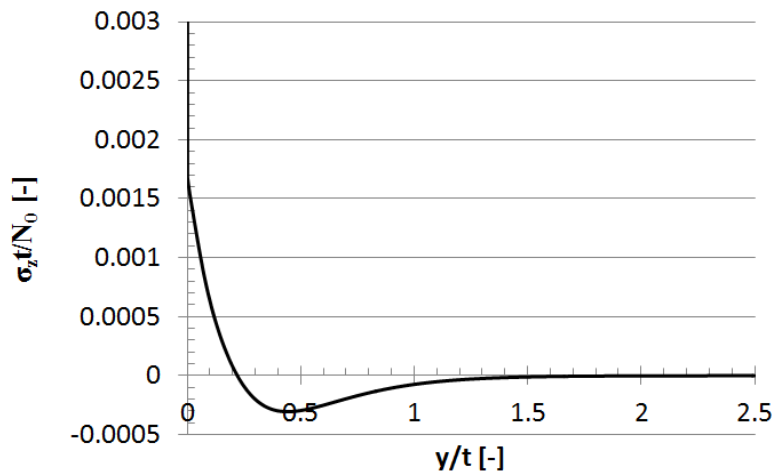


Figure 4.17: INS obtained in the interface between a 0° and a 90° ply in a laminate $[0,90]_S$ under axial load.

A INS distribution in the interface similar to the one obtained by other authors, such as Pagano [65], is obtained. The infinite theoretical value of the INS at the free edge is not obtained as in the other aforementioned approximations. By using different order the zone nearer to the free edge is better approximated obtaining more accurate values closer to the free edge, as is seen in Figure 4.18.

Far from the edge, when the model order increases, the solution converges. However, at the zone very close to the free-edge a very slow and not clear convergence is obtained. Therefore, the model cannot be used for estimating the stresses just in the free-edge, but the distance from the free

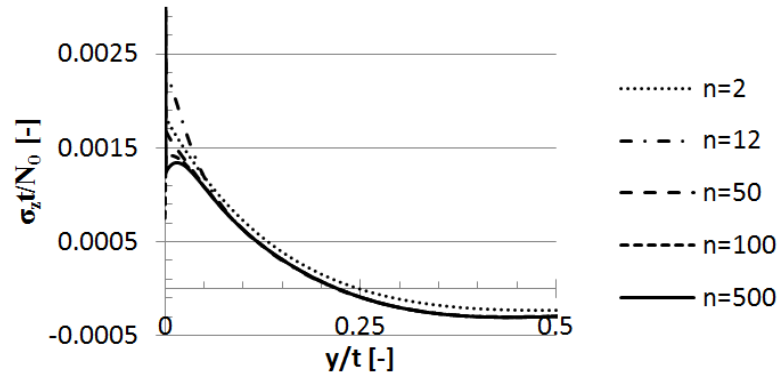


Figure 4.18: INS obtained in the interface between a 0° and a 90° ply for different model orders.

edge where stresses are obtained in an accurate way is reduced by increasing the model order (similarly than the LPBM and the MBM do not predict accurately the stresses just in a change of curvature, but predict accurately the stresses very close to it).

Figure 4.19 shows the ISS obtained along the interface by using the non-regularized model with $n = 500$.

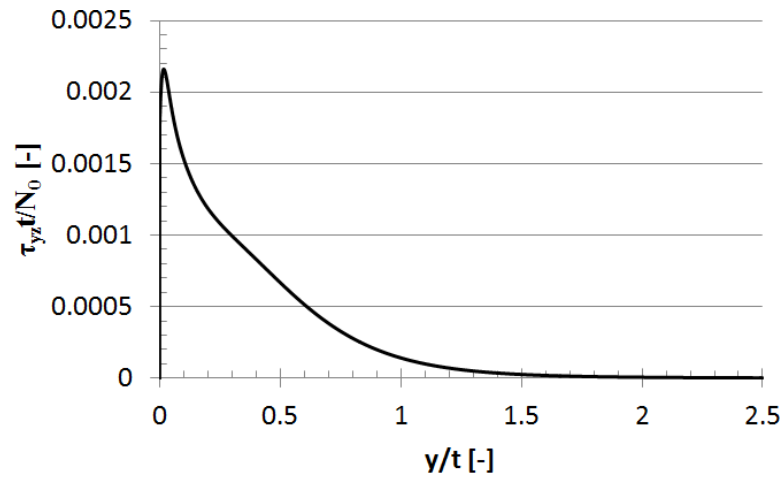


Figure 4.19: ISS obtained in the interface between a 0° and a 90° ply in a laminate $[0,90]_S$ under axial load.

The distribution of the ISS shows that the solution converge to a finite value of the ISS just at the free-edge, due to the infinite value of the INS. The present solution has the maximum value close to the free edge and not

just at the free edge, but doing a sensibility analysis it is observed that the maximum value gets closer to the free edge when the order increases.

Chapter 5

Failure mechanisms involved in the unfolding failure

The unfolding failure has been traditionally associated to the INS, considering that when the maximum INS in the thickness reach the ILTS, a crack is initiated interlaminarly and it is propagated by the INS causing the delamination. The ILTS is typically obtained by using a four-point bending test [3]. However, when applying this testing procedure to a L-shaped composite laminate, the maximum INS calculated, i.e., the apparent ILTS, has a thickness dependence similar to that depicted in Figure 1.2, where a typical distribution of the apparent ILTS with the thickness is shown. This thickness dependence is shown, for example, by Edwards and Thompson [6].

However, the thickness dependence is not generally given in fabric composites as can be seen in the experimental results of Avalon and Donaldson [8], and it is neither observed in unidirectional laminates $[0]_n$, as can be seen in the unidirectional specimens of Hoffmann et al. [7].

Airbus Operations S.L. has provided some experimental results which are used in the present Chapter for the validation of the models developed in the PhD project. The INS calculated for the aforementioned experimental results using the analysis tools existing prior to this Thesis presents the thickness dependence which is found in the literature and which has not been explained yet.

This Chapter explains first the bases of a new idea for giving an explanation to this thickness dependence by introducing a new failure mechanism, which has been denominatated induced unfolding. This new idea assumes that an intralaminar failure may induce defects in the interlaminar direction which propagate as a delamination with the presence of the INS. The classical failure mechanism has been denominatated traditional unfolding in order to distinguish from the new mechanism. After introducing the bases

of the new failure mechanism, the experimental results provided by Airbus Operations S.L. are used to show evidences of the existence of the induced unfolding. These evidences are divided in two groups. First, stresses are accurately calculated using the non-regularized model developed in Chapter 4 showing that intralaminar failures may take place at the loads in which the delamination is produced. Second, the delamination locations in the thickness is estimated by considering the traditional and the induced unfolding, observing that the locations of the delaminations agree in a much higher percentage with those predicted by the induced unfolding.

This new failure mechanism has supposed an important change in the understanding of the unfolding failure and consequently requires a deeper research. Therefore, this Chapter lays the background for a future development of a failure criterion which may include this new concept, requiring a wider experimental and numerical analysis.

5.1 The concept of the induced unfolding failure mechanism

The idea of the induced unfolding lays in an intralaminar failure which introduces defects or cracks that propagates interlaminarly due to the presence of a high INS. This effect has been showed in similar problems in the literature. Roos [117] observed in his PhD Thesis interlaminar cracks in Ω -specimens which have been initiated by a matrix failure, and H el enon et al. [76] observed a similar delamination in T-specimens. Notwithstanding, these authors obtained an initial intralaminar failure which was dominated by an ISS, so the initial intralaminar defect was not perpendicular to the interface between plies and the interlaminar propagation is more evident. For those cases, where the matrix failure has an initial failure which is not perpendicular to the interfaces between plies causing the delamination, the Wisnom delamination criterion [75] is of special interest. This criterion considers the stresses in the matrix in all the directions by calculating an effective stress, where the fibre direction stress is obtained by factoring down the composite stress by the ratio of matrix modulus to the fibre direction modulus.

Notwithstanding, the present idea of induced unfolding establishes that the delamination may be produced also when the intralaminar crack is perpendicular to the interface. Bl azquez et al. [118] and Par is et al. [119, 120] studied the propagation of an intralaminar matrix crack in a flat laminate due to a tensile load. They obtained several possibilities of behaviour when the crack approaches the interface with a stiffer ply. Generally, an interlam-

intra-laminar crack appears in the interface, which may be connected or not with the intralaminar matrix crack. Hence, connecting this concept with the induced unfolding mechanism, the appearance of this interlaminar initial crack due to the matrix failure may propagate interlaminarly as a delamination with a high enough INS. Flat laminates require a load increment to propagate the delamination caused by the intralaminar crack, but high INS are present in curved laminates which may cause the instantaneous propagation of the delamination. An example of the intralaminar cracks perpendicular to the interfaces between plies that have propagated interlaminarly may be found in Figure 5.1.

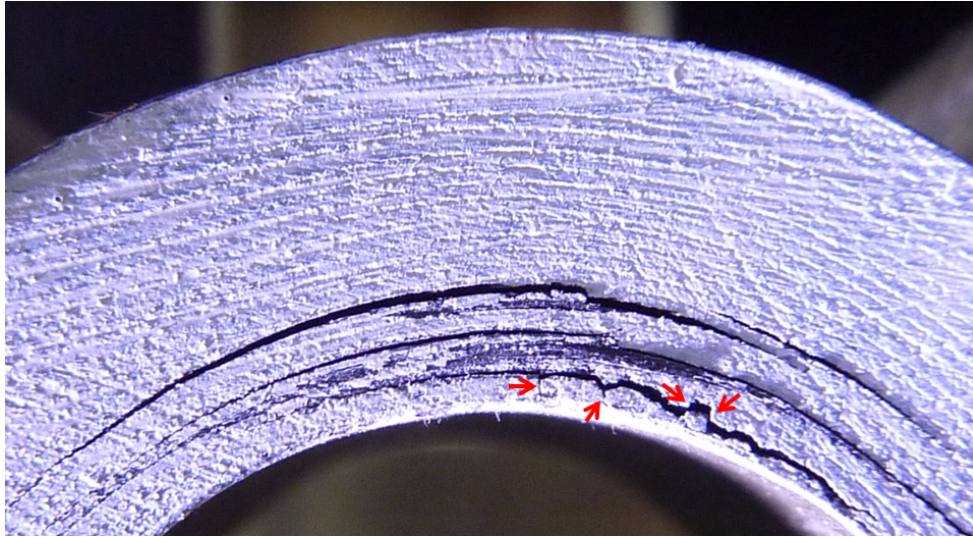


Figure 5.1: Propagation of intralaminar cracks as delaminations causing the induced unfolding.

The intralaminar matrix failure may be predicted with a typical strength failure criterion. However, the propagation of the delamination requires a fracture mechanics criterion, which is not directly applicable with the models developed in the present project. Hence, results of the present Chapter are not conclusive but indicative about if the failure mechanism is possible or not.

The matrix failure is not the only intralaminar failure which may induce a delamination and, therefore, the induced unfolding failure. Another example of intralaminar failure which may induce a delamination may be given by a fibre compressive failure. This kind of induced failure is given then in the compressive side of the specimen (near to the higher radius), so it may be easily identified by the location of the delamination, as seen in Figure 5.2.



Figure 5.2: Induced unfolding initiated by a fibre compressive failure.

The fibre compressive case is typical of fabric composite laminates, where the fibre compressive strength to ILTS ratio is lower. Composite laminates with UD plies have higher fibre compressive strength to ILTS ratios, so traditional unfolding is given at lower loads and the fibre compressive failure is not typically given.

The present Chapter is focused only in the induced unfolding initiated by an intralaminar matrix failure, which is analysed in detail by using the experimental results provided by Airbus Operations S.L.

5.2 Experimental results

The experimental tests consisted in a four-point bending test campaign over L-specimens made by a CFRP of UD plies with different lay-ups. Six kinds of specimens were defined according to Table 5.1, where the stacking sequence of each kind of specimen is shown. Seven coupons of each specimen were tested.

Name	Stacking sequence
CP1	[45 -45 90 45 0 -45 90 -45 45]
CP2	[45 -45 90 -45 45 0 45 -45] _S
CP3	[45 -45 90 -45 45 0 45 -45] _S
CP4	[45 -45 90 90 -45 45 0 45 -45 45 -45 0 45 -45] _S
CP5	[45 0 -45 90] _{6S}
CP6	[45 -45 90 90 90 -45 45 0 0 45 -45 45 -45 0 [45 -45] ₅] _S

Table 5.1: Specimens stacking sequences

The geometry of each kind of coupon is determined by the thickness, t , the outer radius of the curved part, R_o , and the width, W , which are shown

in Table 5.2. Notice that CP2 and CP3 specimens have the same stacking sequence and different width.

Name	t (mm)	R_o (mm)	W (mm)
CP1	1.7	5	25
CP2	2.9	8	25
CP3	2.9	8	50
CP4	5.2	12	40
CP5	8.8	20	40
CP6	8.8	20	40

Table 5.2: Specimens dimensions

The experimental failure load has been obtained from the tests, so applying the non-linear methodology described in Chapter 2, the bending moment in the curved part of the L-shaped laminate can be calculated. The bending moment obtained is introduced as input in the subsequent analytical methodologies employed for the stresses calculation.

These coupons were manufactured for a characterization process, so they have not been designed with the purpose of observing the induced unfolding and the laminates are not optimized for this objective.

5.2.1 Traditional unfolding

The traditional unfolding failure criteria, applied to the tests under consideration, establishes that the curved laminate fails when the maximum value of the INS in the curved zone reaches its maximum allowable value. Therefore, calculating the stresses in the coupons that have been tested, the maximum value of the INS may be assumed as the apparent ILTS.

For the calculation of the stresses the non-regularized three-dimensional model developed in Chapter 4 has been selected. This model includes the effect of the torsion, the combined effect of the anticlastic with the curvature, the effect of the finite width and the free-edge effects. The maximum value of the INS is given by the singularity of the free-edge, which is not considered. Therefore, the maximum value is considered as the maximum value obtained in the inner part of the specimen.

The apparent ILTS is then considered as the maximum INS obtained in the middle of the width of the specimen with the non-regularized three-dimensional model with a high enough order. This apparent ILTS divided by the strength in the intralaminar matrix direction S_{22} is depicted in Figure 5.3 respect to the thickness of the coupons.

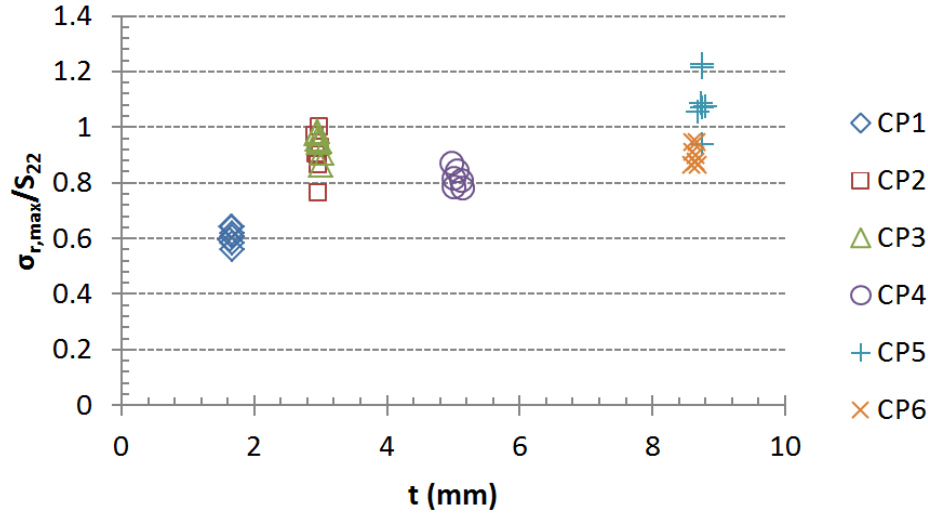


Figure 5.3: Apparent ILTS of the coupons respect to the thickness.

Notice the thickness dependence of the apparent ILTS, where thinnest specimens have lower values of the apparent ILTS than the thickest specimens. Furthermore, assuming that $S_{22} = S_{33}$, the thinnest specimens have an apparent ILTS of 60% of the nominal strength and only CP5 specimens may have failed due to the traditional unfolding while the rest of specimens present a lower value of the INS at the failure onset. Notice also that, for the thickest specimens, two different kind of specimens (CP5 and CP6) are showing different mean values of the apparent ILTS.

5.2.2 Induced unfolding

The induced unfolding hypothesis establishes that the curved laminate is delaminated when a ply fails in an intralaminar direction, requiring a sufficiently high INS for propagating interlaminarly this initial damage.

In order to demonstrate the existence of the induced unfolding, two kind of evidences are shown in the present section. First, evidences associated to the stress state in curved laminates, and second, evidences associated to the delamination location in the thickness of the curved laminate.

Evidences associated to the stress state

The non-regularized three-dimensional model developed in Chapter 4 allows us to obtain with a high accuracy the intralaminar stresses in the

direction perpendicular to the fibres for each ply. Hence, considering the intralaminar failure associated to the matrix as the initial cause of the sample failure, the sample fails when the stress in the intralaminar matrix direction, σ_{22} , reaches the corresponding strength S_{22} .

Figure 5.4 shows the value of the maximum σ_{22} divided by the strength S_{22} respect to the thickness for all the coupons.

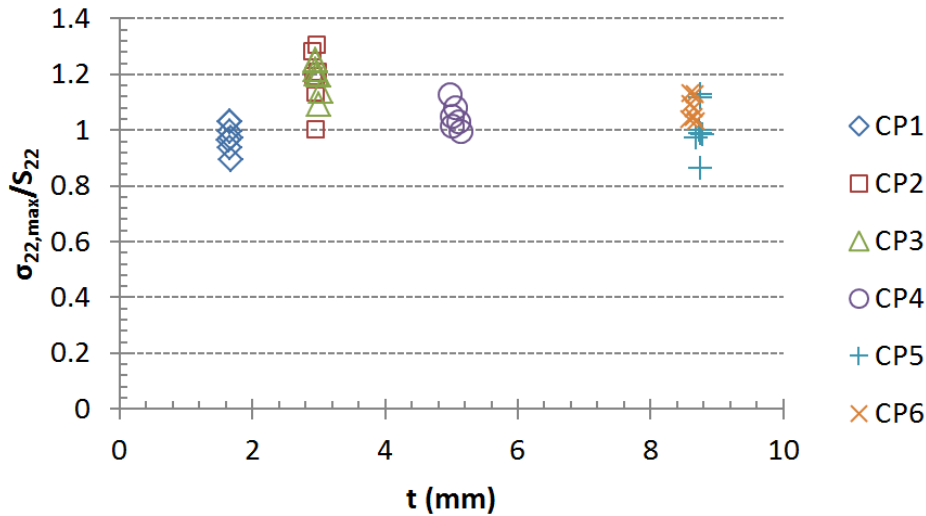


Figure 5.4: Maximum stress in the matrix direction of the coupons respect to the thickness.

It can be observed that all the specimens are bearing a maximum stress in the intralaminar matrix direction which is equal to its strength just in the moment of the failure since the value of σ_{22}/S_{22} is near to the unitary value, without a clear thickness dependence. Therefore, stress analysis carried out suggest that laminates are failing initially by an intralaminar failure causing the induced unfolding and not by the traditional unfolding. Only specimens CP5 have an uncertain failure mechanism while it may have failed by traditional or induced unfolding indifferently.

The maximum of σ_{22} for the present specimens is always given in the 90° plies, although in other stacking sequences it may be also given in the $\pm 45^\circ$ plies.

Evidences associated to the delamination locations

Both traditional unfolding and induced unfolding due to a matrix failure cause a delamination closer to the lower radius than to the higher radius. Moreover, failed composites present multiple delamination cracks in this

zone. This fact hinders identifying which is the first crack causing the failure during the test execution. However, induced unfolding due to a matrix failure causes typically a delamination closer to the lower radius than the traditional unfolding.

A statistical analysis has been carried out over the coupons of each specimen, analysing how many coupons have a particular delamination crack in the position predicted by the stress analysis, assuming that failure is initiated either by traditional unfolding or by induced unfolding, in order to determine which are the more repetitive cracks.

CP1 specimens are difficult to analyse due to their very low thickness, showing a 100% agreement in the delamination location with both failure mechanisms. Figure 5.5 shows a picture of a CP1 coupon.

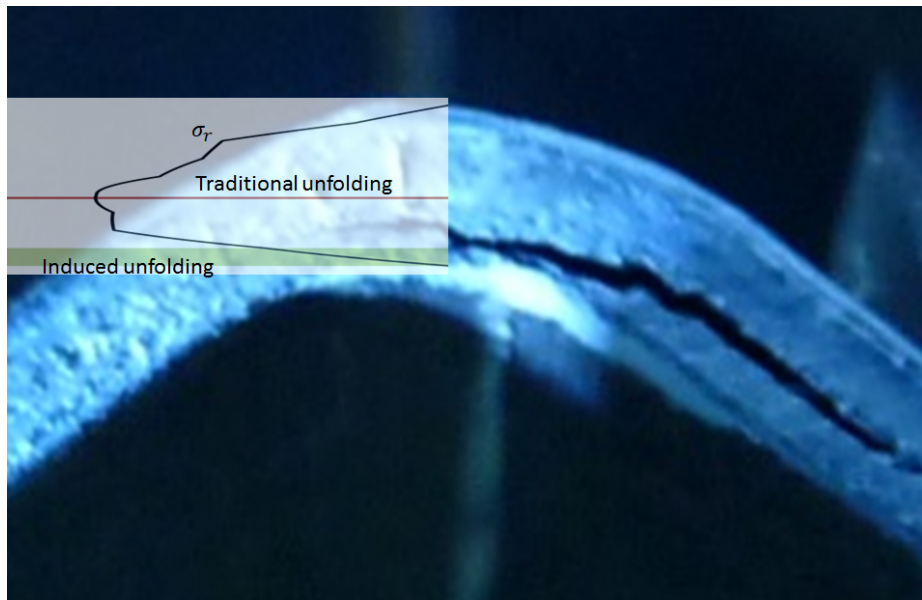


Figure 5.5: Location of the delaminations in a CP1 coupon.

CP2 and CP3 specimens give similar results since they have the same stacking sequence and geometry except the width. This kind of specimens have shown also a 100% agreement with both failure mechanisms. All specimens have a crack at the location predicted by the induced unfolding and also another crack at the location predicted by the traditional unfolding. Figure 5.6 shows a picture of a CP2/CP3 coupon.

CP4 specimens have shown the highest agreement with the induced unfolding. The 100% of CP4 specimens have a crack where the induced unfolding predicts, while only a 29% of the specimens have a crack where the



Figure 5.6: Location of the delaminations in a CP2/CP3 coupon.

traditional unfolding predicts. Figure 5.7 shows a picture of a CP4 coupon.

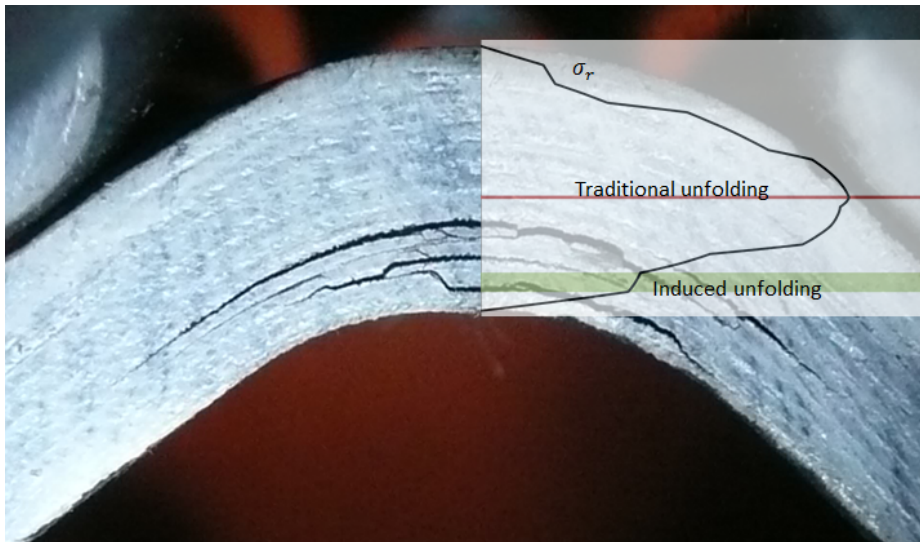


Figure 5.7: Location of the delaminations in a CP4 coupon.

The 100% of CP5 specimens have a delamination crack at the location predicted by the induced unfolding while a 70% have a delamination crack where the traditional unfolding predicts. Figure 5.8 shows a picture of a

CP5 coupon.

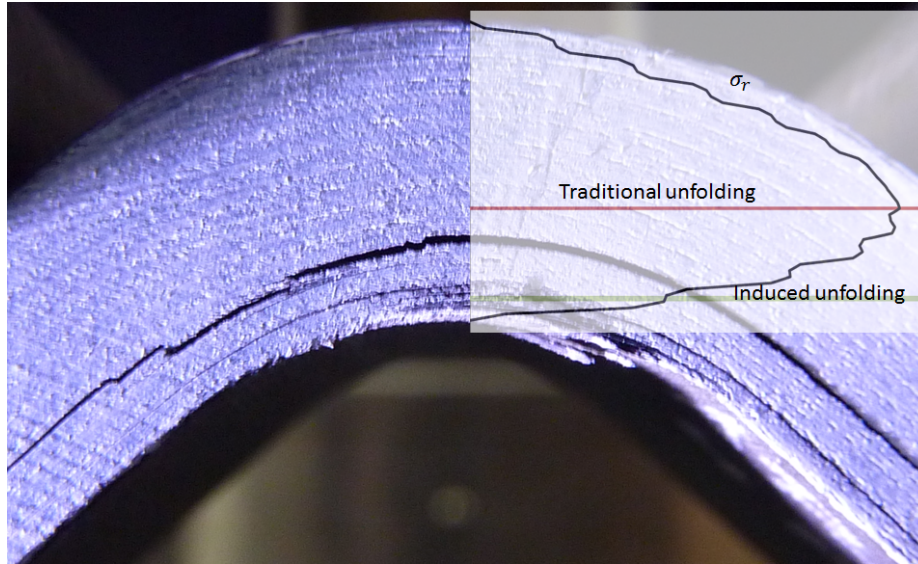


Figure 5.8: Location of the delaminations in a CP5 coupon.

Finally, CP6 specimens have shown also an excellent agreement with the induced unfolding hypothesis, since the 100% of CP6 specimens have a delamination crack at the location predicted by the induced unfolding. Conversely, only a 43% of CP6 specimens have a delamination crack where the traditional unfolding predicts, thus indicating that the intralaminar failure may have triggered the unfolding failure in CP6 samples. Figure 5.9 shows a picture of a CP6 coupon.

More pictures of the delamination cracks in the different kinds of specimens may be observed in [100].

Therefore, the delamination crack locations have shown a 100% agreement with the induced unfolding failure mechanism, thus supporting the hypothesis that this mechanism has initiated the unfolding failure, in particular in CP4 and CP6 specimens where crack locations have shown a good agreement with the traditional unfolding in less than a 50% of the specimen.

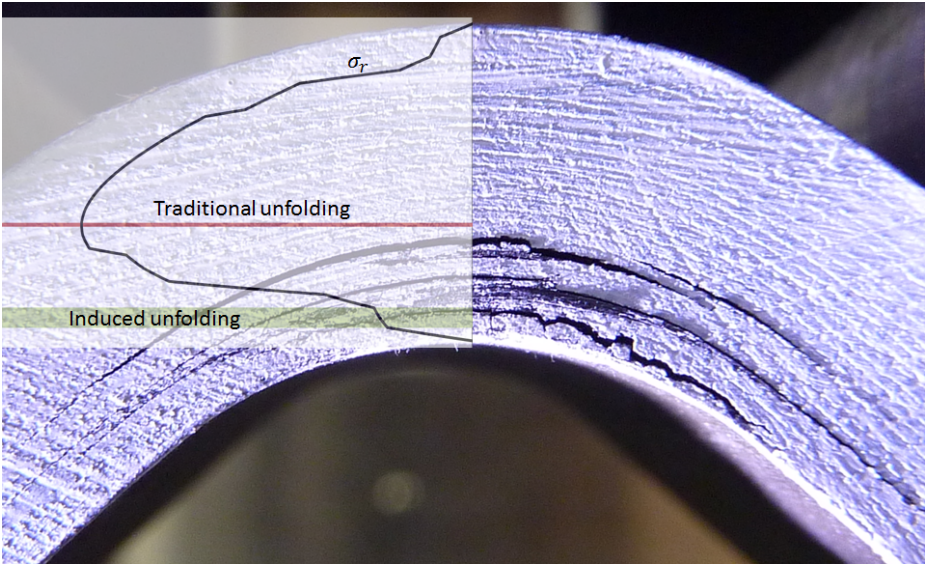


Figure 5.9: Location of the delaminations in a CP6 coupon.

Chapter 6

Design recommendations

In this PhD Thesis several models for the stress calculations based in 2D and 3D approximations have been presented. Those models have been implemented in MatLab, showing very low computational times and a very high accuracy for a high enough model order. This is especially useful for an optimization problem which requires to evaluate many cases and may spend much more time. Furthermore, two kinds of unfolding failure have been separated: the traditional failure and the induced unfolding.

Design recommendations and optimization guidelines may be defined by considering both traditional and induced unfolding failure mechanisms and using the models developed to obtain the stress analysis of multiple configurations. For the analysis of the optimal configurations, a L-shaped laminate of 90° is considered loaded under a pure opening bending moment. The material properties considered are shown in Table 6.1, with a ply thickness of $t_p = 0.2$ mm. S_{22} is the tensile strength in the in-plane direction perpendicular to the fibres corrected with the residual stresses and S_{33} is the ILTS.

Table 6.1: Material properties

E_{11} (MPa)	150	E_{22} (MPa)	10	E_{33} (MPa)	10
ν_{12}	0.3	ν_{13}	0.3	ν_{23}	0.3
G_{12} (MPa)	4.8	G_{13} (MPa)	4.8	G_{23} (MPa)	4.8
S_{22} (MPa)	50	S_{33} (MPa)	50		

The following sections evaluate the maximum bending moment in several kinds of laminates considering both traditional and induced unfolding observing how different parameters affect to the results, and finally summarize the design guidelines by considering the results obtained.

6.1 Evaluation of the maximum bending moment with the combination of traditional and induced unfolding

The simplest approximation for evaluating the maximum INS due to a bending moment is given by Kedward's formula [1], which is shown in equation (2.5). Therefore, the maximum bending moment according to Kedward's formula and the traditional unfolding concept, M_K , that a curved laminate can bear, is given by the following expression:

$$M_K = -\frac{t\sqrt{4R^2 - t^2}}{3}S_{33}. \quad (6.1)$$

This approximation is based on the Lekhnitskii's equations. Therefore, it is valid for homogeneous materials, and does not consider the stacking sequence effect. Notwithstanding, this expression shows that, for a given thickness, it is interesting to increase the mean radius, when possible, to increase the bending moment that the laminate can bear. This bending moment is used as a reference moment in the calculations.

For estimating the moment that the laminate can bear considering the effect of the stacking sequence and the different three-dimensional effects, stresses are calculated according to the three-dimensional non-regularized model with $n = 40$ and $W = 10t$. The three-dimensional effects are generally much more important than the change-of-curvature effects in the considered geometry under a bending moment. The bending problem is one of the cases less affected by the change-of-curvature effects. Therefore, the results of the regularized three-dimensional aforementioned model are used for the optimization, considering that the real value may be modified even in a 6% by the change of curvature.

Applying that three-dimensional model, a bending moment M_{TU} is obtained considering that the INS reaches the ILTS (traditional unfolding) and a bending moment M_{IU} is obtained considering that the matrix stress σ_{22} reaches the corresponding strength S_{22} (induced unfolding). Hence, the maximum bending moment that laminate may bear is given by $M_{\max} = \min(M_{TU}, M_{IU})$.

Six blocks of different kinds of stacking sequences have been considered for the calculations. The first block is composed by a 8-ply laminate 100/0/0/0, where the first number is the percentage of plies at 0° , the second number is the percentage of plies at 90° , the third number is the percentage of plies at 45° and the last number is the percentage of plies at -45° . Therefore, the first laminate considered is a $[0]_8$ laminate.

The second block has four laminates with the different possibilities of 8-ply symmetrical laminates 75/25/0/0. The third block is composed by the four laminates of the different possibilities of 8-ply symmetrical laminates 25/75/0/0. The fourth block has six laminates with the different possibilities of 8-ply symmetrical laminates 50/50/0/0. The fifth block is composed by the 12 possibilities of 8-ply symmetrical laminates 25/25/25/25.

Finally, the sixth block has 12 laminates, defined by the symmetrical laminates $[0,45,-45,90]_{nS}$, $[45,0,-45,90]_{nS}$, $[45,90,0,-45]_{nS}$ and $[45,90,-45,0]_{nS}$ with $n = 2, 3, 4$.

With the purpose of analysing the effect of the stacking sequence, the bending stiffness, E_b [Nm], and the axial stiffness, E_a [N/m], are used. The different results are depicted depending on the non-dimensional parameter $(12E_b)/(E_a t^2)$. Notice that this parameter has an unit value for an isotropic material and for a homogeneous stacking sequence with all plies at 0° or 90° .

For analysing the effect of the radius to thickness ratio, R/t , different values of this parameter are evaluated.

First, considering a laminate with $R/t = 1$, the bending moment associated to the traditional unfolding, M_{TU} , is depicted in Figure 6.1, the bending moment associated to the induced unfolding, M_{IU} , is depicted in Figure 6.2, and the maximum bending moments that the laminates may bear are depicted in Figure 6.3.

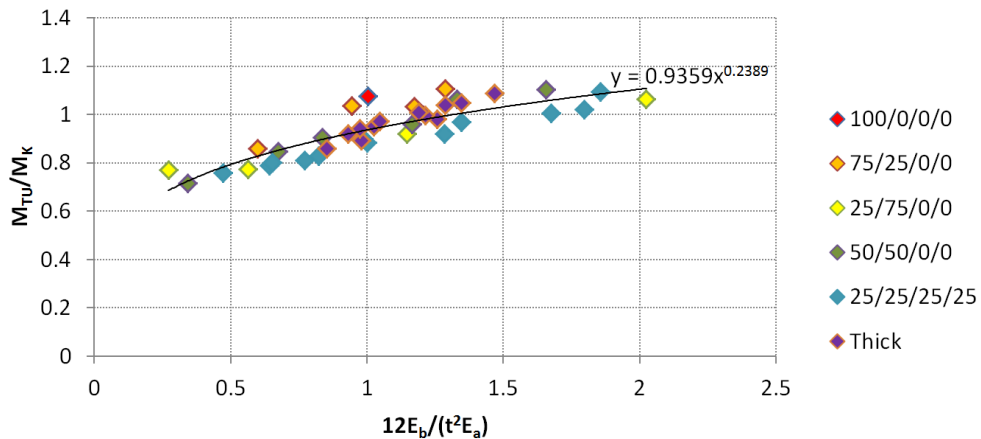


Figure 6.1: Analytical bending moment in the traditional unfolding, M_{TU} , for $R = t$.

As seen in Figure 6.1, the values of M_{TU} for the different stacking sequences and thicknesses follow a defined distribution, which has been in-

terpreted as a potential function. It is observed that the distribution is roughly independent of the number of plies and of the stacking sequence and the percentage of each kind of ply, depending only on the parameter $(12E_b)/(E_a t^2)$.

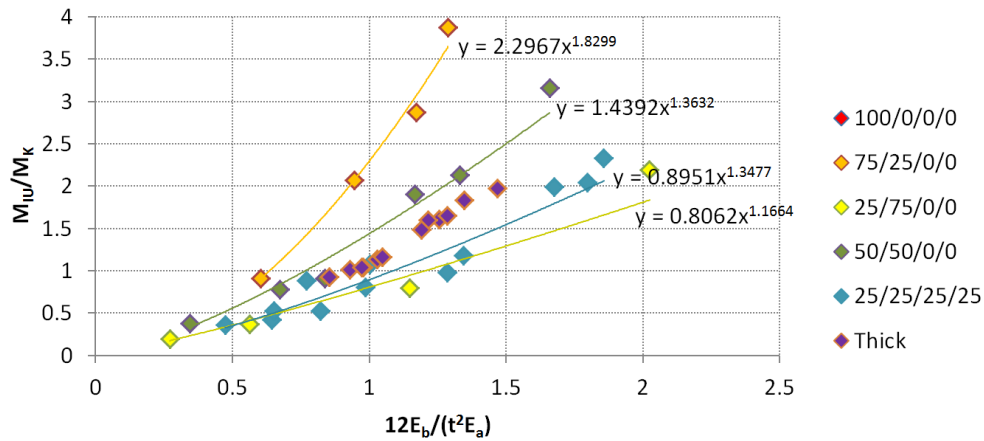


Figure 6.2: Analytical bending moment in the induced unfolding, M_{IU} , for $R = t$.

Respect to Figure 6.2, the values of M_{IU} have not a globally defined distribution. Notwithstanding, each kind of stacking sequence, defined by the percentage of each ply, has a defined distribution which may also be approximated by a potential function.

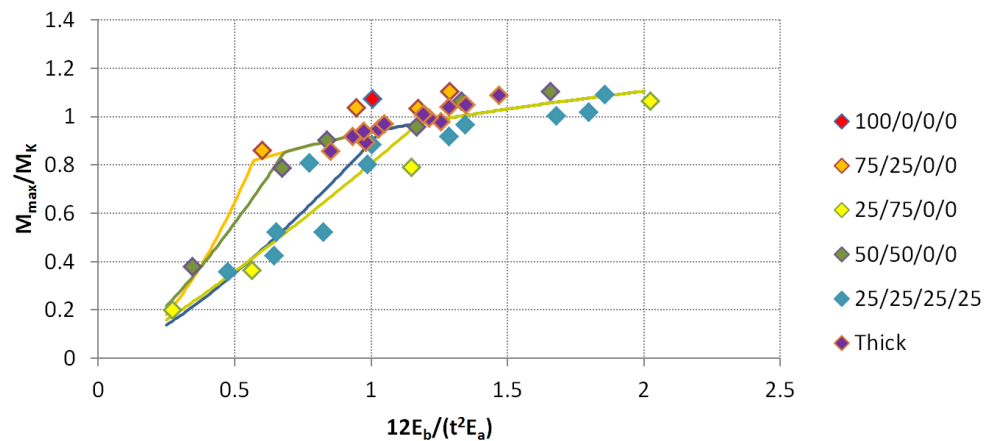


Figure 6.3: Analytical bending moment, M_{max} , for $R = t$.

Hence, considering both M_{TU} and M_{IU} , the maximum bending moment

M_{\max} is obtained as depicted in Figure 6.3. It may be observed that the best design for a curved laminate under bending moment prone to unfolding failure is the one which maximize the parameter $(12E_b)/(E_a t^2)$. Furthermore, stacking sequences which a higher value of that parameter are prone to the traditional unfolding failure, since laminates with a low value are prone to induced unfolding. Furthermore, the reduction of the number of 90° plies causes the increment of M_{IU} and therefore the domination of the traditional unfolding.

Second, considering a laminate with $R/t = 2$, the bending moment associated to the traditional unfolding, M_{TU} , is depicted in Figure 6.4, the bending moment associated to the induced unfolding, M_{IU} , is depicted in Figure 6.5, and the maximum bending moments that the laminates may bear are depicted in Figure 6.6.

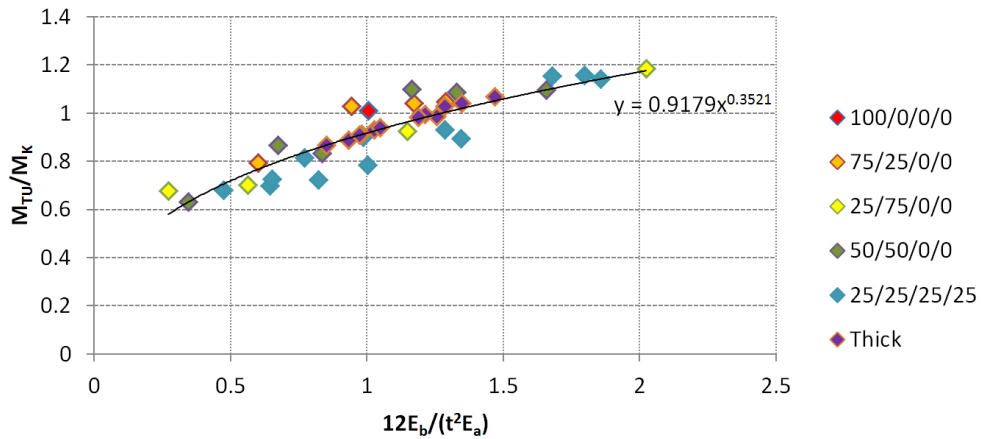


Figure 6.4: Analytical bending moment in the traditional unfolding, M_{TU} , for $R = 2t$.

Comparing Figure 6.4 with Figure 6.1, the case of $R = 2t$ has a higher dispersion of M_{TU} values, although they can be approximated also by a potential function. Furthermore, the potential function of $R = 2t$ has a higher exponent than in the case of $R = t$, causing higher differences of the value of M_{TU} when varying the parameter $(12E_b)/(E_a t^2)$.

Comparing Figure 6.5 with Figure 6.2, the case of $R = 2t$ has a lower dispersion of M_{IU} values, although they can be approximated also by a potential functions. Furthermore, the potential function of $R = 2t$ has a lower exponent and much lower values than in the case of $R = t$.

The maximum bending moment for the $R = 2t$ case, observed in Figure 6.6, shows a higher domination of the induced unfolding due to the much lower values of M_{IU} .

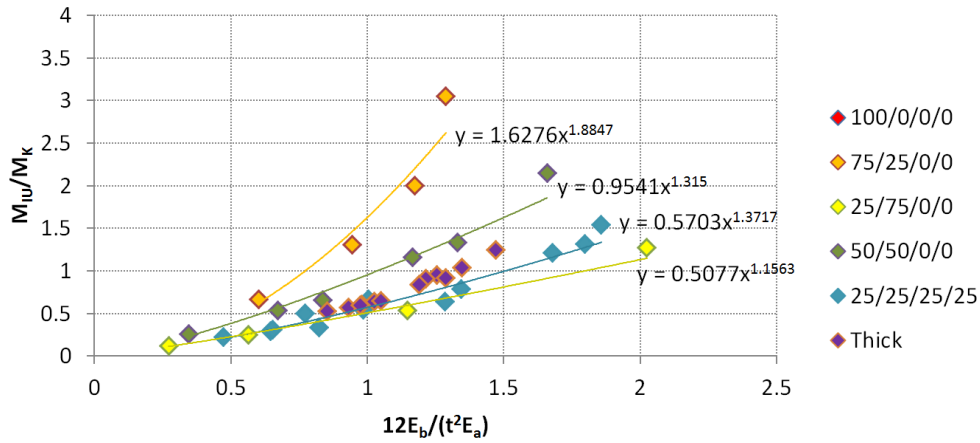


Figure 6.5: Analytical bending moment in the induced unfolding, M_{IU} , for $R = 2t$.

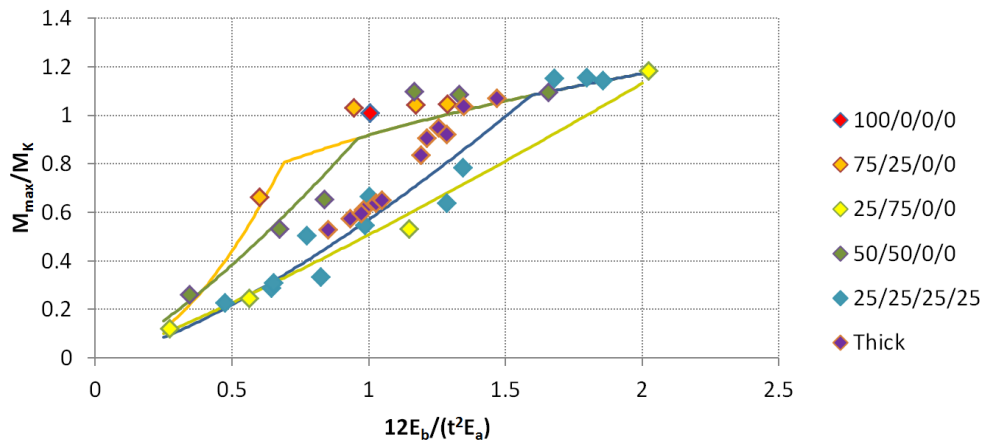


Figure 6.6: Analytical bending moment, M_{\max} , for $R = 2t$.

Finally, considering a laminate with $R/t = 3$, the bending moment associated to the traditional unfolding, M_{TU} , is depicted in Figure 6.7, the bending moment associated to the induced unfolding, M_{IU} , is depicted in Figure 6.8, and the maximum bending moments that the laminates may bear are depicted in Figure 6.9.

In Figure 6.7 it is observed again an increment of the exponent in the potential distribution when the R/t ratio is increased, increasing the slope of the distribution.

Figure 6.8 shows again a decrease of the exponents when the R/t ratio is increased.

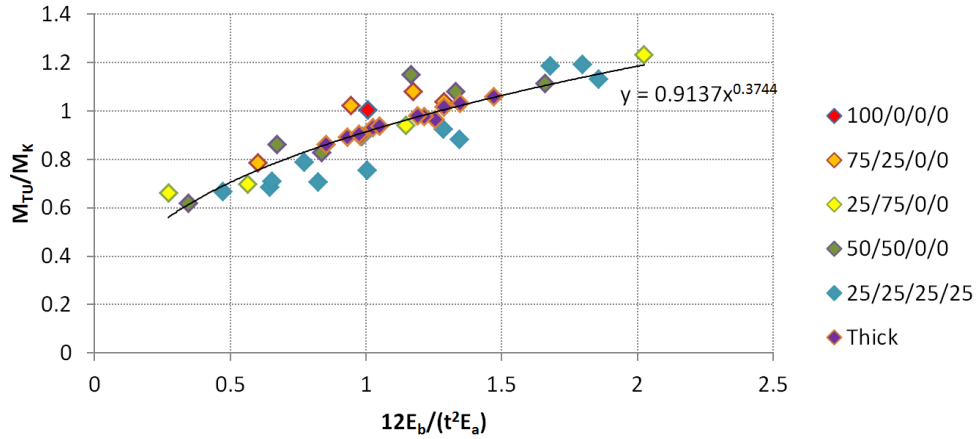


Figure 6.7: Analytical bending moment in the traditional unfolding, M_{TU} , for $R = 3t$.

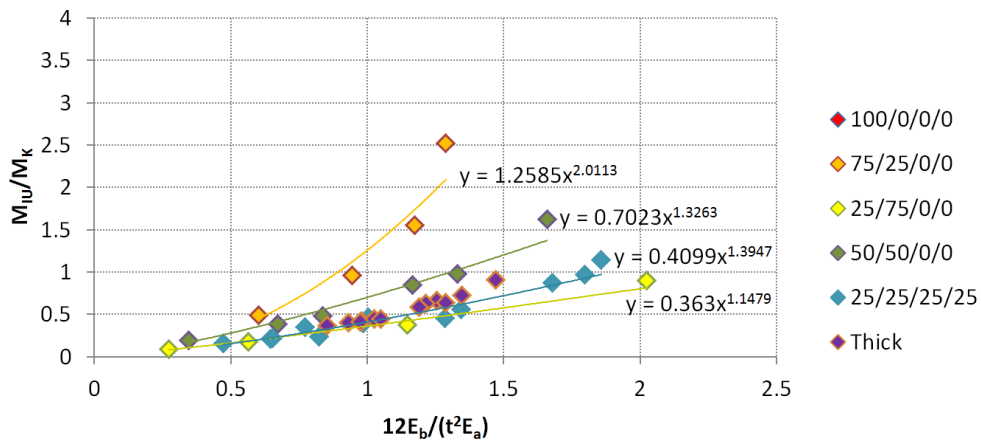


Figure 6.8: Analytical bending moment in the induced unfolding, M_{IU} , for $R = 3t$.

Combining both effects, Figure 6.9 shows a higher domination of the induced unfolding when a higher R/t ratio is chosen. For the depicted laminates, the $R/t = 3$ case is highly dominated by the induced unfolding, and only a few laminates fail by traditional unfolding.

In actual laminates, when a thin laminate is chosen the R/t ratio is usually higher than in thicker laminates due to manufacturability limitations in the inner radius of the curved part. Hence, thinner laminates are more dominated by the induced unfolding, causing higher errors in the traditional calculation based only in the traditional unfolding. Therefore, the induced

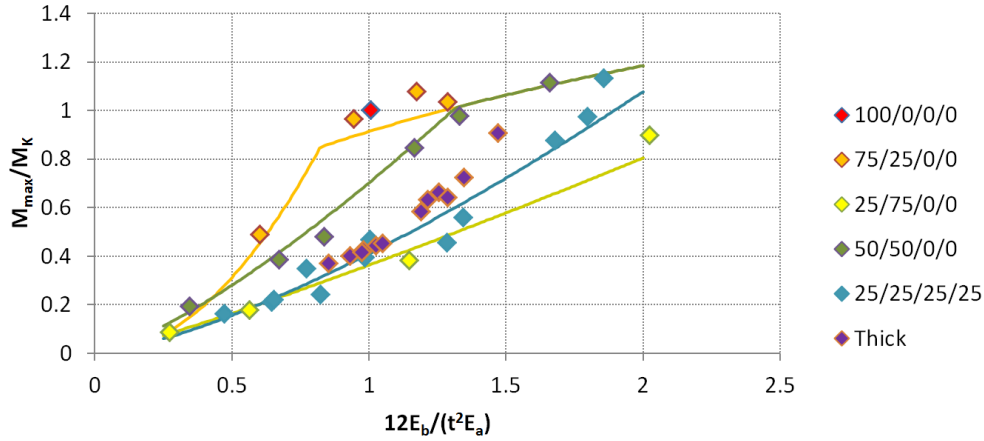


Figure 6.9: Analytical bending moment, M_{\max} , for $R = 3t$.

unfolding constitutes the explanation of the thickness-dependant of the ILTS since thin laminates fail due to a different failure mechanism, the induced unfolding.

6.2 Optimization recommendations based on both failure mechanisms

Considering a fixed R/t ratio and a given proportion of each kind of plies, both failure mechanisms agree in a common optimization criterion based on maximizing the bending stiffness to axial stiffness ratio. Furthermore, due to the higher slope of the induced unfolding correlated curve respect to the traditional unfolding one, small bending stiffness to axial stiffness ratios are usually dominated by the induced unfolding while high ratios are dominated by the traditional unfolding.

When the proportion of plies is not fixed, the traditional unfolding is optimized by maximizing also the bending stiffness to axial stiffness ratio, but the induced unfolding has different correlated curves for different proportions of plies, so detailed study being required for each particular case. Notwithstanding, if the optimum stacking sequence for the traditional unfolding is not failing by induced unfolding it may be considered as the optimum one by considering both failure mechanisms.

Finally, if the R/t ratio is not fixed, a higher ratio improves the traditional unfolding but reduces the maximum bending moment respect to the Kedward bending moment M_K of the induced unfolding. Notwithstanding,

the Kedward bending moment M_K is increased with the R/t ratio, so, finally, the maximum bending moment is always increased when the R/t ratio increases.

The thickness-dependence of the apparent ILTS may be explained using the results of the present Chapter. Notice that when the R/t ratio is increased the relation M_{TU}/M_K remains approximately invariant. However, when the R/t ratio is increased the relation M_{IU}/M_K decreases, and consequently the failure due to the induced unfolding occurs at a lower load and it is more probable that the induced unfolding is given instead of the traditional unfolding. Due to manufacturability reasons, thinner specimens have to be designed typically with higher R/t ratios than the typical ratios of the thicker L-shaped specimens, and then the induced unfolding occurs at a lower load respect to the traditional unfolding and the apparent ILTS, i.e., the value of the INS in the failure load, is lower. Therefore, it causes that the apparent ILTS of thinner specimens is lower than the apparent ILTS of thicker laminates, which may be traduced as the classical thickness dependence.

Chapter 7

Concluding remarks and future developments

Unfolding failure consists in a delamination which appears in curved specimens when they are loaded under a bending moment which tries to open the curvature. This PhD Thesis presents a detailed analysis of the failure mechanisms present in the unfolding failure and the stress states associated to them.

The aims of the Thesis are oriented to give an explanation of the two main problems which are present in the nowadays calculation procedures. The first problem consists in the thickness dependence of the apparent ILTS in typical composite laminates obtained from a four-point bending test procedure, e.g., ASTM D 6415/D 6415M [3]. The second problem consists in a high conservatism of the analytical procedures when applied to some kinds of loading states and geometries, mainly due to non-regularized effects such as the change-of-curvature effect.

The project is divided in three main parts, according to the three main steps involving the failure calculation: obtaining the loads (Chapter 2), calculating the stresses (Chapters 3 and 4) and applying a failure criterion (Chapter 5). Finally, based in the results obtained in the aforementioned Chapters, Chapter 6 has developed some design recommendations.

Chapter 2 is oriented to the bending moment calculation in the four-point bending test. The four-bending point test has been analysed due to its importance in the ILTS calculation, in order to have a wider view of the deformation and the loads distribution during the test. This kind of test is highly non-linear due to the change of the contact point between the rollers and the coupon due to a high displacements problem. Therefore, a non-linear model has been developed to obtain the load-displacements relation and the load-bending moment relation.

The model has shown small differences in the bending moment calculation from the applied load, lesser than a 5%, respect to the model presented in the ASTM procedure [3]. However, it also estimates the displacement by considering the stiffness of the beam, while the ASTM procedure requires the experimental measurements of the load and the displacement. Therefore, the model may be used for monitoring the test while it allows obtaining the force-displacement relation previously to the test.

The force-displacement distribution obtained with the non-linear model for the four-point bending test has been compared with experimental results for the validation of the model, showing a high agreement.

Bi-dimensional models have been developed in Chapter 3 for the calculation of the stresses in curved beams. First, an approximation to the Ko and Jackson equations [4] has been developed. This model is similar to the model presented in [94], using a different notation which makes easier the numerical implementation of the model. Second, the model has been extended by using a series expansion of the displacements and a higher-order moments definition in the stresses side. These higher-order models have allowed the stresses in more complex problems such as the change of curvature problem to be calculated, where the traditional analytical models are not applicable.

Two kinds of higher-order models (MBM and LPBM) have been developed depending on the functions used in the series expansion and the moments definition. MBM model is based in monomials, which let us to obtain a model with very low computational times. This model has a limitation in the maximum order that can be employed due to the increment of the condition number of the stiffness matrix when the order is increased, which limits also the accuracy of the model. Notwithstanding, it has a satisfactory accuracy in the maximum stresses prediction for many interesting situations. LPBM model is based in Legendre polynomials. The Legendre polynomials, due to their orthogonality, suppress the maximum order limitation, and much higher orders can be reached yielding, therefore, much higher accuracies and accurately predicting the whole stress distribution even near to a change of curvature. The computational times of the Legendre polynomials based model are higher than the computational times of the monomials based model, although they are much lower than the computational times required by a FE model with a similar accuracy in the results.

The higher-order models have been used to estimate the regularization distance, which is an important parameter to analyse the extension of the non-regularized effects due to the change of curvature or others factors. This parameter determines the length of the zone in which the Saint-Venant prin-

ciple can be applied. Furthermore, the non-regularized models have been applied to other kinds of problems different from the change of curvature, such as the joint between materials with different properties or the effect of concentrated loads.

The stress analysis in curved specimens has been completed by the development of three-dimensional models in Chapter 4. Three-dimensionality may introduce a torsion, induced by the different length of the outer and inner $\pm 45^\circ$ plies. Furthermore, the anticlastic effect restricted by the curvature of the material introduces a through-the-width moment which is null in the free-edge, modifying the stress distribution and causing a through-the-width distribution of the stress. Finally, the free-edge introduces singularities in the interfaces of the plies.

First, a regularized three-dimensional model has been developed to analyse the effect of a homogeneous change of temperature (causing residual stresses in the laminate), the effect of the torsion and the anticlastic effect. Residual INS have been obtained for curved laminates, observing that, in typical symmetrical laminates, 0° plies (compressed plies) cause a negative increment of the residual INS with the radial coordinate and that 90° plies (tensioned plies) cause a positive increment of the residual INS with the radial coordinate. Therefore, considering that the maximum of the INS due to the bending moment are typically given at lower radii, it is interesting to locate the 0° plies outer than the 90° plies in the stacking sequence in order to use the residual stresses to reduce that maximum INS.

Second, a non-regularized model has been developed to consider also the three-dimensional state, obtaining the free-edge effects and the through-the-width stress distributions. The through-the-width stress distributions have shown a high importance in some kinds of stacking sequences where the maximum stress is a 20% higher than the maximum stress predicted by considering a homogeneous stress distribution in the width. This non-regularized model has similar numerical properties (accuracy, computational times, convergence, etc.) than the bi-dimensional non-regularized models.

The developed non-regularized models have laid the background for a wider analysis of the stress analysis in curved laminates. In particular, the three-dimensional model has provided a much higher accuracy of the stresses in the in-plane matrix direction than that given by the bi-dimensional models, where the stress state approximation (e.g., plane stress or plane strain) plays an important role. This higher accuracy has let us to observe that, when applying the model to experimental results, the matrix direction may be failing approximately at the failure load, which may imply that the unfolding failure could be initiated, not only by the INS, but also by the in-plane stresses.

Following this line, a novel failure mechanism has been presented in Chapter 5, consisting in the concept of induced unfolding which gives a plausible explanation of the thickness-dependence of the apparent ILTS. The induced unfolding is initiated by an intralaminar crack, which, due to the presence of a high enough INS, may propagate interlaminarly when reaching the interface with a stiffer ply.

Hence, intralaminar cracks may anticipate the delamination and, therefore, the unfolding failure, causing that the apparent ILTS (defined as the maximum INS in the failure load) is lower than the actual ILTS. The main intralaminar failure considered has been the in-plane matrix direction failure, which is typically given in composite laminates with UD plies.

Some evidences of the existence of the induced unfolding have been exposed based in some experimental results provided by Airbus Operations S.L. First evidences are based in the maximum stresses calculation, observing that the INS has not always the same value at the failure point, which implies the classical thickness dependence. However, the maximum in-plane matrix direction stress has an almost constant value similar to the matrix direction strength in all the specimens at the failure load. Therefore, results indicate that in all the specimens an in-plane matrix failure should have taken place approximately for the failure load.

Second evidences are based in the location of the delaminations. The location of the first delamination predicted by the traditional unfolding failure mechanism is different generally than the location of the first delamination predicted by the induced unfolding mechanism. Images of the broken coupons after the test have allowed us to observe the cracks that have appeared during the test. The cracks locations have shown a higher correlation with the induced unfolding than with the traditional unfolding. A 100% of the coupons have a delamination where the induced unfolding predicts, while for some kind of specimens only the 50% of the coupons have a delamination where the traditional unfolding predicts.

Finally, based in the results obtained in the previous Chapters, Chapter 6 has developed some design guidelines for optimizing the stacking sequence and geometry of curved laminates prone to unfolding failure.

Both traditional and induced unfolding failure mechanisms may be optimized by maximizing the bending stiffness respect to the axial stiffness. Therefore, if the number of each kind of ply is fixed, the optimizations establishes that the stiffest plies (0° plies) have to be located in the outer part of the stacking sequence, and that the less stiff plies (90° plies) have to be located in the inner part of the stacking sequence.

Furthermore, it may be observed that comparing the maximum bending moment that a curved beam may bear with the maximum bending moment

predicted by Kedward's formula, the relation between them has very small variations in the traditional unfolding mechanism when the mean radius to thickness ratio is increased. However, the variation in the induced unfolding is higher, so that for higher mean radius to thickness ratios the induced unfolding is given at lower bending moments respect to the bending moment predicted by Kedward's formula. Hence, it may explain the classical thickness dependence of the apparent ILTS since thinner laminates require, due to manufacturability reasons, higher mean radius to thickness ratios and, therefore, the bending moment in the induced unfolding to the bending moment in the traditional unfolding ratio decreases anticipating the failure due to the induced unfolding and causing that the apparent ILTS is lower in these cases.

Future developments have to be focused on demonstrating the existence of the induced unfolding with experimental and numerical evidences. Numerical evidences may be focused on modelling the crack propagation from in-plane failures and showing that the onset and propagation of the delamination from that crack is unstable, when the interface is bearing a high enough INS. Experimental evidences may be focused on the realization of experimental tests with stacking sequences and radius to thickness ratios especially chosen for obtaining the desired failure mechanism, and observing the crack initiation and propagation with ultra-high speed cameras.

Finally, a new failure criterion based in both failure mechanisms has to be developed. It is important to include in that failure criterion the necessity of a minimum INS for the propagation of the delamination from the intralaminar crack, which implies the main difficulty in the calculation of the induced unfolding.

Appendix A

Matrices of the differential equation of the 2D non-regularized models

A.1 MBM matrices for the straight beam

The matrices are subdivided in the following submatrices:

$$\mathbf{G} = \begin{bmatrix} \mathbf{G}_{ss} & \mathbf{G}_{sz} \\ \mathbf{G}_{zs} & \mathbf{G}_{zz} \end{bmatrix}, \quad \mathbf{g}_N = \begin{bmatrix} \mathbf{g}_{sN} \\ \mathbf{g}_{zN} \end{bmatrix}, \quad \mathbf{g}_M = \begin{bmatrix} \mathbf{g}_{sM} \\ \mathbf{g}_{zM} \end{bmatrix}, \quad (\text{A.1a})$$

$$\mathbf{g}_{\sigma^+} = \begin{bmatrix} \mathbf{g}_{s\sigma^+} \\ \mathbf{g}_{z\sigma^+} \end{bmatrix}, \quad \mathbf{g}_{\sigma^-} = \begin{bmatrix} \mathbf{g}_{s\sigma^-} \\ \mathbf{g}_{z\sigma^-} \end{bmatrix}, \quad (\text{A.1b})$$

$$\mathbf{g}_{\tau^+} = \begin{bmatrix} \mathbf{g}_{s\tau^+} \\ \mathbf{o} \end{bmatrix}, \quad \mathbf{g}_{\tau^-} = \begin{bmatrix} \mathbf{g}_{s\tau^-} \\ \mathbf{o} \end{bmatrix}, \quad (\text{A.1c})$$

where \mathbf{o} is a vector of zeros and the submatrices are given by:

$$\mathbf{G}_{ss} = -\mathbf{H}_\gamma \mathbf{H}_z \check{\mathbf{D}}_{zz}^{-1} \check{\mathbf{B}}_{sz}^T, \quad \mathbf{G}_{sz} = \mathbf{H}_\gamma \mathbf{H}_z \check{\mathbf{D}}_{zz}^{-1} \mathbf{H}_z^T, \quad (\text{A.2a})$$

$$\mathbf{G}_{zs} = (\mathbf{H}_\gamma^T \check{\mathbf{B}}_{sz} - \check{\mathbf{C}}_{\tau\tau} \mathbf{H}_z) \check{\mathbf{D}}_{zz}^{-1} \check{\mathbf{B}}_{sz}^T - \mathbf{H}_\gamma^T \check{\mathbf{A}}_{ss}, \quad (\text{A.2b})$$

$$\mathbf{G}_{zz} = (\check{\mathbf{C}}_{\tau\tau} \mathbf{H}_z - \mathbf{H}_\gamma^T \check{\mathbf{B}}_{sz}) \check{\mathbf{D}}_{zz}^{-1} \mathbf{H}_z^T, \quad (\text{A.2c})$$

$$\mathbf{g}_{sN} = -\mathbf{H}_\gamma \mathbf{H}_z \check{\mathbf{D}}_{zz}^{-1} \check{\mathbf{b}}_{Nz}, \quad \mathbf{g}_{sM} = -\mathbf{H}_\gamma \mathbf{H}_z \check{\mathbf{D}}_{zz}^{-1} \check{\mathbf{b}}_{Mz}, \quad (\text{A.2d})$$

$$\mathbf{g}_{zN} = -\mathbf{H}_\gamma^T \check{\mathbf{a}}_{Ns} + (\mathbf{H}_\gamma^T \check{\mathbf{B}}_{sz} - \check{\mathbf{C}}_{\tau\tau} \mathbf{H}_z) \check{\mathbf{D}}_{zz}^{-1} \check{\mathbf{b}}_{Nz}, \quad (\text{A.2e})$$

$$\mathbf{g}_{zM} = -\mathbf{H}_\gamma^T \check{\mathbf{a}}_{Ms} + (\mathbf{H}_\gamma^T \check{\mathbf{B}}_{sz} - \check{\mathbf{C}}_{\tau\tau} \mathbf{H}_z) \check{\mathbf{D}}_{zz}^{-1} \check{\mathbf{b}}_{Mz}, \quad (\text{A.2f})$$

$$\mathbf{g}_{s\sigma^+} = -\mathbf{H}_\gamma \hat{\mathbf{f}}_s \left(\frac{t}{2} \right), \quad \mathbf{g}_{s\sigma^-} = \mathbf{H}_\gamma \hat{\mathbf{f}}_s \left(-\frac{t}{2} \right), \quad (\text{A.2g})$$

$$\mathbf{g}_{z\sigma^+} = -\left(\check{\mathbf{C}}_{\tau\tau} \hat{\mathbf{f}}_s \left(\frac{t}{2} \right) + \check{\mathbf{c}}_{Q\tau} \right), \quad (\text{A.2h})$$

$$\mathbf{g}_{z\sigma^-} = \check{\mathbf{C}}_{\tau\tau} \hat{\mathbf{f}}_s \left(-\frac{t}{2} \right) + \check{\mathbf{c}}_{Q\tau}, \quad (\text{A.2i})$$

$$\mathbf{g}_{s\tau^+} = -\mathbf{f}_s \left(\frac{t}{2} \right), \quad \mathbf{g}_{s\tau^-} = \mathbf{f}_s \left(-\frac{t}{2} \right). \quad (\text{A.2j})$$

A.2 MBM matrices for the curved beam

The matrices are subdivided in the following submatrices:

$$\mathbf{G} = \begin{bmatrix} \mathbf{G}_{ss} & \mathbf{G}_{sz} \\ \mathbf{G}_{zs} & \mathbf{G}_{zz} \end{bmatrix}, \quad \mathbf{g}_N = \begin{bmatrix} \mathbf{g}_{sN} \\ \mathbf{g}_{zN} \end{bmatrix}, \quad \mathbf{g}_M = \begin{bmatrix} \mathbf{g}_{sM} \\ \mathbf{g}_{zM} \end{bmatrix}, \quad (\text{A.3a})$$

$$\mathbf{g}_{\sigma^+} = \begin{bmatrix} \mathbf{g}_{s\sigma^+} \\ \mathbf{g}_{z\sigma^+} \end{bmatrix}, \quad \mathbf{g}_{\sigma^-} = \begin{bmatrix} \mathbf{g}_{s\sigma^-} \\ \mathbf{g}_{z\sigma^-} \end{bmatrix}, \quad (\text{A.3b})$$

$$\mathbf{g}_{\tau^+} = \begin{bmatrix} \mathbf{g}_{s\tau^+} \\ \mathbf{o} \end{bmatrix}, \quad \mathbf{g}_{\tau^-} = \begin{bmatrix} \mathbf{g}_{s\tau^-} \\ \mathbf{o} \end{bmatrix}, \quad (\text{A.3c})$$

where \mathbf{o} is a vector of zeros and the submatrices are given by:

$$\mathbf{G}_{ss} = \mathbf{H}_\gamma \left(\mathbf{H}_s - \mathbf{H}_z \check{\mathbf{D}}_{zz}^{-1} \check{\mathbf{B}}_{sz}^T \right), \quad \mathbf{G}_{sz} = \mathbf{H}_\gamma \mathbf{H}_z \check{\mathbf{D}}_{zz}^{-1} \mathbf{H}_z^T, \quad (\text{A.4a})$$

$$\mathbf{G}_{zs} = \check{\mathbf{C}}_{\tau\tau} \mathbf{H}_s + \left(\mathbf{H}_\gamma^T \check{\mathbf{B}}_{sz} - \check{\mathbf{C}}_{\tau\tau} \mathbf{H}_z \right) \check{\mathbf{D}}_{zz}^{-1} \check{\mathbf{B}}_{sz}^T - \mathbf{H}_\gamma^T \check{\mathbf{A}}_{ss}, \quad (\text{A.4b})$$

$$\mathbf{G}_{zz} = \left(\check{\mathbf{C}}_{\tau\tau} \mathbf{H}_z - \mathbf{H}_\gamma^T \check{\mathbf{B}}_{sz} \right) \check{\mathbf{D}}_{zz}^{-1} \mathbf{H}_z^T + \mathbf{H}_\gamma^T \mathbf{H}_s^T, \quad (\text{A.4c})$$

$$\mathbf{g}_{sN} = -\mathbf{H}_\gamma \mathbf{H}_z \check{\mathbf{D}}_{zz}^{-1} \check{\mathbf{b}}_{Nz}, \quad \mathbf{g}_{sM} = \mathbf{H}_\gamma \left(\mathbf{h}_M - \mathbf{H}_z \check{\mathbf{D}}_{zz}^{-1} \check{\mathbf{b}}_{Mz} \right), \quad (\text{A.4d})$$

$$\mathbf{g}_{zN} = \frac{1}{R} \check{\mathbf{c}}_{Q\tau} - \mathbf{H}_\gamma^T \check{\mathbf{a}}_{Ns} + \left(\mathbf{H}_\gamma^T \check{\mathbf{B}}_{sz} - \check{\mathbf{C}}_{\tau\tau} \mathbf{H}_z \right) \check{\mathbf{D}}_{zz}^{-1} \check{\mathbf{b}}_{Nz}, \quad (\text{A.4e})$$

$$\mathbf{g}_{zM} = \check{\mathbf{C}}_{\tau\tau} \mathbf{h}_M - \mathbf{H}_\gamma^T \check{\mathbf{a}}_{Ms} + \left(\mathbf{H}_\gamma^T \check{\mathbf{B}}_{sz} - \check{\mathbf{C}}_{\tau\tau} \mathbf{H}_z \right) \check{\mathbf{D}}_{zz}^{-1} \check{\mathbf{b}}_{Mz}, \quad (\text{A.4f})$$

$$\mathbf{g}_{s\sigma^+} = -\frac{R^+}{R} \mathbf{H}_\gamma \mathbf{f}_z \left(\frac{t}{2} \right), \quad \mathbf{g}_{s\sigma^-} = \frac{R^-}{R} \mathbf{H}_\gamma \mathbf{f}_z \left(-\frac{t}{2} \right), \quad (\text{A.4g})$$

$$\mathbf{g}_{z\sigma^+} = -\frac{R^+}{R} \left(\check{\mathbf{C}}_{\tau\tau} \mathbf{f}_z \left(\frac{t}{2} \right) + \check{\mathbf{c}}_{Q\tau} \right), \quad (\text{A.4h})$$

$$\mathbf{g}_{z\sigma^-} = \frac{R^-}{R} \left(\check{C}_{\tau\tau} \mathbf{f}_z \left(-\frac{t}{2} \right) + \check{c}_{Q\tau} \right), \quad (\text{A.4i})$$

$$\mathbf{g}_{\tau^+} = -\frac{R^+}{R} \mathbf{f}_s \left(\frac{t}{2} \right), \quad \mathbf{g}_{\tau^-} = \frac{R^-}{R} \mathbf{f}_s \left(-\frac{t}{2} \right). \quad (\text{A.4j})$$

A.3 LPBM matrices for the straight beam

The matrices are subdivided in the following submatrices:

$$\mathbf{G} = \begin{bmatrix} \mathbf{G}_{ss} & \mathbf{G}_{sz} \\ \mathbf{G}_{zs} & \mathbf{G}_{zz} \end{bmatrix}, \quad \mathbf{g}_N = \begin{bmatrix} \mathbf{g}_{sN} \\ \mathbf{g}_{zN} \end{bmatrix}, \quad \mathbf{g}_M = \begin{bmatrix} \mathbf{g}_{sM} \\ \mathbf{g}_{zM} \end{bmatrix}, \quad (\text{A.5a})$$

$$\mathbf{g}_{\sigma^+} = \begin{bmatrix} \mathbf{g}_{s\sigma^+} \\ \mathbf{g}_{z\sigma^+} \end{bmatrix}, \quad \mathbf{g}_{\sigma^-} = \begin{bmatrix} \mathbf{g}_{s\sigma^-} \\ \mathbf{g}_{z\sigma^-} \end{bmatrix}, \quad (\text{A.5b})$$

$$\mathbf{g}_{\tau^+} = \begin{bmatrix} \mathbf{g}_{s\tau^+} \\ \mathbf{o} \end{bmatrix}, \quad \mathbf{g}_{\tau^-} = \begin{bmatrix} \mathbf{g}_{s\tau^-} \\ \mathbf{o} \end{bmatrix}, \quad (\text{A.5c})$$

where \mathbf{o} is a vector of zeros and the submatrices are given by:

$$\mathbf{G}_{ss} = -\mathbf{H}_\gamma \mathbf{H}_z \check{D}_{zz}^{-1} \check{B}_{sz}^T, \quad \mathbf{G}_{sz} = \mathbf{H}_\gamma \mathbf{H}_z \check{D}_{zz}^{-1} \mathbf{H}_z^T, \quad (\text{A.6a})$$

$$\mathbf{G}_{zs} = (\mathbf{H}_\gamma^T \check{B}_{sz} - \check{C}_{\tau\tau} \mathbf{H}_z) \check{D}_{zz}^{-1} \check{B}_{sz}^T - \mathbf{H}_\gamma^T \check{A}_{ss}, \quad (\text{A.6b})$$

$$\mathbf{G}_{zz} = (\check{C}_{\tau\tau} \mathbf{H}_z - \mathbf{H}_\gamma^T \check{B}_{sz}) \check{D}_{zz}^{-1} \mathbf{H}_z^T, \quad (\text{A.6c})$$

$$\mathbf{g}_{sN} = -\mathbf{H}_\gamma \mathbf{H}_z \check{D}_{zz}^{-1} \check{b}_{Nz}, \quad \mathbf{g}_{sM} = -\mathbf{H}_\gamma \mathbf{H}_z \check{D}_{zz}^{-1} \check{b}_{Mz}, \quad (\text{A.6d})$$

$$\mathbf{g}_{zN} = -\mathbf{H}_\gamma^T \check{a}_{Ns} + (\mathbf{H}_\gamma^T \check{B}_{sz} - \check{C}_{\tau\tau} \mathbf{H}_z) \check{D}_{zz}^{-1} \check{b}_{Nz}, \quad (\text{A.6e})$$

$$\mathbf{g}_{zM} = -\mathbf{H}_\gamma^T \check{a}_{Ms} + (\mathbf{H}_\gamma^T \check{B}_{sz} - \check{C}_{\tau\tau} \mathbf{H}_z) \check{D}_{zz}^{-1} \check{b}_{Mz}, \quad (\text{A.6f})$$

$$\mathbf{g}_{s\sigma^+} = -\mathbf{H}_\gamma \hat{\mathbf{f}}_s(1) - \mathbf{h}_Q, \quad \mathbf{g}_{s\sigma^-} = \mathbf{H}_\gamma \hat{\mathbf{f}}_s(-1) + \mathbf{h}_Q, \quad (\text{A.6g})$$

$$\mathbf{g}_{z\sigma^+} = -(\check{C}_{\tau\tau} \hat{\mathbf{f}}_s(1) + \check{c}_{Q\tau}), \quad \mathbf{g}_{z\sigma^-} = \check{C}_{\tau\tau} \hat{\mathbf{f}}_s(-1) + \check{c}_{Q\tau}, \quad (\text{A.6h})$$

$$\mathbf{g}_{s\tau^+} = -\mathbf{f}_s(1), \quad \mathbf{g}_{s\tau^-} = \mathbf{f}_s(-1). \quad (\text{A.6i})$$

A.4 LPBM matrices for the curved beam

The matrices are subdivided in the following submatrices:

$$\mathbf{G} = \begin{bmatrix} \mathbf{G}_{ss} & \mathbf{G}_{sz} \\ \mathbf{G}_{zs} & \mathbf{G}_{zz} \end{bmatrix}, \quad \mathbf{g}_N = \begin{bmatrix} \mathbf{g}_{sN} \\ \mathbf{g}_{zN} \end{bmatrix}, \quad \mathbf{g}_M = \begin{bmatrix} \mathbf{g}_{sM} \\ \mathbf{g}_{zM} \end{bmatrix}, \quad (\text{A.7a})$$

$$\mathbf{g}_{\sigma^+} = \begin{bmatrix} \mathbf{g}_{s\sigma^+} \\ \mathbf{g}_{z\sigma^+} \end{bmatrix}, \quad \mathbf{g}_{\sigma^-} = \begin{bmatrix} \mathbf{g}_{s\sigma^-} \\ \mathbf{g}_{z\sigma^-} \end{bmatrix}, \quad (\text{A.7b})$$

$$\mathbf{g}_{\tau^+} = \begin{bmatrix} \mathbf{g}_{s\tau^+} \\ \mathbf{o} \end{bmatrix}, \quad \mathbf{g}_{\tau^-} = \begin{bmatrix} \mathbf{g}_{s\tau^-} \\ \mathbf{o} \end{bmatrix}, \quad (\text{A.7c})$$

where \mathbf{o} is a vector of zeros and the submatrices are given by:

$$\mathbf{G}_{ss} = \mathbf{H}_\gamma \left(\mathbf{H}_s - \mathbf{H}_z \check{\mathbf{D}}_{zz}^{-1} \check{\mathbf{B}}_{sz}^T \right), \quad \mathbf{G}_{sz} = \mathbf{H}_\gamma \mathbf{H}_z \check{\mathbf{D}}_{zz}^{-1} \mathbf{H}_z^T, \quad (\text{A.8a})$$

$$\mathbf{G}_{zs} = \check{\mathbf{C}}_{\tau\tau} \mathbf{H}_s + \left(\mathbf{H}_\gamma^T \check{\mathbf{B}}_{sz} - \check{\mathbf{C}}_{\tau\tau} \mathbf{H}_z \right) \check{\mathbf{D}}_{zz}^{-1} \check{\mathbf{B}}_{sz}^T - \mathbf{H}_\gamma^T \check{\mathbf{A}}_{ss}, \quad (\text{A.8b})$$

$$\mathbf{G}_{zz} = \left(\check{\mathbf{C}}_{\tau\tau} \mathbf{H}_z - \mathbf{H}_\gamma^T \check{\mathbf{B}}_{sz} \right) \check{\mathbf{D}}_{zz}^{-1} \mathbf{H}_z^T + \mathbf{H}_\gamma^T \mathbf{H}_s^T, \quad (\text{A.8c})$$

$$\mathbf{g}_{sN} = \mathbf{H}_\gamma \left(\mathbf{h}_N - \mathbf{H}_z \check{\mathbf{D}}_{zz}^{-1} \check{\mathbf{b}}_{Nz} \right) + \frac{\mathbf{h}_Q}{R}, \quad (\text{A.8d})$$

$$\mathbf{g}_{sM} = \mathbf{H}_\gamma \left(\mathbf{h}_M - \mathbf{H}_z \check{\mathbf{D}}_{zz}^{-1} \check{\mathbf{b}}_{Mz} \right), \quad (\text{A.8e})$$

$$\mathbf{g}_{zN} = \frac{1}{R} \check{\mathbf{c}}_{Q\tau} + \check{\mathbf{C}}_{\tau\tau} \mathbf{h}_N - \mathbf{H}_\gamma^T \check{\mathbf{a}}_{Ns} + \left(\mathbf{H}_\gamma^T \check{\mathbf{B}}_{sz} - \check{\mathbf{C}}_{\tau\tau} \mathbf{H}_z \right) \check{\mathbf{D}}_{zz}^{-1} \check{\mathbf{b}}_{Nz}, \quad (\text{A.8f})$$

$$\mathbf{g}_{zM} = \check{\mathbf{C}}_{\tau\tau} \mathbf{h}_M - \mathbf{H}_\gamma^T \check{\mathbf{a}}_{Ms} + \left(\mathbf{H}_\gamma^T \check{\mathbf{B}}_{sz} - \check{\mathbf{C}}_{\tau\tau} \mathbf{H}_z \right) \check{\mathbf{D}}_{zz}^{-1} \check{\mathbf{b}}_{Mz}, \quad (\text{A.8g})$$

$$\mathbf{g}_{s\sigma^+} = -\frac{R^+}{R} \left(\mathbf{H}_\gamma \mathbf{f}_z(1) + \mathbf{h}_Q \right), \quad \mathbf{g}_{s\sigma^-} = \frac{R^-}{R} \left(\mathbf{H}_\gamma \mathbf{f}_z(-1) + \mathbf{h}_Q \right), \quad (\text{A.8h})$$

$$\mathbf{g}_{z\sigma^+} = -\frac{R^+}{R} \left(\check{\mathbf{C}}_{\tau\tau} \mathbf{f}_z(1) + \check{\mathbf{c}}_{Q\tau} \right), \quad \mathbf{g}_{z\sigma^-} = \frac{R^-}{R} \left(\check{\mathbf{C}}_{\tau\tau} \mathbf{f}_z(-1) + \check{\mathbf{c}}_{Q\tau} \right), \quad (\text{A.8i})$$

$$\mathbf{g}_{\tau^+} = -\frac{R^+}{R} \mathbf{f}_s(1), \quad \mathbf{g}_{\tau^-} = \frac{R^-}{R} \mathbf{f}_s(-1). \quad (\text{A.8j})$$

Appendix B

Matrices expressions of the 3D non-regularized models

B.1 Stiffness matrices for the flat laminate

The stiffness matrices \mathbf{K}_σ and \mathbf{K}_τ are divided in terms associated to the different components of the vector of equations (4.82). These components are denominated as follows:

$$\mathbf{K}_\sigma = \begin{bmatrix} A_{11} & B_{11} & A_{12} & B_{12} & (\mathbf{k}_{12}^A)^T & A_{16} & B_{16} & (\mathbf{k}_{16}^A)^T & (\mathbf{k}_{13}^A)^T \\ B_{11} & D_{11} & B_{12} & D_{12} & (\mathbf{k}_{12}^B)^T & B_{16} & D_{16} & (\mathbf{k}_{16}^B)^T & (\mathbf{k}_{13}^B)^T \\ A_{12} & B_{12} & A_{22} & B_{22} & (\mathbf{k}_{22}^A)^T & A_{26} & B_{26} & (\mathbf{k}_{26}^A)^T & (\mathbf{k}_{23}^A)^T \\ B_{12} & D_{12} & B_{22} & D_{22} & (\mathbf{k}_{22}^B)^T & B_{26} & D_{26} & (\mathbf{k}_{26}^B)^T & (\mathbf{k}_{23}^B)^T \\ \mathbf{k}_{12}^A & \mathbf{k}_{12}^B & \mathbf{k}_{22}^A & \mathbf{k}_{22}^B & \mathbf{K}_{22}^\sigma & \mathbf{k}_{26}^A & \mathbf{k}_{26}^B & \mathbf{K}_{26}^\sigma & \mathbf{K}_{23}^\sigma \\ A_{16} & B_{16} & A_{26} & B_{26} & (\mathbf{k}_{26}^A)^T & A_{66} & B_{66} & (\mathbf{k}_{66}^A)^T & (\mathbf{k}_{63}^A)^T \\ B_{16} & D_{16} & B_{26} & D_{26} & (\mathbf{k}_{26}^B)^T & B_{66} & D_{66} & (\mathbf{k}_{66}^B)^T & (\mathbf{k}_{63}^B)^T \\ \mathbf{k}_{16}^A & \mathbf{k}_{16}^B & \mathbf{k}_{26}^A & \mathbf{k}_{26}^B & \mathbf{K}_{26}^\sigma & \mathbf{k}_{66}^A & \mathbf{k}_{66}^B & \mathbf{K}_{66}^\sigma & \mathbf{K}_{63}^\sigma \\ \mathbf{k}_{13}^A & \mathbf{k}_{13}^B & \mathbf{k}_{23}^A & \mathbf{k}_{23}^B & (\mathbf{K}_{23}^\sigma)^T & \mathbf{k}_{63}^A & \mathbf{k}_{63}^B & (\mathbf{K}_{63}^\sigma)^T & \mathbf{K}_{33}^\sigma \end{bmatrix}, \quad (\text{B.1a})$$

$$\mathbf{K}_\tau = \begin{bmatrix} A_{44} & (\mathbf{k}_{44}^C)^T & A_{45} & (\mathbf{k}_{45}^C)^T \\ \mathbf{k}_{44}^C & \mathbf{K}_{44}^\tau & \mathbf{k}_{45}^C & \mathbf{K}_{45}^\tau \\ A_{45} & (\mathbf{k}_{45}^C)^T & A_{55} & (\mathbf{k}_{55}^C)^T \\ \mathbf{k}_{45}^C & \mathbf{K}_{45}^\tau & \mathbf{k}_{55}^C & \mathbf{K}_{55}^\tau \end{bmatrix}. \quad (\text{B.1b})$$

The components of the stiffness matrices \mathbf{K}_σ and \mathbf{K}_τ , shown in equations (B.1), are calculated from the following expressions:

$$A_{ij} = \sum_{p=1}^{N_p} (z_p^+ - z_p^-) \bar{C}_{ij}^p, \quad i, j = 1, 2, 3, 4, 5, 6, \quad (\text{B.2a})$$

$$B_{ij} = \sum_{p=1}^{N_p} \frac{1}{2} ((z_p^+)^2 - (z_p^-)^2) \bar{C}_{ij}^p, \quad i, j = 1, 2, 3, 6, \quad (\text{B.2b})$$

$$D_{ij} = \sum_{p=1}^{N_p} \frac{1}{3} ((z_p^+)^3 - (z_p^-)^3) \bar{C}_{ij}^p, \quad i, j = 1, 2, 3, 6, \quad (\text{B.2c})$$

$$\mathbf{k}_{ij}^A = \sum_{p=1}^{N_p} \left(\bar{C}_{ij}^p \int_{z_p^-}^{z_p^+} \mathbf{f}_s(z) dz \right), \quad i, j = 1, 2, 6, \quad (\text{B.2d})$$

$$\mathbf{k}_{ij}^A = \sum_{p=1}^{N_p} \left(\bar{C}_{ij}^p \int_{z_p^-}^{z_p^+} \hat{\mathbf{f}}_s(z) dz \right), \quad i = 1, 2, 6, \quad j = 3, \quad (\text{B.2e})$$

$$\mathbf{k}_{ij}^B = \sum_{p=1}^{N_p} \left(\bar{C}_{ij}^p \int_{z_p^-}^{z_p^+} z \mathbf{f}_s(z) dz \right), \quad i, j = 1, 2, 6, \quad (\text{B.2f})$$

$$\mathbf{k}_{ij}^B = \sum_{p=1}^{N_p} \left(\bar{C}_{ij}^p \int_{z_p^-}^{z_p^+} z \hat{\mathbf{f}}_s(z) dz \right), \quad i = 1, 2, 6, \quad j = 3, \quad (\text{B.2g})$$

$$\mathbf{k}_{ij}^C = \sum_{p=1}^{N_p} \left(\bar{C}_{ij}^p \int_{z_p^-}^{z_p^+} \hat{\mathbf{f}}_s(z) dz \right), \quad i, j = 4, 5, \quad (\text{B.2h})$$

$$\mathbf{K}_{ij}^\sigma = \sum_{p=1}^{N_p} \left(\bar{C}_{ij}^p \int_{z_p^-}^{z_p^+} \mathbf{f}_s(z) \mathbf{f}_s^T(z) dz \right), \quad i, j = 1, 2, 6, \quad (\text{B.2i})$$

$$\mathbf{K}_{ij}^\sigma = \sum_{p=1}^{N_p} \left(\bar{C}_{ij}^p \int_{z_p^-}^{z_p^+} \mathbf{f}_s(z) \hat{\mathbf{f}}_s^T(z) dz \right), \quad i = 1, 2, 6, \quad j = 3, \quad (\text{B.2j})$$

$$\mathbf{K}_{33}^\sigma = \sum_{p=1}^{N_p} \left(\bar{C}_{33}^p \int_{z_p^-}^{z_p^+} \hat{\mathbf{f}}_s(z) \hat{\mathbf{f}}_s^T(z) dz \right), \quad (\text{B.2k})$$

$$\mathbf{K}_{ij}^\tau = \sum_{p=1}^{N_p} \left(\bar{C}_{ij}^p \int_{z_p^-}^{z_p^+} \hat{\mathbf{f}}_s(z) \hat{\mathbf{f}}_s^T(z) dz \right), \quad i, j = 4, 5. \quad (\text{B.2l})$$

The matrices \mathbf{K}_σ^A and \mathbf{K}_σ^B yield:

$$\mathbf{K}_\sigma^A = \begin{bmatrix} A_{22} & B_{22} & (\mathbf{k}_{22}^A)^T & A_{26} & B_{26} & (\mathbf{k}_{26}^A)^T & (\mathbf{k}_{23}^A)^T \\ B_{22} & D_{22} & (\mathbf{k}_{22}^B)^T & B_{26} & D_{26} & (\mathbf{k}_{26}^B)^T & (\mathbf{k}_{23}^B)^T \\ \mathbf{k}_{22}^A & \mathbf{k}_{22}^B & \mathbf{K}_{22}^\sigma & \mathbf{k}_{26}^A & \mathbf{k}_{26}^B & \mathbf{K}_{26}^\sigma & \mathbf{K}_{23}^\sigma \\ A_{26} & A_{26} & (\mathbf{k}_{26}^A)^T & A_{66} & B_{66} & (\mathbf{k}_{66}^A)^T & (\mathbf{k}_{36}^A)^T \\ B_{26} & B_{26} & (\mathbf{k}_{26}^B)^T & B_{66} & D_{66} & (\mathbf{k}_{66}^B)^T & (\mathbf{k}_{36}^B)^T \\ \mathbf{k}_{26}^A & \mathbf{k}_{26}^B & \mathbf{K}_{26}^\sigma & \mathbf{k}_{66}^A & \mathbf{k}_{66}^B & \mathbf{K}_{66}^\sigma & \mathbf{K}_{36}^\sigma \\ \mathbf{k}_{23}^A & \mathbf{k}_{23}^B & (\mathbf{K}_{23}^\sigma)^T & \mathbf{k}_{36}^A & \mathbf{k}_{36}^B & (\mathbf{K}_{36}^\sigma)^T & \mathbf{K}_{33}^\sigma \end{bmatrix}, \quad (\text{B.3a})$$

$$\mathbf{K}_\sigma^B = \begin{bmatrix} A_{12} & B_{12} \\ B_{12} & D_{12} \\ \mathbf{k}_{12}^A & \mathbf{k}_{12}^B \\ A_{16} & B_{16} \\ B_{16} & D_{16} \\ \mathbf{k}_{16}^A & \mathbf{k}_{16}^B \\ \mathbf{k}_{13}^A & \mathbf{k}_{13}^B \end{bmatrix}. \quad (\text{B.3b})$$

B.2 Auxiliary matrices for the flat laminate

The auxiliary matrices employed in Chapter 4 in the development of the non-regularized model for the straight laminates are defined as follows:

$$\mathbf{H}_{11}^Q = (\mathbf{H}_\gamma^T)^{-1} \check{\mathbf{K}}_{44}^\tau \mathbf{H}_\gamma^{-1}, \quad (\text{B.4a})$$

$$\mathbf{H}_{12}^Q = (\mathbf{H}_\gamma^T)^{-1} (\check{\mathbf{k}}_{45}^C - \check{\mathbf{K}}_{45}^\tau \mathbf{H}_\gamma^{-1} \mathbf{h}_Q), \quad (\text{B.4b})$$

$$\mathbf{H}_{13}^Q = (\mathbf{H}_\gamma^T)^{-1} \check{\mathbf{K}}_{45}^\tau \mathbf{H}_\gamma^{-1}, \quad (\text{B.4c})$$

$$\mathbf{H}_{21}^Q = (\check{\mathbf{k}}_{45}^C)^T \mathbf{H}_\gamma^{-1} - \mathbf{h}_Q^T \mathbf{H}_{31}^Q, \quad (\text{B.4d})$$

$$\mathbf{H}_{22}^Q = \check{A}_{55} - (\check{\mathbf{k}}_{55}^C)^T \mathbf{H}_\gamma^{-1} \mathbf{h}_Q - \mathbf{h}_Q^T \mathbf{H}_{32}^Q, \quad (\text{B.4e})$$

$$\mathbf{H}_{23}^Q = (\check{\mathbf{k}}_{55}^C)^T \mathbf{H}_\gamma^{-1} - \mathbf{h}_Q^T \mathbf{H}_{33}^Q, \quad (\text{B.4f})$$

$$\mathbf{H}_{31}^Q = (\mathbf{H}_\gamma^T)^{-1} \check{\mathbf{K}}_{45}^\tau \mathbf{H}_\gamma^{-1}, \quad (\text{B.4g})$$

$$\mathbf{H}_{32}^Q = (\mathbf{H}_\gamma^T)^{-1} (\check{\mathbf{k}}_{55}^C - \check{\mathbf{K}}_{55}^\tau \mathbf{H}_\gamma^{-1} \mathbf{h}_Q), \quad (\text{B.4h})$$

$$\mathbf{H}_{33}^Q = (\mathbf{H}_\gamma^T)^{-1} \check{\mathbf{K}}_{55}^\tau \mathbf{H}_\gamma^{-1}. \quad (\text{B.4i})$$

The matrix \mathbf{H}_ϵ yield:

$$\mathbf{H}_\varepsilon = \begin{bmatrix} \check{k}_{22}^A & \check{k}_{22}^B & \check{K}_{22}^\sigma & \check{k}_{26}^A & \check{k}_{26}^B & \check{K}_{26}^\sigma & \check{K}_{23}^\sigma \\ \check{B}_{26} & \check{B}_{26} & (\check{k}_{26}^B)^T & \check{B}_{66} & \check{D}_{66} & (\check{k}_{66}^B)^T & (\check{k}_{36}^B)^T \\ \check{k}_{26}^A & \check{k}_{26}^B & \check{K}_{26}^\sigma & \check{k}_{66}^A & \check{k}_{66}^B & \check{K}_{66}^\sigma & \check{K}_{36}^\sigma \\ \check{k}_{23}^A & \check{k}_{23}^B & (\check{K}_{23}^\sigma)^T & \check{k}_{36}^A & \check{k}_{36}^B & (\check{K}_{36}^\sigma)^T & \check{K}_{33}^\sigma \end{bmatrix} \begin{bmatrix} N_y^\varepsilon \\ M_y^\varepsilon \\ M_y^\varepsilon \\ N_{sy}^\varepsilon \\ M_{sy}^\varepsilon \\ M_{sy}^\varepsilon \\ M_z^\varepsilon \end{bmatrix}. \quad (\text{B.5})$$

Matrices \mathbf{G} and \mathbf{G}_c and vector \mathbf{g}_ε of the final differential equations are obtained from the following expressions:

$$\mathbf{G} = \mathbf{G}_1^{-1} \mathbf{G}_2, \quad \mathbf{G}_c = \mathbf{G}_1^{-1} \mathbf{G}_3, \quad \mathbf{g}_\varepsilon = \mathbf{G}_1^{-1} \mathbf{H}_\varepsilon, \quad (\text{B.6})$$

where the auxiliary matrices \mathbf{G}_1 , \mathbf{G}_2 and \mathbf{G}_3 are defined by:

$$\mathbf{G}_1 = \begin{bmatrix} H_{11}^Q - \check{K}_{23}^\sigma H_z^{-1} H_\gamma^{-1} & H_{12}^Q & H_{13}^Q & -(H_\gamma^T)^{-1} \\ H_{21}^Q - (\check{k}_{36}^B)^T H_z^{-1} H_\gamma^{-1} & H_{22}^Q & H_{23}^Q & 0 \\ H_{31}^Q - \check{K}_{36}^\sigma H_z^{-1} H_\gamma^{-1} & H_{32}^Q & H_{33}^Q & 0 \\ -\check{K}_{33}^\sigma H_z^{-1} H_\gamma^{-1} & 0 & 0 & 0 \end{bmatrix}, \quad (\text{B.7a})$$

$$\mathbf{G}_2 = \begin{bmatrix} \check{K}_{22}^\sigma & \check{k}_{26}^B & \check{K}_{26}^\sigma & 0 \\ (\check{k}_{26}^B)^T & \check{D}_{66} & (\check{k}_{66}^B)^T & 0 \\ \check{K}_{26}^\sigma & \check{k}_{66}^B & \check{K}_{66}^\sigma & 0 \\ (\check{K}_{23}^\sigma)^T & \check{k}_{36}^B & (\check{K}_{36}^\sigma)^T & H_z^T \end{bmatrix}, \quad (\text{B.7b})$$

$$\mathbf{G}_3 = \begin{bmatrix} 0 & \check{k}_{12}^A & \check{k}_{12}^B \\ 2 & \check{B}_{16} & \check{D}_{16} \\ 0 & \check{k}_{16}^A & \check{k}_{16}^B \\ 0 & \check{k}_{13}^A & \check{k}_{13}^B \end{bmatrix}. \quad (\text{B.7c})$$

B.3 Stiffness matrices for the curved laminate

The stiffness matrices \mathbf{K}_σ , \mathbf{K}_τ and $\mathbf{K}_{\varepsilon\gamma}$ are divided in terms associated to the different components of the vector of equations (4.146). These components are denominated as follows:

$$\mathbf{K}_\sigma = \begin{bmatrix} A_{11} & B_{11} & (\mathbf{k}_{11}^A)^T & A_{12} & B_{12} & (\mathbf{k}_{12}^A)^T & A_{16} & B_{16} & (\mathbf{k}_{16}^A)^T & (\mathbf{k}_{13}^A)^T \\ B_{11} & D_{11} & (\mathbf{k}_{11}^B)^T & B_{12} & D_{12} & (\mathbf{k}_{12}^B)^T & B_{16} & D_{16} & (\mathbf{k}_{16}^B)^T & (\mathbf{k}_{13}^B)^T \\ \mathbf{k}_{11}^A & \mathbf{k}_{11}^B & \mathbf{K}_{11}^\sigma & \mathbf{k}_{12}^C & \mathbf{k}_{12}^D & \mathbf{K}_{12}^\sigma & \mathbf{k}_{16}^A & \mathbf{k}_{16}^B & \mathbf{K}_{16}^\sigma & \mathbf{K}_{13}^\sigma \\ A_{12} & B_{12} & (\mathbf{k}_{12}^C)^T & A_{22} & B_{22} & (\mathbf{k}_{22}^A)^T & A_{26} & B_{26} & (\mathbf{k}_{26}^A)^T & (\mathbf{k}_{23}^A)^T \\ B_{12} & D_{12} & (\mathbf{k}_{12}^D)^T & B_{22} & D_{22} & (\mathbf{k}_{22}^B)^T & B_{26} & D_{26} & (\mathbf{k}_{26}^B)^T & (\mathbf{k}_{23}^B)^T \\ \mathbf{k}_{12}^A & \mathbf{k}_{12}^B & (\mathbf{K}_{12}^\sigma)^T & \mathbf{k}_{22}^A & \mathbf{k}_{22}^B & \mathbf{K}_{22}^\sigma & \mathbf{k}_{26}^C & \mathbf{k}_{26}^D & \mathbf{K}_{26}^\sigma & \mathbf{K}_{23}^\sigma \\ A_{16} & B_{16} & (\mathbf{k}_{16}^A)^T & A_{26} & A_{26} & (\mathbf{k}_{26}^C)^T & A_{66} & B_{66} & (\mathbf{k}_{66}^A)^T & (\mathbf{k}_{36}^A)^T \\ B_{16} & D_{16} & (\mathbf{k}_{16}^B)^T & B_{26} & B_{26} & (\mathbf{k}_{26}^D)^T & B_{66} & D_{66} & (\mathbf{k}_{66}^B)^T & (\mathbf{k}_{36}^B)^T \\ \mathbf{k}_{16}^A & \mathbf{k}_{16}^B & \mathbf{K}_{16}^\sigma & \mathbf{k}_{26}^A & \mathbf{k}_{26}^B & (\mathbf{K}_{26}^\sigma)^T & \mathbf{k}_{66}^A & \mathbf{k}_{66}^B & \mathbf{K}_{66}^\sigma & \mathbf{K}_{36}^\sigma \\ \mathbf{k}_{13}^A & \mathbf{k}_{13}^B & (\mathbf{K}_{13}^\sigma)^T & \mathbf{k}_{23}^A & \mathbf{k}_{23}^B & (\mathbf{K}_{23}^\sigma)^T & \mathbf{k}_{36}^A & \mathbf{k}_{36}^B & (\mathbf{K}_{36}^\sigma)^T & \mathbf{K}_{33}^\sigma \end{bmatrix}, \quad (\text{B.8a})$$

$$\mathbf{K}_\tau = \begin{bmatrix} A_{44} & (\mathbf{k}_{44}^F)^T & A_{45} & (\mathbf{k}_{45}^F)^T \\ \mathbf{k}_{44}^F & \mathbf{K}_{44}^\tau & \mathbf{k}_{45}^F & \mathbf{K}_{45}^\tau \\ A_{45} & (\mathbf{k}_{45}^F)^T & A_{55} & (\mathbf{k}_{55}^F)^T \\ \mathbf{k}_{45}^F & \mathbf{K}_{45}^\tau & \mathbf{k}_{55}^F & \mathbf{K}_{55}^\tau \end{bmatrix}, \quad (\text{B.8b})$$

$$\mathbf{K}_{\varepsilon\gamma} = \begin{bmatrix} A_{11}^\varepsilon & A_{16}^\gamma \\ B_{11}^\varepsilon & B_{16}^\gamma \\ \mathbf{k}_{11}^\varepsilon & \mathbf{k}_{16}^\gamma \\ A_{12}^\varepsilon & A_{26}^\gamma \\ B_{12}^\varepsilon & B_{26}^\gamma \\ \mathbf{k}_{12}^\varepsilon & \mathbf{k}_{26}^\gamma \\ A_{16}^\varepsilon & A_{66}^\gamma \\ B_{16}^\varepsilon & B_{66}^\gamma \\ \mathbf{k}_{16}^\varepsilon & \mathbf{k}_{66}^\gamma \\ \mathbf{k}_{13}^\varepsilon & \mathbf{k}_{36}^\gamma \end{bmatrix}. \quad (\text{B.8c})$$

The components of the stiffness matrix \mathbf{K}_σ , shown in equations (B.8), are calculated from the following expressions:

$$A_{11} = \sum_{p=1}^{N_p} \left(\bar{C}_{11}^p \int_{z_p^-}^{z_p^+} \frac{R}{z+R} dz \right), \quad A_{12} = \sum_{p=1}^{N_p} \left(\bar{C}_{12}^p \int_{z_p^-}^{z_p^+} dz \right), \quad (\text{B.9a})$$

$$A_{16} = \sum_{p=1}^{N_p} \left(\bar{C}_{16}^p \int_{z_p^-}^{z_p^+} dz \right), \quad A_{22} = \sum_{p=1}^{N_p} \left(\bar{C}_{22}^p \int_{z_p^-}^{z_p^+} \frac{z+R}{R} dz \right), \quad (\text{B.9b})$$

$$A_{26} = \sum_{p=1}^{N_p} \left(\bar{C}_{16}^p \int_{z_p^-}^{z_p^+} \frac{z+R}{R} dz \right), \quad A_{66} = \sum_{p=1}^{N_p} \left(\bar{C}_{66}^p \int_{z_p^-}^{z_p^+} \frac{z+R}{R} dz \right), \quad (\text{B.9c})$$

$$B_{11} = \sum_{p=1}^{N_p} \left(\bar{C}_{11}^p \int_{z_p^-}^{z_p^+} \frac{R}{z+R} z dz \right), \quad B_{12} = \sum_{p=1}^{N_p} \left(\bar{C}_{12}^p \int_{z_p^-}^{z_p^+} z dz \right), \quad (\text{B.10a})$$

$$B_{16} = \sum_{p=1}^{N_p} \left(\bar{C}_{16}^p \int_{z_p^-}^{z_p^+} z dz \right), \quad B_{22} = \sum_{p=1}^{N_p} \left(\bar{C}_{22}^p \int_{z_p^-}^{z_p^+} \frac{z+R}{R} z dz \right), \quad (\text{B.10b})$$

$$B_{26} = \sum_{p=1}^{N_p} \left(\bar{C}_{16}^p \int_{z_p^-}^{z_p^+} \frac{z+R}{R} z dz \right), \quad B_{66} = \sum_{p=1}^{N_p} \left(\bar{C}_{66}^p \int_{z_p^-}^{z_p^+} \frac{z+R}{R} z dz \right), \quad (\text{B.10c})$$

$$D_{11} = \sum_{p=1}^{N_p} \left(\bar{C}_{11}^p \int_{z_p^-}^{z_p^+} \frac{R}{z+R} z^2 dz \right), \quad D_{12} = \sum_{p=1}^{N_p} \left(\bar{C}_{12}^p \int_{z_p^-}^{z_p^+} z^2 dz \right), \quad (\text{B.11a})$$

$$D_{16} = \sum_{p=1}^{N_p} \left(\bar{C}_{16}^p \int_{z_p^-}^{z_p^+} z^2 dz \right), \quad D_{22} = \sum_{p=1}^{N_p} \left(\bar{C}_{22}^p \int_{z_p^-}^{z_p^+} \frac{z+R}{R} z^2 dz \right), \quad (\text{B.11b})$$

$$D_{26} = \sum_{p=1}^{N_p} \left(\bar{C}_{16}^p \int_{z_p^-}^{z_p^+} \frac{z+R}{R} z^2 dz \right), \quad D_{66} = \sum_{p=1}^{N_p} \left(\bar{C}_{66}^p \int_{z_p^-}^{z_p^+} \frac{z+R}{R} z^2 dz \right), \quad (\text{B.11c})$$

$$\mathbf{k}_{11}^A = \sum_{p=1}^{N_p} \left(\bar{C}_{11}^p \int_{z_p^-}^{z_p^+} \frac{R}{z+R} \mathbf{f}_s(z) dz \right), \quad (\text{B.12a})$$

$$\mathbf{k}_{12}^A = \sum_{p=1}^{N_p} \left(\bar{C}_{12}^p \int_{z_p^-}^{z_p^+} \mathbf{f}_y(z) dz \right), \quad \mathbf{k}_{12}^C = \sum_{p=1}^{N_p} \left(\bar{C}_{12}^p \int_{z_p^-}^{z_p^+} \mathbf{f}_s(z) dz \right), \quad (\text{B.12b})$$

$$\mathbf{k}_{16}^A = \sum_{p=1}^{N_p} \left(\bar{C}_{16}^p \int_{z_p^-}^{z_p^+} \mathbf{f}_s(z) dz \right), \quad \mathbf{k}_{13}^A = \sum_{p=1}^{N_p} \left(\bar{C}_{13}^p \int_{z_p^-}^{z_p^+} \frac{z+R}{R} \hat{\mathbf{f}}_s(z) dz \right), \quad (\text{B.12c})$$

$$\mathbf{k}_{22}^A = \sum_{p=1}^{N_p} \left(\bar{C}_{22}^p \int_{z_p^-}^{z_p^+} \frac{z+R}{R} \mathbf{f}_y(z) dz \right), \quad (\text{B.12d})$$

$$\mathbf{k}_{26}^A = \sum_{p=1}^{N_p} \left(\bar{C}_{26}^p \int_{z_p^-}^{z_p^+} \frac{z+R}{R} \mathbf{f}_s(z) dz \right), \quad (\text{B.12e})$$

$$\mathbf{k}_{26}^C = \sum_{p=1}^{N_p} \left(\bar{C}_{26}^p \int_{z_p^-}^{z_p^+} \frac{z+R}{R} \mathbf{f}_y(z) dz \right), \quad (\text{B.12f})$$

$$\mathbf{k}_{23}^A = \sum_{p=1}^{N_p} \left(\bar{C}_{23}^p \int_{z_p^-}^{z_p^+} \left(\frac{z+R}{R} \right)^2 \hat{\mathbf{f}}_s(z) dz \right), \quad (\text{B.12g})$$

$$\mathbf{k}_{66}^A = \sum_{p=1}^{N_p} \left(\bar{C}_{66}^p \int_{z_p^-}^{z_p^+} \frac{z+R}{R} \mathbf{f}_s(z) dz \right), \quad (\text{B.12h})$$

$$\mathbf{k}_{36}^A = \sum_{p=1}^{N_p} \left(\bar{C}_{36}^p \int_{z_p^-}^{z_p^+} \left(\frac{z+R}{R} \right)^2 \hat{\mathbf{f}}_s(z) dz \right), \quad (\text{B.12i})$$

$$\mathbf{k}_{11}^B = \sum_{p=1}^{N_p} \left(\bar{C}_{11}^p \int_{z_p^-}^{z_p^+} \frac{R}{z+R} \mathbf{f}_s(z) z dz \right), \quad (\text{B.13a})$$

$$\mathbf{k}_{12}^B = \sum_{p=1}^{N_p} \left(\bar{C}_{12}^p \int_{z_p^-}^{z_p^+} \mathbf{f}_y(z) z dz \right), \quad \mathbf{k}_{12}^D = \sum_{p=1}^{N_p} \left(\bar{C}_{12}^p \int_{z_p^-}^{z_p^+} \mathbf{f}_s(z) z dz \right), \quad (\text{B.13b})$$

$$\mathbf{k}_{16}^B = \sum_{p=1}^{N_p} \left(\bar{C}_{16}^p \int_{z_p^-}^{z_p^+} \mathbf{f}_s(z) z dz \right), \quad \mathbf{k}_{13}^B = \sum_{p=1}^{N_p} \left(\bar{C}_{13}^p \int_{z_p^-}^{z_p^+} \frac{z+R}{R} \hat{\mathbf{f}}_s(z) z dz \right), \quad (\text{B.13c})$$

$$\mathbf{k}_{22}^B = \sum_{p=1}^{N_p} \left(\bar{C}_{22}^p \int_{z_p^-}^{z_p^+} \frac{z+R}{R} \mathbf{f}_y(z) z dz \right), \quad (\text{B.13d})$$

$$\mathbf{k}_{26}^B = \sum_{p=1}^{N_p} \left(\bar{C}_{26}^p \int_{z_p^-}^{z_p^+} \frac{z+R}{R} \mathbf{f}_s(z) z dz \right), \quad (\text{B.13e})$$

$$\mathbf{k}_{26}^D = \sum_{p=1}^{N_p} \left(\bar{C}_{26}^p \int_{z_p^-}^{z_p^+} \frac{z+R}{R} \mathbf{f}_y(z) z dz \right), \quad (\text{B.13f})$$

$$\mathbf{k}_{23}^B = \sum_{p=1}^{N_p} \left(\bar{C}_{23}^p \int_{z_p^-}^{z_p^+} \left(\frac{z+R}{R} \right)^2 \hat{\mathbf{f}}_s(z) z dz \right), \quad (\text{B.13g})$$

$$\mathbf{k}_{66}^B = \sum_{p=1}^{N_p} \left(\bar{C}_{66}^p \int_{z_p^-}^{z_p^+} \frac{z+R}{R} \mathbf{f}_s(z) z dz \right), \quad (\text{B.13h})$$

$$\mathbf{k}_{36}^B = \sum_{p=1}^{N_p} \left(\bar{C}_{36}^p \int_{z_p^-}^{z_p^+} \left(\frac{z+R}{R} \right)^2 \hat{\mathbf{f}}_s(z) z dz \right), \quad (\text{B.13i})$$

$$\mathbf{K}_{11}^{\sigma} = \sum_{p=1}^{N_p} \left(\bar{C}_{11}^p \int_{z_p^-}^{z_p^+} \frac{R}{z+R} \mathbf{f}_s(z) \mathbf{f}_s^T(z) dz \right), \quad (\text{B.14a})$$

$$\mathbf{K}_{12}^{\sigma} = \sum_{p=1}^{N_p} \left(\bar{C}_{12}^p \int_{z_p^-}^{z_p^+} \mathbf{f}_s(z) \mathbf{f}_y^T(z) dz \right), \quad (\text{B.14b})$$

$$\mathbf{K}_{16}^{\sigma} = \sum_{p=1}^{N_p} \left(\bar{C}_{16}^p \int_{z_p^-}^{z_p^+} \mathbf{f}_s(z) \mathbf{f}_s^T(z) dz \right), \quad (\text{B.14c})$$

$$\mathbf{K}_{13}^{\sigma} = \sum_{p=1}^{N_p} \left(\bar{C}_{13}^p \int_{z_p^-}^{z_p^+} \frac{z+R}{R} \mathbf{f}_s(z) \hat{\mathbf{f}}_s^T(z) dz \right), \quad (\text{B.14d})$$

$$\mathbf{K}_{22}^{\sigma} = \sum_{p=1}^{N_p} \left(\bar{C}_{22}^p \int_{z_p^-}^{z_p^+} \frac{z+R}{R} \mathbf{f}_y(z) \mathbf{f}_y^T(z) dz \right), \quad (\text{B.14e})$$

$$\mathbf{K}_{26}^{\sigma} = \sum_{p=1}^{N_p} \left(\bar{C}_{26}^p \int_{z_p^-}^{z_p^+} \frac{z+R}{R} \mathbf{f}_y(z) \mathbf{f}_s^T(z) dz \right), \quad (\text{B.14f})$$

$$\mathbf{K}_{23}^{\sigma} = \sum_{p=1}^{N_p} \left(\bar{C}_{23}^p \int_{z_p^-}^{z_p^+} \left(\frac{z+R}{R} \right)^2 \mathbf{f}_s(z) \hat{\mathbf{f}}_s^T(z) dz \right), \quad (\text{B.14g})$$

$$\mathbf{K}_{66}^{\sigma} = \sum_{p=1}^{N_p} \left(\bar{C}_{66}^p \int_{z_p^-}^{z_p^+} \frac{z+R}{R} \mathbf{f}_s(z) \mathbf{f}_s^T(z) dz \right), \quad (\text{B.14h})$$

$$\mathbf{K}_{36}^{\sigma} = \sum_{p=1}^{N_p} \left(\bar{C}_{36}^p \int_{z_p^-}^{z_p^+} \left(\frac{z+R}{R} \right)^2 \mathbf{f}_s(z) \hat{\mathbf{f}}_s^T(z) dz \right), \quad (\text{B.14i})$$

$$\mathbf{K}_{33}^{\sigma} = \sum_{p=1}^{N_p} \left(\bar{C}_{33}^p \int_{z_p^-}^{z_p^+} \left(\frac{z+R}{R} \right)^3 \hat{\mathbf{f}}_s(z) \hat{\mathbf{f}}_s^T(z) dz \right), \quad (\text{B.14j})$$

The components of the stiffness matrix \mathbf{K}_{τ} , shown in equations (B.8), are calculated from the following expressions:

$$A_{44} = \sum_{p=1}^{N_p} \left(\bar{C}_{44}^p \int_{z_p^-}^{z_p^+} \frac{z+R}{R} dz \right), \quad A_{45} = \sum_{p=1}^{N_p} \left(\bar{C}_{45}^p \int_{z_p^-}^{z_p^+} dz \right), \quad (\text{B.15a})$$

$$A_{55} = \sum_{p=1}^{N_p} \left(\bar{C}_{55}^p \int_{z_p^-}^{z_p^+} \frac{R}{z+R} dz \right), \quad (\text{B.15b})$$

$$\mathbf{k}_{44}^F = \sum_{p=1}^{N_p} \left(\bar{C}_{44}^p \int_{z_p^-}^{z_p^+} \frac{z+R}{R} \mathbf{f}_z(z) dz \right), \quad \mathbf{k}_{45}^F = \sum_{p=1}^{N_p} \left(\bar{C}_{45}^p \int_{z_p^-}^{z_p^+} \mathbf{f}_z(z) dz \right), \quad (\text{B.16a})$$

$$\mathbf{k}_{55}^F = \sum_{p=1}^{N_p} \left(\bar{C}_{55}^p \int_{z_p^-}^{z_p^+} \frac{R}{z+R} \mathbf{f}_z(z) dz \right), \quad (\text{B.16b})$$

$$\mathbf{K}_{44}^\tau = \sum_{p=1}^{N_p} \left(\bar{C}_{44}^p \int_{z_p^-}^{z_p^+} \frac{z+R}{R} \mathbf{f}_z(z) \mathbf{f}_z^T(z) dz \right), \quad (\text{B.17a})$$

$$\mathbf{K}_{45}^\tau = \sum_{p=1}^{N_p} \left(\bar{C}_{45}^p \int_{z_p^-}^{z_p^+} \mathbf{f}_z(z) \mathbf{f}_z^T(z) dz \right), \quad (\text{B.17b})$$

$$\mathbf{K}_{55}^\tau = \sum_{p=1}^{N_p} \left(\bar{C}_{55}^p \int_{z_p^-}^{z_p^+} \frac{R}{z+R} \mathbf{f}_z(z) \mathbf{f}_z^T(z) dz \right). \quad (\text{B.17c})$$

The components of the stiffness matrix $\mathbf{K}_{\varepsilon\gamma}$, shown in equations (B.8), are calculated from the following expressions:

$$A_{11}^\varepsilon = \sum_{p=1}^{N_p} \left(\bar{C}_{11}^p \int_{z_p^-}^{z_p^+} dz \right), \quad A_{16}^\gamma = \sum_{p=1}^{N_p} \left(\bar{C}_{16}^p \int_{z_p^-}^{z_p^+} \frac{R}{z+R} dz \right), \quad (\text{B.18a})$$

$$A_{12}^\varepsilon = \sum_{p=1}^{N_p} \left(\bar{C}_{12}^p \int_{z_p^-}^{z_p^+} \frac{z+R}{R} dz \right), \quad A_{26}^\gamma = \sum_{p=1}^{N_p} \left(\bar{C}_{26}^p \int_{z_p^-}^{z_p^+} dz \right), \quad (\text{B.18b})$$

$$A_{16}^\varepsilon = \sum_{p=1}^{N_p} \left(\bar{C}_{16}^p \int_{z_p^-}^{z_p^+} \frac{z+R}{R} dz \right), \quad A_{66}^\gamma = \sum_{p=1}^{N_p} \left(\bar{C}_{66}^p \int_{z_p^-}^{z_p^+} dz \right), \quad (\text{B.18c})$$

$$B_{11}^\varepsilon = \sum_{p=1}^{N_p} \left(\bar{C}_{11}^p \int_{z_p^-}^{z_p^+} z dz \right), \quad B_{16}^\gamma = \sum_{p=1}^{N_p} \left(\bar{C}_{16}^p \int_{z_p^-}^{z_p^+} \frac{R}{z+R} z dz \right), \quad (\text{B.19a})$$

$$B_{12}^\varepsilon = \sum_{p=1}^{N_p} \left(\bar{C}_{12}^p \int_{z_p^-}^{z_p^+} \frac{z+R}{R} z dz \right), \quad B_{26}^\gamma = \sum_{p=1}^{N_p} \left(\bar{C}_{26}^p \int_{z_p^-}^{z_p^+} z dz \right), \quad (\text{B.19b})$$

$$B_{16}^\varepsilon = \sum_{p=1}^{N_p} \left(\bar{C}_{16}^p \int_{z_p^-}^{z_p^+} \frac{z+R}{R} z dz \right), \quad B_{66}^\gamma = \sum_{p=1}^{N_p} \left(\bar{C}_{66}^p \int_{z_p^-}^{z_p^+} z dz \right), \quad (\text{B.19c})$$

$$\mathbf{k}_{11}^\varepsilon = \sum_{p=1}^{N_p} \left(\bar{C}_{11}^p \int_{z_p^-}^{z_p^+} \mathbf{f}_s(z) dz \right), \quad (\text{B.20a})$$

$$\mathbf{k}_{16}^\gamma = \sum_{p=1}^{N_p} \left(\bar{C}_{16}^p \int_{z_p^-}^{z_p^+} \frac{R}{z+R} \mathbf{f}_s(z) dz \right), \quad (\text{B.20b})$$

$$\mathbf{k}_{12}^\varepsilon = \sum_{p=1}^{N_p} \left(\bar{C}_{12}^p \int_{z_p^-}^{z_p^+} \frac{z+R}{R} \mathbf{f}_y(z) dz \right), \quad (\text{B.20c})$$

$$\mathbf{k}_{26}^\gamma = \sum_{p=1}^{N_p} \left(\bar{C}_{26}^p \int_{z_p^-}^{z_p^+} \mathbf{f}_y(z) dz \right), \quad (\text{B.20d})$$

$$\mathbf{k}_{16}^\varepsilon = \sum_{p=1}^{N_p} \left(\bar{C}_{16}^p \int_{z_p^-}^{z_p^+} \frac{z+R}{R} \mathbf{f}_s(z) dz \right), \quad (\text{B.20e})$$

$$\mathbf{k}_{66}^\gamma = \sum_{p=1}^{N_p} \left(\bar{C}_{66}^p \int_{z_p^-}^{z_p^+} \mathbf{f}_s(z) dz \right), \quad (\text{B.20f})$$

$$\mathbf{k}_{13}^\varepsilon = \sum_{p=1}^{N_p} \left(\bar{C}_{13}^p \int_{z_p^-}^{z_p^+} \left(\frac{z+R}{R} \right)^2 \hat{\mathbf{f}}_s(z) dz \right), \quad (\text{B.20g})$$

$$\mathbf{k}_{36}^\gamma = \sum_{p=1}^{N_p} \left(\bar{C}_{36}^p \int_{z_p^-}^{z_p^+} \frac{z+R}{R} \hat{\mathbf{f}}_s(z) dz \right). \quad (\text{B.20h})$$

B.4 Auxiliary matrices for the curved laminate

The auxiliary matrices employed in Chapter 4 in the development of the non-regularized model for the curved laminates are defined as follows:

$$H_{00}^Q = \check{A}_{44} - (\check{\mathbf{k}}_{44}^C)^T \mathbf{H}_\gamma^{-1} \mathbf{h}_Q - \mathbf{h}_Q^T \mathbf{H}_{10}^Q, \quad (\text{B.21a})$$

$$\mathbf{H}_{01}^Q = (\check{\mathbf{k}}_{44}^C)^T \mathbf{H}_\gamma^{-1} - \mathbf{h}_Q^T \mathbf{H}_{11}^Q, \quad (\text{B.21b})$$

$$H_{02}^Q = \check{A}_{45} - (\check{\mathbf{k}}_{45}^C)^T \mathbf{H}_\gamma^{-1} \mathbf{h}_Q - \mathbf{h}_Q^T \mathbf{H}_{12}^Q, \quad (\text{B.21c})$$

$$\mathbf{H}_{03}^Q = (\check{\mathbf{k}}_{45}^C)^T \mathbf{H}_\gamma^{-1} - \mathbf{h}_Q^T \mathbf{H}_{13}^Q, \quad (\text{B.21d})$$

$$\mathbf{H}_{10}^Q = (\mathbf{H}_\gamma^T)^{-1} (\check{\mathbf{k}}_{44}^C - \check{\mathbf{K}}_{44}^\tau \mathbf{H}_\gamma^{-1} \mathbf{h}_Q), \quad (\text{B.21e})$$

$$\mathbf{H}_{11}^Q = (\mathbf{H}_\gamma^T)^{-1} \check{\mathbf{K}}_{44}^\tau \mathbf{H}_\gamma^{-1}, \quad (\text{B.21f})$$

$$\mathbf{H}_{12}^Q = (\mathbf{H}_\gamma^T)^{-1} (\check{\mathbf{k}}_{45}^C - \check{\mathbf{K}}_{45}^\tau \mathbf{H}_\gamma^{-1} \mathbf{h}_Q), \quad (\text{B.21g})$$

$$\mathbf{H}_{13}^Q = (\mathbf{H}_\gamma^T)^{-1} \check{\mathbf{K}}_{45}^\tau \mathbf{H}_\gamma^{-1}, \quad (\text{B.21h})$$

$$\mathbf{H}_{20}^Q = \check{A}_{45} - (\check{\mathbf{k}}_{45}^C)^T \mathbf{H}_\gamma^{-1} \mathbf{h}_Q - \mathbf{h}_Q^T \mathbf{H}_{30}^Q, \quad (\text{B.21i})$$

$$\mathbf{H}_{21}^Q = (\check{\mathbf{k}}_{45}^C)^T \mathbf{H}_\gamma^{-1} - \mathbf{h}_Q^T \mathbf{H}_{31}^Q, \quad (\text{B.21j})$$

$$\mathbf{H}_{22}^Q = \check{A}_{55} - (\check{\mathbf{k}}_{55}^C)^T \mathbf{H}_\gamma^{-1} \mathbf{h}_Q - \mathbf{h}_Q^T \mathbf{H}_{32}^Q, \quad (\text{B.21k})$$

$$\mathbf{H}_{23}^Q = (\check{\mathbf{k}}_{55}^C)^T \mathbf{H}_\gamma^{-1} - \mathbf{h}_Q^T \mathbf{H}_{33}^Q, \quad (\text{B.21l})$$

$$\mathbf{H}_{30}^Q = (\mathbf{H}_\gamma^T)^{-1} (\check{\mathbf{k}}_{45}^C - \check{\mathbf{K}}_{45}^\tau \mathbf{H}_\gamma^{-1} \mathbf{h}_Q), \quad (\text{B.21m})$$

$$\mathbf{H}_{31}^Q = (\mathbf{H}_\gamma^T)^{-1} \check{\mathbf{K}}_{45}^\tau \mathbf{H}_\gamma^{-1}, \quad (\text{B.21n})$$

$$\mathbf{H}_{32}^Q = (\mathbf{H}_\gamma^T)^{-1} (\check{\mathbf{k}}_{55}^C - \check{\mathbf{K}}_{55}^\tau \mathbf{H}_\gamma^{-1} \mathbf{h}_Q), \quad (\text{B.21o})$$

$$\mathbf{H}_{33}^Q = (\mathbf{H}_\gamma^T)^{-1} \check{\mathbf{K}}_{55}^\tau \mathbf{H}_\gamma^{-1}. \quad (\text{B.21p})$$

The matrix $\check{\mathbf{K}}_A$ yield:

$$\check{\mathbf{K}}_A = \begin{bmatrix} \check{K}_{11}^A & \check{K}_{12}^A & \check{K}_{13}^A & \check{K}_{14}^A & \check{K}_{15}^A & \check{K}_{16}^A & \check{K}_{17}^A & \check{K}_{18}^A \\ \check{K}_{21}^A & \check{K}_{22}^A & \check{K}_{23}^A & \check{K}_{24}^A & \check{K}_{25}^A & \check{K}_{26}^A & \check{K}_{27}^A & \check{K}_{28}^A \\ \check{K}_{31}^A & \check{K}_{32}^A & \check{K}_{33}^A & \check{K}_{34}^A & \check{K}_{35}^A & \check{K}_{36}^A & \check{K}_{37}^A & \check{K}_{38}^A \\ \check{K}_{41}^A & \check{K}_{42}^A & \check{K}_{43}^A & \check{K}_{44}^A & \check{K}_{45}^A & \check{K}_{46}^A & \check{K}_{47}^A & \check{K}_{48}^A \\ \check{K}_{51}^A & \check{K}_{52}^A & \check{K}_{53}^A & \check{K}_{54}^A & \check{K}_{55}^A & \check{K}_{56}^A & \check{K}_{57}^A & \check{K}_{58}^A \\ \check{K}_{61}^A & \check{K}_{62}^A & \check{K}_{63}^A & \check{K}_{64}^A & \check{K}_{65}^A & \check{K}_{66}^A & \check{K}_{67}^A & \check{K}_{68}^A \\ \check{K}_{71}^A & \check{K}_{72}^A & \check{K}_{73}^A & \check{K}_{74}^A & \check{K}_{75}^A & \check{K}_{76}^A & \check{K}_{77}^A & \check{K}_{78}^A \\ \check{K}_{81}^A & \check{K}_{82}^A & \check{K}_{83}^A & \check{K}_{84}^A & \check{K}_{85}^A & \check{K}_{86}^A & \check{K}_{87}^A & \check{K}_{88}^A \\ \check{K}_{91}^A & \check{K}_{92}^A & \check{K}_{93}^A & \check{K}_{94}^A & \check{K}_{95}^A & \check{K}_{96}^A & \check{K}_{97}^A & \check{K}_{98}^A \\ \check{K}_{z1}^A & \check{K}_{z2}^A & \check{K}_{z3}^A & \check{K}_{z4}^A & \check{K}_{z5}^A & \check{K}_{z6}^A & \check{K}_{z7}^A & \check{K}_{z8}^A \end{bmatrix}, \quad (\text{B.22})$$

where the columns of $\check{\mathbf{K}}_A$ are defined from the columns of \mathbf{K}_σ as follows:

$$\begin{bmatrix} \check{K}_{11}^A \\ \check{K}_{21}^A \\ \vdots \\ \check{K}_{z1}^A \end{bmatrix} = \begin{bmatrix} \check{B}_{11} \\ \check{D}_{11} \\ \vdots \\ \check{\mathbf{k}}_{13}^B \end{bmatrix} - \begin{bmatrix} (\check{\mathbf{k}}_{13}^A)^T \\ (\check{\mathbf{k}}_{13}^B)^T \\ \vdots \\ \check{\mathbf{K}}_{33}^\sigma \end{bmatrix} \mathbf{H}_z^{-1} \mathbf{h}_M, \quad (\text{B.23a})$$

$$\begin{bmatrix} \check{K}_{12}^A \\ \check{K}_{22}^A \\ \vdots \\ \check{K}_{z2}^A \end{bmatrix} = \begin{bmatrix} (\check{k}_{11}^A)^T \\ (\check{k}_{11}^B)^T \\ \vdots \\ (\check{K}_{13}^\sigma)^T \end{bmatrix} - \begin{bmatrix} (\check{k}_{13}^A)^T \\ (\check{k}_{13}^B)^T \\ \vdots \\ \check{K}_{33}^\sigma \end{bmatrix} \mathbf{H}_z^{-1} \mathbf{H}_s, \quad (\text{B.23b})$$

$$\begin{bmatrix} \check{K}_{13}^A \\ \check{K}_{23}^A \\ \vdots \\ \check{K}_{z3}^A \end{bmatrix} = R \begin{bmatrix} \check{A}_{11} \\ \check{B}_{11} \\ \vdots \\ \check{k}_{13}^A \end{bmatrix} - \begin{bmatrix} (\check{k}_{13}^A)^T \\ (\check{k}_{13}^B)^T \\ \vdots \\ \check{K}_{33}^\sigma \end{bmatrix} \mathbf{H}_z^{-1} (\mathbf{H}_\gamma^{-1} \mathbf{h}_Q + R \mathbf{h}_N), \quad (\text{B.23c})$$

$$\begin{bmatrix} \check{K}_{14}^A \\ \check{K}_{24}^A \\ \vdots \\ \check{K}_{z4}^A \end{bmatrix} = \begin{bmatrix} \check{B}_{12} \\ \check{D}_{12} \\ \vdots \\ \check{k}_{23}^B \end{bmatrix}, \quad \begin{bmatrix} \check{K}_{15}^A \\ \check{K}_{25}^A \\ \vdots \\ \check{K}_{z5}^A \end{bmatrix} = \begin{bmatrix} (\check{k}_{13}^A)^T \\ (\check{k}_{13}^B)^T \\ \vdots \\ \check{K}_{33}^\sigma \end{bmatrix} \mathbf{H}_z^{-1} \mathbf{H}_\gamma^{-1}, \quad (\text{B.23d})$$

$$\begin{bmatrix} \check{K}_{16}^A \\ \check{K}_{26}^A \\ \vdots \\ \check{K}_{z6}^A \end{bmatrix} = \begin{bmatrix} (\check{k}_{12}^A)^T \\ (\check{k}_{12}^B)^T \\ \vdots \\ (\check{K}_{23}^\sigma)^T \end{bmatrix}, \quad \begin{bmatrix} \check{K}_{17}^A \\ \check{K}_{27}^A \\ \vdots \\ \check{K}_{z7}^A \end{bmatrix} = \begin{bmatrix} \check{B}_{16} \\ \check{D}_{16} \\ \vdots \\ \check{k}_{36}^B \end{bmatrix} - \frac{1}{R} \begin{bmatrix} \check{A}_{16} \\ \check{B}_{16} \\ \vdots \\ \check{k}_{36}^A \end{bmatrix}, \quad (\text{B.23e})$$

$$\begin{bmatrix} \check{K}_{18}^A \\ \check{K}_{28}^A \\ \vdots \\ \check{K}_{z8}^A \end{bmatrix} = \begin{bmatrix} (\check{k}_{16}^A)^T \\ (\check{k}_{16}^B)^T \\ \vdots \\ (\check{K}_{36}^\sigma)^T \end{bmatrix}, \quad (\text{B.23f})$$

The matrices \check{K}_B and \check{K}_C and the vector \check{K}_D are obtained by the following equations:

$$\begin{aligned} \check{K}_B &= \begin{bmatrix} \check{K}_{11}^B & \check{K}_{12}^B & \check{K}_{13}^B & \check{K}_{14}^B & \check{K}_{15}^B & \check{K}_{16}^B & \check{K}_{17}^B \\ \check{K}_{21}^B & \check{K}_{22}^B & \check{K}_{23}^B & \check{K}_{24}^B & \check{K}_{25}^B & \check{K}_{26}^B & \check{K}_{27}^B \end{bmatrix} = \\ &- \begin{bmatrix} \check{K}_{21}^A & \check{K}_{32}^A \\ \check{K}_{31}^A & \check{K}_{32}^A \end{bmatrix}^{-1} \begin{bmatrix} \check{K}_{23}^A & \check{K}_{24}^A & \check{K}_{25}^A & \check{K}_{26}^A & \check{K}_{27}^A & \check{K}_{28}^A \\ \check{K}_{33}^A & \check{K}_{34}^A & \check{K}_{35}^A & \check{K}_{36}^A & \check{K}_{37}^A & \check{K}_{38}^A \end{bmatrix} \begin{bmatrix} -\mathbf{h}_M^T \\ -\mathbf{H}_s^T \end{bmatrix}, \end{aligned} \quad (\text{B.24a})$$

$$\check{K}_C = \begin{bmatrix} K_{11}^C & K_{12}^C \\ K_{21}^C & K_{22}^C \end{bmatrix} = - \begin{bmatrix} \check{K}_{21}^A & \check{K}_{22}^A \\ \check{K}_{31}^A & \check{K}_{32}^A \end{bmatrix}^{-1} \begin{bmatrix} B_{11}^\varepsilon & B_{16}^\gamma \\ k_{11}^\varepsilon & k_{16}^\gamma \end{bmatrix}, \quad (\text{B.24b})$$

$$\check{K}_D = \begin{bmatrix} \check{K}_1^D \\ \check{K}_2^D \end{bmatrix} = \begin{bmatrix} \check{K}_{21}^A & \check{K}_{22}^A \\ \check{K}_{31}^A & \check{K}_{32}^A \end{bmatrix}^{-1} \begin{bmatrix} \check{k}_2^\varepsilon \\ \check{k}_3^\varepsilon \end{bmatrix}, \quad (\text{B.24c})$$

where the components \check{k}_i^ε , $i = 1, 2, \dots, 9, z$, are defined in equation (4.149).

Finally, matrices \mathbf{G} and \mathbf{G}_c and vector \mathbf{g}_ε are defined by the following expressions:

$$\mathbf{G} = \mathbf{G}_A^{-1} \mathbf{G}_B, \quad \mathbf{G}_c = \mathbf{G}_A^{-1} \mathbf{G}_C, \quad \mathbf{g}_\varepsilon = \mathbf{G}_A^{-1} \mathbf{H}_\varepsilon, \quad (\text{B.25})$$

where the auxiliary matrices \mathbf{G}_A , \mathbf{G}_B and \mathbf{G}_C and the auxiliary vector \mathbf{H}_ε are defined by the following expressions:

$$\mathbf{G}_A = \begin{bmatrix} G_{11}^A & G_{12}^A & G_{13}^A & G_{14}^A & G_{15}^A & G_{16}^A \\ G_{21}^A & G_{22}^A & G_{23}^A & G_{24}^A & G_{25}^A & G_{26}^A \\ G_{31}^A & G_{32}^A & G_{33}^A & G_{34}^A & G_{35}^A & G_{36}^A \\ G_{41}^A & G_{42}^A & G_{43}^A & G_{44}^A & G_{45}^A & G_{46}^A \\ G_{51}^A & G_{52}^A & G_{53}^A & G_{54}^A & G_{55}^A & G_{56}^A \\ G_{61}^A & G_{62}^A & G_{63}^A & G_{64}^A & G_{65}^A & G_{66}^A \end{bmatrix}, \quad (\text{B.26a})$$

$$\mathbf{G}_B = \begin{bmatrix} G_{11}^B & G_{12}^B & G_{13}^B & G_{14}^B & G_{15}^B & G_{16}^B \\ G_{21}^B & G_{22}^B & G_{23}^B & G_{24}^B & G_{25}^B & G_{26}^B \\ G_{31}^B & G_{32}^B & G_{33}^B & G_{34}^B & G_{35}^B & G_{36}^B \\ G_{41}^B & G_{42}^B & G_{43}^B & G_{44}^B & G_{45}^B & G_{46}^B \\ G_{51}^B & G_{52}^B & G_{53}^B & G_{54}^B & G_{55}^B & G_{56}^B \\ G_{61}^B & G_{62}^B & G_{63}^B & G_{64}^B & G_{65}^B & G_{66}^B \end{bmatrix}, \quad (\text{B.26b})$$

$$\mathbf{G}_C = \begin{bmatrix} G_{11}^C & G_{12}^C \\ G_{21}^C & G_{22}^C \\ G_{31}^C & G_{32}^C \\ G_{41}^C & G_{42}^C \\ G_{51}^C & G_{52}^C \\ G_{61}^C & G_{62}^C \end{bmatrix}, \quad \mathbf{H}_\varepsilon = \begin{bmatrix} H_1^\varepsilon \\ H_2^\varepsilon \\ H_3^\varepsilon \\ H_4^\varepsilon \\ H_5^\varepsilon \\ H_6^\varepsilon \end{bmatrix}, \quad (\text{B.26c})$$

the components of matrix \mathbf{G}_A yielding:

$$G_{11}^A = H_{00}^Q - \check{K}_{53}^A - \check{K}_{51}^A \check{K}_{11}^B - \check{K}_{52}^A \check{K}_{21}^B, \quad (\text{B.27a})$$

$$G_{12}^A = H_{01}^Q - \check{K}_{55}^A - \check{K}_{51}^A \check{K}_{13}^B - \check{K}_{52}^A \check{K}_{23}^B, \quad (\text{B.27b})$$

$$G_{13}^A = H_{02}^Q, \quad G_{14}^A = H_{03}^Q, \quad G_{15}^A = -1, \quad G_{16}^A = h_Q^T (\mathbf{H}_\gamma^T)^{-1}, \quad (\text{B.27c})$$

$$G_{21}^A = H_{10}^Q - \check{K}_{63}^A - \check{K}_{61}^A \check{K}_{11}^B - \check{K}_{62}^A \check{K}_{21}^B, \quad (\text{B.27d})$$

$$G_{22}^A = H_{11}^Q - \check{K}_{65}^A - \check{K}_{61}^A \check{K}_{13}^B - \check{K}_{62}^A \check{K}_{23}^B, \quad (\text{B.27e})$$

$$G_{23}^A = H_{12}^Q, \quad G_{24}^A = H_{13}^Q, \quad G_{25}^A = 0, \quad G_{26}^A = -(\mathbf{H}_\gamma^T)^{-1}, \quad (\text{B.27f})$$

$$G_{31}^A = H_{20}^Q - \check{K}_{83}^A + \frac{\check{K}_{73}^A}{R} - \left(\check{K}_{81}^A - \frac{\check{K}_{71}^A}{R} \right) \check{K}_{11}^B - \left(\check{K}_{82}^A - \frac{\check{K}_{72}^A}{R} \right) \check{K}_{21}^B, \quad (\text{B.27g})$$

$$\mathbf{G}_{32}^A = \mathbf{H}_{21}^Q - \check{\mathbf{K}}_{85}^A + \frac{\check{\mathbf{K}}_{75}^A}{R} - \left(\check{\mathbf{K}}_{81}^A - \frac{\check{\mathbf{K}}_{71}^A}{R} \right) \check{\mathbf{K}}_{13}^B - \left(\check{\mathbf{K}}_{82}^A - \frac{\check{\mathbf{K}}_{72}^A}{R} \right) \check{\mathbf{K}}_{23}^B, \quad (\text{B.27h})$$

$$G_{33}^A = H_{22}^Q, \quad \mathbf{G}_{34}^A = \mathbf{H}_{23}^Q, \quad G_{35}^A = 0, \quad \mathbf{G}_{36}^A = \mathbf{0}, \quad (\text{B.27i})$$

$$\mathbf{G}_{41}^A = \mathbf{H}_{30}^Q - \check{\mathbf{K}}_{93}^A - \check{\mathbf{K}}_{91}^A \check{\mathbf{K}}_{11}^B - \check{\mathbf{K}}_{92}^A \check{\mathbf{K}}_{21}^B, \quad (\text{B.27j})$$

$$\mathbf{G}_{42}^A = \mathbf{H}_{31}^Q - \check{\mathbf{K}}_{95}^A - \check{\mathbf{K}}_{91}^A \check{\mathbf{K}}_{13}^B - \check{\mathbf{K}}_{92}^A \check{\mathbf{K}}_{23}^B, \quad (\text{B.27k})$$

$$\mathbf{G}_{43}^A = \mathbf{H}_{32}^Q, \quad \mathbf{G}_{44}^A = \mathbf{H}_{33}^Q, \quad G_{45}^A = 0, \quad \mathbf{G}_{46}^A = \mathbf{0}, \quad (\text{B.27l})$$

$$G_{51}^A = -\check{\mathbf{K}}_{13}^A - \check{\mathbf{K}}_{11}^A \check{\mathbf{K}}_{11}^B - \check{\mathbf{K}}_{12}^A \check{\mathbf{K}}_{21}^B, \quad (\text{B.27m})$$

$$\mathbf{G}_{52}^A = -\check{\mathbf{K}}_{15}^A - \check{\mathbf{K}}_{11}^A \check{\mathbf{K}}_{13}^B - \check{\mathbf{K}}_{12}^A \check{\mathbf{K}}_{23}^B, \quad (\text{B.27n})$$

$$G_{53}^A = 0, \quad \mathbf{G}_{54}^A = \mathbf{0}, \quad G_{55}^A = 0, \quad \mathbf{G}_{56}^A = \mathbf{0}, \quad (\text{B.27o})$$

$$\mathbf{G}_{61}^A = -\check{\mathbf{K}}_{z3}^A - \check{\mathbf{K}}_{z1}^A \check{\mathbf{K}}_{11}^B - \check{\mathbf{K}}_{z2}^A \check{\mathbf{K}}_{21}^B, \quad (\text{B.27p})$$

$$\mathbf{G}_{62}^A = -\check{\mathbf{K}}_{z5}^A - \check{\mathbf{K}}_{z1}^A \check{\mathbf{K}}_{13}^B - \check{\mathbf{K}}_{z2}^A \check{\mathbf{K}}_{23}^B, \quad (\text{B.27q})$$

$$\mathbf{G}_{63}^A = \mathbf{0}, \quad \mathbf{G}_{64}^A = \mathbf{0}, \quad \mathbf{G}_{65}^A = \mathbf{0}, \quad \mathbf{G}_{66}^A = \mathbf{0}, \quad (\text{B.27r})$$

the components of matrix \mathbf{G}_B yielding:

$$G_{11}^B = \check{\mathbf{K}}_{54}^A + \check{\mathbf{K}}_{51}^A \check{\mathbf{K}}_{12}^B + \check{\mathbf{K}}_{52}^A \check{\mathbf{K}}_{22}^B, \quad \mathbf{G}_{12}^B = \check{\mathbf{K}}_{56}^A + \check{\mathbf{K}}_{51}^A \check{\mathbf{K}}_{14}^B + \check{\mathbf{K}}_{52}^A \check{\mathbf{K}}_{24}^B, \quad (\text{B.28a})$$

$$G_{13}^B = \check{\mathbf{K}}_{57}^A + \check{\mathbf{K}}_{51}^A \check{\mathbf{K}}_{15}^B + \check{\mathbf{K}}_{52}^A \check{\mathbf{K}}_{25}^B, \quad \mathbf{G}_{14}^B = \check{\mathbf{K}}_{58}^A + \check{\mathbf{K}}_{51}^A \check{\mathbf{K}}_{16}^B + \check{\mathbf{K}}_{52}^A \check{\mathbf{K}}_{26}^B, \quad (\text{B.28b})$$

$$G_{15}^B = 0, \quad \mathbf{G}_{16}^B = \check{\mathbf{K}}_{51}^A \check{\mathbf{K}}_{17}^B + \check{\mathbf{K}}_{52}^A \check{\mathbf{K}}_{27}^B, \quad (\text{B.28c})$$

$$\mathbf{G}_{21}^B = \check{\mathbf{K}}_{64}^A + \check{\mathbf{K}}_{61}^A \check{\mathbf{K}}_{12}^B + \check{\mathbf{K}}_{62}^A \check{\mathbf{K}}_{22}^B, \quad \mathbf{G}_{22}^B = \check{\mathbf{K}}_{66}^A + \check{\mathbf{K}}_{61}^A \check{\mathbf{K}}_{14}^B + \check{\mathbf{K}}_{62}^A \check{\mathbf{K}}_{24}^B, \quad (\text{B.28d})$$

$$\mathbf{G}_{23}^B = \check{\mathbf{K}}_{67}^A + \check{\mathbf{K}}_{61}^A \check{\mathbf{K}}_{15}^B + \check{\mathbf{K}}_{62}^A \check{\mathbf{K}}_{25}^B, \quad \mathbf{G}_{24}^B = \check{\mathbf{K}}_{68}^A + \check{\mathbf{K}}_{61}^A \check{\mathbf{K}}_{16}^B + \check{\mathbf{K}}_{62}^A \check{\mathbf{K}}_{26}^B, \quad (\text{B.28e})$$

$$\mathbf{G}_{25}^B = \mathbf{0}, \quad \mathbf{G}_{26}^B = \check{\mathbf{K}}_{61}^A \check{\mathbf{K}}_{17}^B + \check{\mathbf{K}}_{62}^A \check{\mathbf{K}}_{27}^B, \quad (\text{B.28f})$$

$$G_{31}^B = \check{\mathbf{K}}_{84}^A - \frac{\check{\mathbf{K}}_{74}^A}{R} + \left(\check{\mathbf{K}}_{81}^A - \frac{\check{\mathbf{K}}_{71}^A}{R} \right) \check{\mathbf{K}}_{12}^B + \left(\check{\mathbf{K}}_{82}^A - \frac{\check{\mathbf{K}}_{72}^A}{R} \right) \check{\mathbf{K}}_{22}^B, \quad (\text{B.28g})$$

$$\mathbf{G}_{32}^B = \check{\mathbf{K}}_{86}^A - \frac{\check{\mathbf{K}}_{76}^A}{R} + \left(\check{\mathbf{K}}_{81}^A - \frac{\check{\mathbf{K}}_{71}^A}{R} \right) \check{\mathbf{K}}_{14}^B + \left(\check{\mathbf{K}}_{82}^A - \frac{\check{\mathbf{K}}_{72}^A}{R} \right) \check{\mathbf{K}}_{24}^B, \quad (\text{B.28h})$$

$$G_{33}^B = \check{\mathbf{K}}_{87}^A - \frac{\check{\mathbf{K}}_{77}^A}{R} + \left(\check{\mathbf{K}}_{81}^A - \frac{\check{\mathbf{K}}_{71}^A}{R} \right) \check{\mathbf{K}}_{15}^B + \left(\check{\mathbf{K}}_{82}^A - \frac{\check{\mathbf{K}}_{72}^A}{R} \right) \check{\mathbf{K}}_{25}^B, \quad (\text{B.28i})$$

$$\mathbf{G}_{34}^B = \check{\mathbf{K}}_{88}^A - \frac{\check{\mathbf{K}}_{78}^A}{R} + \left(\check{\mathbf{K}}_{81}^A - \frac{\check{\mathbf{K}}_{71}^A}{R} \right) \check{\mathbf{K}}_{16}^B + \left(\check{\mathbf{K}}_{82}^A - \frac{\check{\mathbf{K}}_{72}^A}{R} \right) \check{\mathbf{K}}_{26}^B, \quad (\text{B.28j})$$

$$G_{35}^B = 0, \quad \mathbf{G}_{36}^B = \left(\check{\mathbf{K}}_{81}^A - \frac{\check{\mathbf{K}}_{71}^A}{R} \right) \check{\mathbf{K}}_{17}^B + \left(\check{\mathbf{K}}_{82}^A - \frac{\check{\mathbf{K}}_{72}^A}{R} \right) \check{\mathbf{K}}_{27}^B, \quad (\text{B.28k})$$

$$\mathbf{G}_{41}^B = \check{\mathbf{K}}_{94}^A + \check{\mathbf{K}}_{91}^A \check{\mathbf{K}}_{12}^B + \check{\mathbf{K}}_{92}^A \check{\mathbf{K}}_{22}^B, \quad \mathbf{G}_{42}^B = \check{\mathbf{K}}_{96}^A + \check{\mathbf{K}}_{91}^A \check{\mathbf{K}}_{14}^B + \check{\mathbf{K}}_{92}^A \check{\mathbf{K}}_{24}^B, \quad (\text{B.28l})$$

$$\mathbf{G}_{43}^B = \check{\mathbf{K}}_{97}^A + \check{\mathbf{K}}_{91}^A \check{\mathbf{K}}_{15}^B + \check{\mathbf{K}}_{92}^A \check{\mathbf{K}}_{25}^B, \quad \mathbf{G}_{44}^B = \check{\mathbf{K}}_{98}^A + \check{\mathbf{K}}_{91}^A \check{\mathbf{K}}_{16}^B + \check{\mathbf{K}}_{92}^A \check{\mathbf{K}}_{26}^B, \quad (\text{B.28m})$$

$$\mathbf{G}_{45}^B = 0, \quad \mathbf{G}_{46}^B = \check{\mathbf{K}}_{91}^A \check{\mathbf{K}}_{17}^B + \check{\mathbf{K}}_{92}^A \check{\mathbf{K}}_{27}^B, \quad (\text{B.28n})$$

$$G_{51}^B = \check{\mathbf{K}}_{14}^A + \check{\mathbf{K}}_{11}^A \check{\mathbf{K}}_{12}^B + \check{\mathbf{K}}_{12}^A \check{\mathbf{K}}_{22}^B, \quad \mathbf{G}_{52}^B = \check{\mathbf{K}}_{16}^A + \check{\mathbf{K}}_{11}^A \check{\mathbf{K}}_{14}^B + \check{\mathbf{K}}_{12}^A \check{\mathbf{K}}_{24}^B, \quad (\text{B.28o})$$

$$G_{53}^B = \check{\mathbf{K}}_{17}^A + \check{\mathbf{K}}_{11}^A \check{\mathbf{K}}_{15}^B + \check{\mathbf{K}}_{12}^A \check{\mathbf{K}}_{25}^B, \quad \mathbf{G}_{54}^B = \check{\mathbf{K}}_{18}^A + \check{\mathbf{K}}_{11}^A \check{\mathbf{K}}_{16}^B + \check{\mathbf{K}}_{12}^A \check{\mathbf{K}}_{26}^B, \quad (\text{B.28p})$$

$$G_{55}^B = -\frac{1}{R}, \quad \mathbf{G}_{56}^B = \check{\mathbf{K}}_{11}^A \check{\mathbf{K}}_{17}^B + \check{\mathbf{K}}_{12}^A \check{\mathbf{K}}_{27}^B - \mathbf{h}_N^T, \quad (\text{B.28q})$$

$$\mathbf{G}_{61}^B = \check{\mathbf{K}}_{z4}^A + \check{\mathbf{K}}_{z1}^A \check{\mathbf{K}}_{12}^B + \check{\mathbf{K}}_{z2}^A \check{\mathbf{K}}_{22}^B, \quad \mathbf{G}_{62}^B = \check{\mathbf{K}}_{z6}^A + \check{\mathbf{K}}_{z1}^A \check{\mathbf{K}}_{14}^B + \check{\mathbf{K}}_{z2}^A \check{\mathbf{K}}_{24}^B, \quad (\text{B.28r})$$

$$\mathbf{G}_{63}^B = \check{\mathbf{K}}_{z7}^A + \check{\mathbf{K}}_{z1}^A \check{\mathbf{K}}_{15}^B + \check{\mathbf{K}}_{z2}^A \check{\mathbf{K}}_{25}^B, \quad \mathbf{G}_{64}^B = \check{\mathbf{K}}_{z8}^A + \check{\mathbf{K}}_{z1}^A \check{\mathbf{K}}_{16}^B + \check{\mathbf{K}}_{z2}^A \check{\mathbf{K}}_{26}^B, \quad (\text{B.28s})$$

$$\mathbf{G}_{65}^B = 0, \quad \mathbf{G}_{66}^B = \check{\mathbf{K}}_{10,1}^A \check{\mathbf{K}}_{17}^B + \check{\mathbf{K}}_{10,2}^A \check{\mathbf{K}}_{27}^B - \mathbf{H}_z^T, \quad (\text{B.28t})$$

the components of matrix \mathbf{G}_C yielding:

$$G_{11}^C = B_{12}^\varepsilon + \check{\mathbf{K}}_{51}^A K_{11}^C + \check{\mathbf{K}}_{52}^A K_{21}^C, \quad G_{12}^C = B_{26}^\gamma + \check{\mathbf{K}}_{51}^A K_{12}^C + \check{\mathbf{K}}_{52}^A K_{22}^C, \quad (\text{B.29a})$$

$$G_{21}^C = k_{12}^\varepsilon + \check{\mathbf{K}}_{61}^A K_{11}^C + \check{\mathbf{K}}_{62}^A K_{21}^C, \quad G_{22}^C = k_{26}^\gamma + \check{\mathbf{K}}_{61}^A K_{12}^C + \check{\mathbf{K}}_{62}^A K_{22}^C, \quad (\text{B.29b})$$

$$G_{31}^C = B_{16}^\varepsilon - \frac{A_{16}^\varepsilon}{R} + \left(\check{\mathbf{K}}_{81}^A - \frac{\check{\mathbf{K}}_{71}^A}{R} \right) K_{11}^C + \left(\check{\mathbf{K}}_{82}^A - \frac{\check{\mathbf{K}}_{72}^A}{R} \right) K_{21}^C, \quad (\text{B.29c})$$

$$G_{32}^C = B_{66}^\gamma - \frac{A_{66}^\gamma}{R} + \left(\check{K}_{81}^A - \frac{\check{K}_{71}^A}{R} \right) K_{12}^C + \left(\check{K}_{82}^A - \frac{\check{K}_{72}^A}{R} \right) K_{22}^C, \quad (\text{B.29d})$$

$$\mathbf{G}_{41}^C = \mathbf{k}_{16}^\varepsilon + \check{\mathbf{K}}_{91}^A K_{11}^C + \check{\mathbf{K}}_{92}^A K_{21}^C, \quad \mathbf{G}_{42}^C = \mathbf{k}_{66}^\gamma + \check{\mathbf{K}}_{91}^A K_{12}^C + \check{\mathbf{K}}_{92}^A K_{22}^C, \quad (\text{B.29e})$$

$$G_{51}^C = A_{11}^\varepsilon + \check{K}_{11}^A K_{11}^C + \check{K}_{12}^A K_{21}^C, \quad G_{52}^C = A_{16}^\gamma + \check{K}_{11}^A K_{12}^C + \check{K}_{12}^A K_{22}^C, \quad (\text{B.29f})$$

$$\mathbf{G}_{61}^C = \mathbf{k}_{13}^\varepsilon + \check{\mathbf{K}}_{10,1}^A K_{11}^C + \check{\mathbf{K}}_{10,2}^A K_{21}^C, \quad (\text{B.29g})$$

$$\mathbf{G}_{62}^C = \mathbf{k}_{36}^\gamma + \check{\mathbf{K}}_{10,1}^A K_{12}^C + \check{\mathbf{K}}_{10,2}^A K_{22}^C, \quad (\text{B.29h})$$

and the components of matrix \mathbf{H}_ε yielding:

$$H_1^\varepsilon = \check{K}_{51}^A \check{K}_1^D + \check{\mathbf{K}}_{52}^A \check{\mathbf{K}}_2^D - \check{k}_5^\varepsilon, \quad \mathbf{H}_2^\varepsilon = \check{\mathbf{K}}_{61}^A \check{K}_1^D + \check{\mathbf{K}}_{62}^A \check{\mathbf{K}}_2^D - \check{\mathbf{k}}_6^\varepsilon, \quad (\text{B.30a})$$

$$H_3^\varepsilon = \left(\check{K}_{81}^A - \frac{\check{K}_{71}^A}{R} \right) \check{K}_1^D + \left(\check{\mathbf{K}}_{82}^A - \frac{\check{\mathbf{K}}_{72}^A}{R} \right) \check{\mathbf{K}}_2^D - \check{k}_8^\varepsilon + \frac{\check{k}_7^\varepsilon}{R}, \quad (\text{B.30b})$$

$$\mathbf{H}_4^\varepsilon = \check{\mathbf{K}}_{91}^A \check{K}_1^D + \check{\mathbf{K}}_{92}^A \check{\mathbf{K}}_2^D - \check{\mathbf{k}}_9^\varepsilon, \quad H_5^\varepsilon = \check{K}_{11}^A \check{K}_1^D + \check{K}_{12}^A \check{K}_2^D - \check{k}_1^\varepsilon, \quad (\text{B.30c})$$

$$\mathbf{H}_6^\varepsilon = \check{\mathbf{K}}_{10,1}^A \check{K}_1^D + \check{\mathbf{K}}_{10,2}^A \check{\mathbf{K}}_2^D - \check{\mathbf{k}}_z^\varepsilon. \quad (\text{B.30d})$$

Bibliography

- [1] K.T. Kedward, R.S. Wilson, and S. K. Mclean. Flexure of simply curved composite shapes. *Composites*, 20:527–536, 1989.
- [2] P.C. Paul, C.R. Saff, K.B. Sanger, M.A. Mahler, H.P. Kan, and E.F. Kautz. Out of plane analysis for composite structures. In *Eighth DoD/NASA/FAA Conference on Fibrous Composites in Structural Design*, pages 263–279, 1992. Norfolk, Virginia.
- [3] ASTM D 6415/D 6415M - 06a. Standard test method for measuring the curved beam strength of a fibre-reinforced polymer-matrix composite. ASTM Standards, 2007.
- [4] W.L. Ko and R.H. Jackson. Multilayer theory for delamination analysis of a composite curved bar subjected to end forces and end moments. *NASA Technical Memorandum 4139*, 1989.
- [5] R.Y. Kim and S.R. Soni. Failure of composite laminates due to combined interlaminar normal and shear stresses. In *Composites'86: recent advances in Japan and the United States, Proceedings of Japan-U.S. CCM-III*, pages 341–350, 1986.
- [6] T. Edwards and J. Thompson. Spar corner radius integrity for the A400M wing. *Applied Mechanics and Materials*, 3-4:197–202, 2005.
- [7] M. Hoffmann, K. Zimmermann, B. Bautz, and P. Middendorf. Size effect on through-thickness strength properties of 3D loaded composite laminates. In *Proceedings of the 17th European Conference on Composite Materials ECCM17*, 2016. 26-30 of June, Munich, Germany.
- [8] S.C. Avalon and S.L. Donaldson. Strength of composite angle brackets with multiple geometries and nanofiber-enhanced resins. *Journal of Composite Materials*, 45(9):1017–1030, 2010.
- [9] M.R. Wisnom. Size effects in the testing of fibre-composite materials. *Composites Science and Technology*, 59:1937–1957, 1999.

-
- [10] A. Makeev, G. Seon, Y. Nikishkov, and E. Lee. Methods for assessment of interlaminar tensile strength of composite materials. *Journal of Composite Materials*, 49(7):783–794, 2015.
- [11] T.A. Fletcher, T. Kim, T.J. Dodwell, R. Butler, R. Scheichl, and R. Newley. The influence of free edges on curved beam strength. In *Proceedings of the 21th International Conference on Composite Materials ICCM20*, 2015. 19-24 of July, Copenhagen, Denmark.
- [12] T.A. Fletcher, A.K. Reinartz, T.J. Dodwell, R. Butler, R. Scheichl, and R. Newley. Efficient modelling and accurate certification of curved aerospace laminates. In *Proceedings of the 17th European Conference on Composite Materials ECCM17*, 2016. 26-30 of June, Munich, Germany.
- [13] T. Kim, T.A. Fletcher, T.J. Dodwell, R. Butler, R. Scheichl, J. Ankersen, and R. Newley. The effect of free edges on inter-laminar performance of curved laminates. In *56th AIAA/ASCE/AHS/ASC Structures, Structural Dynamics, and Materials Conference*, 2015.
- [14] J. Most, D. Stegmair, and D. Petry. Error estimation between simple, closed-form analytical formulae and full-scale FEM for interlaminar stress prediction in curved laminates. *Composite Structures*, 131:72–81, 2015.
- [15] R.M. Jones. *Mechanics of Composite Materials*. Mc Graw-Hill, 1975.
- [16] J.M. Whitney and N.J. Pagano. Shear deformation in heterogeneous anisotropic plates. *Journal of Applied Mechanics*, 37:1031–1036, 1970.
- [17] K.C. Lin and C.M. Hsieh. The closed form general solutions of 2-D curved laminated beams of variable curvatures. *Composite Structures*, 79(4):606–618, 2007.
- [18] K.C. Lin and C.W. Lin. Finite deformation of 2-D laminated curved beams with variable curvatures. *International Journal of Non-Linear Mechanics*, 46(10):1293–1304, 2011.
- [19] S.G. Lekhnitskii, S.W. Tsai, and T. Cheron. *Anisotropic Plates*. Gordon and Breach Science Publishers, 1968.
- [20] W.L. Ko. Delamination stresses in semicircular laminated composite curved bars. *NASA Technical Memorandum 4026*, 1988.

-
- [21] A. Sharma and C.E. Bakis. Analysis of elastic stresses in thick, polar-orthotropic, C-shaped rings. *Journal of Composite Materials*, 38:1619–1638, 2004.
- [22] A. Sharma and C.E. Bakis. C-shape specimen for tensile radial strength of thick, filament-wound rings. *Journal of Composite Materials*, 40(2):97–116, 2006.
- [23] A. Schmitz and P. Horst. Bending deformation limits of corrugated unidirectionally reinforced composites. *Composite Structures*, 107:103–111, 2014.
- [24] W. Cui, T. Liu, J. Len, and R. Ruo. Interlaminar tensile strength (ILTS) measurement of woven glass/polyester laminates specimen using four-point curved beam specimen. *Composites Part A*, 27A:1097–1105, 1996.
- [25] S. Smidt. Bending of curved sandwich beams. *Composite Structures*, 33:211–225, 1995.
- [26] R.A. Shenoi and W. Wang. Through-thickness stresses in curved composite laminates and sandwich beams. *Composites Science and Technology*, 61(11):1501–1512, 2001.
- [27] M.S. Qatu. Theories and analyses of thin and moderately thick laminated composite curved beams. *International Journal of Solids and Structures*, 30(20):2743–2756, 1993.
- [28] G. Kress, R. Roos, M. Barbezat, C. Dransfeld, and P. Ermanni. Model for interlaminar normal stress in singly curved laminates. *Composite Structures*, 69(4):458–469, 2005.
- [29] R.M. Guedes and A. Sá. Numerical analysis of singly curved shallow composite panels under three-point bend load. *Composite Structures*, 83(2):212–220, 2008.
- [30] G. Kress. Minimized computational effort for the thick-walled composite tube problem. *Computers and Structures*, 54(4):633–639, 1995.
- [31] V. Rodríguez de la Cruz, D. Fernández Caballero, F. Mujika, and J.M. Muñoz Guijosa. Analysis of out-of-plane stresses in sandwich beams subjected to pure bending with large deflections. *Journal of Composite Materials*, 47(22):2809–2822, 2012.

-
- [32] G. Vargas, A. Arrese, N. Carbajal, and F. Mujika. Analysis of in-plane and out-of-plane thermo-mechanical stresses in un-symmetric cross-ply curved laminated strips. *Journal of Composite Materials*, 43:3157–3184, 2009.
- [33] D. Bruno, R. Carpino, F. Greco, and P. Lonetti. Energy release rate and mode partition for interlaminar crack in circular laminated beams. *International Journal of Solids and Structures*, 43:1201–1223, 2006.
- [34] E. Carrera, M. Filippi, and E. Zappino. Free vibration analysis of laminated beam by polynomial, trigonometric, exponential and zig-zag theories. *Journal of Composite Materials*, 48(19):2299–2316, 2014.
- [35] S.P. Timoshenko. On the correction factor for shear of the differential equation for transverse vibrations of bars of uniform cross-section. *Philosophical Magazine*, 41:744–746, 1921.
- [36] S.P. Timoshenko. On the transverse vibrations of bars of uniform cross-section. *Philosophical Magazine*, 43:125–131, 1922.
- [37] H. Matsunaga. Interlaminar stress analysis of laminated composite beams according to global higher-order deformation theories. *Composite Structures*, 55:105–114, 2002.
- [38] H. Matsunaga. Interlaminar stress analysis of laminated composite and sandwich circular arches subjected to thermal/mechanical loading. *Composite Structures*, 60:345–358, 2003.
- [39] J.G. Ren. Exact solutions for laminated cylindrical shells in cylindrical bending. *Composites Science and Technology*, 29:169–187, 1987.
- [40] E. Carrera. On the use of the Murakami’s zig-zag function in the modeling of layered plates and shells. *Computers and Structures*, 82:541–554, 2004.
- [41] U. Icardi and L. Ferrero. Multilayered shell model with variable representation of displacements across the thickness. *Composites: Part B*, 42:18–26, 2011.
- [42] A. Alibeigloo and M. Shakeri. Elasticity solution for static analysis of laminated cylindrical panel using differential quadrature method. *Engineering Structures*, 31:260–267, 2009.

-
- [43] P. Malekzadeh. A two-dimensional layerwise-differential quadrature static analysis of thick laminated composite circular arches. *Applied Mathematical Modelling*, 33:1850–1861, 2009.
- [44] K. Bhaskar and T.K. Varadan. A higher-order theory for bending analysis of laminated shells of revolution. *Computers and Structures*, 40(4):815–819, 1991.
- [45] K. Bhaskar and G. Balasubramanyam. Accurate analysis of end-loaded laminated orthotropic cylindrical shells. *Composite Structures*, 58:209–216, 2002.
- [46] G.Y. Cui and C. Ruiz. Through-thickness failure of laminated carbon/epoxy composites under combined stress. *Composites Science and Technology*, 53:253–258, 1995.
- [47] M.R. Wisnom, Z.J. Petrossian, and M.I. Jones. Interlaminar failure of unidirectional glass/epoxy due to combined through thickness shear and tension. *Composites Part A*, 27A:921–929, 1996.
- [48] S. McRobbie, A.J. Longmuir, J. Wilcox, A.G. Gibson, and H.W. Chandler. Through-thickness stress in curved laminates of single- and double-skinned construction. *Composites*, 26:339–345, 1995.
- [49] E. Graff and G.S. Springer. Stress analysis of thick, curved composite laminates. *Computers and Structures*, 38(1):41–55, 1991.
- [50] N. Rattanawangcharoen. An analysis of weakly bonded laminated cylindrical panels. *Journal of Reinforced Plastics and Composites*, 25(15):1611–1628, 2006.
- [51] G. Kress and M. Winkler. Corrugated laminate analysis: A generalized plane-strain problem. *Composite Structures*, 93:1493–1504, 2011.
- [52] M. Cinefra and E. Carrera. Shell finite elements with different through-the-thickness kinematics for the linear analysis of cylindrical multi-layered structures. *International Journal for Numerical Methods in Engineering*, 93:160–182, 2013.
- [53] P. Vidal, L. Gallimard, and O. Polit. Shell finite element based on the proper generalized decomposition for the modeling of cylindrical composite structures. *Computers and Structures*, 132:1–11, 2014.
- [54] F. Fraternali and G. Bilotti. Nonlinear elastic stress analysis in curved composite beams. *Computers and Structures*, 62(5):837–859, 1997.

- [55] M.R. Wisnom, M. Gigliotti, N. Ersoy, M. Campbell, and K.D. Potter. Mechanisms generating residual stresses and distortion during manufacture of polymer–matrix composite structures. *Composites Part A: Applied Science and Manufacturing*, 37(4):522–529, 2006.
- [56] J.W. Kim and D.G. Lee. Measurement of residual stresses in thick composite cylinders by the radial-cut-cylinder-bending method. *Composite Structures*, 77:444–456, 2007.
- [57] K. Takagaki, S. Minakuchi, and N. Takeda. Fiber-optic-based life-cycle monitoring of through-thickness strain in thick CFRP pipes. *Advanced Composite Materials*, 23(3):195–209, 2014.
- [58] N.N. Huang and T.R. Tauchert. Thermal stresses in doubly-curved cross-ply laminates. *International Journal of Solids and Structures*, 29(8):991–1000, 1992.
- [59] M.S. Qatu. Accurate equations for laminated composite deep thick shells. *International Journal of Solids and Structures*, 36:2917–2941, 1999.
- [60] E. Asadi, W. Wanga, and M.S. Qatu. Static and vibration analyses of thick deep laminated cylindrical shells using 3D and various shear deformation theories. *Composite Structures*, 94:494–500, 2012.
- [61] E. Asadi and M.S. Qatu. Static analysis of thick laminated shells with different boundary conditions using GDQ. *Thin-Walled Structures*, 51:76–81, 2012.
- [62] F. Tornabene, A. Liverani, and G. Caligiana. Static analysis of laminated composite curved shells and panels of revolution with a posteriori shear and normal stress recovery using generalized differential quadrature method. *International Journal of Mechanical Sciences*, 61:71–87, 2012.
- [63] R.B. Pipes and N.J. Pagano. Interlaminar stresses in composite laminates under uniform axial extension. *Journal of Composite Materials*, 4(4):538–548, 1970.
- [64] R.B. Pipes and N.J. Pagano. Interlaminar stresses in composite laminates: An approximate elasticity solution. *Journal of Applied Mechanics*, 41(3):668–672, 1975.
- [65] N.J. Pagano. On the calculation of interlaminar normal stress in composite laminate. *Journal of Composite Materials*, 8:65–81, 1974.

- [66] W. Becker. Closed-form solution for the free-edge effect in cross-ply laminates. *Composite Structures*, 26:39–45, 1993.
- [67] C. Kassapoglou and P.A. Lagace. Closed form solutions for the interlaminar stress field in angle-ply and cross-ply laminates. *Journal of Composite Materials*, 21(4):292–308, 1987.
- [68] C. Mittelstedt and W. Becker. Free-edge effects in composite laminates. *Applied Mechanics Reviews*, 60(5):217–245, 2007.
- [69] C. Wenzel, M. D’Ottavio, O. Polit, and P. Vidal. Assessment of free-edge singularities in composite laminates using higher-order plate elements. *Mechanics of Advanced Materials and Structures*, 23:948–959, 2016.
- [70] T. Kant and K. Swaminathan. Estimation of transverse/interlaminar stresses in laminated composites - a selective review and survey of current developments. *Composite Structures*, 49:65–75, 2000.
- [71] A.C. Orifici, I. Herszberg, and R.S. Thomson. Review of methodologies for composite material modelling incorporating failure. *Composite Structures*, 86:194–210, 2008.
- [72] Z. Hashin. Failure criteria for unidirectional composites. *Journal of Applied Mechanics*, 47:329–334, 1980.
- [73] J.C. Brewer and P.A. Lagacé. Quadratic stress criterion for initiation of delamination. *Journal of Composite Materials*, 22:1141–55, 1988.
- [74] L. Tong. An assessment of failure criteria to predict the strength of adhesively bonded composite double lap joints. *Journal of Reinforced Plastics and Composites*, 16(8):698–713, 1997.
- [75] M.R. Wisnom, G.F.J. Hill, and M.I. Jones. Through thickness failure prediction of composite structural elements. In *Proceedings of the 13th International Conference on Composite Materials ICCM13*, 2001. Beijing, China.
- [76] F. Hélénon, M.R. Wisnom, S.R. Hallett, and R.S. Trask. Numerical investigation into failure of laminated composite T-piece specimens under tensile loading. *Composites: Part A*, 43:1017–1027, 2012.
- [77] ASTM D 2344/D 2344M - 13. Standard test method for short-beam strength of polymer matrix composite materials and their laminates. ASTM Standards, 2013.

-
- [78] A. Makeev, Y. He, P. Carpentier, and B. Shonkwiler. A method for measurement of multiple constitutive properties for composite materials. *Composites: Part A*, 43:2199–2210, 2012.
- [79] A. Makeev, P. Carpentier, and B. Shonkwiler. Methods to measure interlaminar tensile modulus of composites. *Composites: Part A*, 56:256–261, 2014.
- [80] ASTM D 7291/D 7291M - 07. Through-thickness "flatwise" tensile strength and elastic modulus of a fiber-reinforced polymer matrix composite material. ASTM Standards, 2007.
- [81] M. Hoffmann, K. Zimmermann, B. Bautz, and P. Middendorf. A new specimen geometry to determine the through-thickness tensile strength of composite laminates. *Composites Part B*, 77:145–152, 2015.
- [82] M. Hoffmann, K. Zimmermann, and P. Middendorf. Determination of the through-thickness strength properties to predict the failure of thick-walled composite lugs. In *Proceedings of the 21th International Conference on Composite Materials ICCM20*, 2015. 19-24 of July, Copenhagen, Denmark.
- [83] W. Cui, M. Wisnom, and M. Jones. Effect of specimen size on interlaminar shear strength of unidirectional carbon fibre-epoxy. *Composites Engineering*, 4:299–307, 1994.
- [84] J. Hitchon and D. Phillips. The effect of specimen size on the strength of CFRP. *Composites*, 9:119–124, 1978.
- [85] W. Weibull. A statistical distribution function of wide applicability. *Journal of Applied Mechanics*, 18:293–297, 1951.
- [86] T.J. Lu, Z.C. Xia, and J.W. Hutchinson. Delamination of beams under transverse shear and bending. *Materials Science and Engineering*, A188:103–112, 1994.
- [87] G. Wimmer and H.E. Pettermann. A semi-analytical model for the simulation of delamination in laminated composites. *Composites Science and Technology*, 68:2332–2339, 2008.
- [88] G. Wimmer, W. Kitzmüller, G. Pinter, T. Wettemann, and H.E. Pettermann. Computational and experimental investigation of delamination in L-shaped laminated composite components. *Engineering Fracture Mechanics*, 76:2810–2820, 2009.

- [89] G. Wimmer, C. Schuecker, and H.E. Pettermann. Numerical simulation of delamination in laminated composite components – A combination of a strength criterion and fracture mechanics. *Composites: Part B*, 40:158–165, 2009.
- [90] B. Gözlüklü and D. Coker. Modeling of the dynamic delamination of L-shaped unidirectional laminated composites. *Composite Structures*, 94:1430–1442, 2012.
- [91] B. Gözlüklü, I. Uyar, and D. Coker. Intersonic delamination in curved thick composite laminates under quasi-static loading. *Mechanics of Materials*, 80:163–182, 2015.
- [92] R.Y. Kim and S.R. Soni. Experimental and analytical studies on the onset of delamination in laminated composites. *Journal of Composite Materials*, 18(70):70–80, 1984.
- [93] J.M. González-Cantero, E. Graciani, F. París, B. López-Romano, and J.A. Rodríguez-Sánchez. Study of the composite ILTS test in CFRP angles by means of analytical and FEM models. In *7th International Conference on Composites Testing and Model Identification*, 2015. IMDEA, Getafe, Spain.
- [94] J.M. González-Cantero, E. Graciani, A. Blázquez, and F. París. A new analytical model for evaluating interlaminar stresses in the unfolding failure of composite laminates. *Composite Structures*, 147:260–273, 2016.
- [95] J.M. González-Cantero, E. Graciani, F. París, and B. López-Romano. Semi-analytic model to evaluate non-regularized stresses causing unfolding failure in composites. *Composite Structures*, 171:77–91, 2017.
- [96] J.M. González-Cantero, E. Graciani, B. López-Romano, and F. París. Enhanced semi-analytic model for the evaluation of non-regularized stresses in the unfolding failure by using Legendre polynomials. *In preparation*.
- [97] A.J.M. Spencer, P. Watson, and T.G. Rogers. Mathematical analysis of the springback effect in laminated thermoplastic channel sections. *Composites Manufacturing*, 2(3-4):253–258, 1991.
- [98] J.M. González-Cantero. 3D analytical model for evaluating stresses in curved aerostructural composite laminates. ECSE2016-1, Airbus Group Chair of Aeronautical Studies, School of Engineering, University of Seville, 2016.

- [99] J.M. González-Cantero, E. Graciani, F. París, and B. López-Romano. Stacking sequence optimization of curved UD-CFRP laminates for improving unfolding strength considering thermal residual stresses. In *Proceedings of the 17th European Conference on Composite Materials ECCM17*, 2016. 26-30 of June, Munich, Germany.
- [100] J.M. González-Cantero, E. Graciani, B. López-Romano, and F. París. Induced unfolding: a new mechanism of unfolding failure in composite laminates. *Submitted to Composites Science and Technology*, 2017.
- [101] W.C. Jackson and R.H. Martin. An interlaminar tensile strength specimen. *Composite Materials: Testing and Design (11th Volume), ASTM STP 1206*, pages 333–354, 1993.
- [102] L. Ramírez López. Fabricación y ensayo de probetas ILTS. Degree Final Project, Superior Engineering School, University of Seville, 2015.
- [103] J.M. González-Cantero, E. Graciani, A. Blázquez, and F. París. Analytic evaluation of radial stresses in unfolding failure of composite materials. Comparison with numerical solutions. In *Proceedings of the 16th European Conference on Composite Materials ECCM16*, 2014. 22-26 of June, Seville, Spain.
- [104] G. Arfken. *Orthogonal Polynomials*. Mathematical Methods for Physicists, 3rd edition, 1985.
- [105] M. Abramowitz and I.A. Stegun. *Handbook of Mathematical Functions with Formulas, Graphs, and Mathematical Tables*, chapter 8. Dover Books on Mathematics, 1965.
- [106] D. Zwillinger. *Handbook of Differential Equations*, chapter 22. Boston, MA: Academic Press, 3rd edition, 1997.
- [107] M.E.A. El-Mikkawy and G.-S. Cheon. Combinatorial and hypergeometric identities via the Legendre polynomials - A computational approach. *Applied Mathematics and Computation*, 166(1):181–195, 2005.
- [108] J.M. González-Cantero, E. Graciani, F. París, B. López-Romano, and D. Meizoso-Latova. Semi-analytic solution of non-regularized unfolding stresses in composite beams employing a series approximation based on Legendre polynomials. In *Proceedings of the 21th International Conference on Composite Materials ICCM20*, 2015. 19-24 of July, Copenhagen, Denmark.

- [109] J.M. González-Cantero, E. Graciani, F. París, D. Meizoso-Latova, and J.A. Rodríguez-Sánchez. Resultados semi-analíticos de tensiones no regularizadas en barras curvas de material compuesto usando un desarrollo en serie de funciones monomiales. In *Proceedings of the XI Congreso Nacional de Materiales Compuestos, Matcomp'15*, 2015. 6-8 of July, Móstoles, Spain.
- [110] J.M. González-Cantero, E. Graciani, F. París, and B. López-Romano. Semi-analytical stress calculation in composite materials using a 2D series expansion of the displacements. In *Proceedings of the 19th International Conference on Composite Structures ICCS19*, 2016. 5-9 of September, Porto, Portugal.
- [111] E.E. Theotokoglou and E. Sideridis. Study of composite beams in asymmetric four-point bending. *Journal of Reinforced Plastics and Composites*, 30(13):1125–1137, 2011.
- [112] Y.C. Chiang. Curved laminate analysis. *Structural Engineering and Mechanics*, 39(2):169–186, 2011.
- [113] C.P. Wu and Y.W. Chi. Three-dimensional nonlinear analysis of laminated cylindrical shells under cylindrical bending. *European Journal of Mechanics A/Solids*, 24:837–856, 2005.
- [114] O.G. Kravchenko, C. Li, A. Strachanand, S.G. Kravchenko, and R.B. Pipes. Prediction of the chemical and thermal shrinkage in a thermoset polymer. *Composites: Part A*, 66:35–43, 2014.
- [115] O.G. Kravchenko, S.G. Kravchenko, and R.B. Pipes. Chemical and thermal shrinkage in thermosetting prepreg. *Composites Part A*, 80:72–81, 2016.
- [116] Wilhelm Flügge. *Stresses in Shells*. Springer-Verlag Berlin, second edition, 1973.
- [117] R. Roos. *Model for Interlaminar Normal Stresses in Doubly Curved Laminates*. PhD thesis, Swiss Federal Institute of Technology, Zurich, 2008.
- [118] A. Blázquez, V. Mantič, F. París, and N.L. McCartney. BEM analysis of damage progress in 0/90 laminates. *Engineering Analysis with Boundary Elements*, 33:762–769, 2009.

-
- [119] F. París, A. Blázquez, N.L. McCartney, and V. Mantić. Characterization and evolution of matrix and interface related damage in $[0/90]_S$ laminates under tension. Part I: Numerical predictions. *Composites Science and Technology*, 70:1168–1175, 2010.
- [120] F. París, A. Blázquez, N.L. McCartney, and A. Barroso. Characterization and evolution of matrix and interface related damage in $[0/90]_S$ laminates under tension. Part II: Experimental evidence. *Composites Science and Technology*, 70:1176–1183, 2010.

Curriculum Vitae

Name: Juan Manuel González Cantero
Date of Birth: December 30, 1990
Nationality: Spanish
E-mail: Juan.Manuel.Gonzalez@fidamc.es

Education:

- PhD, Universidad de Sevilla, Escuela Técnica Superior de Ingenieros (Sept 2014 - Jul 2017).
- 63 credits in Advanced Design in Mechanical Engineering Master at the University of Seville (2014).
- Aeronautical Engineer at the Engineering School of Seville University with an average mark of 8.93/10 (Sept 2008 - Oct 2013). Awards:
 - Award for the Outstanding Graduate of the Year.
 - Best final year project on an aeronautical topic (Cátedra EADS).
- Erasmus FORMAT-EO (FORMATION of Multi-disciplinary Approaches to Training in Earth Observation) intensive course in the University of Leicester (July 2013).

Working experience:

- PhD Student and stress engineer in FIDAMC (Spain) since February 2014, working on national and European R&D projects.
- Internship at Airbus Group Innovations, within the department "Lightweight Design & Optimization" at the Airbus Group site Otto-brunn (Germany) since the 01/04/2016 until 31/07/2016.
- Internship at the Armament and Experimentation Logistic Center of the Spanish Air Force at August 2013.

Publications:

- J.M. González-Cantero, E. Graciani, A. Blázquez, and F. París. A new analytical model for evaluating interlaminar stresses in the unfolding failure of composite laminates. *Composite Structures*, 147:260–273, 2016.
- J.M. González-Cantero, E. Graciani, F. París, and B. López-Romano. Semi-analytic model to evaluate non-regularized stresses causing unfolding failure in composites. *Composite Structures*, 171:77–91, 2017.
- J.M. González-Cantero, E. Graciani, B. López-Romano, and F. París. Induced unfolding: a new mechanism of unfolding failure in composite laminates. *Submitted to Composites Science and Technology*, 2017.
- J.M. González-Cantero, E. Graciani, B. López-Romano, and F. París. Enhanced semi-analytic model for the evaluation of non-regularized stresses in the unfolding failure by using Legendre polynomials. *In preparation*.
- J.M. González-Cantero. 3D analytical model for evaluating stresses in curved aerostructural composite laminates. ECSE2016-1, Airbus Group Chair of Aeronautical Studies, School of Engineering, University of Seville, 2016.

Conferences:

- J.M. González-Cantero, E. Graciani, A. Blázquez, and F. París. Analytical evaluation of radial stresses in unfolding failure of composite materials. Comparison with numerical solutions. In *Proceedings of the 16th European Conference on Composite Materials ECCM16*, 2014. 22-26 of June, Seville, Spain.
- J.M. González-Cantero, E. Graciani, F. París, B. López-Romano, and J.A. Rodríguez-Sánchez. Study of the composite ILTS test in CFRP angles by means of analytical and FEM models. In *7th International Conference on Composites Testing and Model Identification*, 2015. IMDEA, Getafe, Spain.
- J.M. González-Cantero, E. Graciani, F. París, D. Meizoso-Latova, and J.A. Rodríguez-Sánchez. Resultados semi-analíticos de tensiones no regularizadas en barras curvas de material compuesto usando un desarrollo en serie de funciones monomiales. In *Proceedings of the XI Congreso Nacional de Materiales Compuestos, Matcomp'15*, 2015. 6-8 of July, Móstoles, Spain.

-
- J.M. González-Cantero, E. Graciani, F. París, B. López-Romano, and D. Meizoso-Latova. Semi-analytic solution of non-regularized unfolding stresses in composite beams employing a series approximation based on Legendre polynomials. In *Proceedings of the 21th International Conference on Composite Materials ICCM20*, 2015. 19-24 of July, Copenhagen, Denmark.
 - J.M. González-Cantero, E. Graciani, F. París, and B. López-Romano. Stacking sequence optimization of curved UD-CFRP laminates for improving unfolding strength considering thermal residual stresses. In *Proceedings of the 17th European Conference on Composite Materials ECCM17*, 2016. 26-30 of June, Munich, Germany.
 - J.M. González-Cantero, E. Graciani, F. París, and B. López-Romano. Semi-analytical stress calculation in composite materials using a 2D series expansion of the displacements. In *Proceedings of the 19th International Conference on Composite Structures ICCS19*, 2016. 5-9 of September, Porto, Portugal.